Ferrocene-based Electrochemical Chiral Sensors

by

Giorgio Mirri

A thesis submitted to

The University of Birmingham

For the degree of

DOCTOR OF PHILOSOPHY

Dedicata alla memoria di mio
Padre e mio Nonno

Acknowledgements

There are a few people without whom this thesis would be never finished. First of all I am very grateful to my supervisor Dr. Jim Tucker to allow me to work in his group, to be always present during all my PhD and also for his patience in these last few months. Secondly past and present members of the Tucker group for bearing me singing in the lab, along with being available for any question and problem I incurred in.

All the electrochemistry characterisation and experiments would have been much harder if not impossible if I was not supported by my second supervisor Dr. Sarah Horswell who has been very helpful with many tips to better carry out electrochemical experiments, in addition to a big help in the characterisation of the SAMs.

I also thank the analytical facility of the University of Birmingham, Dr. Neil Spencer for the help in characterising compounds and in running boron NMR; Mr Graham Burns for the HPLC characterisation, Mr Peter Ashton for the Mass spectroscopy and Dr. Louise Male for the resolution of crystal structures.

I am grateful to the School of Chemistry for the funding for my research and for a travel grant. In the same way I owe acknowledgements to SCI for contributing to the expenses to go to an international conference.

I could not be at the end of the path without the support of my family, my mother, my brothers, my grandparents, uncles and aunts who have been always encouraging and supportive throughout the whole PhD.

A special mention goes to a special person, who in the bad and in the good was always there, felt close even when far away.

I cannot finish without thanking all the people that accompanied me during these three years in the UK, my housemates at the “Restaurant” Bick, Bene, Pete, Vicka, Susana and Eleni who made me feeling at home.

But also the Italian family, Luca, Carlos, Lucia, Luciana e (il capitano) Santiago, Mino, Alessio Ludovico and Irina for the “merende” (Dai, dai, dai alla cazzo di cane!). Last but not least Natalia, Andrea and Damian for hosting me (and my stuff!!) in their house.

I hope I didn’t forget anyone. This acknowledgements have been written at 4.30am after a long overnight printing session, which is not finished yet!

List of Abbreviations

A	Electrode surface area (cm^2)
α	transfer coefficient
AE	Auxiliary Electrode
Ar	Aromatic
Bn	Benzyl
Γ	Surface coverage (mol cm^{-2})
C	Concentration (M)
$CDCl_3$	Deuterated chloroform
COSY	Correlation Spectroscopy
Cp	Cyclopentadienyl
CV	Cyclic Voltammetry
δ	Chemical shift
d	in NMR doublet
D	Diffusion coefficient
dmfc	Decamethylferrocene
ΔE_p	Peak separation
ΔE_{HG}	$\lvert E°'_{HG} - E°'_{H} \rvert$
E	potential (V)
$E°'$	formal potential (V)
E_{pa}	Anodic peak (V)
E_{pc}	Cathodic peak (V)
Ee	enantiomeric excess
Fc	Ferrocene
$FcMe_{10}$	decamethylferrocene
FWHM	Full width half maximum

HMBC	Hetronuclear multiple bond correlation
HSQC	Heteronuclear single quantum coherence
i_p^a	Anodic peak current (A)
i_p^c	Cathodic peak current (A)
J	Coupling constant (Hz)
K	equilibrium constant
$k°$	rate constant of the heterogeneous electron transfer
Me	Methyl
MeOD-d_4	Deutereted methanol
n	number of electrons
v	scan rate (mV s^{-1})
^iPr	isopropyl
R	Ideal gas constant, 8.314 J K^{-1} mol^{-1}
RE	Reference electrode
r.t.	Room temperature
SAMs	Self assemblied monolayers
SWV	Square Wave Voltammetry
σ	charge density
T	Absolute temperature (K)
TBA·PF_6	tetrabutylammonium hexafluorophosphate
WE	Working electrode

Abstract

Chiral recognition, determination of enantiomeric excess and the separation of enantiomers are challenging problems for the chemist. This work has as its aim the design and syntheses of new electrochemical chiral receptors for neutral molecules. All the receptors prepared contain a ferrocene group as electroactive reporting unit. The differences among the receptors mainly relate to the binding site and the chiral group.

The first type of receptor, presented in Chapter 2, consists of chiral ferrocene containing boronic acids that have been used to electrochemically sense aromatic and aliphatic chiral and achiral diols. The electrochemical determination of the enantiomeric excess of a mixture of two enantiomers of Binol performed with one of these boronic acids represents a new advance in supramolecular chiral sensing.

In Chapter 3 the synthesis of ferrocene-containing chiral macrocycles of different sizes is described. The binding site is a cavity featuring a diamidopyridine moiety, with the chirality introduced through a Binol unit. These receptors showed low interaction with achiral cyclic ureas and chiral carboxylic acids.

Chapter 4 describes the study of self-assembled monolayers onto gold surfaces. The monolayers are formed by ferrocene-containing amides of lipoic (thioctic) acid and, for the first time, isolipoic acid. The studies indicate that isolipoic acid could be an attractive anchor group for SAM formation when strong control over the chirality of the monolayer is required.

1. Introduction

1.1 Supramolecular Chemistry

"Chemistry beyond the molecule",[1] probably the most famous and comprehensive definition of supramolecular chemistry was given in 1985 by Jean-Marie Lehn, Nobel prize winner in 1987, together with Cram and Pedersen.[2] However, the term *übermoleküle* was used from the mid '30s of the 20th century to indicate structurally organized systems interacting by metal coordination.[3] This branch of chemistry investigates systems based predominantly on weak and reversible interaction between molecules: i.e. H-bonds, coordination bonds, Van der Waals interactions, π-π interactions, ion-dipole interactions, etc.

Naturally occurring macromolecules like enzymes and membrane receptors have been a great source of inspiration in the design of supramolecular systems. The terms *receptor* and *substrate,* borrowed from natural systems are still commonly used to indicate two different molecular units interacting by means of non-covalent interactions. The *receptor* is the bigger molecular unit whereas the *substrate* is the smaller one.

It was necessary at some point to distinguish between natural and artificial supramolecular systems. Therefore the terms *host* and *guest* were introduced by Cram, generally used to describe the *receptor* and the *substrate* respectively. However, the difference between *host* and *guest* does not rely only on dimensions but in the direction of the interactions that allow the formation of the supramolecular system. The *host* is the species the interaction converge to and the *guest* is the species that interactions diverge from.[4] H*ost-guest* chemistry is, therefore, the investigation of systems characterised by the

presence of a highly organised binding geometry between two complementary molecular units, due to the presence of multiple binding sites. This means that, in these systems, non-covalent interactions are not randomly displayed but rather there is a compatibility between the host and the guest according to the *lock-key* principle expressed by Fischer in 1894.[5]

The complementarity between host and guest depends on their structures possessing sites and groups strategically positioned on the structures, allowing the non-covalent positive interactions to be greater than repulsive interactions.[6] The magnitude of these interactions increases with the number of groups participating in the binding.[7] A typical example is the DNA double helix; complementary base pairing allows the two polyanionic strands to overcome their electrostatic repulsion and strongly bind together.[8]

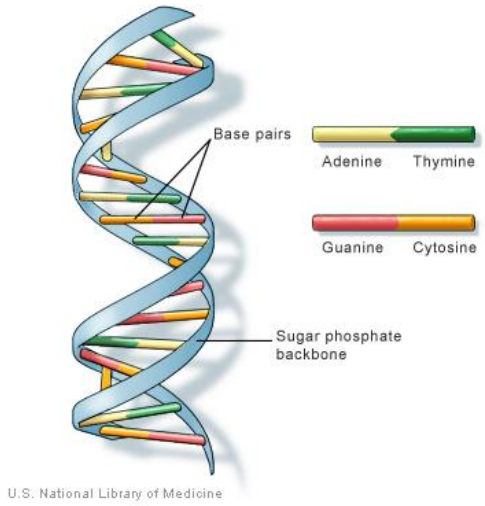

Figure 1. DNA double helix.U.S. National Library of Medicine.

Artificial supramolecular systems have been used to bind cations,[9] anions[10] and neutral molecules.[11] A particular effect can be correlated to the formation of a supramolecular complex. This effect could be a change in a chemical or physical property of the system resulting in the formation of a supramolecular sensor;[12] a change in the substrate, i.e.

supramolecular catalysis,[13] or an increase in the solubility of the guest in a solvent in which it is not normally soluble.[14]

1.2 Dynamic Covalent Chemistry

The main interest of supramolecular chemists with regards to weak interactions is how the thermodynamics govern such processes. Non-covalent interactions tend to be reversible and with small activation energies; for these reasons a series of processes leads to the most stable product. This concept is the basis of self-assembly where molecules adopt ordered structures due to intermolecular interactions. As described by a recent comprehensive review,[15] this field is extremely wide, ranging from the synthesis of mechanically interlocked systems, i.e. rotaxanes, catenanes and borromean rings,[16] to materials chemistry.[17]

When reversible interactions are covalent bonds we are in the field of dynamic covalent chemistry. Reversibility implies the possibility of error checking and can lead to self-repairing systems in contrast to the traditional synthetic chemistry, which relies on kinetically controlled reactions with the formation of irreversible bonds.

Before the term dynamic covalent chemistry was introduced to describe this field,[18] studies on the self-assembling and dynamic synthesis of macrocycles had already been reported (Scheme 1).[19]

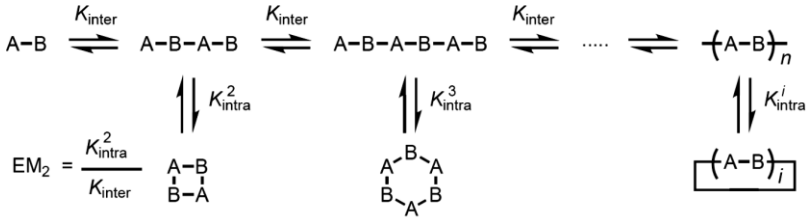

Scheme 1. Dynamic formation of macrocycles.[19]

1.3 Molecular and Supramolecular Devices and Sensors

A molecular device can be defined as an assembly of a discrete number of molecular components designed to achieve a specific function.[20] The same function is not performed by the single components not bound together. A device usually works by giving a response to a certain stimulus and if either the stimulus or the response involves a non-covalent interaction, we obtain a supramolecular device. For example with the ferrocene Hamilton-like receptor, **(i),** shown in Figure 2 the stimulus is the binding of the guest that gives as a response a difference in the electrode potential compared to that of the host alone.[21]

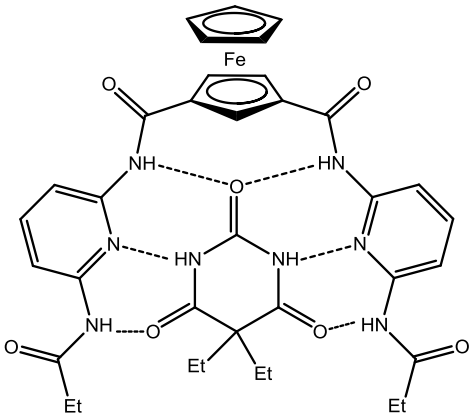

(i)

Figure 2. Ferrocene Hamilton-like receptor

On the other hand the device **(ii)** shown in Figure 3 works in an opposite way; it is a Hamilton-like receptor equipped with two pendant arms with an anthracene unit at each terminus. The stimulus in this case is irradiation with a particular wavelength, allowing the photodimerisation of the two antracene units. This leads to a change in the structure of the binding site, thereby reducing the affinity of the host for the barbiturate, causing the displacement of the guest.[22]

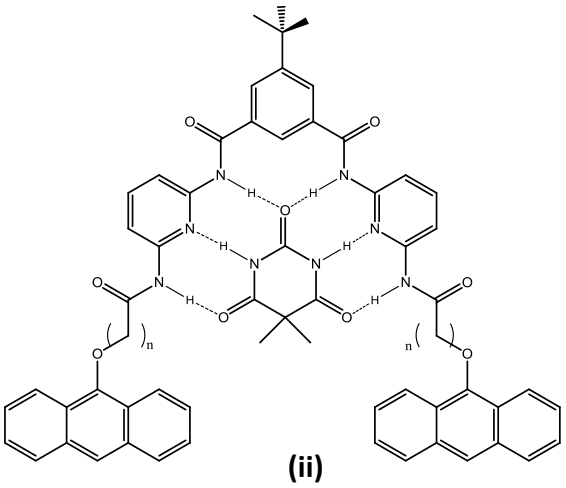

(ii)

Figure 3. Photo-active Hamilton like receptor.

A sensor could therefore be seen as a supramolecular device where the stimulus is the binding of a guest species and the response being a change in a chemical or physical property of the device. Thus a sensor is essentially constituted by a binding site and a signalling unit (Figure 4).[7]

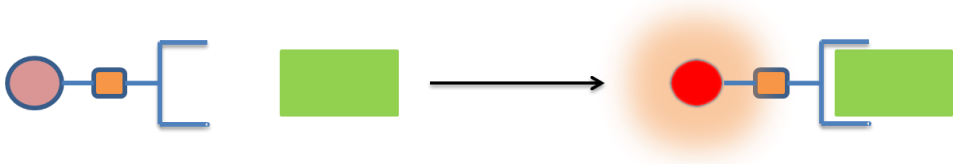

Figure 4. Schematic representation of supramolecular sensors.

Most commonly used reporting units are redox-active and photoactive groups. This is because this kind of reporting group can be assessed using rather inexpensive instruments, in addition to giving large responses to the analyte at relatively low concentrations.[12]

A classic example is compound **(iii)**, an *AND* logic gate for H^+ and Na^+ reported by de Silva in 1993. This receptor possess two binding sites, a tertiary amine for H^+ and a crown ether for Na^+; the fluorescence emission of the antracene unit is switched on only when both the

cations are bound. When either of the binding sites is free it quenches the fluorescence via electron transfer.[23]

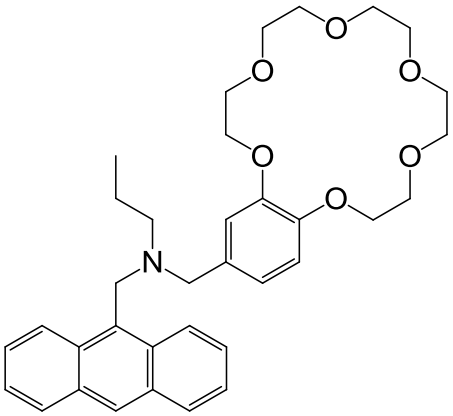

(iii)

Another interesting example is compound **(iv)** which can bind a series of saccharides; the receptors itself is achiral, but it can be used to differentiate enantiomers using a chiral technique, i.e circular dicroism.[24]

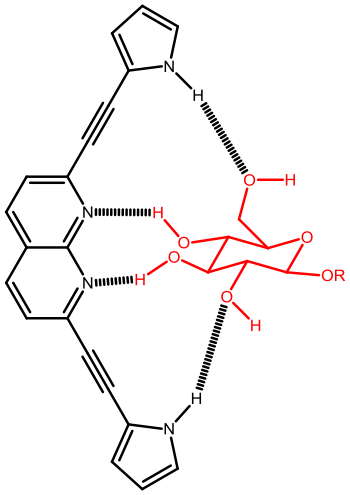

(iv)

1.4 Chiral recognition and chiral sensing

The etymology of the term chirality comes from the Greek χείρ (kheir) which means hand and it represents the property of objects that are not superimposable on their mirror images.

Chirality is therefore a geometrical property due to the absence of rotoreflexing elements in the molecule. The major difficulty in enantiomeric recognition relies on the fact that two enantiomers possess the same physical and chemical properties when observed in an achiral environment. However, they interact differently with chiral objects. Hence one of the first observations was that two enantiomers interact with circularly polarised light rotating the plane of polarisation with the same magnitude but in opposite directions. Therefore the recognition of two enantiomers can be performed only if a sensor possesses asymmetry or if the binding event with a symmetrical sensor happens in an asymmetrical fashion.

Chiral recognition was first performed by Cram who reported a method to resolve racemic mixtures of chiral ammonium salts using compound **(v)**. This compound was able to bind only one of the two enantiomers in aqueous solution, allowing it to permeate a layer of an organic solvent and then release it in another aqueous layer not containing any of the two enantiomers.[25]

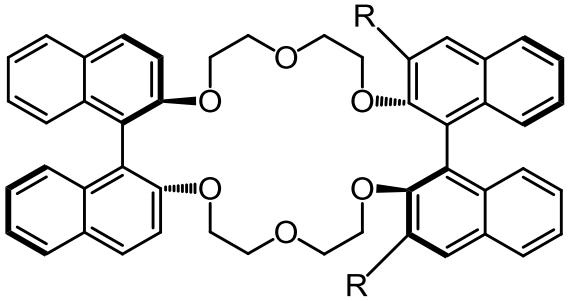

(v)

In order to perform chiral sensing, the sensor seen in the previous section has to be equipped with an enantiopure chiral moiety in close proximity to the binding site.

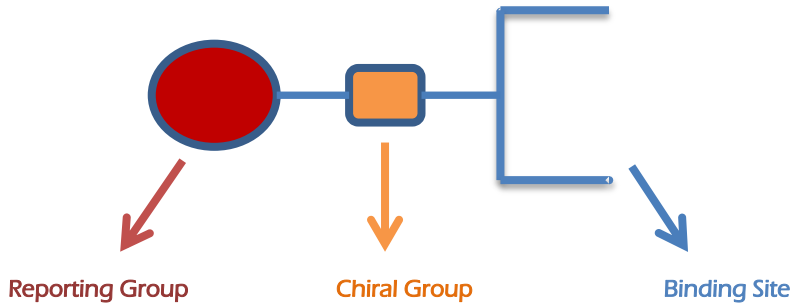

Figure 5. Schematic representation of a chiral supramolecular sensor.

Among supramolecular chiral sensors those that possess a photoactive reporting group have been far preferred to other kind of receptors, as described by Pu in a recent review.[26] This is probably due to the greater pedigree of this kind of reporting units as choice for sensors for charged and neutral achiral guests compared to sensors based on redox-active reporting groups.

One example is compound **(vi)** reported by Beer in 2004, which underwent different fluorescence quenching responses when exposed to either enantiomer of 1-phenyl ethyl amine.[27]

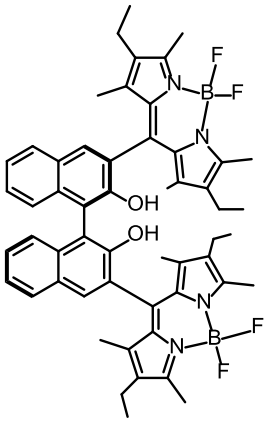

(vi)

Another example of a photoactive chiral receptor is the water-soluble salophen-zinc **(vii)**, reported by Dalla Cort and co-workers, which demonstrated enantioselective binding towards phenylalanine in water with a maximum K_L/K_D of 9.6. The read-out was a change in the intensity of the absorbtion of UV-Vis light which allowed binding constants to be determined.[28]

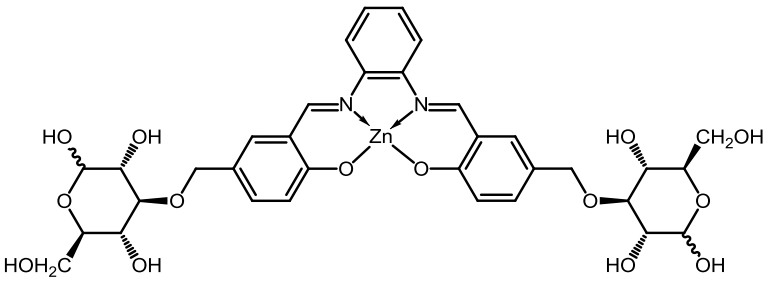

(vii)

A fluorescent receptor **(viii)** for monosaccharides was reported by Shinkai and James. The binding site was constituted by two boronic acid units, with the chiral group a Binol unit which also acted as fluorescent signalling unit.[29]

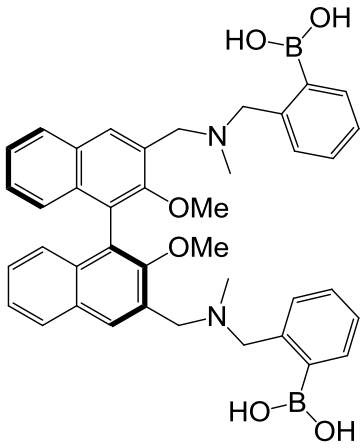

(viii)

1.5 Electrochemical sensing

When performing electrochemical sensing, the thermodynamics of the processes in both the oxidised and the reduced states must be taken into account, along with the redox processes of the free host and the complex. All the processes involved are represented in the square scheme shown below (Scheme 2).

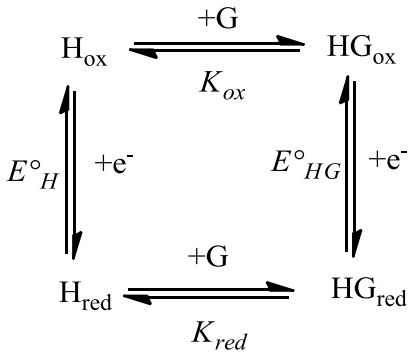

Scheme 2. Square scheme of electrochemical sensing.

The thermodynamic equilibria and electrode potentials are connected to each other by the Nernst equation (***1.1***)

$$E = E^{o'}_{Ox/\mathrm{Red}} + \frac{RT}{nF}\ln\left(\frac{[Ox]}{[\mathrm{Red}]}\right) \qquad (\textbf{\textit{1.1}})$$

Combining the Nernst equations for the free host, (***1.1bis***) and for the complex, (***1.2***), gives Equation (***1.3***) which can be rearranged to Equations (***1.3bis***) and (***1.3ter***)

$$(E - E^{o}_{H})nF/RT = \ln\left(\frac{[H_{ox}]}{[H_{red}]}\right) \qquad (\textbf{\textit{1.1bis}})$$

$$(E - E^{o}_{HG})nF/RT = \ln\left(\frac{[HG_{ox}]}{[HG_{red}]}\right) \qquad (\textbf{\textit{1.2}})$$

$$(E^{o}_{HG} - E^{o}_{H})nF/RT = -\Delta E°nF/RT = \ln\left(\frac{[HG_{ox}][H_{red}]}{[HG_{red}][H_{ox}]}\right) \quad (\textbf{\textit{1.3}})$$

$$-\Delta E°nF/RT = \ln\left(\frac{K_{ox}}{K_{red}}\right) \quad (\textbf{\textit{1.3bis}})$$

$$\frac{K_{ox}}{K_{red}} = e^{-\Delta EnF/RT} \quad (\textbf{\textit{1.3ter}})$$

In these equations, *n* is the number of electrons involved in the redox process, *F* the Faraday constant, *R* the constant for the ideal gas and T the absolute temperature. E_H° and E_{HG}° are the formal electrode potential for the free host and the complex respectively and ΔE° is (E_{HG}°- E_H°).

From Equation (***1.3bis***) it is clear that with redox-active sensors, a negative shift in the potential upon complexation is correlated to the complexation being stronger in the oxidised state ($K_{ox}/K_{red} > 1$). Similarly, a positive shift is correlated to a destabilisation of the complex upon oxidation ($K_{ox}/K_{red} < 1$).

1.5.1 Redox-active receptors

Electrochemistry has been recognised as a powerful tool for supramolecular sensing.[30] However, the extension of the field of electrochemical sensing goes beyond the realm of supramolecular chemistry to include enzyme-based biosensors and the sensing of redox-active analytes.[31]

Redox-active units commonly used as reporting group in supramolecular sensors, are inorganic and organic groups which can be easily oxidised and reduced, ideally between only two redox states. Organic redox reporting groups have been extensively used in molecular sensors as demonstrated by a variety of reviews.[32] Two organic units which have been used as electroactive signalling units are described below. Tetrathiafulvalene (TTF) can be readily

oxidised twice to give a radical cation ($TTF^{\cdot+}$) and a dication species (TTF^{2+}). The relatively low potential for the two oxidation processes (0.34 V and 0.78 V *vs.* Ag/AgCl, for E^1 and E^2 respectively) is explained by the gain in energy from the formation of the aromatic 1,3-dithiolium cation rings, as described in Scheme 3.[32a]

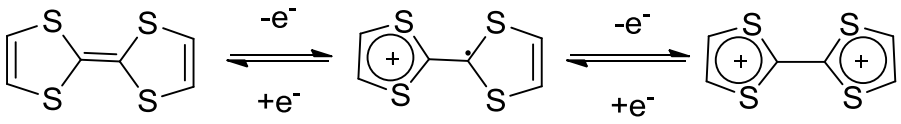

Scheme 3. Redox processes of TTF.

Another organic redox-active group widely used as a reporting unit is anthraquinone. In contrast to TTF, this group readily undergoes a 2 electron reduction process, as described in Scheme 4.

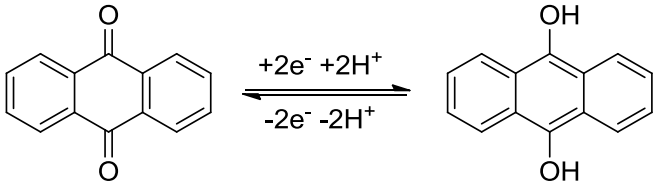

Scheme 4. Redox process of anthraquinone.

Receptors for metallic cations equipped with these two reporting groups have been described, and they are represented in Figure 6. Compound **(ix)** is a receptor for sodium cations.[33] The second example **(x)** is a sensor for the DNA base thymine in aqueous solution.[34]

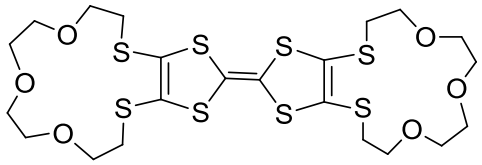

(ix)

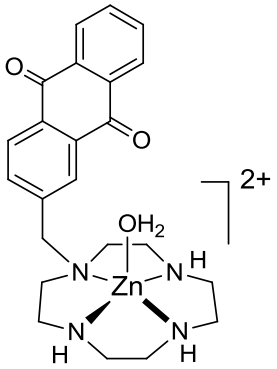

(x)

Figure 6. Examples of receptors with organic reporting group.

1.5.2 Ferrocene-based receptors

Among various inorganic groups, metallocenes, and in particular ferrocene, have been the redox-active units of choice for electrochemical sensors. This is due to the fact that they are relatively easy to functionalise via reactions characteristic of aromatic compounds, i.e. lithiation, Friedel-Craft reactions, etc., leading to a plethora of receptors.[21,35]

Furthermore, ferrocene is a coloured compound and likewise are its derivatives (from dark red to yellow). It undergoes a one-electron oxidation process from the stable Cp-Fe(II)-Cp species to the Cp-Fe(III)-Cp]$^+$ (ferrocenium ion) species. Salts of ferrocenium possess an intense blue colour and are used as oxidising agents.[36]

The redox potential of the Fc^+/Fc semi-reaction is 0.64 V (*vs.* SHE). This one-electron process is electrochemically reversible, being not affected by the polarity of the solvent nor by the presence of molecular oxygen.[32c,37] However, the potential is sensitive to substitutions on the Cp rings, in particular a correlation between the Hammett coefficient, σ_p, and the electrode potential has been demonstrated.[38] Hence electron-withdrawing substituents cause an increase in the potential; whereas electron-donating groups cause a decrease in the potential. This is due to the fact that when the electron cloud around the ferrocene unit decreases, the ferrocene becomes more difficult to oxidise and thus a higher

potential must be applied in order to obtain the ferronium ion. On the other hand when the electron cloud increases around the Fe(II) nucleus the species is easier to oxidise and for this reason the required potential is lower.

Ferrocene-based sensors for cations were one of the first supramolecular sensors to be reported and were originally based on the incorporation of crown ethers or cryptands.[39] When cations are sensed, the introduction of a positively charged species in the *host-guest* complex destabilises the ferrocenium ion, making the ferrocene harder to oxidise. This results in an increase in the potential of the ferrocene upon addition of the guest. Examples of some ferrocene-based cation sensors are shown in Figure 7. Compounds **(xi), (xii)** and **(xiii)** have been used to sense alkali metal ions in organic solvents.[40] Receptor **(xiii)** displayed an unusual negative shift in the electrode potential probably due to a structural rearrangement upon complexation.[39,41] Compound **(xiv)** showed an high selectivity towards the binding of Mg^{2+}.[42] Compound **(xv)** is an example of a sensor for a non-metallic cation; in this case amino acids were bound and sensed.[43]

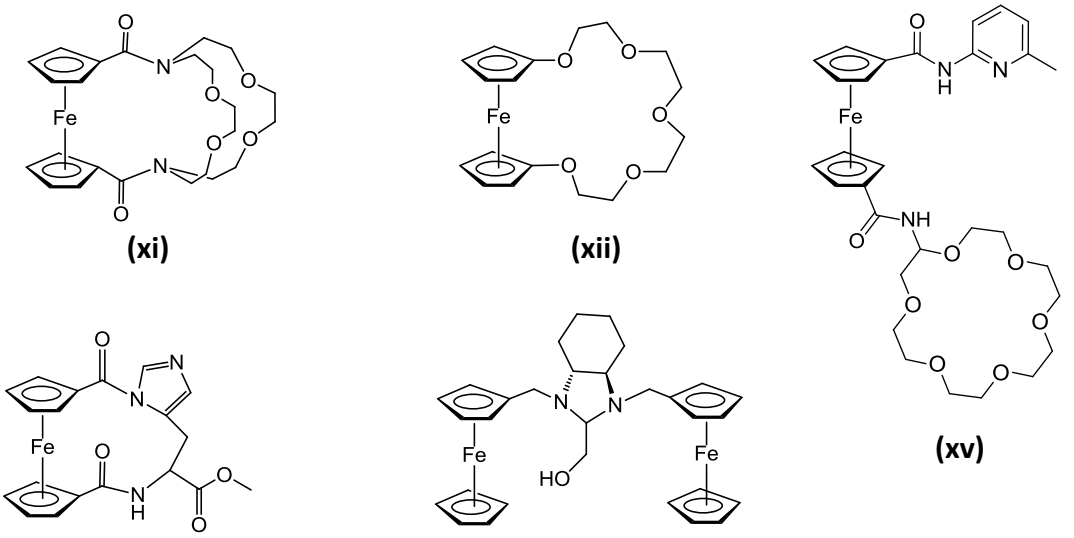

Figure 7. Examples of redox-active receptors for cations

Anions present more challenges for binding than cations due to their larger radius/charge ratio, their dimensions and their geometric preferences.[44] Electrochemical sensors for anions based on ferrocene generally undergo negative shifts in potential upon the binding of the analyte. This is due to the negative charge stabilising the ferrocenium ion, making the oxidation of the redox unit easier.

Receptor **(xvi)** has been used to complex hydrogen sulphate (HSO_4^-) in aqueous media[45] and **(xvii)** was demonstrated to be able to bind the natural ubiquitous *"energy currency"* ATP in organic solvents. In this latter case the polyanion stabilised the dicationic species formed upon oxidation, as evidenced by a rather large negative shift of -470 mV.[46] Shinkai developed the ferrocenyl boronic acid, **(xviii)**, for the selective binding of fluoride over mixtures of halides.[47] More recently Aldridge used a hindered 1,2 diboryl ferrocene, **(xix)**, to selectively recognise cyanide in the presence of fluoride.[48]

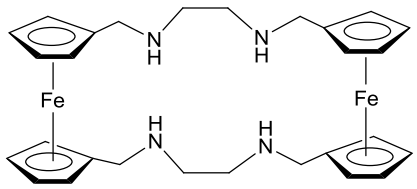

(xvi)

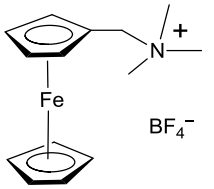

(xvii)

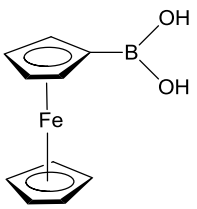

(xviii)

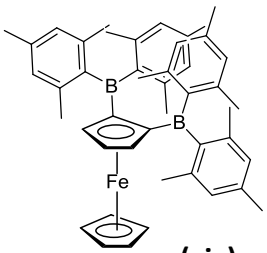

(xix)

Figure 8. Examples of receptors for anions.

Neutral molecule electrochemical sensing accounts for fewer examples compared to the recognition of charged species. This is probably due to the rather small response that the

binding event causes to the signalling unit. Examples of redox-active sensors for neutral molecules were described in previous sections (**(i)** and **(iv)**). One further example is **(xx)**; the 1,1'-bis-(amido)-pyridine has been demonstrated to bind carboxylic acids in chlorinated organic solvents causing a negative shift in the electrode potential of the ferrocene unit upon the binding of the guest.[49]

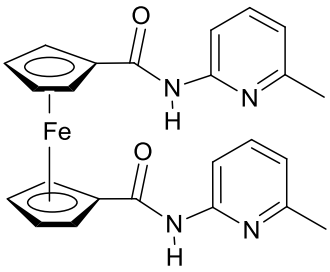

(xx)

1.5.3 Electrochemical chiral sensing

When the guest consists of a pair of enantiomers the reasoning described in previous sections must take into account both species. The square scheme is therefore doubled to describe the adducts formed between the free host and each of the two enantiomers in both the reduced and oxidised forms (Scheme 5).

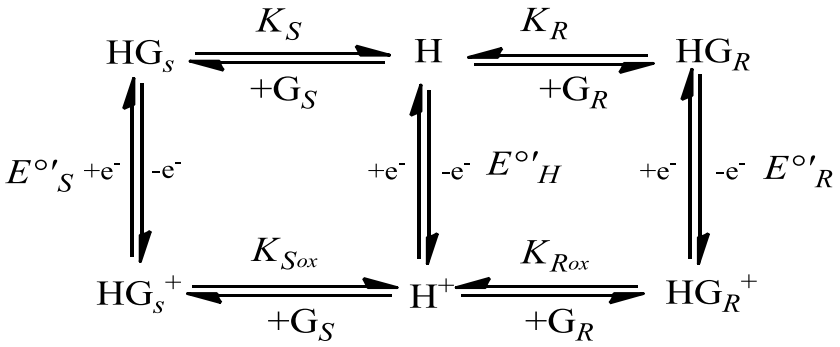

Scheme 5. Square scheme of electrochemical chiral sensing.

Having two different guests also means that the rearranged Nernst equation doubles up (Equations (***1.4***) and (***1.5***)).

$$\Delta E_R = -\frac{RT}{nF}\ln\frac{K_{R_{ox}}}{K_R} \qquad (\textbf{\textit{1.4}})$$

$$\Delta E_S = -\frac{RT}{nF}\ln\frac{K_{S_{ox}}}{K_S} \qquad (\textbf{\textit{1.5}})$$

From Equations (***1.4***) and (***1.5***) it follows that for electrochemical chiral sensing (i.e. where $\Delta E_R \neq \Delta E_S$) the condition required is

$$\frac{K_{R_{ox}}}{K_R} \neq \frac{K_{S_{ox}}}{K_S} \qquad (\textbf{\textit{1.6}})$$

A schematic representation of an enantioselective electrochemical sensor is shown in Figure 9.

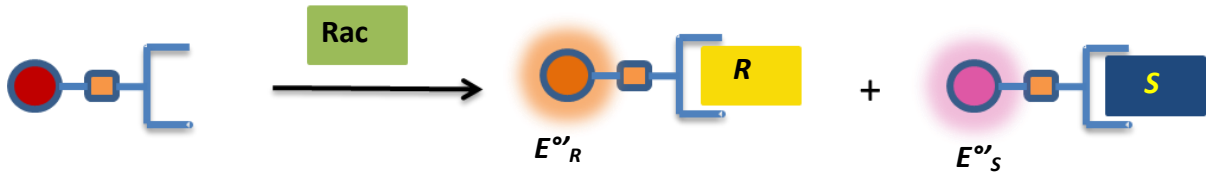

Figure 9. Schematic representation of electrochemical chiral sensing, where $E^{\circ\prime}_R \neq E^{\circ\prime}_S$.

When the two complexes formed with either enantiomer possess the same electrode potential (i.e. $\Delta E_R^{\circ\prime} = \Delta E_S^{\circ\prime}$), chiral recognition might still be possible if the thermodynamic constants for the formation of the two diasteromeric complexes are different in either the oxidised or in the reduced states. An example of this method of detection is described in the next section.

1.5.4 Electrochemical chiral sensors

In contrast to the large number of photo-active sensors reported, chiral recognition performed with redox-active receptors accounts for only a few examples.[31b] In 1995 Shinkai reported a redox-active boronic acid saccharide sensor **(xxi)** which could sense different linear saccharides and also perform chiral discrimination between D and L forms for some of them.[50]

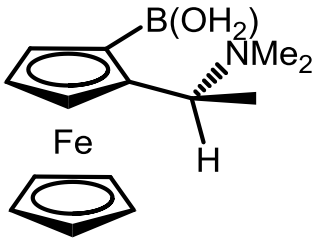

(xxi)

More recently Tucker reported the chiral recognition of carboxylate anions by the chiral ferrocenyl urea **(xxii)** shown in Figure 10.[35e]

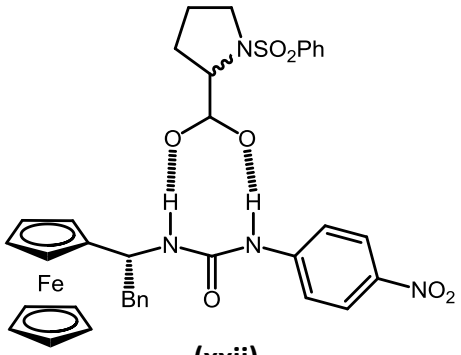

(xxii)

Figure 10. Chiral ferrocenyl urea **(xxii)** with chiral prolinate guest.

This system based its chiral sensing ability more in the difference of the binding constants for the formation of the two diasteromeric host-guest complexes than on the difference in the electrode potentials, which were, in fact, whithin experimental error when more than 2 equivalents of guest were added. However, $\delta\Delta E_{obs}$ (which is $|\Delta E_R^{\circ\prime} - \Delta E_S^{\circ\prime}|$) was larger in the

presence of between 0.5 and 1 molar equivalents of the guest, allowing the the enantiomers to be distinguish electrochemically (Figure 11).

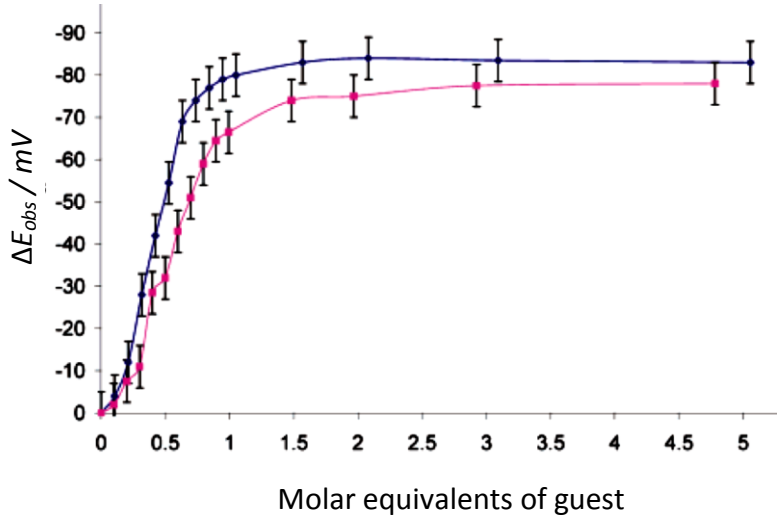

Figure 11. ΔE_{obs} of **(xxii)** *vs.* molar equivalent of guests. Blue (*S*)-prolinate guest; Pink (*R*)-prolinate guest

In 2006 Kim *et al.* reported compound **(xxiii)** which could distinguish various enantiomers of chiral amines. Moreover the potential of the host **(xxiii)** showed a linear relationship between the enantiomeric composition of the guest solution (2-amino-2-phenyl-ethanol), allowing the determination of large differences in the enantiomeric composition of guest solutions.[51]

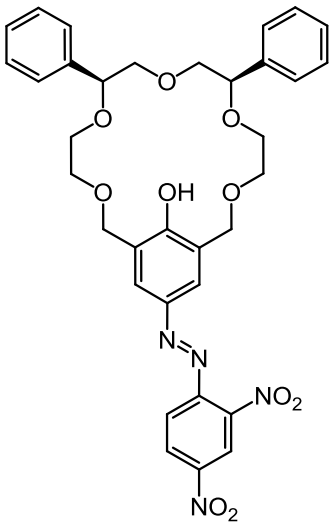

(xxiii)

As evidenced by Shinkai's works described above, the boronic acid moiety is widely used as a binding site for 1,2 and 1,3 diols, as also described in a very recent review by James.[52]

James and co-workers have also reported a facile protocol for the determination of enantiomeric excess of mixtures of chiral diols[53] and amines[54] by ^{1}H-NMR using boronic acids.

1.6 Electrochemical Techniques

Redox-active sensors are generally assessed using techniques that measure the current as a function of the applied potential.[44b] The simplest set-up required to carry out these experiments is a three-electrode cell as shown in Figure 12. This cell is constituted by a working electrode, a reference electrode and an auxiliary electrode.

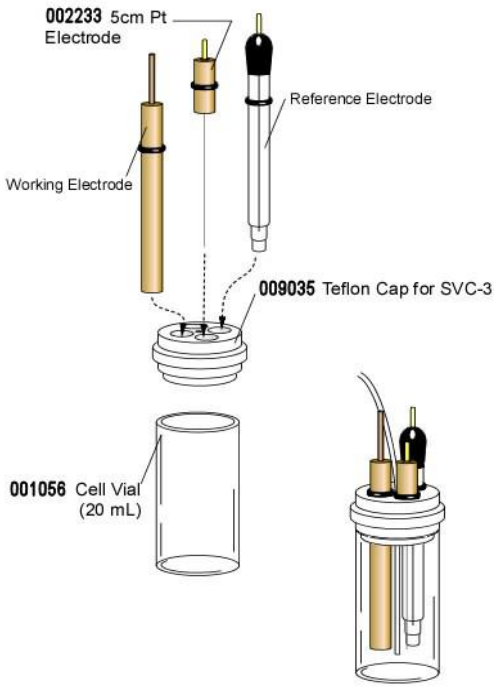

Figure 12. Three-electrode cell. http://www.als-japan.com/1025.html

The cell is connected to a potentiostat that allows the potential between the working electrode and the reference electrode to be controlled. The presence of the auxiliary electrode is necessary to allow the current flowing through the reference electrode to be small, as the potential is affected by the current and the potential of the reference electrode is required to be constant during the experiment.

The reference electrode commonly used is the Ag/AgCl (KCl, 3 M) electrode. This redox couple possesses a potential of +0.21 V *vs.* the standard hydrogen electrode (SHE) which, as the universal reference, has a value of 0.00 V. The potential is not an absolute physical quantity and always has to be related to another potential which acts as a reference.

The Ag/AgCl electrode is constituted by a silver wire immersed in an aqueous solution of silver chloride separated from the analyte solution by a vycro septum. The relative stability of the potential and the ease of the set-up allows this electrode to be widely used in electrochemical sensing experiments. However, when the experiment is carried out in non-aqueous solvents, an interphase potential will establish between the aqueous solution of the electrode and the solution of the analyte. The magnitude of this potential is not measurable but it affects the reference potential itself. For this reason when experiments are carried out in organic solvents that are immiscible with water, an internal reference is generally used. Hence electrode potentials observed during the experiments are reported *vs*. the internal reference. Two voltammetric techniques that use the set-up described above are described in the next sections.

1.6.1 Cyclic Voltammetry

Cyclic voltammetry is a linear sweep potential technique. The potential is scanned linearly forward and backwards in a cycle (or cycles).[55] The current flowing during the sweep peaks when the potential reaches the electrode potential of one of the analytes. Figure 13 shows the potential vs. time and an example of a cyclic voltammogram.

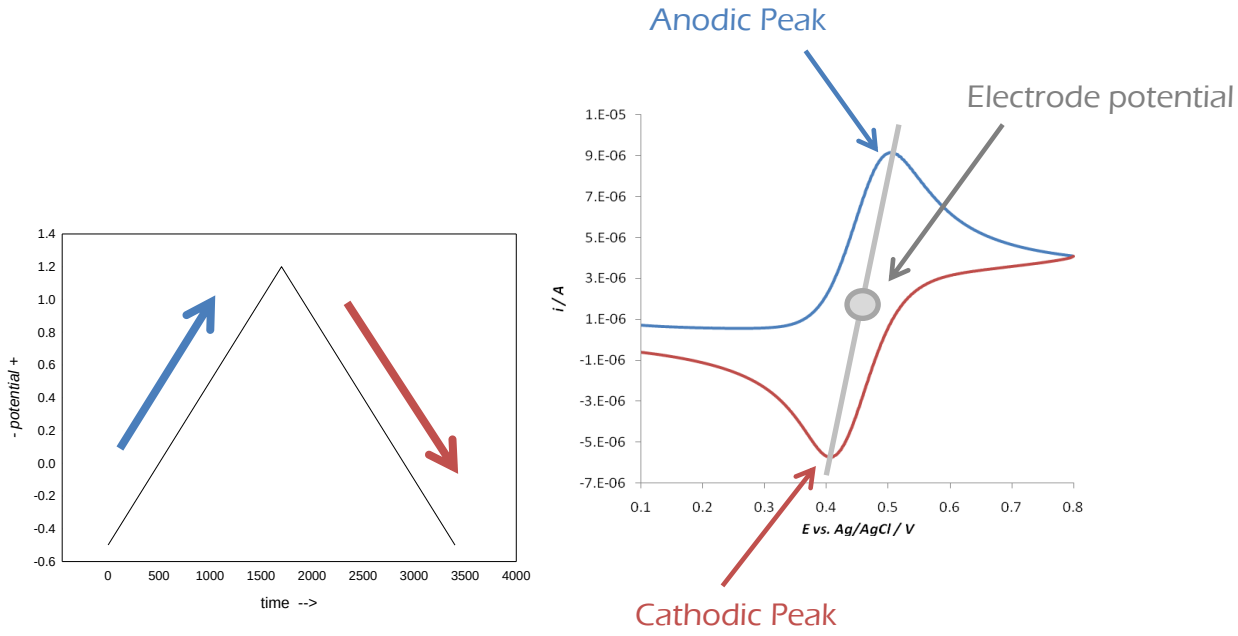

Figure 13. Potential *vs.* time in cyclic voltammetry experiments and an example of cyclic voltammogram.

The anodic peak is due to the current flowing during the oxidation process, whereas the cathodic peak is due to the current from the reduction process. Cyclic voltammograms of electrochemically reversible species appear with a characteristic "duck" shape. The two peaks are not symmetrical and the formal electrode potential, *E°',* is approximated as the mid-point between the two peak potentials.

Mass transport and the kinetics of electron transfer affect the potential as described in Equation (***1.7***).

$$k_{ET} = k^{\circ} e^{\frac{-\alpha n F}{RT}(E - E^{\circ\prime})} \qquad (\textbf{\textit{1.7}})$$

Here k_{ET} is the rate constant for the electron transfer, k° the rate constant for the standard heterogeneous electron transfer, α the transfer coefficient, *n* the number of electrons transferred per molecule, *F* the Faraday constant, *R* the universal gas constant, T the absolute temperature (K) and $E^{\circ\prime}$ the formal potential. ($E-E^{\circ\prime}$) is called the overpotential and is also indicated as η; it indicates the extra potential that should be applied to the solution in order to observe electron transfer.[56] The overpotential is the reason why the anodic and cathodic current peaks are shifted with respect to the electrode potential of the analyte. For reversible systems the difference is 59/n mV.[57] Moreover, mass transport prevents the current from increasing exponentially indefinitely, when the mass transport becomes the rate determining step the current reaches a maximum and then decreases without going back to 0.000 A.

As mentioned above, the electrode potential of an analyte can be determined by calculating the mid-point between the anodic and the cathodic peak potentials (Equation (***1.8***)).

$$E^{\circ\prime} = \frac{E_{pa} + E_{pc}}{2} \qquad (\textbf{\textit{1.8}})$$

The current depends also on the scan-rate and according to the Randles-Sevcik Equation (***1.9***), is proportional to the square root of the scan-rate[58]

$$i_p = 2.69 \times 10^5 n^{3/2} A D^{1/2} C v^{1/2} \qquad (\textbf{\textit{1.9}})$$

i_p is the peak current (Ampere), *n* the number of electron exchanged, *A* the electrode surface (cm^2), D the diffusion coefficient ($cm^2\ s^{-1}$), C the bulk concentration (M) and v is the

potential scan rate (V s^{-1}). It can be demonstrated that at high scan rates, there is an increase in the peak separation which can be erroneously interpreted as slow electron-transfer. However, this is due to the Ohmic drop of the solution that acts as a resistance, which affects the observed potential.[59]

1.6.2 Square Wave Voltammetry

Square wave voltammetry (SWV) is a pulsed potential technique invented by Ramaey and Krause in 1969.[60] It was then further developed by Osteryoung and for this reason is also indicated as Osteryoung voltammetry.[61] In this technique, pulses of potential are superimposed on a staircase and Figure 14 shows the graph of the potential *vs.* time. The current is measured twice, before and after each step. The square wave voltammogram (dotted red line in Figure 14) is the net current, i.e. the result of the difference between the two currents measured (red and blue line respectively). The peak is centred on the electrode potential of the electrode potential of the analyte.

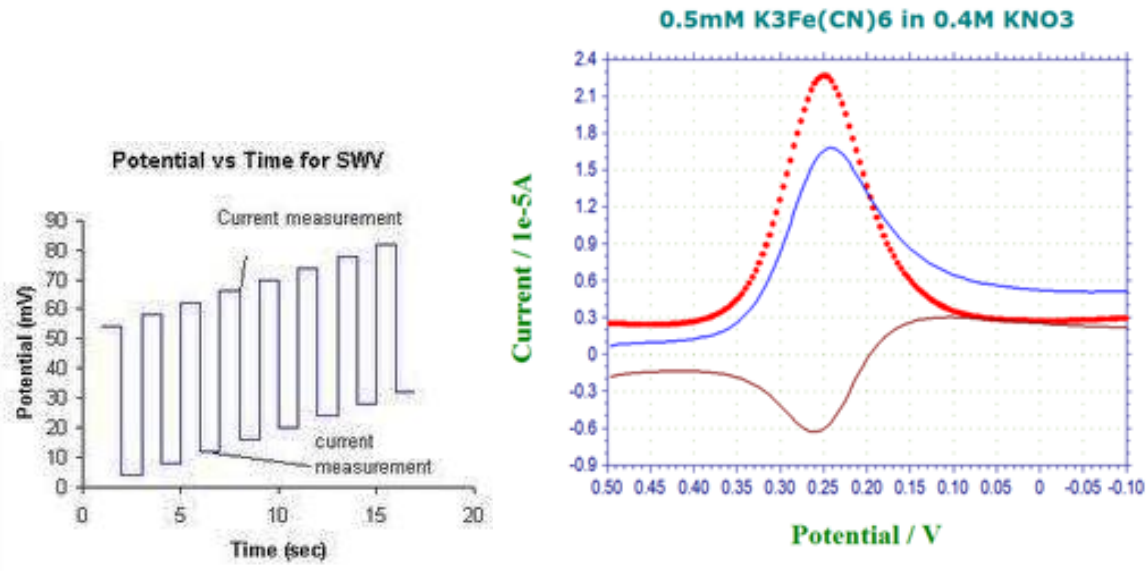

Figure 14. Potenital *vs.* time in square wave voltammetry experiments and an example of a square wave voltammogram.

There are some advantages to using this technique, firstly the limit of detection is lower than other electrochemical techniques (10^{-8} M)[57] and secondly the solutions do not need to be purged prior to each experiment since in the region of oxygen reduction, the two currents have the same value, giving a zero net current.

1.7 References

(1) Lehn, J. M. *Science* **1985**, *227*, 849.
(2) Lehn, J., Nobel Lecture.
(3) (a) Wolf, K. L.; Frahm, H.; Harms, H. *Z. Phys. Chem. Abt. B* **1937**, *36*, 237(b) Wolf, K. L.; Dunken, H.; Merkel, K. *Z. Phys. Chem. Abt. B* **1940**, *46*, 287.
(4) Kyba, E. P.; Helgeson, R. C.; Madan, K.; Gokel, G. W.; Tarnowski, T. L.; Moore, S. S.; Cram, D. J. *J. Am. Chem. Soc.* **1977**, *99*, 2564.
(5) Fischer, E. *Ber. Deutsch. Chem. Gesell.* **1894**, *27*.
(6) Cram, D. J.; Lein, G. M. *J. Am. Chem. Soc.* **1985**, *107*, 3657.
(7) Schneider, H.-J. *Angew. Chem., Int. Ed. Engl.* **1991**, *30*, 1417.
(8) Watson, J. D.; Crick, F. H. C. *Nature* **1953**, *171*, 737.
(9) Pedersen, C. J. *J. Am. Chem. Soc.* **1967**, *89*, 2495.
(10) Steed, J. W. *Chem. Soc. Rev.* **2009**, *38*, 506.
(11) Chang, S. K.; Hamilton, A. D. *J. Am. Chem. Soc.* **1988**, *110*, 1318.
(12) Fabbrizzi, L.; Poggi, A. *Chem. Soc. Rev.* **1995**, *24*, 197.
(13) Wiester, M. J.; Ulmann, P. A.; Mirkin, C. A. *Angew. Chem., Int. Ed.* **2011**, *50*, 114.
(14) Pedersen, C. J. *J. Am. Chem. Soc.* **1967**, *89*, 7017.
(15) Ariga, K.; Hill, J. P.; Lee, M. V.; Vinu, A.; Charvet, R.; Acharya, S. *Science and Technology of Advanced Materials* **2008**, *9*.
(16) Chichak, K. S.; Cantrill, S. J.; Pease, A. R.; Chiu, S.-H.; Cave, G. W. V.; Atwood, J. L.; Stoddart, J. F. *Science* **2004**, *304*, 1308.
(17) Elemans, J. A. A. W.; Rowan, A. E.; Nolte, R. J. M. *J. Mater. Chem.* **2003**, *13*, 2661.
(18) Rowan, S. J.; Cantrill, S. J.; Cousins, G. R. L.; Sanders, J. K. M.; Stoddart, J. F. *Angew. Chem., Int. Ed.* **2002**, *41*, 898.
(19) Ercolani, G.; Mandolini, L.; Mencarelli, P.; Roelens, S. *J. Am. Chem. Soc.* **1993**, *115*, 3901.
(20) Balzani, V.; Credi, A.; Venturi, M. *Nano Today* **2007**, *2*, 18.
(21) Westwood, J.; Coles, S. J.; Collinson, S. R.; Gasser, G.; Green, S. J.; Hursthouse, M. B.; Light, M. E.; Tucker, J. H. R. *Organometallics* **2004**, *23*, 946.
(22) Molard, Y.; Bassani, D. M.; Desvergne, J. P.; Moran, N.; Tucker, J. H. R. *J. Org. Chem.* **2006**, *71*, 8523.
(23) Desilva, A. P.; Gunaratne, H. Q. N.; Mccoy, C. P. *Nature* **1993**, *364*, 42.
(24) Fang, J. M.; Selvi, S.; Liao, J. H.; Slanina, Z.; Chen, C. T.; Chou, P. T. *J. Am. Chem. Soc.* **2004**, *126*, 3559.
(25) (a) Newcomb, M.; Toner, J. L.; Helgeson, R. C.; Cram, D. J. *J. Am. Chem. Soc.* **1979**, *101*, 4941(b) Newcomb, M.; Helgeson, R. C.; Cram, D. J. *J. Am. Chem. Soc.* **1974**, *96*, 7367.
(26) Pu, L. *Chem. Rev.* **2004**, *104*, 1687.
(27) Beer, G.; Rurack, K.; Daub, J. *Chem. Commun.* **2001**, 1138.
(28) Dalla Cort, A.; De Bernardin, P.; Schiaffino, L. *Chirality* **2009**, *21*, 104.
(29) James, T. D.; Sandanayake, K. R. A. S.; Shinkai, S. *Nature* **1995**, *374*, 345.
(30) (a) Lehn, J. *Supramolecular Chemistry, Concepts and Perspectives*; VCH: Weinheim, 1995(b) Kaifer, A. E.; Gomez-Kaifer, M. *Supramolecular Electrochemistry*; Wiley-VCH, 1999.
(31) (a) Bakker, E.; Telting-Diaz, M. *Anal. Chem.* **2002**, *74*, 2781(b) Privett, B. J.; Shin, J. H.; Schoenfisch, M. H. *Anal. Chem.* **2008**, *80*, 4499.
(32) (a) Canevet, D.; SallA, M.; Zhang, G.; Zhang, D.; Zhu, D. *Chem. Commun.* **2009**, 2245(b) D. Beer, P.; A. Gale, P.; Z. Chen, G. *J. Chem. Soc., Dalton Trans.* **1999**, 1897(c) Tucker, J. H. R.; Collinson, S. R. *Chem. Soc. Rev.* **2002**, *31*, 147.

(33) Liu, S.-G.; Echegoyen, L. *Eur. J. Org. Chem.* **2000**, *2000*, 1157.
(34) Tucker, J. H. R.; Shionoya, M.; Koike, T.; Kimura, E. *Bull. Chem. Soc. Jpn.* **1995**, *68*, 2465.
(35) (a) Casas-Solvas, J. M.; Ortiz-Salmeron, E.; Fernandez, I.; Garcia-Fuentes, L.; Santoyo-Gonzalez, F.; Vargas-Berenguel, A. *Chem.-Eur. J.* **2009**, *15*, 8146(b) Mirri, G.; Bull, S. D.; Horton, P. N.; James, T. D.; Male, L.; Tucker, J. H. R. *J. Am. Chem. Soc.* **2010**, *132*, 8903(c) Wade, C. R.; Broomsgrove, A. E. J.; Aldridge, S.; Gabbai, F. P. *Chem. Rev.* **2010**, *110*, 3958(d) Miller, S. R.; Gustowski, D. A.; Chen, Z. H.; Gokel, G. W.; Echegoyen, L.; Kaifer, A. E. *Anal. Chem.* **1988**, *60*, 2021(e) Willener, Y.; Joly, K. A.; Moody, C. J.; Tucker, J. H. R. *J. Org. Chem.* **2008**, *73*, 1225(f) Broomsgrove, A. E. J.; A. Addy, D.; Di Paolo, A.; Morgan, I. R.; Bresner, C.; Chislett, V.; Fallis, I. A.; Thompson, A. L.; Vidovic, D.; Aldridge, S. *Inorg. Chem.* **2009**, *49*, 157.
(36) Connelly, N. G.; Geiger, W. E. *Chem. Rev.* **1996**, *96*, 877.
(37) Fujihira, M.; Hoshino, K.; Saji, T.; Aoyagui, S. *Chem. Lett.* **1985**, 1419.
(38) (a) Emília, M.; Silva, N. P. R. A.; Pombeiro, A. J. L.; da Silva, J. J. R. F.; Herrmann, R.; Deus, N.; Castilho, T. J.; Silva, M. F. C. G. *J. Organomet. Chem.* **1991**, *421*, 75(b) N.P.R.A. Silva, M. E.; Pombeiro, A. J. L.; Fraústo da Silva, J. J. R.; Herrmann, R.; Deus, N.; E.Bozak, R. *J. Organomet. Chem.* **1994**, *480*, 81.
(39) Medina, J. C.; Goodnow, T. T.; Bott, S.; Atwood, J. L.; Kaifer, A. E.; Gokel, G. W. *J. Chem. Soc. Chem. Commun.* **1991**, 290.
(40) (a) Medina, J. C.; Goodnow, T. T.; Rojas, M. T.; Atwood, J. L.; Lynn, B. C.; Kaifer, A. E.; Gokel, G. W. *J. Am. Chem. Soc.* **1992**, *114*, 10583(b) Saji, T.; Kinoshita, I. *J. Chem. Soc., Chem. Commun.* **1986**, 716.
(41) Chowdhury, S.; Schatte, G.; Kraatz, H.-B. *Eur. J. Inorg. Chem.* **2006**, *2006*, 988.
(42) Sutcliffe, O. B.; Bryce, M. R.; Batsanov, A. S. *J. Organomet. Chem.* **2002**, *656*, 211.
(43) Miyaji, H.; Gasser, G.; Green, S. J.; Molard, Y.; Strawbridge, S. M.; Tucker, J. H. R. *Chem. Commun.* **2005**, 5355.
(44) (a) Beer, P. D. *Chem. Commun.* **1996**, 689(b) Beer, P. D.; Gale, P. A.; Chen, G. Z. *Coord. Chem. Rev.* **1999**, *185-186*, 3.
(45) Beer, P. D.; Cadman, J.; Lloris, J. M.; Martinez-Manez, R.; Padilla, M. E.; Pardo, T.; Smith, D. K.; Soto, J. *J. Chem. Soc., Dalton Trans.* **1999**, 127.
(46) Reynes, O.; Moutet, J. C.; Pecaut, J.; Royal, G.; Saint-Aman, E. *New J. Chem.* **2002**, *26*, 9.
(47) Dusemund, C.; Sandanayake, K. R. A. S.; Shinkai, S. *J. Chem. Soc., Chem. Commun.* **1995**, 333.
(48) Morgan, I. R.; Broomsgrove, A. E. J.; Fitzpatrick, P.; Vidovic, D.; Thompson, A. L.; Fallis, I. A.; Aldridge, S. *Organometallics* **2010**, *29*, 4762.
(49) Carr, J. D.; Goles, S. J.; Hursthouse, M. B.; Light, M. E.; Tucker, J. H. R.; Westwood, J. *Angew. Chem., Int. Ed.* **2000**, *39*, 3296.
(50) Ori, A.; Shinkai, S. *J. Chem. Soc. Chem. Commun.* **1995**, 1771.
(51) Chun, K.; Kim, T. H.; Lee, O.-S.; Hirose, K.; Chung, T. D.; Chung, D. S.; Kim, H. *Anal. Chem.* **2006**, *78*, 7597.
(52) Nishiyabu, R.; Kubo, Y.; James, T. D.; Fossey, J. S. *Chem. Commun. (Cambridge, U. K.)* **2011**, *47*, 1106.
(53) Kelly, A. M.; Perez-Fuertes, Y.; Fossey, J. S.; Yeste, S. L.; Bull, S. D.; James, T. D. *Nat. Protoc.* **2008**, *3*, 215.
(54) Perez-Fuertes, Y.; Kelly, A. M.; Fossey, J. S.; Powell, M. E.; Bull, S. D.; James, T. D. *Nat. Protoc.* **2008**, *3*, 210.
(55) Kissinger, P. T.; Heineman, W. R. *J. Chem. Educ.* **1983**, *60*, 702.
(56) Erdey-Gruz, T.; Volmer, M. *Z. Phys. Chem. Abt. A* **1930**, *150*, 203.

(57) Brett, C. M.; Oliveira-Brett, A. M. *Voltammetric Sensors in Electroanalysis*; University Press: Oxford, 1998.
(58) Randles, J. E. B. *Trans. Faraday Soc.* **1948**, *44*, 327.
(59) Nicholso.Rs *Anal. Chem.* **1965**, *37*, 1351.
(60) Ramaley, L.; Krause, M. S. *Anal. Chem.* **1969**, *41*, 1362.
(61) Osteryoung, R. A.; Osteryoung, J. *Phil. Trans. R. Soc. A* **1981**, *302*, 315.

2. Ferrocene Boronic Acids as Chiral Sensors

2.1 Introduction and Aim of the Studies

With the increasing preference for asymmetric synthesis,[1] the preparation and further separation of racemates[1] and the production of drugs and enantiopure compounds in general, synthetic chemists are continuously seeking for a rapid determination of the enantiomeric excess (*ee*) of a mixture of enantiomers.[2]

In principle the *ee* of a mixture of enantiomers can be calculated from the optical rotation of the solution, but the rotational power of the enantiopure compound is a fundamental parameter which is not always accurately determined and it is completely unknown in the case of newly prepared compounds.

In general, methods for the recognition of enantiomers are based on the interaction between the analyte and an enantiopure chiral object: e.g. other small enantiopure molecules; chiral HPLC solid phases;[3] NMR shift reagents;[3b] etc. This is due to the fact that two enantiomers possess the same chemical and physical properties; however, when interacting with the chiral object they will display different behaviours, allowing their recognition and, in some cases, their separation.

Some methods, however, are based on a different factor; that is the rate of the reaction between an enantiopure reactive compound and two enantiomers that require resolution. This causes the less reactive enantiomer to be present in excess in the solution. Kinetic resolution, as defined by the IUPAC, is the achievement of partial or complete resolution by virtue of unequal rates of reaction of the enantiomers in a racemate with a chiral agent

(reagent,catalyst, solvent, etc).[4] Within this category, the earliest examples of the separation of two enantiomers were reported[5] as well as new features such as the use of dynamic kinetic resolution, as described in a recent review.[6]

NMR spectroscopy has been used as a tool for enantiomeric recognition and determination of the enantiomeric excess (*ee*) of mixtures of enantiomers by means of shift reagents. The first example of this class of compound was Mosher's acid[7] (Figure 1) which can be readily transformed into the corresponding acyl chloride, allowing the resolution of spectra of chiral α alcohols and amines via the formation of diasteromeric esters or amides.

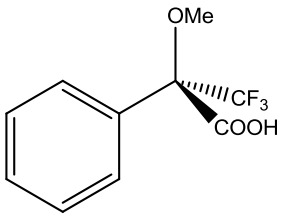

Figure 1. Mosher's acid (MTPA methoxytrifluoromethylphenylacetic acid)

Shift reagents which do not involve the formation of covalent bonds have also been developed and are mainly based on lanthanides,[8] but there are also recent examples of supramolecular shift reagents based on hydrogen bonding interactions.[8b] With these systems, the enantiomeric composition of the mixture being studied can be evaluated by inspecting the integrals of the signals corresponding to the two diasteromeric adducts, with the integral ratio corresponding to the enantiomeric composition of the mixture.

Drawbacks in the use of NMR shift reagents include the requirement of rather high concentrations of analyte in order to obtain more precise integrals, especially at high *ee* values, in addition to the need to have a good separation of the peaks.

As described below, another approach sees the use of molecular sensors, thus the introduction of a reporting unit, i.e. a photo or redox-active group, which displays a change in a physico-chemical property, the magnitude of which depends on the amount of enantiomer that is bound.

Molecular recognition is a wide branch of supramolecular chemistry and the guest sensing performed using electro-active hosts is well established and widely described in the literature.[9] However, chiral recognition performed with such sensors only amounts to a few examples.[10] By contrast, chiral receptors equipped with photo-active reporting groups are widely described and reported.[11] Moreover, among the few examples of electrochemical chiral sensing, until now none of them has reported the determination of the enantiomeric excess in the 90-100% range that is the most useful for the synthetic chemist.[12]

For example, previous work in Tucker group reported the use of Hamilton-like ferrocene receptors containing amidopyridine moieties to sense carboxylic acids,[13] barbiturates and cyclic ureas.[14] From these studies chiral ferrocene urea systems were then prepared and used to sense chiral carboxylate anions (Figure 2). However, only a moderate enantioselectivity, with a K_S/K_R = 1.66, was observed along with a maximum difference in the shift of the potentials ($\delta\Delta E_{obs}$, Chapter 1, p. 19) for the complexes formed with the two enantiomers of ca. 20 mV.[10a]

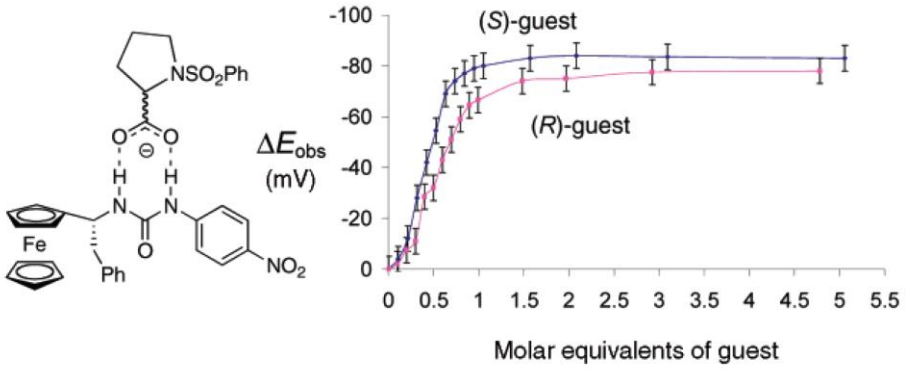

Figure 2. Chiral ferrocenyl urea systems for the electrochemical recognition of chiral carboxilates

Boronic acids and boronate esters have a great pedigree in supramolecular chemistry as binding sites for diols and anions. Ferrocene based boronic acids have been used as sensors for different chiral substrates.[10b] Given this precedent and the recent description of boronic acids based NMR-shift reagents for the determination of the enantiomeric excess of chiral diols[15] and amines,[16] (Figure 3) we decided to investigate whether chiral ferrocene boronic acids could be used as electrochemical chiral sensors for diols. The results of these studies are presented in this chapter in which we also demonstrate that enantiomeric excess can be determined using electrochemical methods in a way that competes with other more established systems in terms of concentration and sensitivity.

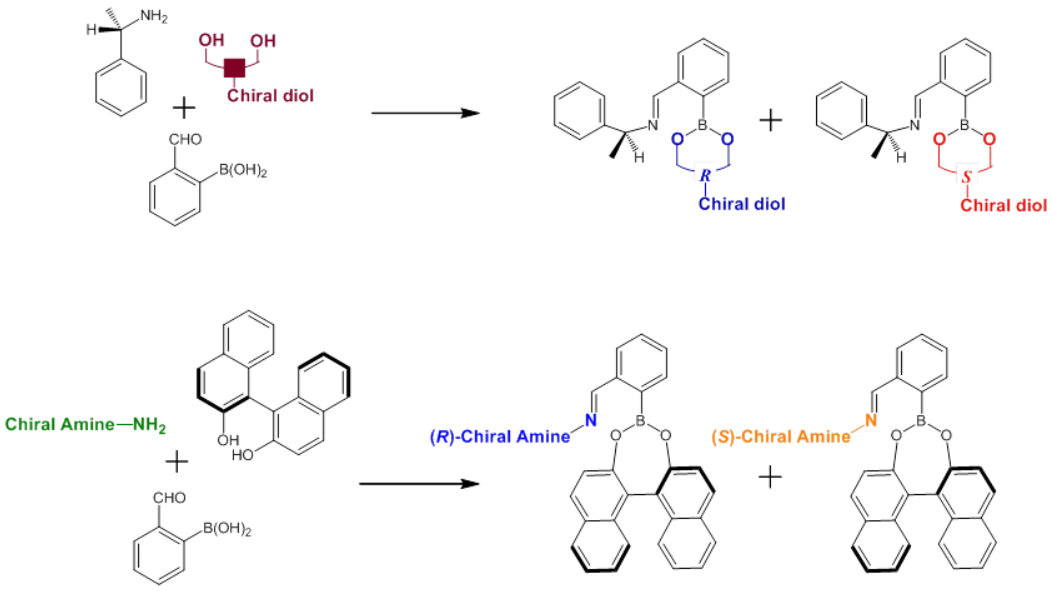

Figure 3. Pictorial representation of the NMR protocol for ee determination based on boronic acids.

The objectives of this work were firstly to assess how the electrode potential of the ferrocene unit of chiral boronic acids sensors would change upon the formation of the boronate esters of the two different enantiomers of various chiral diols (Scheme 1). Secondly we would then investigate whether there was any link between the electrode potential observed and the enantiomeric composition when a mixture of two enantiomers was sensed (Scheme 2).

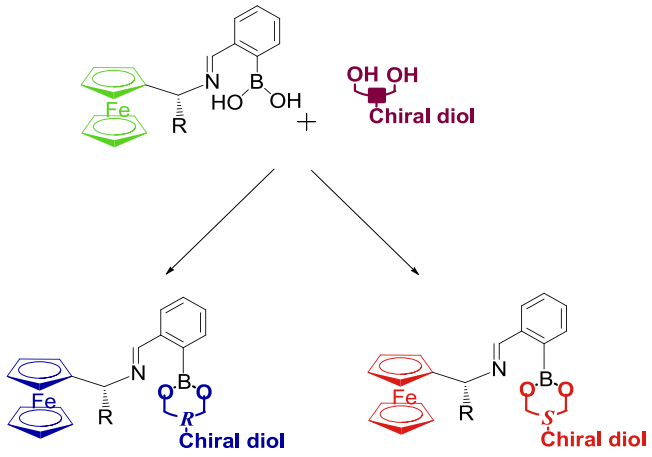

Scheme 1. Formation of diasteromeric boronate ester adducts. Different colours for the ferrocene units symbolise different electrode potentials.

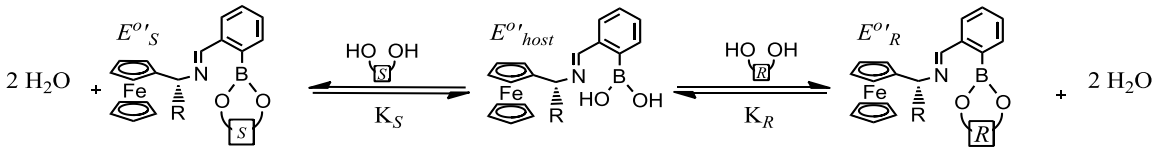

Scheme 2. Equilibria involved when a mixture of two enantiomers of guest is treated with a ferrocenyl boronic acid.

2.2 Synthesis of the Chiral boronic acid

In order to work as chiral sensors these systems needed to possess an enantiopure chiral centre and this was installed α to the ferrocenyl unit using a chiral amine precursor. The asymmetric synthesis of the chiral amine[17] is shown in Scheme 3 and was achieved using a chiral auxiliary[18] obtained via a Mizunobou reaction between N-hydroxyphthalimide and (*S*)-1-phenylbutanol. This reaction proceeded with inversion of configuration of the alcohol, with the chiral auxiliary then activated via the *in situ* formation of (*R*)-1-phenyl-butanoxyamine and reacted with ferrocenecarboxyaldehyde, yielding a chiral ferrocenyl oxime ether. This has been previously shown to undergo stereoselective nucleophilic addition by Grignard reagents.[18] Benzyl and ^{i}Pr magnesium chloride are commercially available and were used as purchased from Sigma-Aldrich, whereas the newly reported amine **(*R*)-1c** was obtained by generating methylnaphthalene magnesium chloride *in situ* using a common lab procedure for the formation of Grignards from alkyl chlorides in diethylether. The highly enantiopure amines **(*R*)-1a-c** were then obtained via a reductive cleavage of the diasteromeric N-alkoxy-amines performed with Zn and acetic acid in an ultrasound bath.

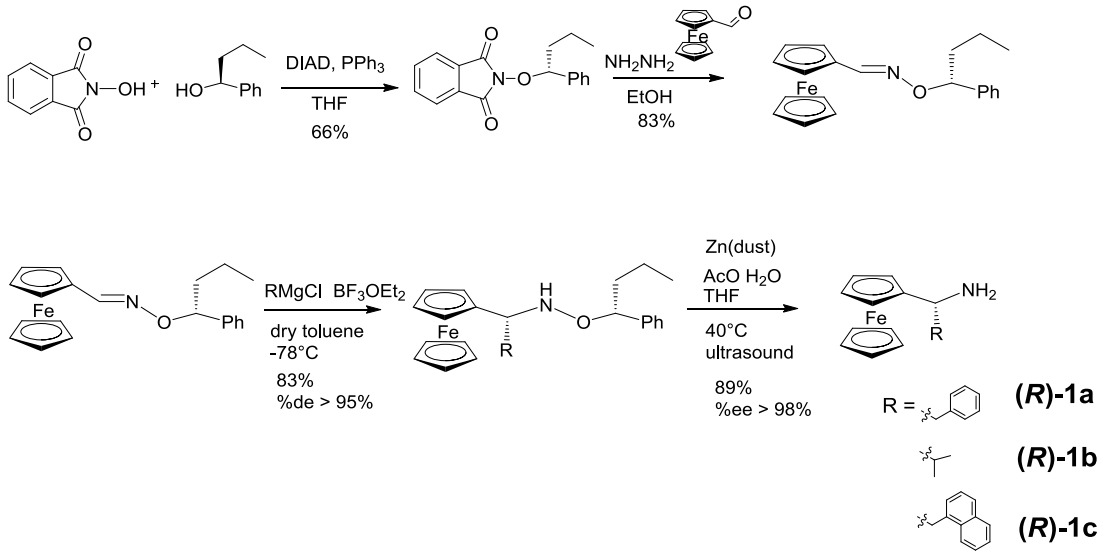

Scheme 3. Reaction scheme of the formation of chiral amines.

(*S*)-1a was obtained using the same reaction scheme using a chiral alcohol with the opposite configuration. This amine was prepared in order to assess whether an opposite configuration would give opposite enantioselection towards the binding of chiral guests. Enantiopurity of amines was assessed by HPLC.

Achiral amine **1d** was obtained by reductive amination performed with ammonium acetate and consequent reduction with sodium cyano borohydride in methanol (Scheme 4).[19]

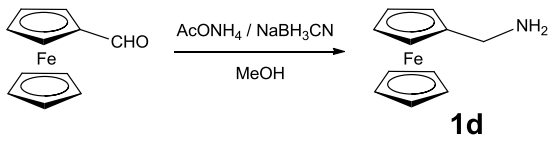

Scheme 4

Electrochemical sensors **2a-d** were then obtained adding equimolar quantities of a solution of the corresponding amine **1a-d** to 2-formyl-phenyl boronic acid (Scheme 5). This solution was then used as prepared in either $CDCl_3$ or in the electrolyte depending on the experiment and not further purified.

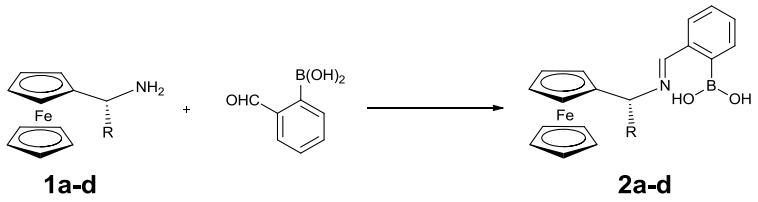

Scheme 5. Formation of the chiral boronic acid.

Chiral and achiral diols (Figure 4) were chosen as guests for their ability to form boronate esters with boronic acids. Similarly to the hosts, solutions of guests were prepared in $CDCl_3$ or electrolyte, depending on the experiment.

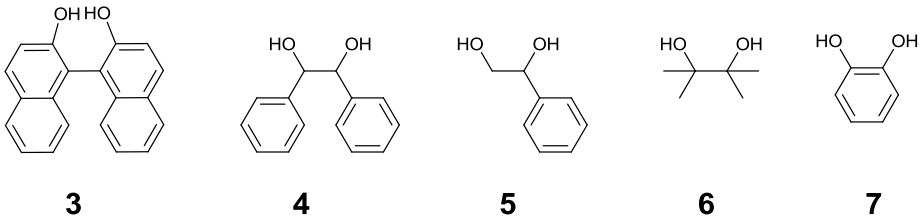

Figure 4. Chiral and achiral diols used as guests.

The boronates formed via the reaction shown in Scheme 1 are presented in Figure 5. The configuration nomenclature is indicated as the following order: chiral centre of the sensor; chiral centre(s) of the guest. For example the boronate formed by **(*R*)-2a** and hydrobenzoin **(*S,S*)-4** is **(*R,S,S*)-9a**. Moreover, despite the systems described in this chapter all being made via the formation of covalent bonds, a supramolecular notation is used to describe them. Thus boronic acids **(*R*)-2a-d** will also be called *hosts, receptors or sensors,* the diols *guests or analytes* and the boronates *adducts.* This approach is adopted not only to reinforce the supramolecular nature of the work, but also because the thermodynamic equilibria have been shown to be dramatically affected by the presence of water (this is particularly true for **(*R,R*)** and **(*R,S*)-8a-d**), leading to interactions that have a magnitude comparable to non-covalent interactions.

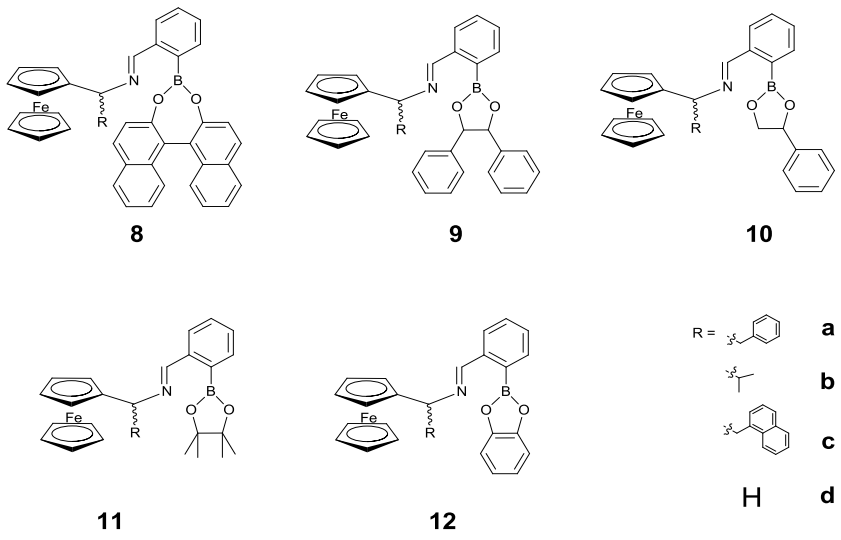

Figure 5. Boronate adducts formed with different guests.

2.2 Crystal structure‡

Among all the adducts made, only **(*R,R*)-8a** formed crystals, which were grown from a toluene solution and the structure was determined by X-Ray diffraction (Figure 6).

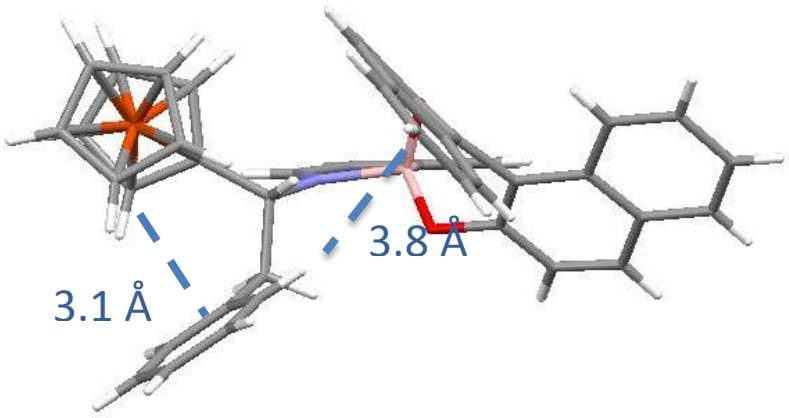

Figure 6. Crystal structure of **(*R,R*)-8a** with spatial distances between different units of the molecule.

From the structure, a spatial interaction of the benzyl group with the ferrocene unit and a naphthyl of the Binol is evident. In particular the aromatic ring on the benzyl group lies 3.8 Å from the centroid of the naphthyl unit which indicates an *edge-face* π-interaction. In solution

‡ Crystal structure resolved by Dr. P. N. Horton and Dr. L. Male

the benzyl group would be free to rotate and the interaction could become *face-face* as demonstrated by the up-field shift of the signals of the benzyl group (vide infra). π-π-stacking is a favourable interaction especially if one π system interacting is electron-rich and the other electron-deficient.[20]

In addition to the spatial interaction from the crystal structure, the sp^3 hybridisation of the boron atom is also evident (Figure 7) with the bond angles centred at this atom being less than 120° (expected for sp^2 hybridisation), consistent with a tetrahedrical geometry (Table 1). It is also worth noting that B-O bonds appear to be shorter than the C-B bond (Table 2). The coordination of the nitrogen by the boron is thought to increase the electronic communication between the boronic acid binding site and the ferrocenyl reporting unit.

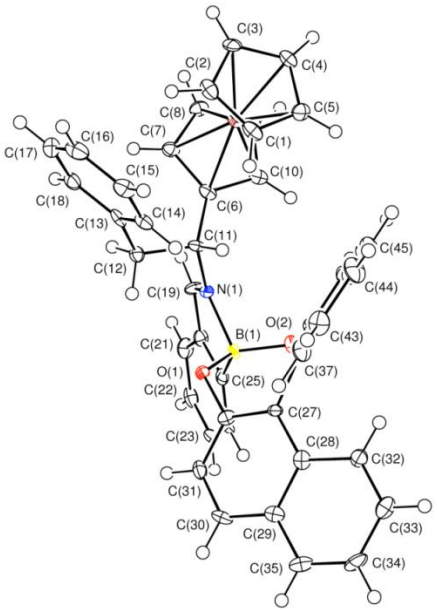

Figure 7. Crystal structure of **(*R,R*)-8a** with position of the different atoms.

Table 1. Angles (°) between bonds centred on the boron atom.

Atom 1	Atom 2	Atom 3	Angle (°)
C_{25}	B_1	N_1	96.2(4)
C_{25}	B_1	O_1	117.1(4)
C_{25}	B_1	O_2	111.5(4)
N_1	B_1	O_1	104.5(4)
N_1	B_1	O_2	109.1(4)
O_1	B_1	O_2	115.9(4)

Table 2. Bond lengths of bonds including the boron.

Bond	Length / Å
N_1-B_1	1.663(7)
C_{25}-B_1	1.623(7)
B_1-O_1	1.453(7)
B_1-O_2	1.451(6)

2.3 Electrochemistry

Electrochemical studies on amines, imines and boronate adducts were performed in order to investigate the change in the electrode potential undergone by the ferrocene unit upon the formation of host-guest complexes. As revealed in this section, the ability of **2a-d** to act as a sensor for diols is proven by the fact that upon addition of the guest, a shift of the potential is displayed.

In addition to the electronic effect of the guest, the results also show that opposite enantiomers of certain chiral guests display significant differences in electrode potential, allowing these systems to be used as chiral sensors for the recognition of enantiomers. In order to better understand what is behind electrochemical chiral sensing, we need to consider not only the difference in thermodynamics of the reduced state, but also the thermodynamic processes in the oxidised state and how they change upon the redox process as described in Chapter 1 (Scheme 7).

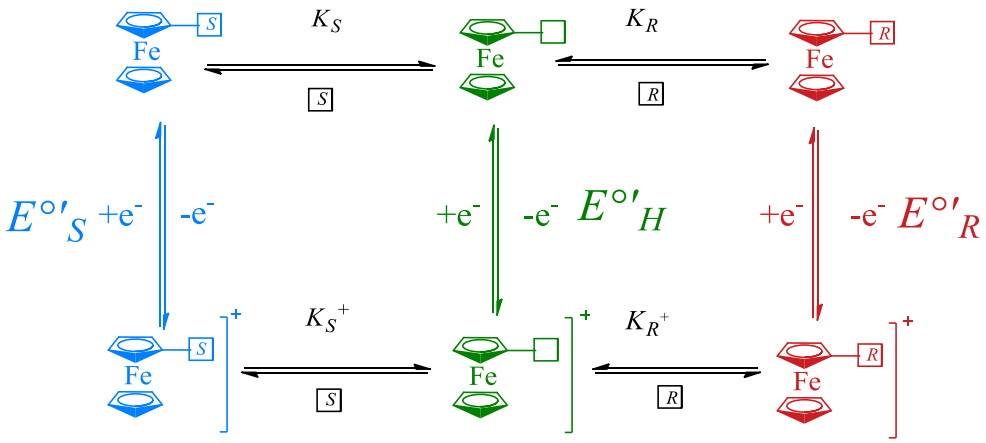

Scheme 6. Square scheme of the electrochemical chiral sensing, for ferrocene-based sensors.

The thermodynamic constants in the two redox states are linked to the change in the electrode potential upon binding by the Nernst Equations (***2.1***) and (***2.2***)

$$\Delta E_R = E_R^{\circ'} - E_H^{\circ'} = -\frac{RT}{nF}\ln\frac{K_R^+}{K_R} \qquad (\textbf{2.1})$$

$$\Delta E_S = E_S^{\circ'} - E_H^{\circ'} = -\frac{RT}{nF}\ln\frac{K_S^+}{K_S} \qquad (\textbf{2.2})$$

From Equation (***2.1***) and (***2.2***) we can say that a different shift of the potential upon the binding of the two enantiomers, $\delta\Delta E^{\circ\prime} \neq 0$ ($\delta\Delta E^{\circ\prime} = |E_R^{\circ\prime} - E_S^{\circ\prime}|$), is due to $K_R^+/K_R \neq K_S^+/K_S$; therefore the lack of enantioselectivity in one of the redox states (e.g. $K_R = K_s$) does not necessarily mean that electrochemical chiral sensing cannot be performed.

All the systems described in this chapter (i.e. amines, boronic acids and boronates) displayed electrochemically reversible behaviour, the peak currents for each of them being proportional to the scan rate (Figure 8) according to Equation (***2.3***). The electrode potential of the amines and imines studied are displayed in Table 3.

$$i_p = 269 \times 10^5 n^{3/2} A D^{1/2} C \nu^{1/2} \qquad (\textbf{2.3})$$

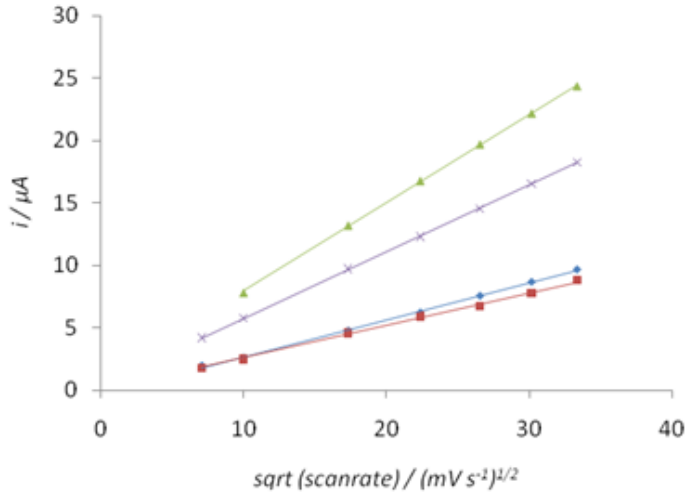

Figure 8. Peak current *vs.*scan rate plot. (R)-1a blue, (R)-2a red, (*R,R*)-8a green, (*R,S*)-8a purple

Table 3. Electrode potential of the amines **1a-d** and of the boronic acids **2a-d** calculated *vs.* dmfc in dcm TBA·PF_6 0.1 M solution. [a] determined with SWV (error ±2 mV); [b] determined with CV (error ±5 mV).

	a	**b**	**c**	**d**
(*R*)-1	533[a]	512[a]	542[a]	524[b]
(*R*)-2	565[a]	548[a]	580[a]	540[a]

The next sections describe interactions of various guests with imines 2a-d. The formation of the adduct is very sensitive to the presence of water (Scheme 6). For this reason a large excess of guest (>10 equivalents) was used each time in order to shift the equilibrium towards the formation of the adduct. Furthermore drying agents such as molecular sieves and $MgSO_4$ were used during the electrochemical experiments. No electrochemical activity of the guests in the potential window studied (-300 – 900 mV) was found.

2.3.1 Achiral guests: Pinacol and Catechol

Adducts **11a-d** and **12a-d** formed by hosts **2a-d** with neutral molecules pinacol **6** and catechol **7** show an opposite effect on the potential (Table 4). Clearly the direction of the shift, with respect to the potential of the free boronic acid, depends on the nature of the guest, with the aliphatic diol pinacol inducing a negative shift in potential, and aromatic diol catechol inducing a positive shift.

Table 4. Electrode potentials in mV *vs.* dmfc of **11a-d** (corresponding to the adducts formed by **2a-d** with pinacol, **6**) and **12a-d** (corresponding to the adducts formed by **2a-d** with catechol, **7**) determined via SWV. [a] not determined.

	(*R*)-2a	**(*R*)-2b**	**(*R*)-2c**	**2d**
6	-48	[a]	-64	-14
7	+40	[a]	+38	+108

As previously reported this effect depends on the electronic effect of the diol on the ferrocene unit.[21,22] Despite the long distance between the ferrocene and the binding site (six covalent bonds between the ferrocene and the boron atom), the redox unit is in communication with the binding site by the 'shortcut' provided by the dative bond between the nitrogen and the boron (Scheme 7) as suggested by the X-Ray structure of the analogous Binol adduct (Figure 6). Boronate esters formed with different guests possess differences in the acidity; boronate esters of aromatic diols are more acidic than boronates formed by aliphatic diols. The difference in acidity affects the strength of the dative bond and therefore the potential of the ferrocene unit. The increase in the polarisation of the dative bond due to the binding of aromatic guests causes the electron density around the redox-active unit, which means that a higher potential is needed in order to oxidise it. In contrast, the electron-donating effect of aliphatic diols, makes the boron a weaker Lewis acid, in this case the dative bond is less polarised causing an increase in the electron cloud of the ferrocene unit, which is translated in a lower potential needed for the oxidation.

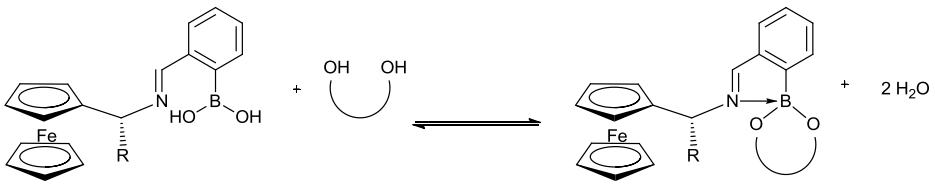

Scheme 7. Formation of the adducts

The cyclic and square wave voltammograms of adducts **11d** and **12d** formed from the achiral boronic acid are displayed in Figure 9.

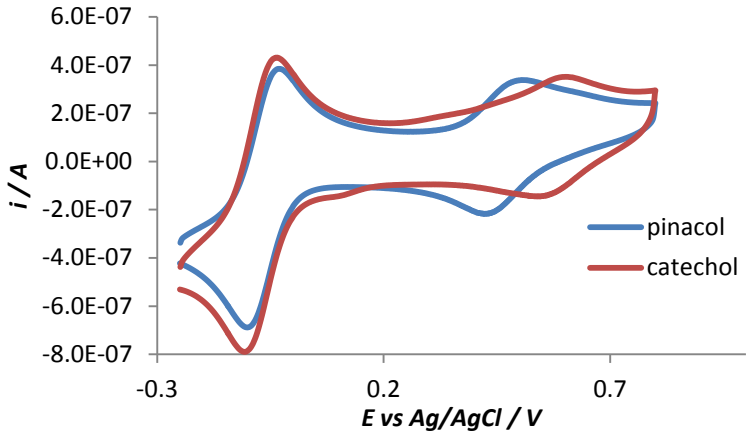

Figure 9. Cyclic voltammograms of **11d** (blue) and **12d** (red) recorded at 100 mV/s. Solvent dcm, TBA PF_6 0.1 M as supporting electrolyte and decamethyl ferrocene as internal reference

2.3.2 Binol

Binol **3**, is a bulky aromatic diol which gives a classic example of axial chirality. The chirality arises from the steric hindrance between the two naphthyl units which results in rotation about the bond between the two naphthyl units being blocked at room temperature. For this reason the absolute configuration is not comparable to those of other guests that all possess one or two chiral stereogenic centres. This means that the effect of **(*R*)-3** on the hosts should not be compared to the effect of other guests with the same absolute configuration (for example **(*R*)-5**).

Adducts **8a-d** formed by **(*R*)-2a-d** with **3** always show a positive shift in potential, in agreement with previous results with the achiral catechol (Section 0). Figure 10 depicts the CVs for the binding of **3** by the achiral sensor **2d** to form adducts **(*R*)-8d** and **(*S*)-8d**, and as expected, no chiral sensing is displayed by this host, i.e. $\delta\Delta E^{\circ\prime}$= 3 mV (Table 5) ($\delta\Delta E^{\circ\prime}$ corresponds to the difference in the potential of the adducts formed by two different enantiomers with the same sensor, Chapter 1). The value is within the experimental error (±5 mV for CV and ±2 mV for SWV). However, Figure 11 shows that when a chiral centre is

added to the host (in this case **(*R*)-2a**), the two enantiomers of **3** cause different shifts in potential. Electrochemical data for the adducts **8a-d** formed by the hosts with **3** are summarised in Table 5, and from these data the ability to discriminate between the two enantiomers of **3** is evident. $\delta\Delta E^{\circ\prime}$ is proven to be high for these systems, with a maximum of 51 mV between the potentials for **(*R,R*)-8a** and **(*R,S*)-8a.** In fact all three chiral receptors showing good enantio-discrimination that compares favourably with literature data.[10a]

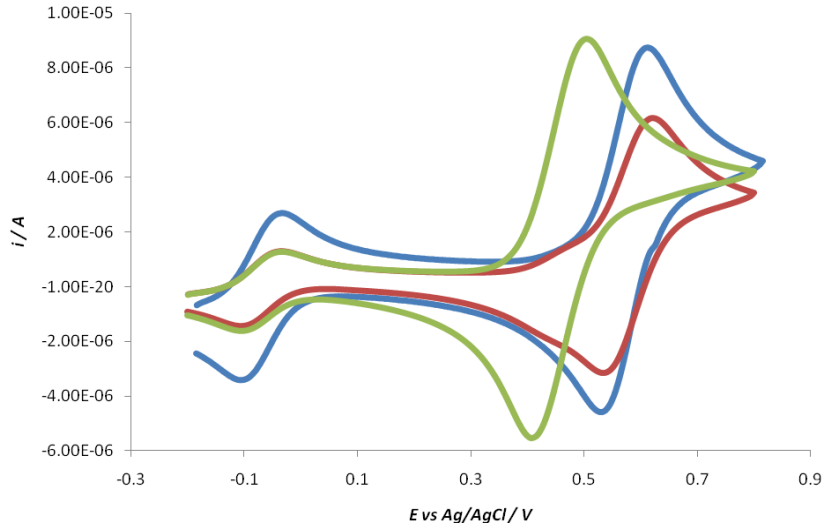

Figure 10. Cyclic voltammograms of **1d** (green); **(*R*)-8d** (red) and **(*S*)-8d** (blue). Solvent dcm, TBA PF_6 0.1 M as supporting electrolyte and decamethyl ferrocene as internal reference

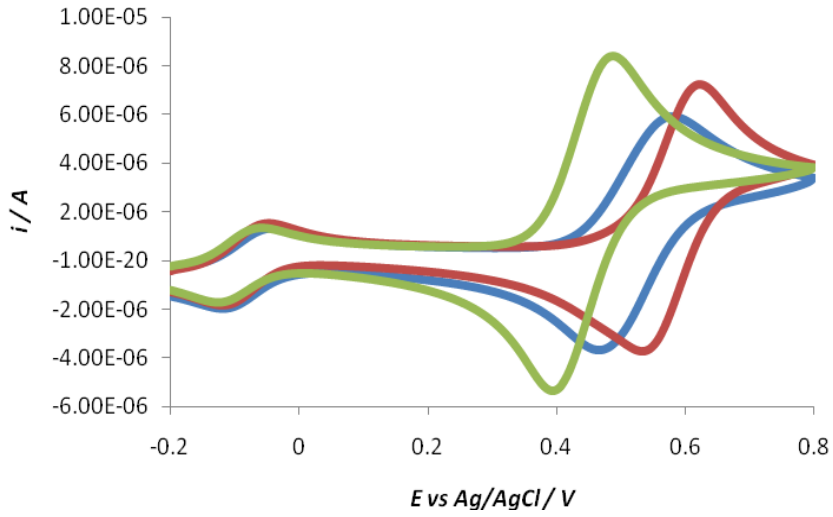

Figure 11. Cyclic voltammograms of **(R)-2a** (green); **(*R,R*)-1d** (red) and **(*R,S)*-1d** (blue). Solvent dcm, TBA PF_6 0.1 M as supporting electrolyte and decamethyl ferrocene as internal reference

Table 5. ΔE°′ in mV *vs.* dmfc of **(*R,R*)8a-d** (corresponding to the adducts formed by **2a-d** with **(*R*)-3**) and **(*R,S*)8a-d** (corresponding to the adducts formed by **2a-d** with **(*S*)-3**). [a] determined by SWV; [b] determined by CV

	(*R*)-2a	**(*R*)-2b**	**(*R*)-2c**	**2d**
(*R*)-3	+100[a]	+86[a]	+81[a]	+105[b]
(*S*)-3	+49[a]	+49[a]	+41[a]	+102[b]
δΔE°′	51	37	40	3

In titrating receptors **(*R*)-2a-c** with Binol **(*R*)-3** and **(*S*)-3** respectively, the square wave voltammograms appear very different for the two enantiomers of the guest. **(*R*)-3**, in fact, causes a new wave to rise at the potential of the adduct while the wave corresponding the free host decreases (Figures 12, 14 and 16). This effect is better known as *two-wave* behaviour.[9a] However, the opposite enantiomer of **(S)-3**, shows *one-wave* behaviour (Figures

13, 15 and 17), which means that, upon the addition of aliquots of guest, the wave shifts without the clear formation of a new one.

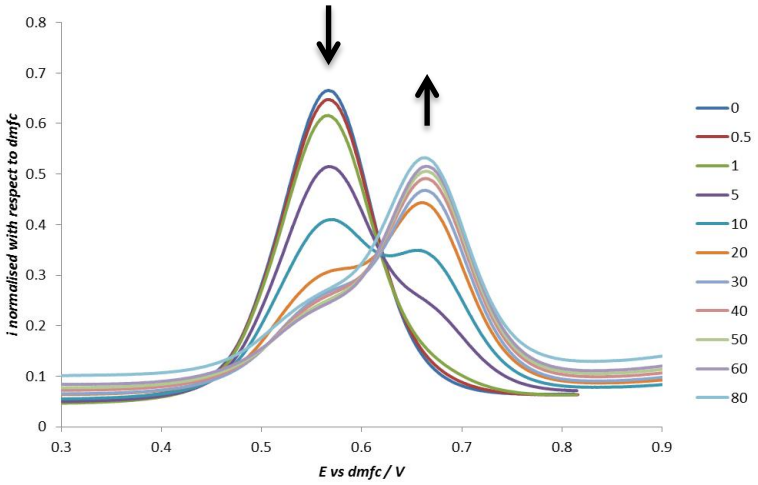

Figure 12. Square wave voltammetric titration of **(*R*)-2a** with **(*R*)-3.** In the legend values of molar equivalents of guest added. Solvent dcm, TBA PF_6 0.1 M as supporting electrolyte and decamethyl ferrocene as internal reference. Guest added from a similar solution without internal reference. The current was normalised with respect to dmfc in order to overcome dilution effects.

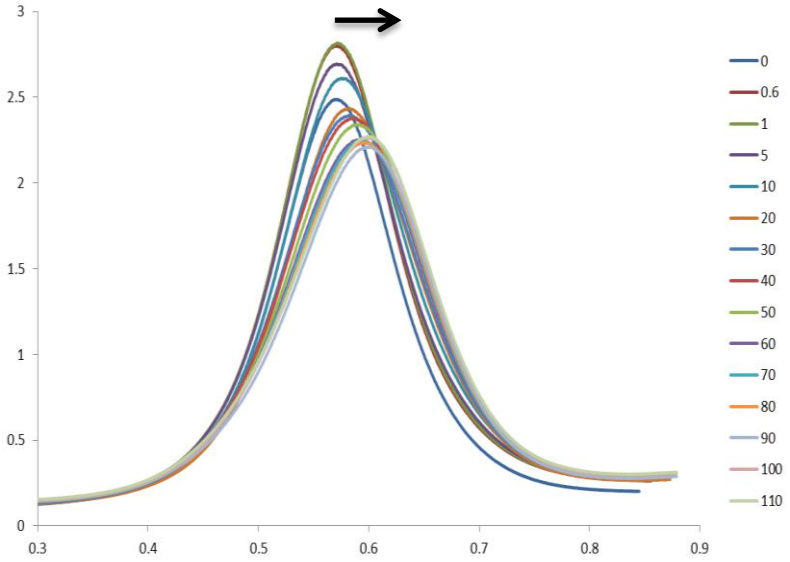

Figure 13. Square wave voltammetric titration of **(*R*)-2a** with **(*S*)-3.** In the legend values of molar equivalents of guest added. Solvent dcm, TBA PF_6 0.1 M as supporting electrolyte and decamethyl ferrocene as internal reference. Guest added from a similar solution without internal reference. The current was normalised with respect to dmfc in order to overcome dilution effects.

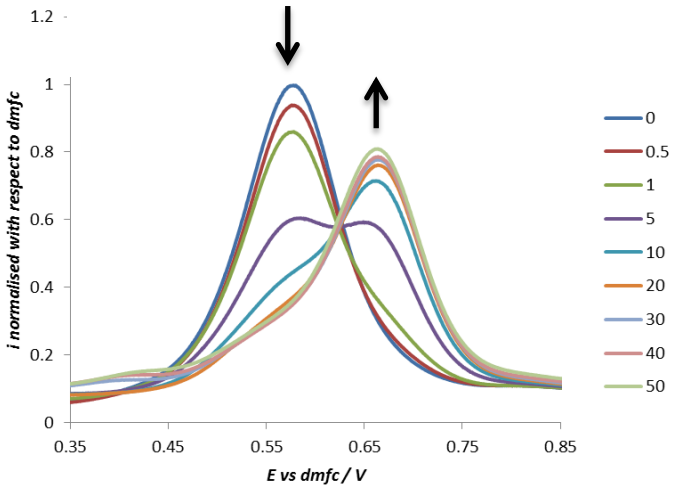

Figure 14. Square wave voltammetric titration of **(*R*)-2c** with **(*R*)-3.** In the legend values of molar equivalents of guest added. Solvent dcm, TBA PF_6 0.1 M as supporting electrolyte and decamethyl ferrocene as internal reference. Guest added from a similar solution without internal reference. The current was normalised with respect to dmfc in order to overcome dilution effects.

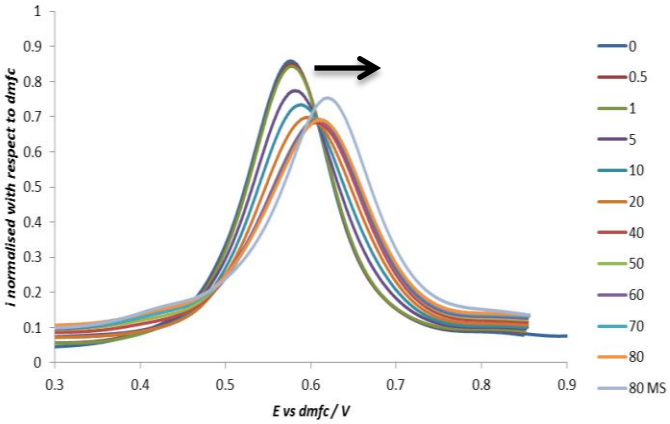

Figure 15. Square wave voltammetric titration of **(*R*)-2c** with **(*S*)-3.** In the legend values of molar equivalents of guest added. 80MS corresponds to the addition of molecular sieves to the solution of 80 eq. of guest. Solvent dcm, TBA PF_6 0.1 M as supporting electrolyte and decamethyl ferrocene as internal reference. Guest added from a similar solution without internal reference. The current was normalised with respect to dmfc in order to overcome dilution effects.

The receptor containing a naphthyl unit **(*R*)-2c** has similar binding constants for the equilibria with ***R*** and ***S*-3** compared to **(*R*)-2a**, considering the similarity in the equivalents of guest needed to be added in order to have a full shift (Figures 12-15). However, even after the addition of more than 120 equivalents of **(R)-3, (*R*)-2b** still showed incomplete formation of the adduct. The constants appear to be even smaller when **(*S*)-3** is titrated (Figure 17).

Generally for all the adducts with Binol, a large excess of guest is needed to obtain the full shifts in potential recorded in Table 5, due to the low equilibrium constants.

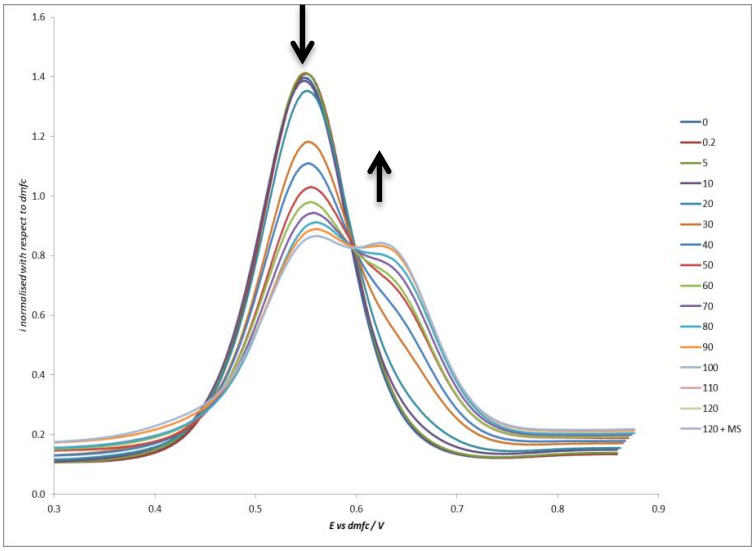

Figure 16. Square wave voltammetric titration of **(*R*)-2b** with **(*R*)-3.** In the legend values of molar equivalents of guest added 80MS corresponds to the addition of molecular sieves to the solution of 80 eq. of guest. Solvent dcm, TBA PF_6 0.1 M as supporting electrolyte and decamethyl ferrocene as internal reference. Guest added from a similar solution without internal reference. The current was normalised with respect to dmfc in order to overcome dilution effects.

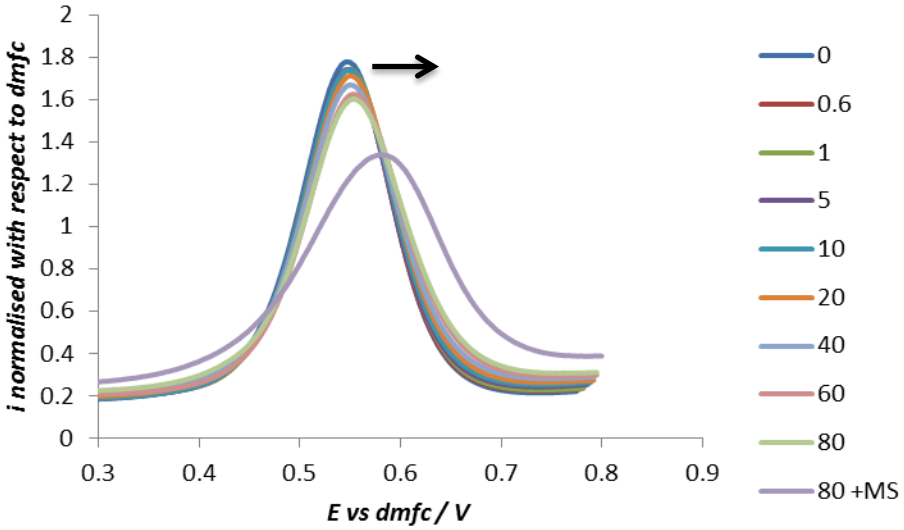

Figure 17. Square wave voltammetric titration of **(*R*)-2b** with **(*S*)-3.** In the legend values of molar equivalents of guest added. Solvent dcm, TBA PF_6 0.1 M as supporting electrolyte and decamethyl ferrocene as internal reference. Guest added from a similar solution without internal reference. The current was normalised with respect to dmfc in order to overcome dilution effects.

Two-wave behaviour is usually associated with a strong binding constant ($K > 10^4$ M^{-1}) for the initial complex (which could be either the reduced or the oxidised state).[23] In this case, however, the adducts formed with Binol **3** are those that possess the lowest constants when compared with the boronates formed with the other guests. As evidenced by the number of equivalents of guest necessary to generate a full shift of the wave. Titrations of the hosts **(*R*)-2a-c** with aliphatic guests **4** and **5** show a full shift of the potential after the addition of less than 10 equivalents (vide infra). In contrast, when these hosts are titrated with either enantiomer of **3**, a full shift is displayed only for a large excess and only if molecular sieves 3Å are added to the electrochemical cell. The addition of molecular sieves contributes to the full complexation for two reasons; firstly because they subtract water, which shifts the equilibrium towards the product; secondly because of a small amount of adsorbtion of the free hosts onto the molecular sieves, which changes the stoichiometry of the processes by increasing the number of equivalents of guest. In either case, the effect is always the shift of the equilibrium towards the products.

2.3.3 Hydrobenzoin

Hydrobenzoin, **4** Figure 4, is a vicinal diol with two chiral centres. It possesses three stereoisomers, the pair of enantiomers (*R,R*) and (*S,S*) and a *meso* form. It is an aliphatic diol but it also possesses two phenyl groups which were expected to sterically interact with the chiral group of the host, thereby enhancing the enantioselectivity.

Square wave voltammetry titrations of all the hosts with **(*R,R*)-4** and **(*S,S*)-4** revealed *one-wave* behaviour in all cases. This allowed a correlation of the potential of the wave with the equivalent of guest added. **(*R*)-2a** displayed a very peculiar behaviour towards the binding of hydrobenzoin in that, the addition of **(*S,S*)-4** caused a +10 mV positive shift, which

was unexpected considering the aliphatic nature of the diol. By contrast, the addition of **(*R,R*)-4** caused the expected negative shift of ca. -13 mV (Figure 18).

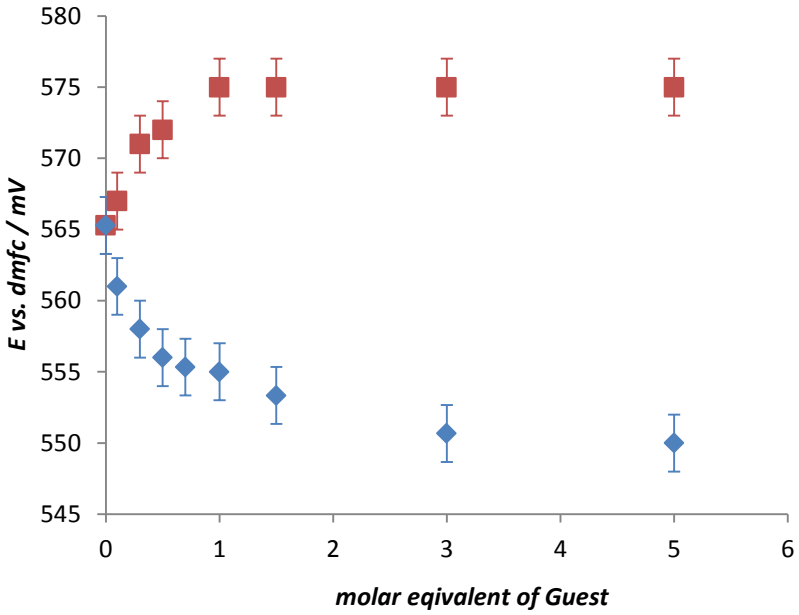

Figure 18. Plot of the potential of the wave vs. the amount of guest added when **(*R*)-2a** was titrated with **(*R,R*)-4** (blue diamonds) and **(*S,S*)-4** (red squares). The error considered is ± 2 mV.

(*meso*)-4 induced a maximum shift in the potential that falls in between the potentials of the two other enantiomers (-4mV, Table 6). This might depend on the formation of two different diasteromers, The observed potential is therefore an average of the two electrode potentials of the adducts.

Table 6. ΔE°' mV *vs.* dmfc of **(*R,R,R*)-9a-d** (corresponding to the adducts formed by **2a-d** with **(*R,R*)-4**), **(*R,R,*S)-9a-d** (corresponding to the adducts formed by **2a-d** with **(*meso*)-4** and **(*R,S,*S)-9a-d** (corresponding to the adducts formed by **2a-d** with **(*S,S*)-4**)

	(*R*)-2a	**(*R*)-2b**	**(*R*)-2c**	**2d**
(*R,R*)-4	-13	-43	-42	+4
(*S,S*)-4	+10	-13	-15	+8
δΔE°'	23	30	27	4
(*meso*)-4	-4	-37	-25	+6

Both **(*R*)-2b** and **(*R*)-2c** underwent negative shifts in potential upon binding of enantiomers of guest **4** (Figures 19 and 20). However, the two hosts were still able to discriminate the two enantiomers of hydrobenzoin, since the potential shifts were different for the two diasteromeric adducts formed **(*R,R,R*)-9b-c** and **(*R,S,S*)-9b-c**. **(*R*)-2b** is the host that displayed the greatest $\delta\Delta E^{\circ\prime}$ (30 mV). However, the other hosts possess similar enantio-discrimination power for this guest. All the electrochemical data for the adducts formed with hydrobenzoin, **4,** are summarised in Table 6.

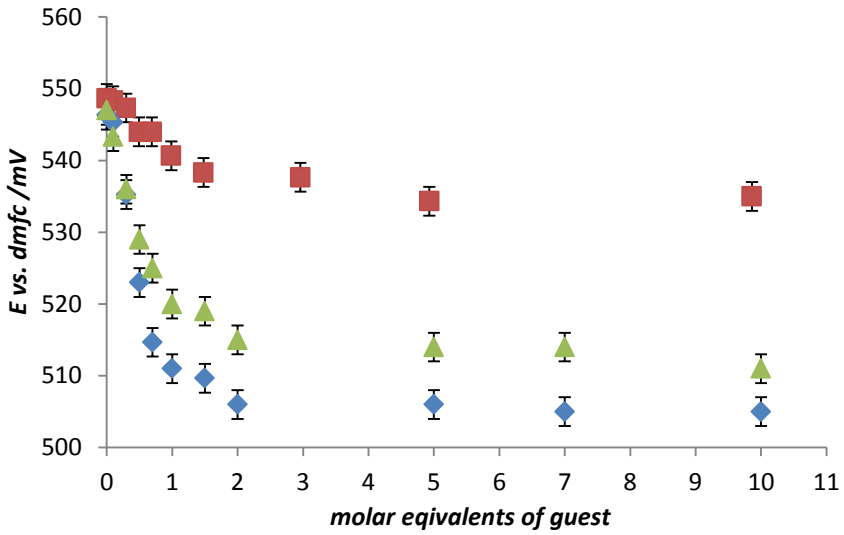

Figure 19. Plot of the observed potential of the wave vs. the amount of guest added when **(*R*)-2b** was titrated with **(*R,R*)-4** (blue diamonds), **(*S,S*)-4** (red squares) and **(*meso*)-4** (green triangles). The error considered is ± 2 mV.

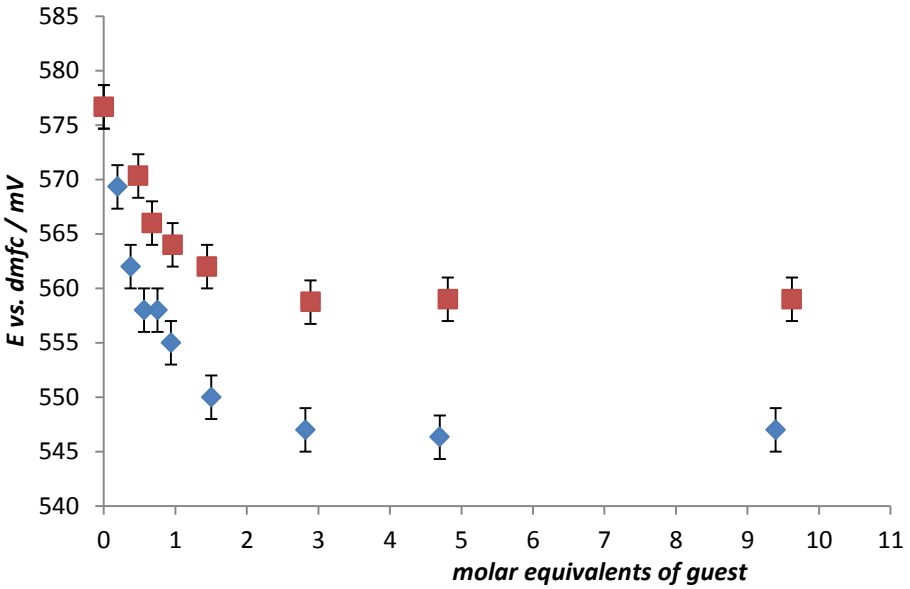

Figure 20. Plot of the observed potential of the wave vs. the amount of guest added when **(*R*)-2c** was titrated with **(*R,R*)-4** (blue diamonds) and **(*S,S*)-4** (red squares). The error considered is ± 2 mV.

2.3.4 1-phenyl-1,2-ethanediol

1-phenyl-ethane-1,2-diol, **5**, is a vicinal aliphatic diol that only has one chiral centre and a bulky phenyl group which may interact with the R group of the host. With this guest the three hosts all displayed a negative shift with comparable and moderate electrochemical chiral discrimination, the maximum difference in the potential for the two diasteromeric adducts being 10 mV, obtained with **(*R*)-2a** and **(*R*)-2b** (Table 7). The low chiral sensing ability compared to the other guests studied was expected considering the structure of the guest. In fact, to avoid steric hindrance this can bind with the bulky phenyl group far away from the R group on the host, decreasing the interaction likely to be responsible for the chiral sensing. Figures 21, 22 and 23 show the plots of observed potential against molar equivalents of guest for the two enantiomers of **5**. Table 7 summarises the electrochemical data for the adducts **10a-d**.

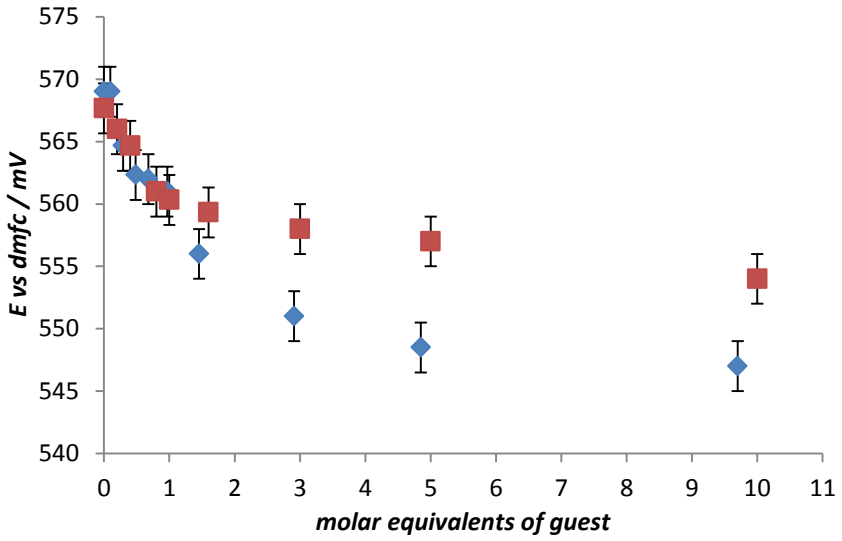

Figure 21. Plot of the observed potential of the wave vs. the amount of guest added when **(*R*)-2a** was titrated with **(*R*)-5** (blue diamonds) and **(*S*)-5** (red squares). The error considered is ± 2 mV.

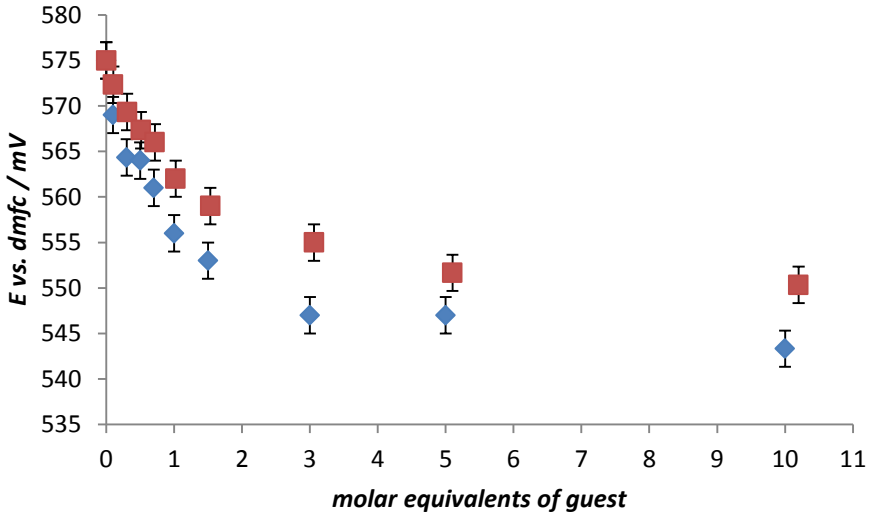

Figure 22. Plot of the observed potential of the wave vs. the amount of guest added when **(*R*)-2c** was titrated with **(*R*)-5** (blue diamonds) and **(*S*)-5** (red squares). The error considered is ± 2 mV.

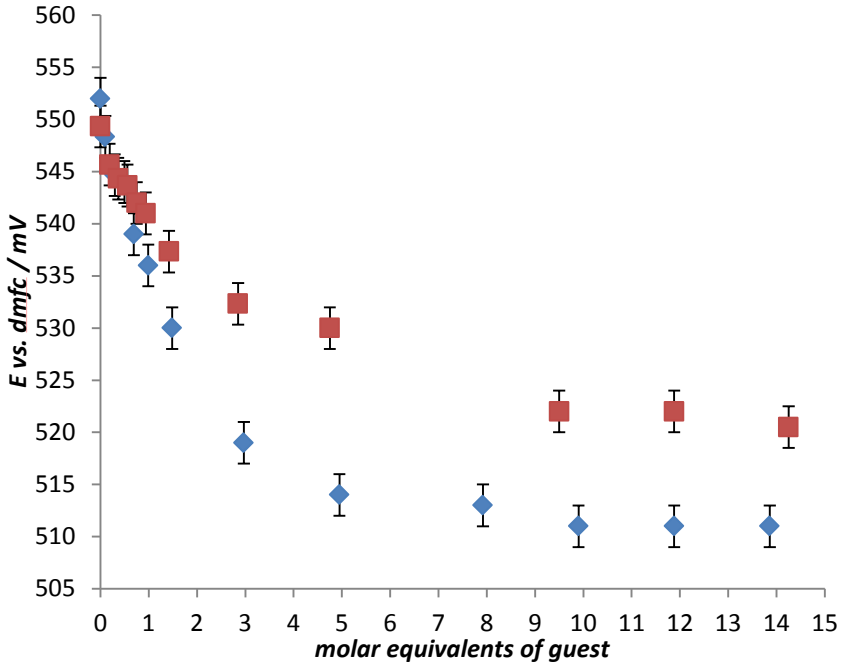

Figure 23. Plot of the observed potential of the wave vs. the amount of guest added when **(*R*)-2b** was titrated with **(*R*)-5** (blue diamonds) and **(*S*)-5** (red squares). The error considered is ± 2 mV.

Table 7. Electrode potentials in mV *vs.* dmfc of **(*R*,*R*)-10a-d** (corresponding to the adducts formed by **2a-d** with **(*R*)-5**) and **(*R*,S)-10a-d** (corresponding to the adducts formed by **2a-d** with **(*S*)-5**)

	(*R*)-2a	**(*R*)2b**	**(*R*)-2c**	**2d**
***(R)*-5**	-19	-37	-40	-4
***(S)*-5**	-9	-27	-31	-1
δΔE°'	10	10	9	3

2.4 NMR binding studies

The formation of the host-guest adducts could also be monitored via ^{1}H-NMR spectroscopy. However, the fact that full complexation was difficult to achieve without the addition of a large excess of guest along with the additional problem of water affecting the equilibrium, led to poor spectra in general. For example, in many spectra the signals of the free host and sometimes even those of the chiral amines are displayed together with the boronate adducts.

The formation of the boronate adducts could be assessed by following the change in the chemical shift of certain diagnostic peaks, i.e. free Cp ring and imine proton. In these equilibria the adducts are formed via formation of new covalent bonds, which means that the diagnostic peaks do not change their chemical shift gradually, as would happen in an H-bonded host/guest system. In other words, slow exchange on the NMR timescale is observed with the peak appearing at the final chemical shift and its integral changing upon the addition of guest.

Unfortunately, as already reported for other boron and iron containing systems,[24] the combined presence of a Fe and a B nucleus leads to a quadrupole relaxation which does not allow the ^{13}C spectra to be recorded (see the Appendix for examples of ^{13}C-NMR spectra of the systems described in this chapter). However, this effect would regard in principle only the carbon bound to the boron, the effect on the whole spectrum could therefore be addressed also to a partial oxidation of the substrate, the Fe^{3+} ion is paramagnetic and would greatly affect the relaxation of all the nuclei. For these reasons a complete assignment of all the peaks was impossible. Nevertheless, NMR remains a powerful tool to assess the enantioselectivity of the systems under study.

2.4.1 Effects on imine and Cp signals

Boronate ester adducts formed between **(*R*)-2a** and Binol show a large difference in the chemical shifts for the free Cp ring in both the free host and in the (*R*) and (*S*) adducts. The peaks shifted *upfield* for both the enantiomers but with a different magnitude (Table 8). Similar effects were observed for the boronates formed by the two enantiomers of **3** with methyl naphthyl receptor **(*R*)-2c** (Table 9). These observations are probably due to a shielding effect arising from the close proximity of the free Cp ring to the aromatic R group and one of the naphthyl units of Binol. In fact, for the ^{i}Pr receptor **(*R*)-2b,** the formation of the boronates caused a downfield shift of the free Cp ring signal upon the binding of **3, 4** and **5** (Table 10), and in the case of **(*R,R*)** and **(*R,S*)-8c** (adduct formed by the naphthyl host with Binol, **3**), the upfield shift of the Cp signals was greater than the correspondent adducts formed with the benzyl system, **(*R,R*)** and **(*R,S*)-8a.** This can be explained by a larger shielding effect by the more extended aromatic naphthyl unit compared to the phenyl ring of the benzyl group.

Table 8. Chemical shift of the free Cp ring and imine protons and the electrode potential *vs.* dmfc for all the adducts formed by **(*R*)-2a** with the chiral guests **3, 4** and **5.**

	(*R*)-2a	**(*R,R*)-8a**	**(*R,S*)-8a**	**(*R,R,R*)-9a**	**(*R,S,S*)-9a**	**(*R,meso*)-9a**	**(*R*)-10a**	**(*S*)-10a**
Cp / δ	4.11	3.60	3.75	3.99	3.99	4.13	4.05	4.03
Imine / δ	7.87	7.94	8.17	8.21	7.98	7.94	7.96	7.87
***E°'* / mV**	565	665	614	552	575	561	546	552

Table 9. Chemical shift of the free Cp ring and imine protons and the electrode potential for all the adducts formed by **(*R*)-2c** with the chiral guests **3, 4** and **5.** [a] not determined

	(*R*)-2c	**(*R,R*)-8c**	**(*R,S*)-8c**	**(*R,R,R*)-9c**	**(*R,S,S*)-9c**	**(*R,meso*)-9c**	**(*R*)-10c**	**(*S*)-10c**
Cp / δ	4.11	3.37	3.61	3.99	3.99	4.09	4.01	4.06
Imine / δ	7.62	8.27	8.34	8.39	8.12	[a]	8.04	7.91
***E°'* / mV**	580	661	621	538	565	555	540	549

Hydrobenzoin also shows a different behaviour when bound to **(*R*)-2a** or **(*R*)-2c**. However, despite there being a difference in the ferrocene-unit electrode potentials for the adducts formed between these hosts and each enantiomer, the free Cp ring does not show any difference in the chemical shift (δ 3.99 for each adduct, Tables 8 and 9).

However, adducts formed by (*R,R*) and (*S,S*) hydrobenzoin with **(*R*)-2b** do show a difference in these signals both when compared with the host and between themselves. On the other hand the imine protons always show a different chemical shift for all the hosts and their adducts with all the guests (Table 10).

Table 10. Chemical shift of the free Cp ring and imine protons and the electrode potential for all the adducts formed by **(*R*)-2b** with the chiral guests **3, 4** and **5.** [a] not determined

	(*R*)-2b	**(*R,R*)-8b**	**(*R,S*)-8b**	**(*R,R,R*)-9b**	**(*R,S,S*)-9b**	**(*R,meso*)-9b**	**(*R*)-10b**	**(*S*)-10b**
Cp / δ	3.99	4.21	4.04	4.04	4.18	[a]	4.05	4.08
Imine / δ	8.43	8.43	8.73	8.74	8.59	[a]	8.62	8.62
***E°'* / mV**	548	634	597	505	536	511	505	511

2.4.1.1 Chemical shift of free Cp rings and imine protons *vs.* electrode potentials

The effect on the free Cp ring of the ferrocene unit is usually a good indication of the binding event and it is generally caused by a through-space interaction between the R groups and the ferrocene unit. However, observing such a change does not necessarily mean that a change in the electrode potential is observed. In particular when considering hosts with an aromatic R side group the upfield shift of the Cp signals is caused by a shielding effect generated by a local magnetic field engendered by an induced ring current of the π electrons of the aromatic group experiencing the main magnetic field of the NMR instrument B_0. Thus this effect is merely magnetic and does not involve any exchange of electrons. However, all the systems under study show a rather large difference in the electrode potential for adducts formed with the two enantiomers of the guests that, from an electronic point of view, should affect the system in the same way.

Figure 24 Figure 25 show that there is no strong correlation between the chemical shifts of the Cp rings or of the imine protons and the electrode potential of the respective adduct.

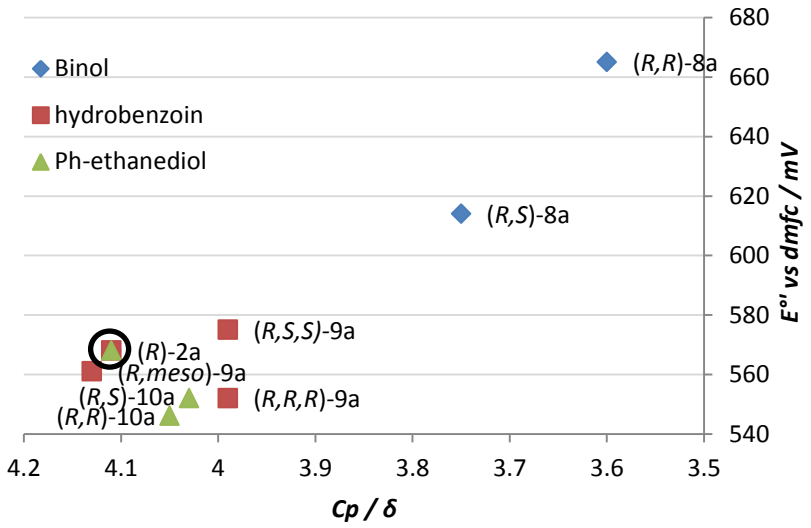

Figure 24. Plot of the chemical shift of the Cp ring *vs.* the potential of each adduct formed by **(*R*)-2a**

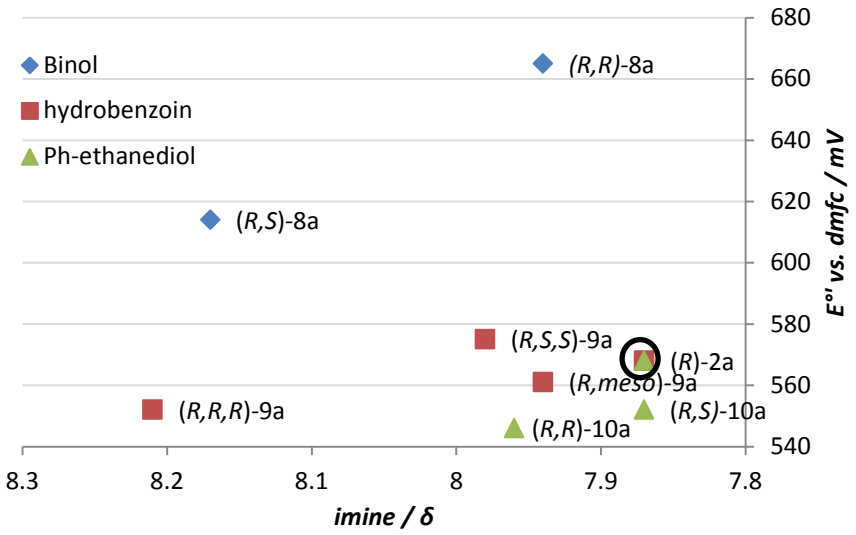

Figure 25. Plot of the chemical shift of imine protons *vs.* the potential of each adduct formed by **(*R*)-2a**

The only significant observation is that Binol **3** gives the most upfield Cp chemical shifts and the most positive electrode potential (Figure 24). In contrast, the **(*R,R,R*)-9a** and **(*R,S,S*)-9a** adducts possess the same chemical shift for the signals of their Cp rings, even though they display an electrode potential difference of 23 mV, in addition to opposite shifts in potential compared to the free host **(*R*)-2a**.

From Figure 26 it is evident that for adducts formed with **(*R*)-2b** a downfield shift of the Cp ring signals compared to the free host (in the black circle) is not linked to a particular direction of the shift in potential.

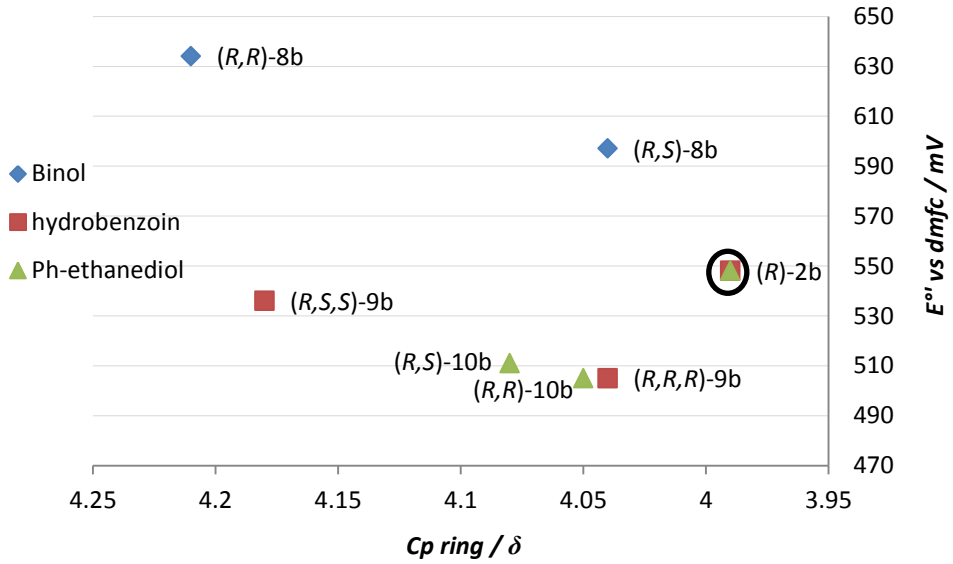

Figure 26. Plot of the chemical shift of free Cp ring protons *vs.* the potential of each adduct formed by **(*R*)-2b**

In particular **(*R,S*)-8b** and **(*R,R,R*)-9b** display a difference in the potential of 92 mV, with a positive shift with respect to the free host for the first one and a negative shift for the latter; however, the Cp rings of these two adducts possess exactly the same chemical shift (δ 4.04). For this reason we can state that there is no absolute dependence between the potential and the chemical shifts of the free Cp ring for substituted ferrocenes, since the two adducts compared above belong to different series and are made from different diols.

To summarise, the interaction of the guests with the side groups R and their interaction with the redox unit are fundamental for ensuring chiral recognition through electrochemistry. It is clear that changes to the chemical shift of the Cp rings by ^{1}H-NMR are linked to the chiral sensing process, and this is the basis of the enantiomeric recognition made via NMR shift reagents. However, the direction and the magnitude of the Cp rings shift are not directly linked to the changes in the electrode potential.

2.4.2 Effects on R groups

The position and the multiplicity of the signals of the R groups can give information about the binding event. For example the signals of the benzyl group of **(*R*)-2a** are different for adducts formed with the two enantiomers of **3**; **(*R*)-3** causes a significant upfield shift in the benzyl proton signals which is not displayed in the boronate formed with the (*S*) enantiomer (Figure 27). As previously discussed in section 2.2, the π-π interaction between the aromatic ring of the benzyl group and the naphthyl unit of the guest is believed to increase the stability of **(*R,R*)-8a** compared to **(*R,S*)-8a**, where for steric reasons the stacking is not possible. On the other hand the 3.1 Å distance between the same benzyl unit and the ferrocene, measured from the X-ray structure, is believed to be the cause of the upfield shift of the Cp ring signal. Moreover, this rather small distance leads to the potential being affected by the benzyl group.

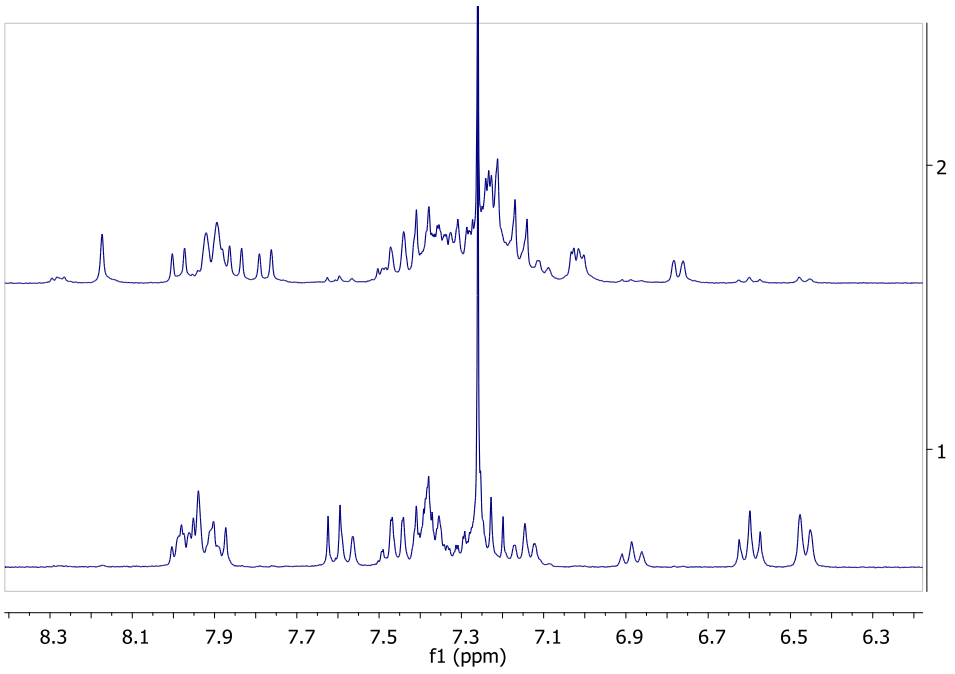

Figure 27. Aromatic region of NMR spectra of **(*R,R*)-8a** (host : guest 1:1) (spectrum 1) and **(*R,S*)-8a** (host : guest 1:1) (spectrum 2). Benzyl protons resonate at 6.91, 6.63 and 6.49 ppm (spectrum 1)

This effect is less pronounced in the adducts formed with hydrobenzoin, since the signals resonate in the aromatic region and are not so evident. However, it is possible to identify some differences in this area upon the binding of the two different enantiomers. In fact **(*R,R,R*)-9a** shows peaks in the region δ7.0-7.2 (Figure 28), and this multiplet is shifted downfield in **(*R,S,S*)-9a** (Figure 29). In each case, differences compared to the free imine are shown by both adducts.

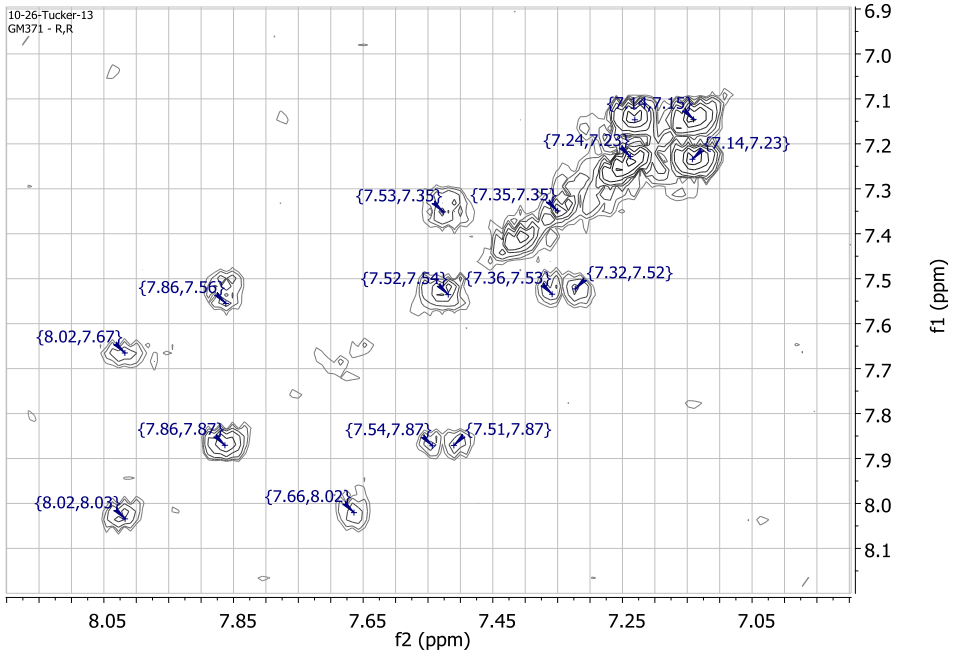

Figure 28. (^{1}H-^{1}H) COSY of **(*R,R,R*)-9a**

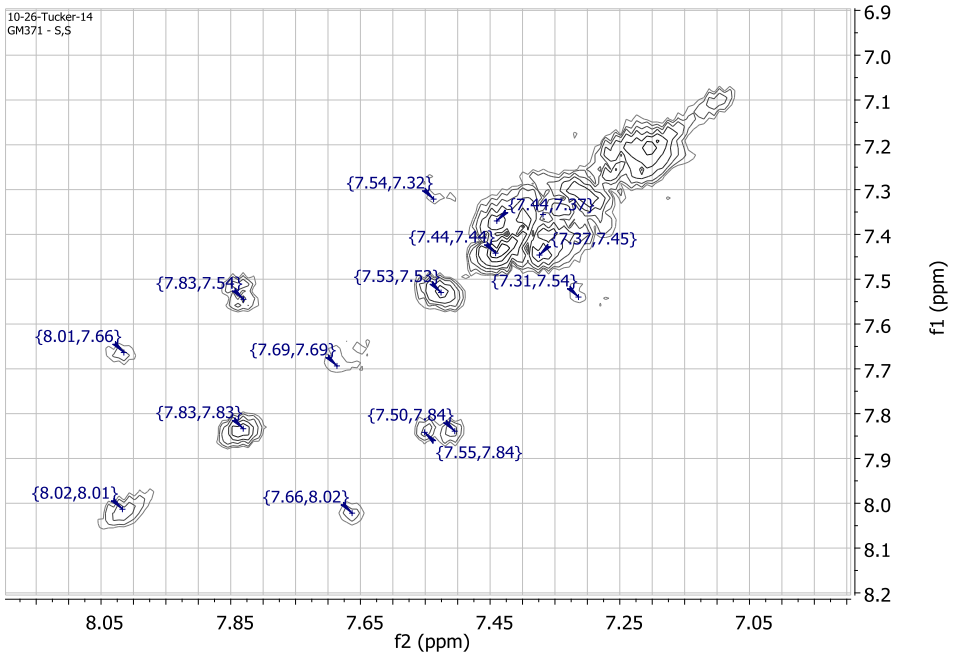

Figure 29. (^{1}H-^{1}H) COSY of **(*R,S,S*)-9a**

In the same way, the isopropyl group for **(*R*)-2b** displays a different appearance when binding **3** or **4**. In fact, when the complex with **3** is formed, the signal of the diasterotopic methyl protons of the isopropyl group appear as a doublet of doublets for both the *R* and *S* enantiomers. For **(*S*)-3** the signal is a doublet of doublets with a very large value ^2J (highlighted in blue in Figure 30). Due to the low equilibrium constant this effect can only be seen with a large excess of Binol. In Figure 30 the formation of the **(*R,S*)-8b** and **(*R,R*)-8b** adducts respectively can only be seen under conditions where there are 4 molar equivalents of **(*S*)-3** and 2 molar equivalents of **(*R*)-3**.

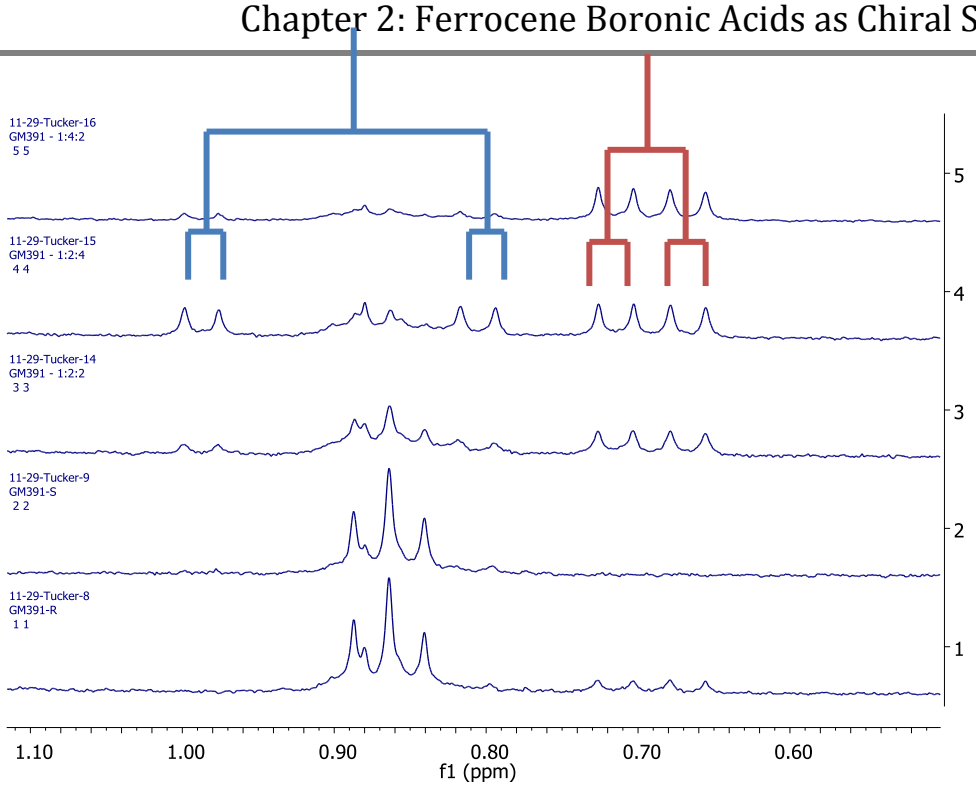

Figure 30. Stack plot of ^{1}H-NMR spectra ($CDCl_3$ 300 MHz) of **(*R,R*)-8b** (spectrum 1)**, (*R,S*)-8b** (spectrum 2) and the spectra obtained by **(*R*)-2b** with **(*R*)-3** and **(*S*)-3** in the respective ratio of 1:2:2 (spectrum 3); 1:2:4 (spectrum 4) and 1:4:2 (spectrum 5).

When hydrobenzoin is added to **(*R*)-2b** (Figure 31, spectrum 3) again the R group changes its chemical shift and multiplicity. In **(*R,S,S*)-9b** (Figure 31, spectrum 2) the signal of the methyl groups is an apparent triplet shifted downfield with respect to the free host. For **(*R,R,R*)-9b** the same signals become a doublet of doublets shifted downfield (Figure 31, spectrum 1) with respect to the free host.

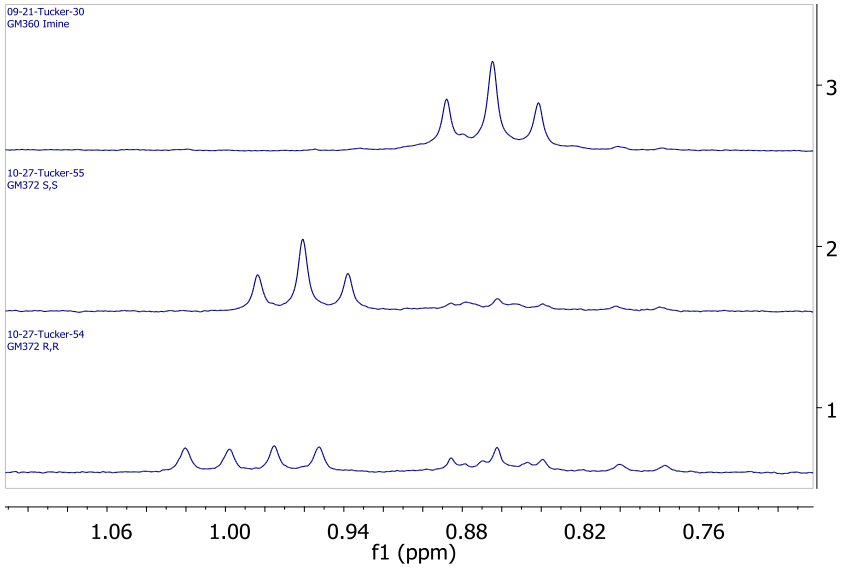

Figure 31. Stack plot of ^{1}H-NMR spectra ($CDCl_3$ 300 MHz) of **(*R,R,R*)-9b** (spectrum 1)**, (*R,S,S*)-9b** (spectrum 2) and **(*R*)-2b** (spectrum 3)

The fact that the signals of the isopropyl group become a doublet of doublets is evidence for an interaction between this group and the guest. This in fact happens when the two methyl groups are in a different magnetic environment.

Similarly to what is displayed by the other hosts, **(*R*)-2c** also shows a change in the appearance of the NMR signals of the naphthyl unit. In the free host, four doublets of the naphthalene are relatively downfield with respect the other aromatic signals (Figure 32, spectrum 3). However, upon the binding of the two enantiomers of Binol these signals move upfield and in the case of **(*R,R*)-8c** some signals fall outside the usual area for aromatic protons,(Figure 32, Spectrum 1). The upfield shift is probably due to a shielding effect by the Binol on the naphthyl unit which is similar to the effect of the Binol on the benzyl group for **(*R,R*)-8a**.

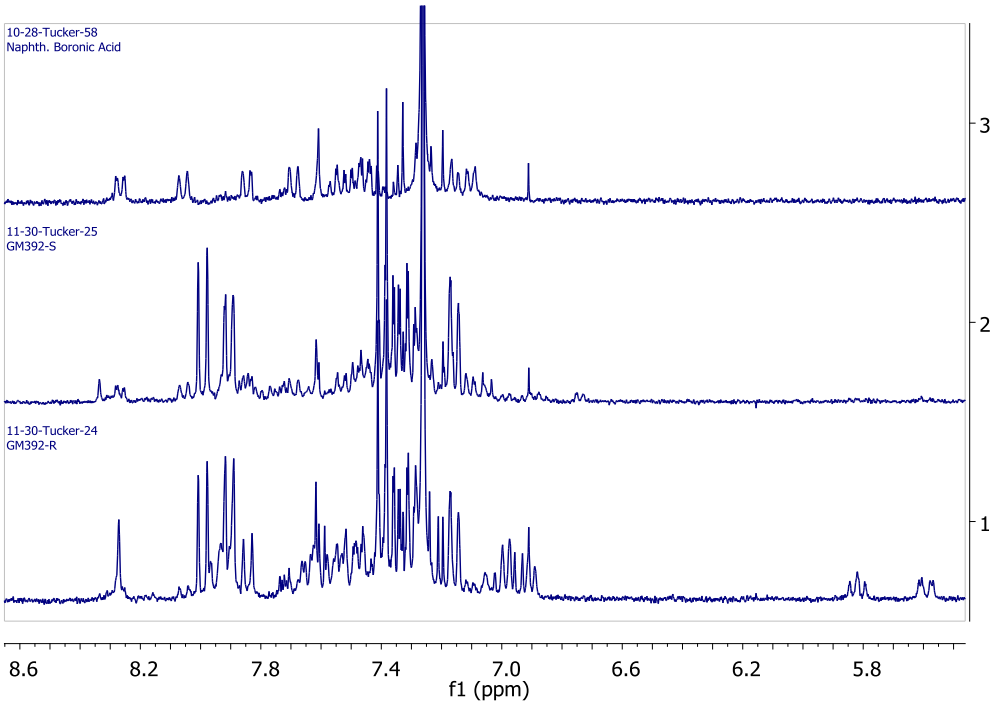

Figure 32. Stack plot of ^{1}H-NMR spectra ($CDCl_3$ 300 MHz) of **(*R,R*)-9c** (host : guest 1:1) (spectrum 1)**, (*R,S*)-9c** (host : guest 1:1) (spectrum 2) and **(*R*)-2c** (spectrum 3)

2.5 K_R / K_S determination

The large difference in the chemical shift of particular nuclei in the free host and in the two diasteromeric assemblies allowed the ratio between the thermodynamic constants K_R and K_S to be determined (Equation (***2.4***)).

$$2H_2O + HG_S \underset{K_S}{\overset{G_S}{\rightleftharpoons}} H \underset{K_R}{\overset{G_R}{\rightleftharpoons}} HG_R + 2H_2O$$

$$K_R = \frac{[HG_R][H_2O]^2}{[H][G_R]}$$

$$\frac{K_R}{K_S} = \frac{[HG_R][G_S]}{[HG_S][G_R]} \qquad (\mathbf{2.4})$$

During these experiments, initial concentrations of the host H, and the two enantiomers of guest G_R and G_S were known ($[\ ]_{TOT}$). The concentration of the different species at

equilibrium were evaluated from integrals of NMR signals of mixtures prepared as described by Equations (***2.5***), (***2.6***) and (***2.7***):

$$[\mathrm{H}]_{TOT} = [\mathrm{HG}_R]_{eq} + [\mathrm{HG}_S]_{eq} + [\mathrm{H}]_{eq} \qquad (\mathbf{2.5})$$

$$[\mathrm{G}_R]_{TOT} = [\mathrm{HG}_R]_{eq} + [\mathrm{G}_R]_{eq} \qquad (\mathbf{2.6})$$

$$[\mathrm{G}_S]_{TOT} = [\mathrm{HG}_S]_{eq} + [\mathrm{G}_S]_{eq} \qquad (\mathbf{2.7})$$

A proportionality constant, *x*, relates the integral ***I*** for each ferrocene species with the total ferrocene concentration, as shown below:

$$[\mathrm{H}]_{TOT} = \boldsymbol{I}_{\mathrm{H}}x + \boldsymbol{I}_{\mathrm{HG}_S}x + \boldsymbol{I}_{\mathrm{HG}_R}x \qquad (\mathbf{2.8})$$

$$x = \frac{[\mathrm{H}]_{TOT}}{\boldsymbol{I}_{\mathrm{H}} + \boldsymbol{I}_{\mathrm{HG}_S} + \boldsymbol{I}_{\mathrm{HG}_R}} \qquad (\mathbf{2.9})$$

Using this parameter, it was possible to work out the equilibrium concentration of both enantiomers of guest by rearranging Equations (***2.5***) and (***2.6***):

$$[\mathrm{G}_R]_{eq} = [\mathrm{G}_R]_{TOT} - \boldsymbol{I}_{\mathrm{HG}_R}x \qquad (\mathbf{2.10})$$

$$[\mathrm{G}_S]_{eq} = [\mathrm{G}_S]_{TOT} - \boldsymbol{I}_{\mathrm{HG}_S}x \qquad (\mathbf{2.11})$$

Similarly, the equilibrium concentrations of HG_R and HG_S can also be determined:

$$[\mathrm{HG}_R]_{eq} = \boldsymbol{I}_{\mathrm{HG}_R}x \qquad (\mathbf{2.12})$$

$$[\mathrm{HG}_S]_{eq} = \boldsymbol{I}_{\mathrm{HG}_S}x \qquad (\mathbf{2.13})$$

From equations (***2.10***), (***2.11***), (***2.12***) and (***2.13***) it is possible to estimate the binding constant ratio K_R/K_S using equation (***2.4***). Figure 33 shows one of the NMR spectra used to determine the constant ratio for **8a** adducts.

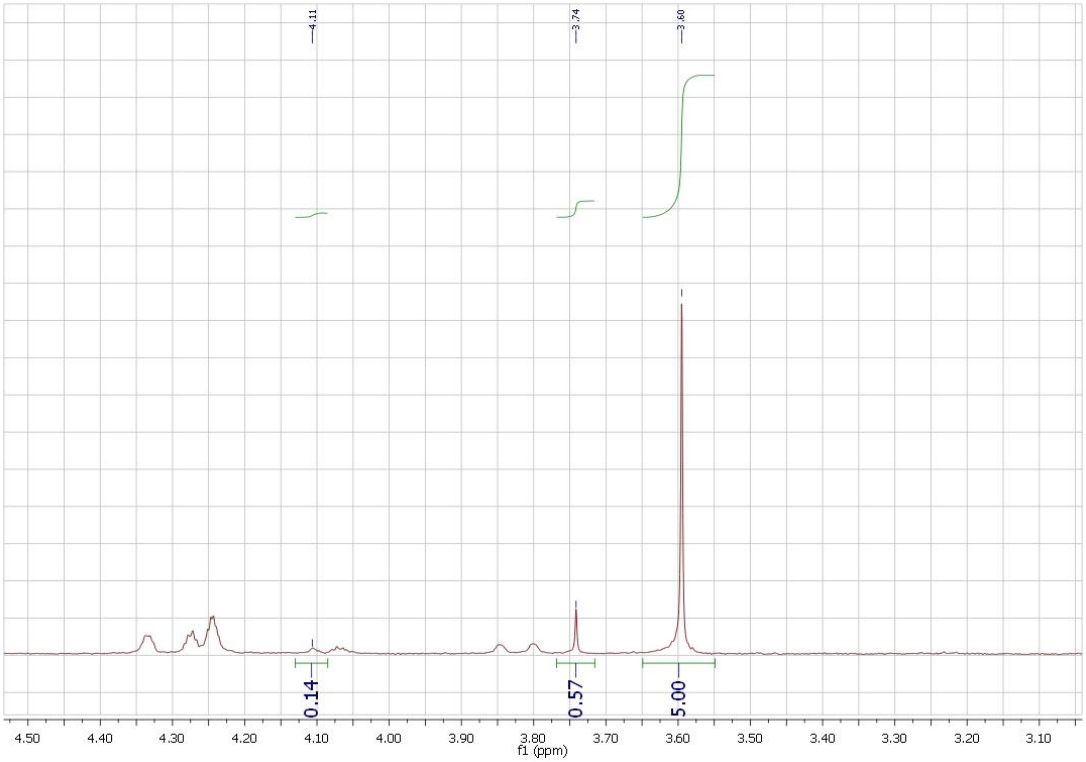

Figure 33. Detail of the ^{1}H-NMR spectrum of the Cp ring nuclei ($CDCl_3$ 300 MHz) of **(*R*)-2a, (*R*)-3** and **(*S*)-3** in a 1:2:2 ratio. (δ 4.11 **(*R*)-2a;** δ 3.74 **(*R,S*)-8a** δ **(*R,R*)-8a.**

Table 11. K_R/K_S of adducts formed with **3** and K_{RR}/K_{SS} of adducts formed with **4.** [a] determined from Cp signals; [b] determined from imine signals (294 K);

	(*R*)-2a	**(R)2b**	**(*R*)-2c**
3	18.7±3.8[a]	2.7±0.29[a]	19.8±5.9[a]
4	0.99±0.14[b]	0.19±0.03[b]	0.30±0.14[b]

From these values it is evident that when Binol, **3**, is bound, hosts with an aromatic side group (**(*R*)-2a** and **(*R*)2c**) demonstrated the best enantioselectivity. In each case (*R*)-Binol is preferred over (*S*)-Binol, Which is consistent with the optimal geometry observed in the X-Ray structure. However, the ^{i}Pr host **(*R*)-2b** displays the best enantioselectivity towards the binding of the aliphatic diol hydrobenzoin, **4**, and in this case, the host with the benzyl group, **(*R*)-2a**, shows no selectivity ($K_R/K_S \approx 1$).

For the adducts formed with **4,** the signal used to evaluate the binding constant ratio was the one for the imine proton, since the Cp ring signals displayed a very similar δ value ($\Delta\delta < 0.01$ ppm). The constants ratio was worked out considering the imine protons which possess very different chemical shift (Figure 34). On the other hand the Cp rings of the two diasteromers are recognisable (**(*R,R,R*)-9a** red arrow, **(*R,S,S*)-9a** blue arrow) but it is not possible to work out a precise value of the integrals.

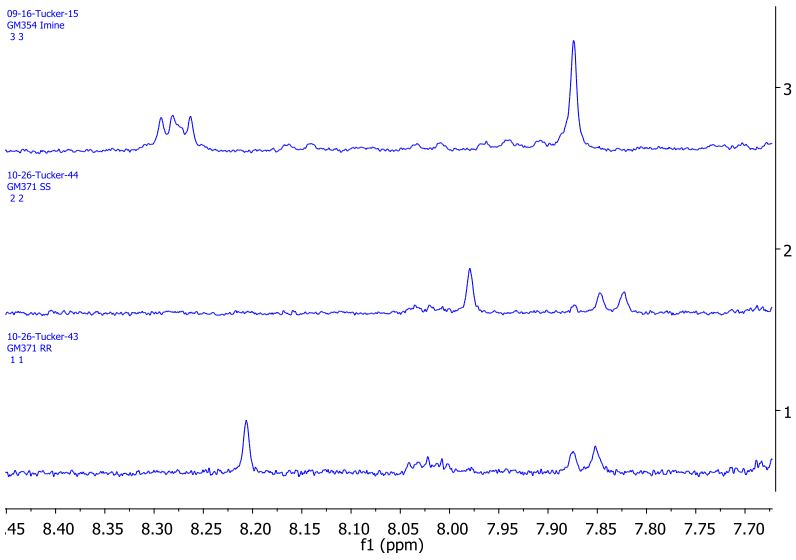

Figure 34 . Stack plot of details of ^{1}H-NMR spectrum ($CDCl_3$ 300 MHz) of the imine signals for **(*R,R,R*)-9a** (spectrum 1), **(*R,S,S*)-9a** (spectrum 2) and **(*R*)-2a** (spectrum 3)

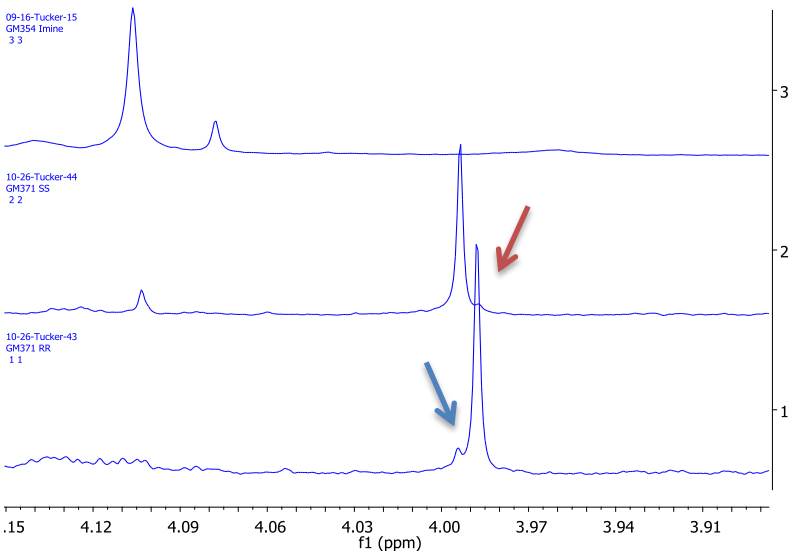

Figure 35. Stack plot of details of ^{1}H-NMR spectrum ($CDCl_3$ 300 MHz) of the Cp ring signals for **(*R,R,R*)-9a** (spectrum 1), **(*R,S,S*)-9a** (spectrum 2) and **(*R*)-2a** (spectrum 3)

From Table 11 it is clear that **(*R*)-2b** shows only a moderate enantioselectivity towards the binding of Binol, **3**, whereas the selectivity is larger with the aliphatic guest hydrobenzoin, **4**. From the NMR it is also evident how low the equilibrium constant for the formation of Binol complexes **(*R,R*)** and **(*R,S*)-8b** is. The NMR spectra in Figure 36 show that upon the addition of one equivalent of either enantiomer of **3** only a small quantity forms the adduct (Figure 36, green arrow Cp ring of **(*R*)-2b**, red arrow Cp ring of **(*R,R*)-8b** and blue arrow Cp ring of **(*R,S*)-8b**).

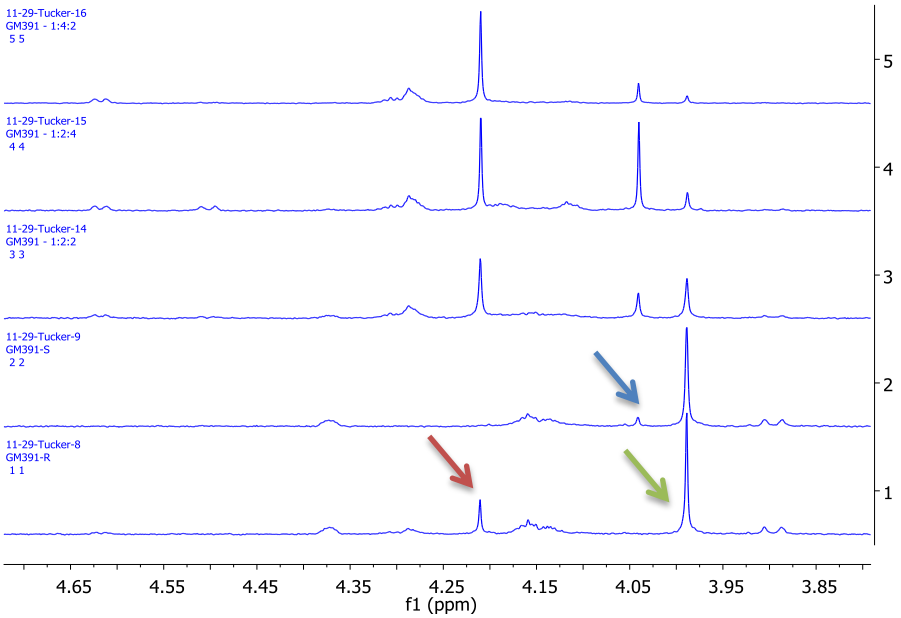

Figure 36. Stack plot of the ^{1}H-NMR spectrum ($CDCl_3$ 300 MHz) detail of the Cp ring of **(*R,R*)-8b** (spectrum 1), **(*R,S*)-8b** (spectrum 2) and of the adducts formed by **(*R*)-2b** with **(*R*)-3** and **(*S*)-3** in the respective ratio: 1:2:2 (spectrum 3); 1:2:4 (spectrum 4) and 1:4:2 (spectrum 5)

However, the equilibrium of the adduct formed with hydrobenzoin, **4**, is shifted more towards the formation of the boronate as shown in Figure 37 (green arrow Cp free host, red arrow Cp ring of **(*R,R,R*)-9b** and blue arrow Cp of **(*R,S,S*)-9b**). For these two examples the signals of the Cp ring were chosen to assess and determine the ratio of the thermodynamic constants. Note that during the NMR experiments many precautions were used to keep the system dry (Dry solvents passed through alumina, 3Å molecular sieves).

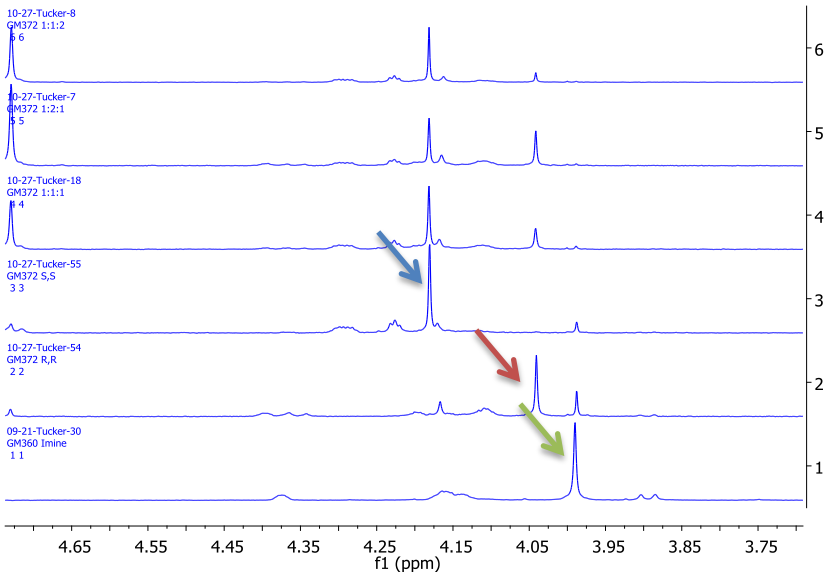

Figure 37. Stack plot of the ^{1}H-NMR spectrum ($CDCl_3$ 300 MHz) detail of the Cp ring of **(*R*)-2b** (spectrum 1), **(*R,R,R*)-9b** (spectrum 2), **(*R,S,S*)-9b** (spectrum 3) and of the adducts formed by **(*R*)-2b** with **(*R,R*)-4** and **(*S,S*)-4** in the respective ratio: 1:1:1 (spectrum 4); 1:2:1 (spectrum 5) and 1:1:2 (spectrum 6)

Similarly to the benzyl adducts, the ratio of the equilibrium constants for the formation of the two diasteromeric naphthyl adducts was obtained from the integrals of the signals of the free Cp rings. However the ratio with Binol, **3**, for the naphthyl system with hydrobenzoin, **9c,** was affected by a great error. In this case the two diasteromers possessed identical signals for the Cp rings, as was the case with **9a**, but in that case the ratio could be calculated by observing changes to the imine protons. Unfortunately for **9c**, the imine proton for the free host overlaped with a ^{13}C-^{1}H satellite peak (Figure 38) leading to a K_{RR}/K_{SS} affected by a large error estimated to be ±0.14.

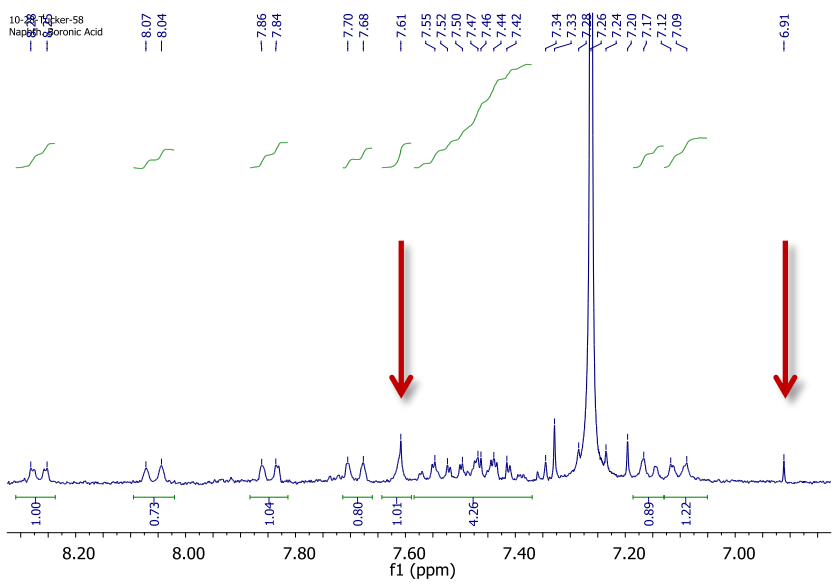

Figure 38. NMR spectrum of **(*R*)-2c** with the ^{13}C-^{1}H satellite peaks highlighted by the arrows

2.5.1 K_R^+ / K_S^+ determination

From the Nernst equation (Equations (***2.1***) and (***2.2***)) and from the previously determined K_R/K_S it is possible to determine the ratio between the binding constants in the oxidised state for the formation of the two diasteromeric complexes for each diol. According to the Nernst equation a positive shift of the potential upon the formation of the boronate is associated with a drop in the equilibrium constant in the oxidised form. In the same way an increase in the thermodynamic constant in the oxidised state will lead to a negative shift in the potential.

$$K_R^+/K_R = \exp[-nF\Delta E^{0\prime}/RT] \qquad (\textbf{\textit{2.14}})$$

$$K_S^+/K_S = \exp[-nF\Delta E^{0\prime}/RT] \qquad (\textbf{\textit{2.15}})$$

K_R^+/K_S^+ can be obtained combining equations (***2.14***) and (***2.15***) with the ratio of the thermodynamic constants obtained from the NMR $(K_R^+/K_R)/(K_S^+/K_S)\times(K_R/K_S)$. This can be done

with the reasonable assumption that the enantiomer binding ratios are not affected by the change in the solvent ($CDCl_3$ for NMR experiments and DCM for electrochemical experiments). The K_R^+/K_S^+ ratios (K_{RR}^+/K_{SS}^+ when hydrobenzoin, **4**, is analysed) are shown in Table 12 and Table 13 for the adducts formed with Binol, **3** and hydrobenzoin, **4** respectively.

Table 12. Ratio of thermodynamic constants in the reduced and oxidised form for adducts formed with the two enantiomers of **3** with the three different chiral guests.

	8a	**8b**	**8c**
K_R/K_S	18.7	2.72	19.8
K_R^+/K_S^+	2.5	0.57	4.11

Table 13. Ratio of thermodynamic constants in the reduced and oxidised form for adducts formed with the two enantiomers of **4** with the three different chiral guests.

	9a	**9b**	**9c**
K_{RR}/K_{SS}	0.99	0.19	0.30
K_{RR}^+/K_{SS}^+	0.39	0.63	0.86

From the values in Table 12 it is evident that upon oxidation, the adducts formed with **(*R*)-3** experience a greater drop in the equilibrium constant, in accordance with a greater $\Delta E^{\circ\prime}$ value for this enantiomer. This can be explained by the dative bond N**:->**B being loosened during the redox process since the electronic cloud is pulled towards the ferrocenium unit. The boronate ester would then be freer to rotate about the Ar-B bond, leading to poorer enantioselectivity. The drop in stability for the adduct **(*R,R*)-8b** is so great that the enantioselectivity in the oxidised state is reversed with respect to the one in the reduced form. When hydrobenzoin, **4**, is sensed, however, with adducts **9b** and **9c** there is an increase in the ratio upon oxidation,

which is linked to the negative shift in the potentials (greater for **(*R,R,R*)-9b-c** than **(*R,S,S*)-9b-c**), but again this means that enantioselectivity decreases upon oxidation. On the other hand, the peculiar behaviour in the electrochemistry for the adducts formed with receptor **(*R*)-2a** also affects the ratio of the equilibrium constants in the oxidised state and for these adducts a drop in the value is found, which leads to an increase in the enantioselectivity upon oxidation of the host.

2.6 ^{11}B-NMR

The hybridisation of the B nucleus can be assessed by considering ^{11}B-NMR spectroscopy. The spectra recorded for the free host **(*R*)-2a** and for its adducts with the two enantiomers of Binol **(*R*)-3** and **(*S*)-3** show an upfield shift in the signal for the boron, which corresponds to a change from sp^2 to sp^3 hybridisation,[25] in agreement with the crystal structure (Figure 7). As shown in Figure 39 the chemical shift for the boron nucleus is 28.5 ppm for the free benzyl host **(*R*)-2a** which shift to ca. 11.5 and 11 ppm for the corresponding **(*R*)-3** and **(*S*)-3** adducts respectively. This is consistent with the effect of increase in the electron density of the boronic acid due to the dative bond formed with the lone pair on the nitrogen atom being present as indicated in the crystal structure. These results were obtained taking into account the boronates present in the glass, with the spectrum of a blank solution subtracted from the NMR spectra obtained.

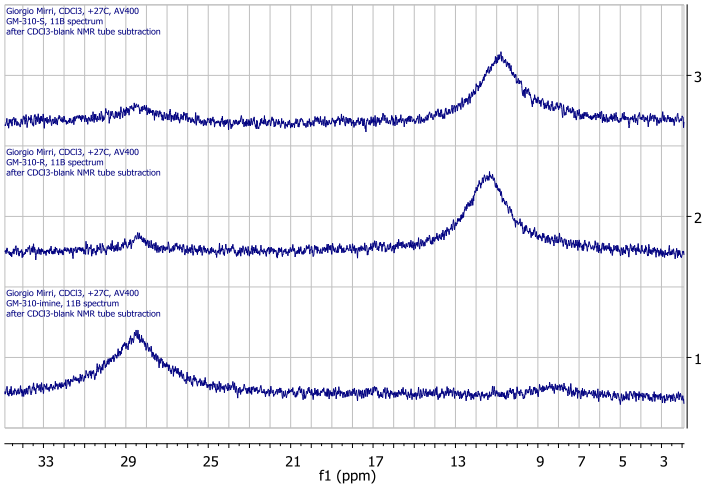

Figure 39. ^{11}B-NMR spectrum ($CDCl_3$ 128 MHz) spectra of **(*R*)-2a** (spectrum 1), **(*R,R*)-8a** (spectrum 2) and **(*R,S*)-8a** (spectrum 3)

2.7 Adducts formed with (*S*)-2a

In order to assess how much the configuration of the chiral centre of the amine affected the binding and also for a useful control for the enantiomeric determination, chiral boronic acid **(*S*)-2a** was prepared in the usual way as shown in Scheme 5. The chiral amine precursor **(*S*)-1a** was prepared following the same reaction pathway (Scheme 4) with the only change being the configuration of the chiral centre of the starting alcohol.

Figure 40 shows that the NMR spectra of **(*S,S*)-8a** and **(*S,R*)-8a** are identical to the spectra of **(*R,R*)-8a** and **(*R,S*)-8a** respectively. The result is not surprising since these adducts are two pairs of enantiomers and thus they possess identical physical and chemical properties in an achiral environment. For this reason also the electrochemical properties are the same (identical electrode potentials within experimental error) as shown in Figure 41 for **(*R,R*)-8a**, **(*S,S*)-8a, (*R,S*)-8a** and **(*S,R*)-8a**. In Table 14 the electrode potential of adducts formed with different guests are presented.

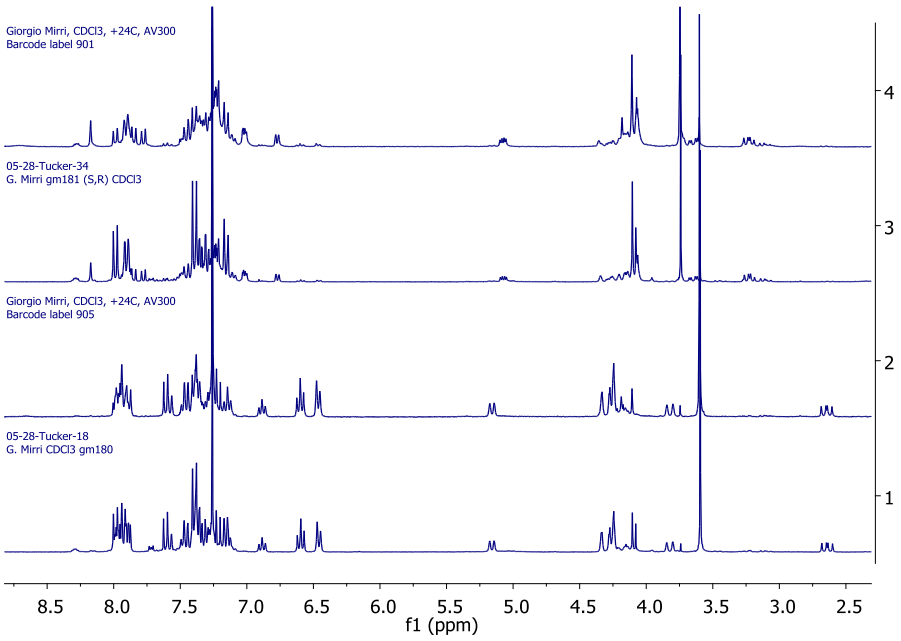

Figure 40. (*S,S*)-8a (spectrum 1), **(*R,R*)-8a** (spectrum 2), **(*S,R*)-8a** (spectrum 3) and **(*R,S*)-8a** (spectrum 4),

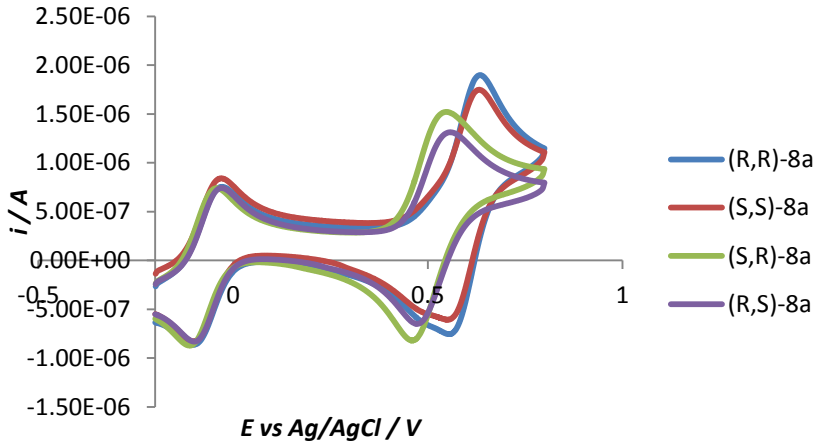

Figure 41. Cyclic voltammogams of **8a** adducts. Solvent: dcm, supporting electrolyte: TBA PF_6 0.1 M and dmfc as internal reference.

Table 14. Electrode potentials in mV *vs.* dmfc of adducts formed by **(*R*)-2a** and **(*S*)-2a** with all the chiral guests, measured by CV.

	(*R,R*)-4	**(*S,S*)-4**	**(*meso*)-4**	**(*R*)-5**	**(*S*)-5**
(*S*)-2a	579	551	559	560	547
(*R*)-2a	552	576	561	546	556

2.8 Electrochemical *%ee* read out

All the hosts display a rather large $\Delta E^{\circ\prime}$ and in some cases also a large difference in the equilibrium constants. It is thus possible to think about correlating the enantiomeric composition of the guests to the potential of the adducts formed with different hosts. In this way it could be possible to electrochemically read out the enantiomeric excess (*ee*) of a mixture of enantiomers.

The read-out was carried out by preparing different solutions, each with the same total concentration of guest but with a different enantiomeric ratio. To allow a complete complexation the solutions were prepared in a way that the guest would be in a 10 fold excess compared to that of the host, with molecular sieves 3Å added to the solution. The large excess of guest does not affect the electrochemistry since the guests were not electro-active in the potential window under study.

2.8.1 Binol

As described above, it was decided to assess the enantiomeric composition of enantiomeric mixtures of Binol by adding 10% of the host **(*R*)-2a** in order to ensure a complete formation of the boronate ester adduct. The observed potential was recorded using SWV which was then plotted against the % *enantiomeric excess* of (*S*)-Binol. The fitting of the points in the region *%ee* = 100 – 60, which is the one that most interests synthetic chemists, showed a linear dependence of the potential with the enantiomeric composition of the solution (Figure 42).

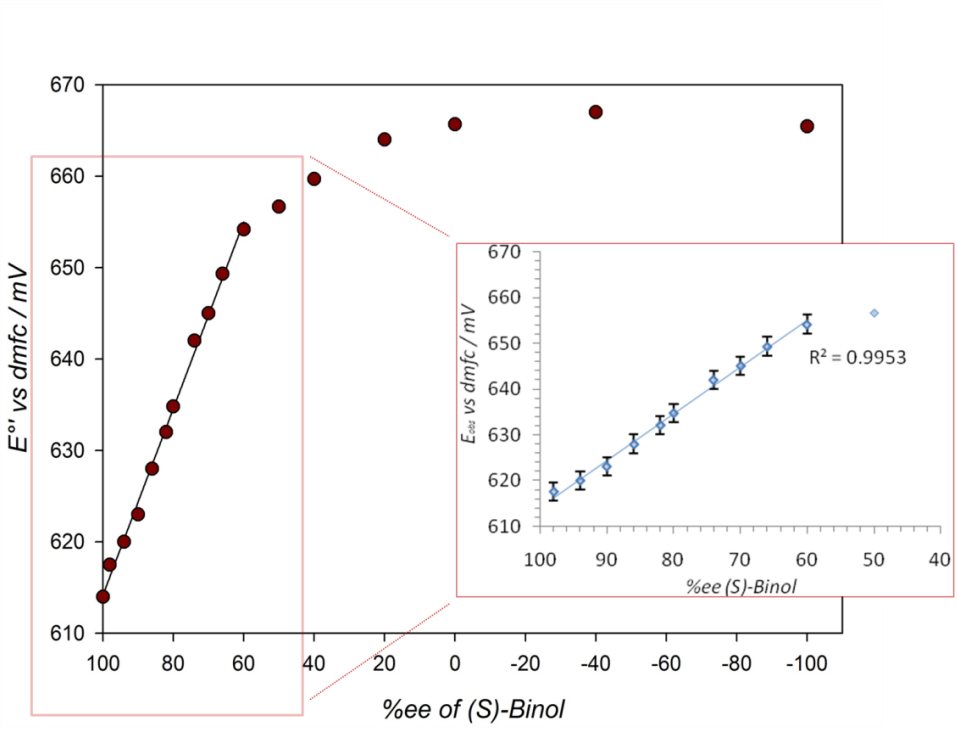

Figure 42. Plot of the peak potential of **(*R*)-2a** *vs.* %ee of **(*S*)-3** added showing the linear dependence between 60% and 98%

Moreover, this method allowed discrimination between 98% and 90% using an analyte concentration of ca. 10^{-4} M. This is at least one order of magnitude lower than the usual concentration for similar NMR methods.[26] The behaviour of the potential *vs.* the enantiomeric composition depends on the large difference in the binding constants for the two enantiomers with the host. This is the cause of the steep linear part along with the plateau at high percentage of the enantiomer that binds more strongly. On the other hand the plateau is caused by the difference in the binding constants, i.e., when mixtures with high percentages of the enantiomer with the higher binding constant are studied, small variations in the composition cause only small changes in the potential.

The square wave voltammograms of the different solutions always displayed *one-wave* behaviour, even when (*R*)-Binol was present in a 7:3 ratio (-40% *ee* in the graph) (Figure 43).

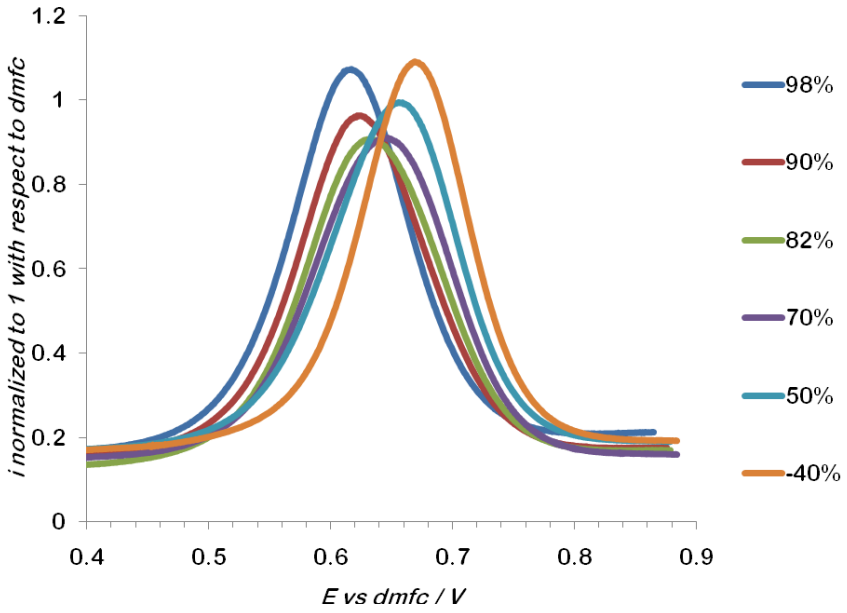

Figure 43. Square wave voltammograms of **(*R*)-2a** (dcm, 3.14×10^{-5} M, 0.1 M TBA·PF_6) each in the presence of a 10-fold excess of **3** with varying enatiomeric composition as expressed by % ee of **(*S*)-3** in the legend. (- 40% equates to 40% ee of **(*R*)-3**).

The isopropyl host **(*R*)-2b** showed a similar behaviour towards enantiomeric mixtures of of Binol. However, the accuracy in the determination of the *ee* is this time lower due to the smaller magnitude of the $\delta\Delta E^{\circ\prime}$ (ca. 30 mV) in addition to the smaller difference in the K_R/K_S ratio for the formation of the two adducts. This ratio in fact, affects the slope of the linear part, which is shallower compared to the one obtained with **(*R*)-2a.** The result is a poorer accuracy for high values of *%ee*. Figure 44 shows the plot of the potential of the ferrocene unit on **(*R*)-2b** *vs.* the *ee* of the solution analysed.

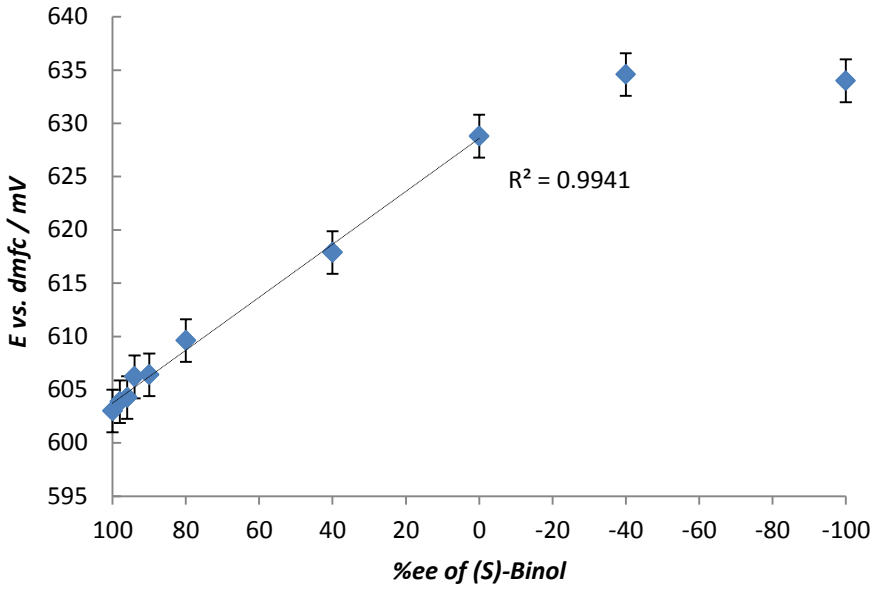

Figure 44. Plot of the peak potential of **(*R*)-2b** *vs*. %ee of **(*S*)-3** added showing the linear dependence between 0% and 98%

2.8.2 Hydrobenzoin

The aliphatic guest which gives the best results in terms of differences in potentials and enantioselectivity is hydrobenzoin, **4**. The correlation between potential and enantiomeric excess assessed using **(*R*)-2b** gives a linear behaviour for 100-40 %*ee* (Figure 45). However, the accuracy, is also affected by the rather small $\delta\Delta E^{\circ\prime}$ (ca. 30 mV) and the low enantioselectivity in the reduced state. It is however possible to detect 10% of the (*S,S*) enantiomer (80% *ee*).

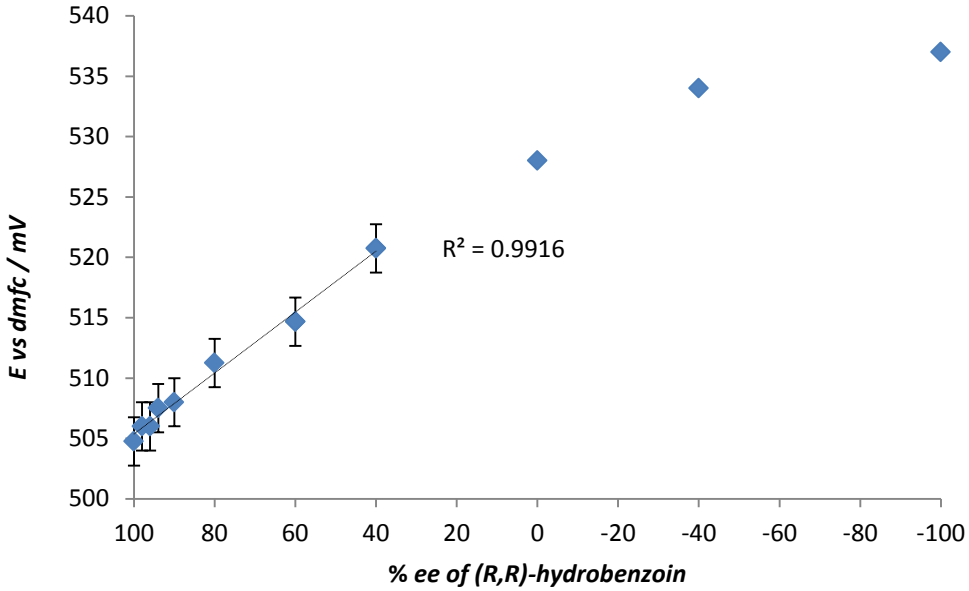

Figure 45. Plot of the peak potential of **(*R*)-2b** *vs*. %ee of **(*R,R*)-4** added showing the linear dependence between 40% and 98%

Interestingly, the potential/*%ee* correlation shows unusual behaviour when hydrobenzoin is analysed using the benzyl host **(*R*)-2a**. Since the equilibrium constant ratio is ≈1, a linear dependence was expected for the whole 100 <-> -100 % *ee* range, without a plateau. However, clearly this does not happen for high values of *%ee* of **(*R,R*)-4** with a deviation from linearity observed that is not displayed in the corresponding negative region (-100 %*ee* of (*R,R*) corresponds to 100 %*ee* (*S,S*)) as shown in Figure 46. The reason for this behaviour could be due to a cooperative binding, however, further studies are needed to confirm this theory.

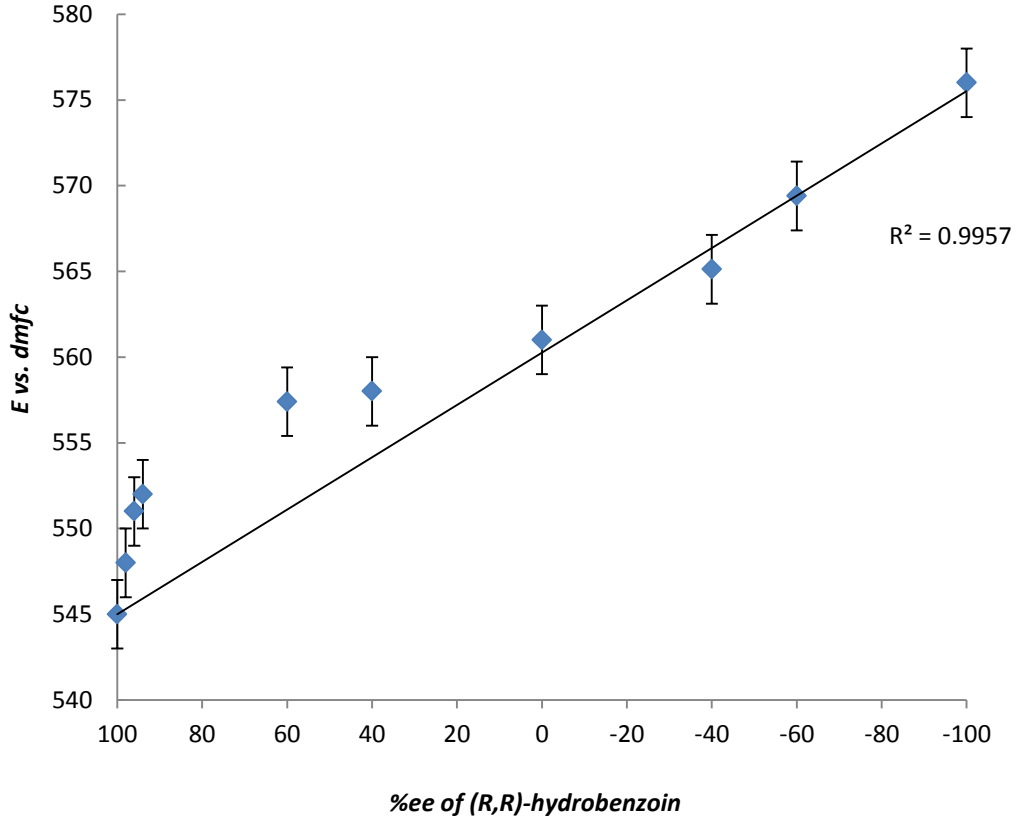

Figure 46. Plot of the peak potential of **(*R*)-2a** *vs*. %ee of **(*R,R*)-4** added showing the linear dependence between -100% and 0% and a deviation from linearity between 0% and 98%

2.9 Digital simulation of CV

As already mentioned in Section **2.3.2**, the addition of each enantiomers of Binol to receptors **(*R*)-2a** gave unusual results in that (*R*)-Binol, **(*R*)-3**, gave *two-wave* behaviour whereas (*S*)-Binol, **(*S*)-3**, gave *one-wave* behaviour. A high binding constant is commonly associated with *two-wave* behaviour whereas systems that are characterised by a low binding constant display *one-wave* behaviour. Usually the two behaviours are displayed by substrates which possess a very different binding constants.[9a,23]

However, the thermodynamics in the oxidised state must also be considered. The Nernst equation (Equations (***2.1***) and (***2.2***)) links the difference in the thermodynamics in the two

redox states to the difference in the electrode potential between the free host and the *host-guest* adduct. The values for adducts formed with Binol **3** are presented in Table 15.

Table 15. Values of the ratio in of the thermodynamic constants evaluated from Equation (**1**) and (**2**) from ΔE°' obtained from electrochemical experiment with Binol **3**.

	8a	**8b**	**8c**
K_R^+ / K_R	0.024	0.031	0.042
K_S^+ / K_S	0.176	0.149	0.202

According to the simulation carried out using DigiSim®[27] it could be demonstrated that the presence of the two behaviours depend on the magnitude of Δ*E*°'. The simulations carried out took into account the effect of the dilution upon the addition of the guest. Simulated voltammograms of the titration of **(*R*)-2a** with **(*R*)-3** and **(*S*)-3** are presented in Figures 47 and 49 respectively, in contrast, Figures 48 and 50 show the experimental titrations for the same systems.

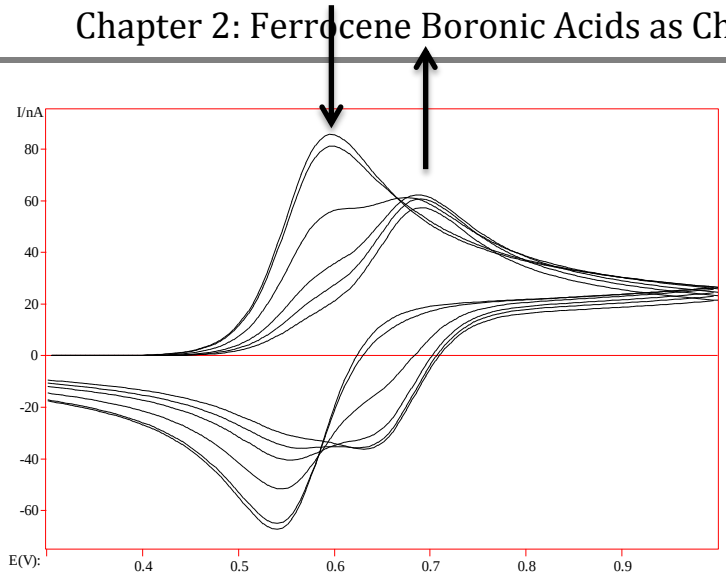

Figure 47 . Simulation of the titration of **(*R*)-2a** with **(*R*)-3.** Initial concentration of **(*R*)-2a** = 4.3×10^{-4} M; molar equivalent of guest added: 0, 1, 10, 30, 50, 80. The arrows show the wave appearing and the one disapperaring upon the addition of aliquots of guest. Correction for the dilution were made for each simulation

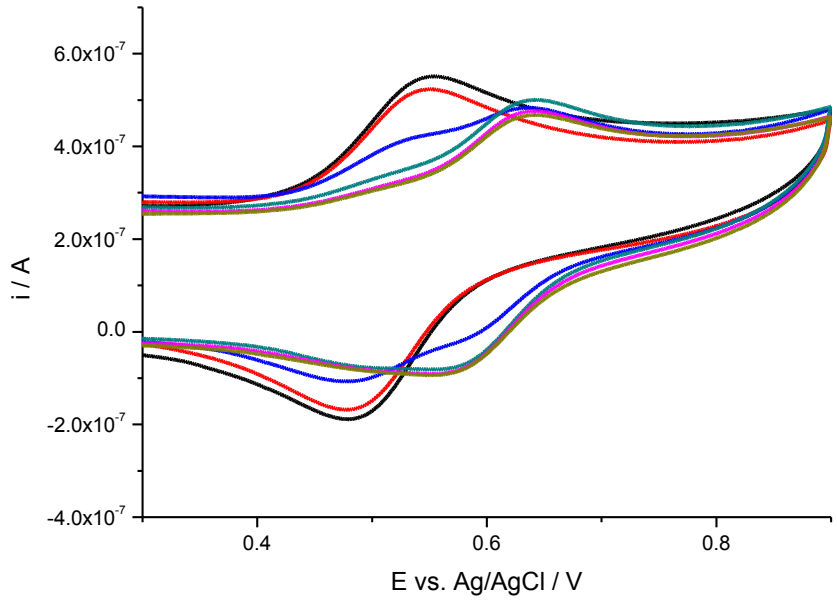

Figure 48 . Cyclic voltammograms of the titration of **(*R*)-2a** with **(*R*)-3.** Initial concentration of **(*R*)-2a** = 4.3×10^{-4} M; molar equivalent of guest added: 0 (black), 1 (red), 10 (blue), 30(cyano), 50 (purple), 80 (gold).

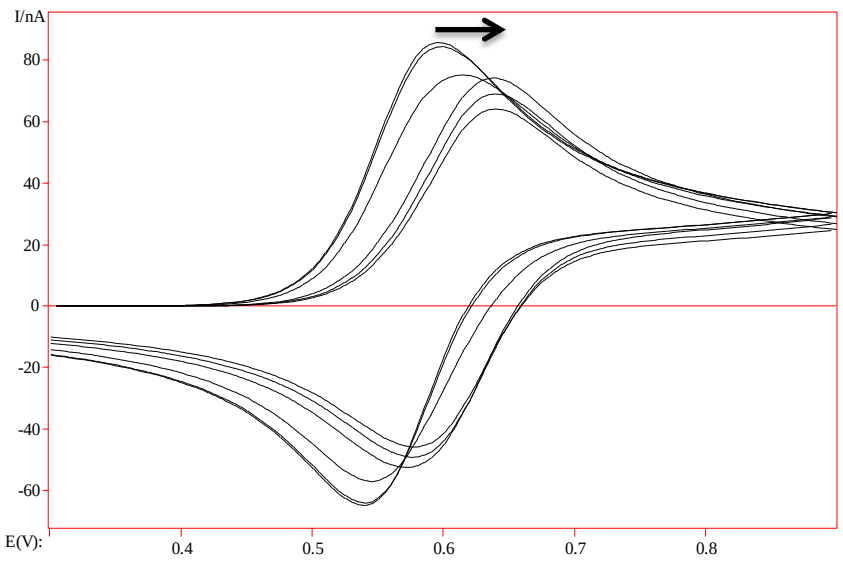

Figure 49. Simulation of the titration of **(*R*)-2a** with **(*S*)-3.** Initial concentration of **(*R*)-2a** = 4.3×10^{-4} M; molar equivalent of guest added: 0, 1, 50, 90, 150, 190. The arrow indicates the direction of the shifting upon the addition of aliquots of guest. Correction for the dilution were made for each simulation

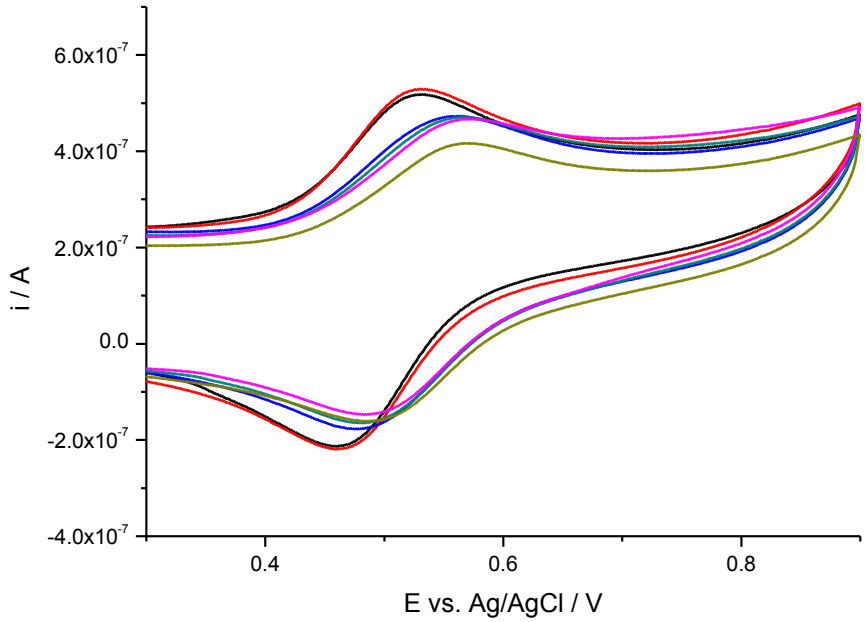

Figure 50. Titration of **(*R*)-2a** with **(*S*)-3.** Initial concentration of **(*R*)-2a** = 4.3×10^{-4} M; molar equivalent of guest added: 0 (black), 1 (red), 50(blue), 90 (cyano), 150 (pink), 190 (gold).

However, another parameter that could affect the behaviour is the diffusion coefficient; this is an indication of how quickly a species diffuses to and from the electrode in solution. Other simulation carried out in our group on H-bonding systems[27] have shown that this parameter can affect the appearance of voltammograms when $\Delta E^{\circ\prime}$ values are similar. Diffusion coefficient can be calculated from equation (***2.3***) and the following values for **(*R*)-2a**, **(*R,R*)-8a** and **(*R,S*)-8a** were obtained 8.6×10^{-10} cm^2/s, 7.06×10^{-10} cm^2/s and 8.53×10^{-10} cm^2/s respectively. These values where used in the digital simulation in Figures 47 and 49.

2.10 Conclusions

In this chapter, it has been demonstrated that chiral receptors based on ferrocene and boronic acids can be used to sense and electrochemically recognise different stereoisomers of chiral diols. Furthermore, with certain guests, it was also possible to perform the first examples of an accurate determination of the enantiomeric excess of a mixture of enantiomers by electrochemical means.

Changing the R group from an aromatic to an alkyl one increases the enantioselectivity towards the binding of aliphatic diols. However, extended aromatic R groups (methyl naphthalene) do not appear to increase the interaction with aromatic diols such as Binol, with the enantioselectivity in the reduced state only moderately higher than that obtained with R = Benzyl. The $\delta\Delta E^{\circ\prime}$ values were generally larger with the benzyl receptor **(*R*)-2a**.

Hydrobenzoin, when sensed with **(*R*)-2a** displays a peculiar behaviour, with the boronate formed by the (*S,S*) isomer leading to an unexpected positive shift in the potential. The electronic nature of the diol would be expected to cause a negative shift in the potential for

both enantiomers. The reason behind this behaviour is still not clear and it will be the subject of further studies.

2.11 Work in progress and future work

Taking inspiration from the work of Shinkai who used a planar chiral ferrocenylboronic acid to electrochemically distinguish glucose from fructose,[10b] we have considered the preparation of planar chiral boronate esters and their use in sensing chiral amines in a similar way to the systems we previously described in this chapter. This approach would be innovative in molecular sensing because the sensor possesses a reporting group, a chiral centre *and* a binding site all in just one unit.

Scheme 8 depicts the synthetic pathway to obtain planar chiral ferrocene carboxyaldehydes via chiral 1,2,4 butanetriol, which acts as a chiral auxiliary.[28] This could be installed onto the ferrocene aldehyde as an acetal, which also works as a protecting group for the formyl moiety during the deprotonation of the ferrocene unit. The chiral auxiliary directs the metallation via the coordination of the Li^+. The coordination is preferential for one of the two diasterotopic ortho positions.

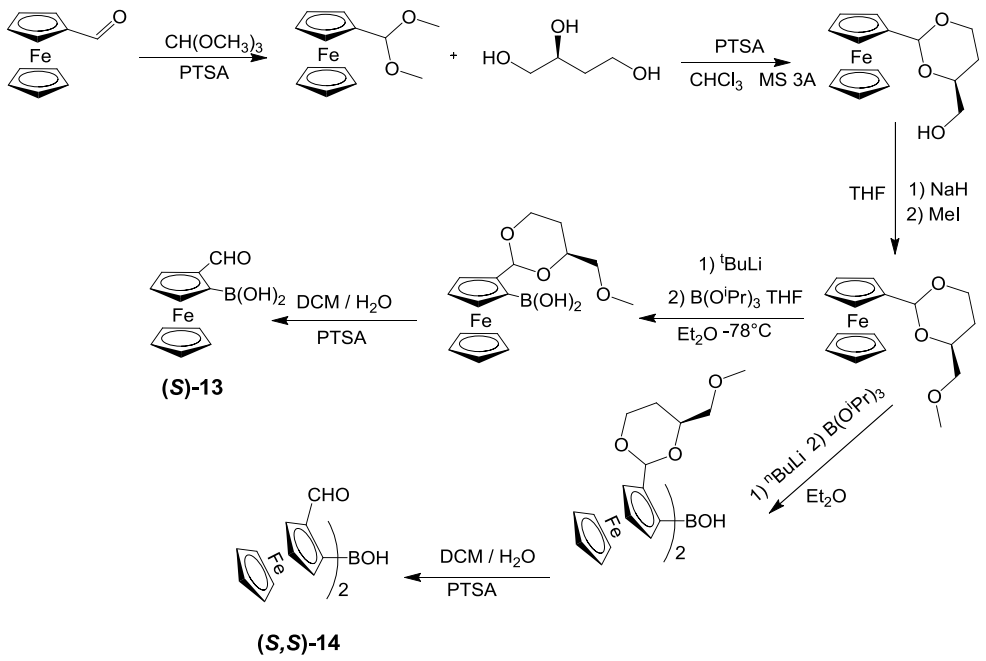

Scheme 8. Formation of planar chiral ferrocene carboxyaldehydes

The formation of the boronic acid **(*S*)-13** over the borinic acid **(*S,S*)-14** is regulated by the dilution of the electrophile and the temperature. In order to obtain the boronic acid, THF was added right after the addition of the electrophile and the temperature was adjusted at -78°C. However the borinic acid was obtained carrying on the reaction at 0°C and without further additions of solvent after the addition of the electrophile.

(*S*)-15 was obtained from **(*S*)-13** by reaction with pinacol (Scheme 9).

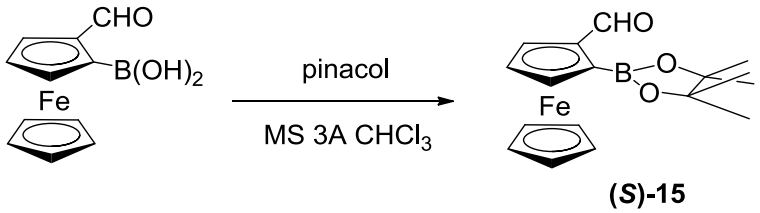

Scheme 9

The aim is to use this compound to form Schiff bases with chiral amines (Figure 51), allowing chiral recognition by electrochemical techniques.

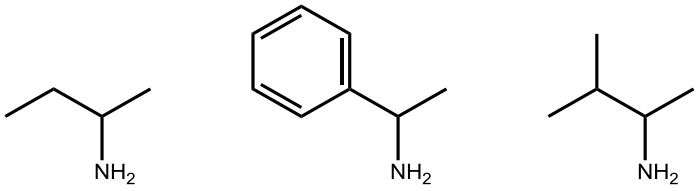

Figure 51

(*S*)-15 could also be used to form imines with a racemic mixture of an amine allowing the separation of the two enantiomers, which could be recovered after an acidic work up that should also allow the chiral sensor to be recovered. This could be a convenient way of obtaining enantiopure *α* alkyl amines which are rather expensive on the market.[29]

2.12 References

(1) (a) Nunez, M. C.; Garcia-Rubino, M. E.; Conejo-Garcia, A.; Cruz-Lopez, O.; Kimatrai, M.; Gallo, M. A.; Espinosa, A.; Campos, J. M. *Curr. Med. Chem.* **2009**, *16*, 2064(b) Farina, V.; Reeves, J. T.; Senanayake, C. H.; Song, J. H. J. *Chem. Rev.* **2006**, *106*, 2734.

(2) Traverse, J. F.; Snapper, M. L. *Drug Discovery Today* **2002**, *7*, 1002.

(3) (a) Zhang, Y. W.; Yao, S.; Zeng, H.; Song, H. *Curr. Pharm. Anal.* **2010**, *6*, 114(b) Uccello-Barretta, G.; Balzano, F.; Salvadori, P. *Curr. Pharm. Des.* **2006**, *12*, 4023.

(4) Moss, G. P. *Pure Appl. Chem.* **1996**, *68*, 2193.

(5) (a) Fischer, E. *Ber. Dtsch. Ges.* **1890**, 5(b) Marckwald, W.; Mc Kenzie, A. *Ber. Dtsch. Ges.* **1899**.

(6) Vedejs, E.; Jure, M. *Angew. Chem., Int. Ed.* **2005**, *44*, 3974.

(7) Dale, J. A.; Dull, D. L.; Mosher, H. S. *J. Org. Chem.* **1969**, *34*, 2543.

(8) (a) Wenzel, T. J.; Wilcox, J. D. *Chirality* **2003**, *15*, 256(b) Ema, T.; Tanida, D.; Sakai, T. *J. Am. Chem. Soc.* **2007**, *129*, 10591.

(9) (a) Amendola, V.; Boiocchi, M.; Colasson, B.; Fabbrizzi, L.; Monzani, E.; Douton-Rodriguez, M. J.; Spadini, C. *Inorg. Chem.* **2008**, *47*, 4808(b) Casas-Solvas, J. M.; Ortiz-Salmeron, E.; Fernandez, I.; Garcia-Fuentes, L.; Santoyo-Gonzalez, F.; Vargas-Berenguel, A. *Chem.-Eur. J.* **2009**, *15*, 8146(c) Bresner, C.; Aldridge, S.; Fallis, I. A.; Jones, C.; Ooi, L. L. *Angew. Chem., Int. Ed.* **2005**, *44*, 3606(d) Bayly, S. R.; Gray, T. M.; Chmielewski, M. J.; Davis, J. J.; Beer, P. D. *Chem. Commun.* **2007**, 2234.

(10) (a) Willener, Y.; Joly, K. A.; Moody, C. J.; Tucker, J. H. R. *J. Org. Chem.* **2008**, *73*, 1225(b) Ori, A.; Shinkai, S. *J. Chem. Soc., Chem. Commun.* **1995**, 1771(c) Arimori, S.; Ushiroda, S.; Peter, L. M.; Jenkins, A. T. A.; James, T. D. *Chem. Commun.* **2002**, 2368.

(11) (a) Liu, H. L.; Peng, Q.; Wu, Y. D.; Chen, D.; Hou, X. L.; Sabat, M.; Pu, L. *Angew. Chem., Int. Ed.* **2010**, *49*, 602(b) Zhang, X.; Chi, L. N.; Ji, S. M.; Wu, Y. B.; Song, P.; Han, K. L.; Guo, H. M.; James, T. D.; Zhao, J. Z. *J. Am. Chem. Soc.* **2009**, *131*, 17452.

(12) Trojanowicz, M.; Kaniewska, M. *Electroanalysis* **2009**, *21*, 229.

(13) Carr, J. D.; Goles, S. J.; Hursthouse, M. B.; Light, M. E.; Tucker, J. H. R.; Westwood, J. *Angew. Chem., Int. Ed.* **2000**, *39*, 3296.

(14) Westwood, J.; Coles, S. J.; Collinson, S. R.; Gasser, G.; Green, S. J.; Hursthouse, M. B.; Light, M. E.; Tucker, J. H. R. *Organometallics* **2004**, *23*, 946.

(15) Kelly, A. M.; Perez-Fuertes, Y.; Fossey, J. S.; Yeste, S. L.; Bull, S. D.; James, T. D. *Nat. Protoc.* **2008**, *3*, 215.

(16) Perez-Fuertes, Y.; Kelly, A. M.; Fossey, J. S.; Powell, M. E.; Bull, S. D.; James, T. D. *Nat. Protoc.* **2008**, *3*, 210.

(17) Laurent, P.; Miyaji, H.; Collinson, S. R.; Prokes, I.; Moody, C. J.; Tucker, J. H. R.; Slawin, A. M. Z. *Org. Lett.* **2002**, *4*, 4037.

(18) Moody, C. J. *Chem. Commun.* **2004**, 1341.

(19) Kraatz, H. B. *J. Organomet. Chem.* **1999**, *579*, 222.

(20) Hunter, C. A.; Sanders, J. K. M. *J. Am. Chem. Soc.* **1990**, *112*, 5525.

(21) Emilia, M.; Silva, N. P. R. A.; Pombeiro, A. J. L.; Dasilva, J. J. R. F.; Herrmann, R.; Deus, N.; Bozak, R. E. *J. Organomet. Chem.* **1994**, *480*, 81.

(22) (a) Batterjee, S. M.; Marzouk, M. I.; Aazab, M. E.; El-Hashash, M. A. *Appl. Organomet. Chem.* **2003**, *17*, 291(b) Emília, M.; Silva, N. P. R. A.; Pombeiro, A. J. L.; da Silva, J. J. R. F.; Herrmann, R.; Deus, N.; Castilho, T. J.; Silva, M. F. C. G. *J. Organomet. Chem.* **1991**, *421*, 75.

(23) Miller, S. R.; Gustowski, D. A.; Chen, Z. H.; Gokel, G. W.; Echegoyen, L.; Kaifer, A. E. *Anal. Chem.* **1988**, *60*, 2021.
(24) Graziani, O.; Hamon, P.; Thepot, J. Y.; Toupet, L.; Szilagyi, P. A.; Molnar, G.; Bousseksou, A.; Tilset, M.; Hamon, J. R. *Inorg. Chem.* **2006**, *45*, 5661.
(25) Zhu, L.; Shabbir, S. H.; Gray, M.; Lynch, V. M.; Sorey, S.; Anslyn, E. V. *J. Am. Chem. Soc.* **2006**, *128*, 1222.
(26) Mirri, G.; Bull, S. D.; Horton, P. N.; James, T. D.; Male, L.; Tucker, J. H. R. *J. Am. Chem. Soc.* **2010**, *132*, 8903.
(27) Mulas, A., 2011.
(28) Riant, O.; Samuel, O.; Flessner, T.; Taudien, S.; Kagan, H. B. *J. Org. Chem.* **1997**, *62*, 6733.
(29) Carr, R.; Alexeeva, M.; Enright, A.; Eve, T. S. C.; Dawson, M. J.; Turner, N. J. *Angew. Chem., Int. Ed.* **2003**, *42*, 4807.

3. Ferrocene-based macrocyclic chiral receptors

3.1 Introduction

Molecular recognition is based on selective interactions between a host and guest. The selectivity of the binding depends largely on the nature and the shape of the binding site. Natural occurring systems, i.e. enzymes, membrane receptors, etc., have been a great source of inspiration in the drive for even more selective sensors.[1] In these systems very often the binding site consists of a 'pocket' with particular groups strategically positioned in the cavity. The binding of the guest, which is entropically disfavoured, is then stabilised by positive non-covalent interactions between the guest and the groups in the pocket. An example of a naturally occurring macrocyclic host is the ionophore valinomycin (Figure 1), an oligopeptide that is able to selectively bind K^+ in the presence of Na^+ and transport it through the cell membrane, giving this compound antibiotic properties.[2] The process is concentration driven based on the fact that the cytosol is deficient in K^+ which the antibiotic carries from outside the membrane. However, the process does not select between mammalian and bacterial cells and for this reason valinomycin is not an efficient therapeutic agent.[3]

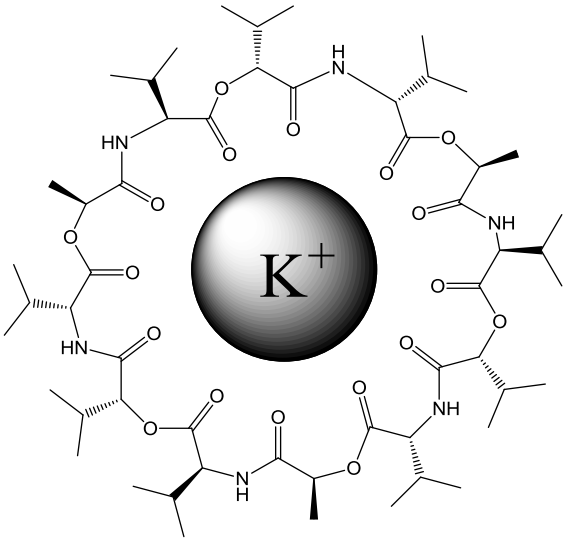

Figure 1 Valinomycin.

Artificial macrocyclic compounds are therefore chosen to mimic Nature in creating selective binding along with the fabrication of nanoporous materials.[4] Moreover, such compounds can be functionalised with particular side groups, increasing the selectivity towards the binding of a particular class of molecule.

As already shown in Chapter 1, the binding of charged molecules by macrocyclic hosts has been the object of investigation for the last 20 years and it is the basis of supramolecular chemistry. Crown ethers and polyamino cryptands have been extensively studied for the binding of cations and anions respectively.[5] The presence of multiple binding sites stabilise the host-guest adducts.[5b] Chiral crown ethers have also been used as receptors for chiral guests.[6]

An example of a sensor for neutral molecules is the Hamilton receptor. This is a macrocycle containing 2,6-diamidopyridine moieties that has been proven to bind barbiturates through the formation of six H-bonds, as shown in Figure 2.[7]

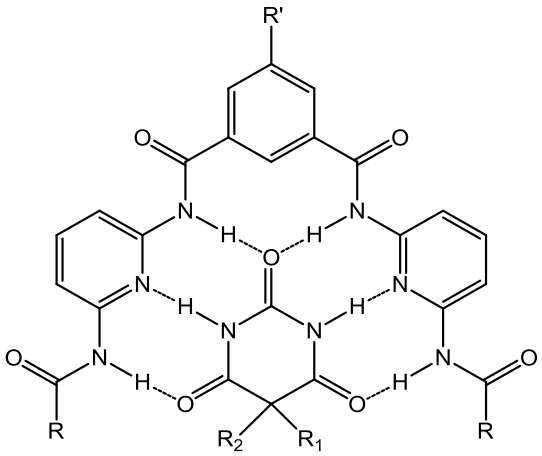

Figure 2 Hamilton receptor binding barbiturates

Chiral macrocycles containing 2,6-diamidopyridine moieties have been recently reported as NMR supramolecular shift reagents for chiral carboxylic acids, dialcohols and sulphoxides.[8] This compound is also commercially available and it is sold as Chirabite® (Figure 3).[9]

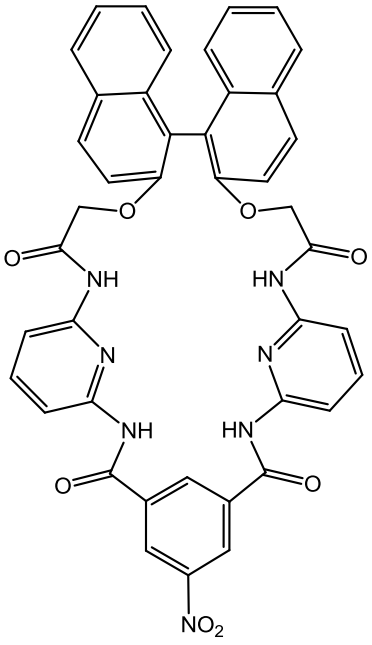

Figure 3 Chirabite®.

Previous work in Tucker group involved the use of ferrocene based receptors with amidopyridine moieties to sense mono and dicarboxylic acids (Figure 4).[10]

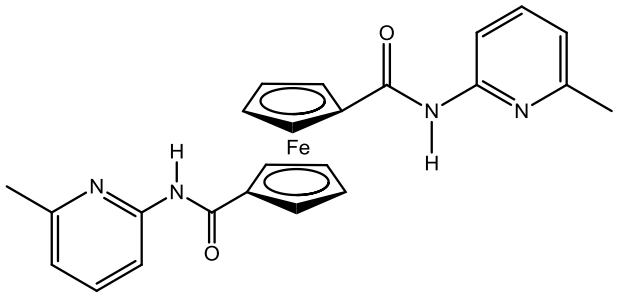

Figure 4 1,1' ferrocene bis-amidopyridine receptor

1,3 ferrocene Hamilton-like receptors were also prepared and proven to be able to sense barbirturates and cyclic ureas. The potential of the ferrocene unit of the compound shown in Figure 5 undergoes a small negative shift upon the addition of barbital (-20 mV), although analogous 1,1'-systems give slightly larger shifts.[11]

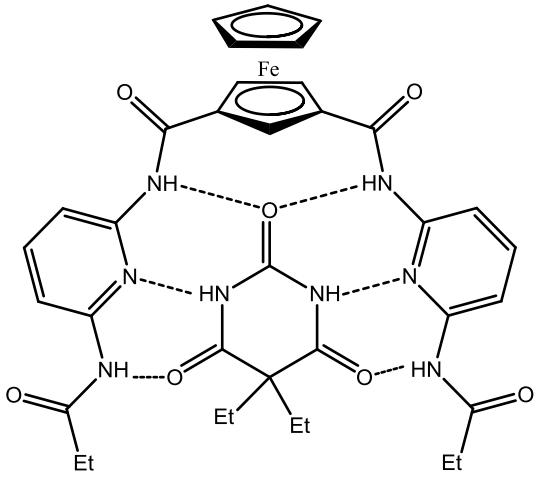

Figure 5 Ferrocene hmilton-like receptor

Ferrocene-containing macrocycles have been reported as long ago as 1986 as redox-switchable membrane carriers for cations.[12] Later, ferrocene containing crown ethers and cryptands have also been used as electrochemical sensors for cations.[13] More recently ferrocene-based ureas were used as metal cation receptors.[14]

3.2 Aim of the studies

In this chapter the synthesis of two chiral macrocycles containing a ferrocene unit (Figure 6) is reported.

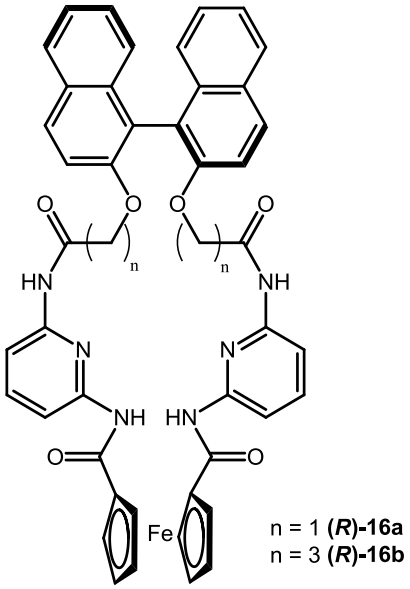

Figure 6 Macrocycles n=1 and n=3.

Preliminary sensing studies carried out using chiral and achiral guests are also presented in order to determine whether these compounds can be used as electrochemical chiral sensors. Achiral cyclic ureas (**17** and **18**) and a barbiturate derivative **19**, 2-phenyl-butyrric acid **20,** and mandelic acid **21**, were chosen as chiral guests.

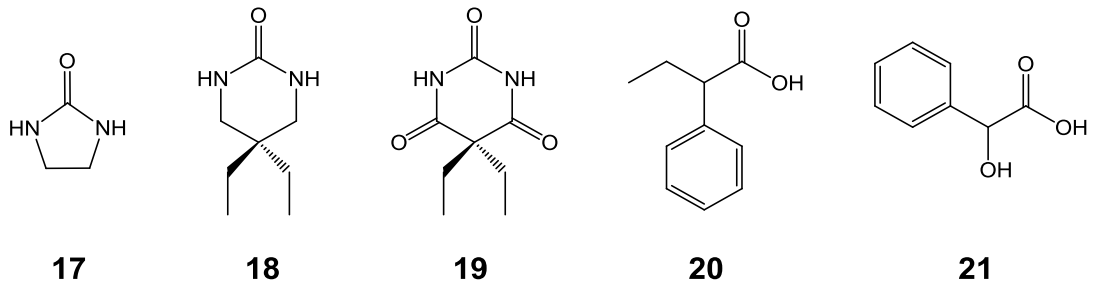

Figure 7 Chiral and achiral guests.

3.3 Synthesis of the macrocycles

The macrocyles were obtained by the reaction of two individually prepared subunits, one carrying the redox unit and the other one carrying the chiral unit Binol.

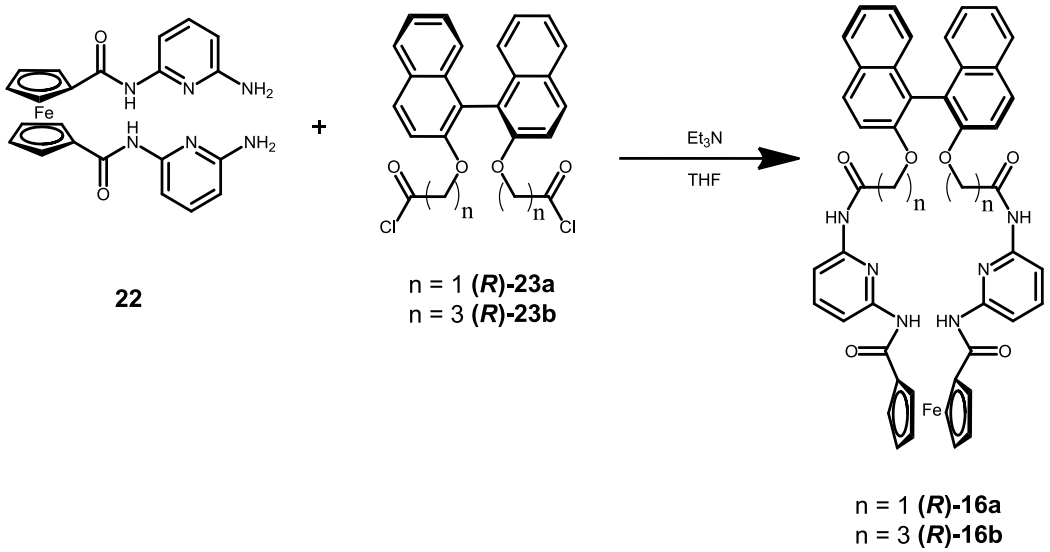

Scheme 1 Cyclisation.

In order to avoid polymerisation, the macrocyclization reactions were carried out under basic conditions with the reacting concentration of the two compounds being very low. Other macrocyclisation methods would involve the use of templates.[15] The high dilution condition could be obtained by adding the two compounds dropwise to the reaction flask over a rather long period of time (1-2 hours) using a syringe pump.[16]

Compound **22** was obtained from ferrocene via formation of a ferrocenyl organolithium which was then reacted directly with dry ice in diethyl ether to obtain the 1,1'-dicarboxylic acid. This compound was then readily converted to the ferrocene-1-1'-diacylchloride with oxalyl chloride. The reaction proceeded in a good yield and the final purification was carried out with a Soxhlet extraction. The diacyl chloride was then reacted with diaminopyridine to obtain the bisamine **22**. (Scheme 2).[17]

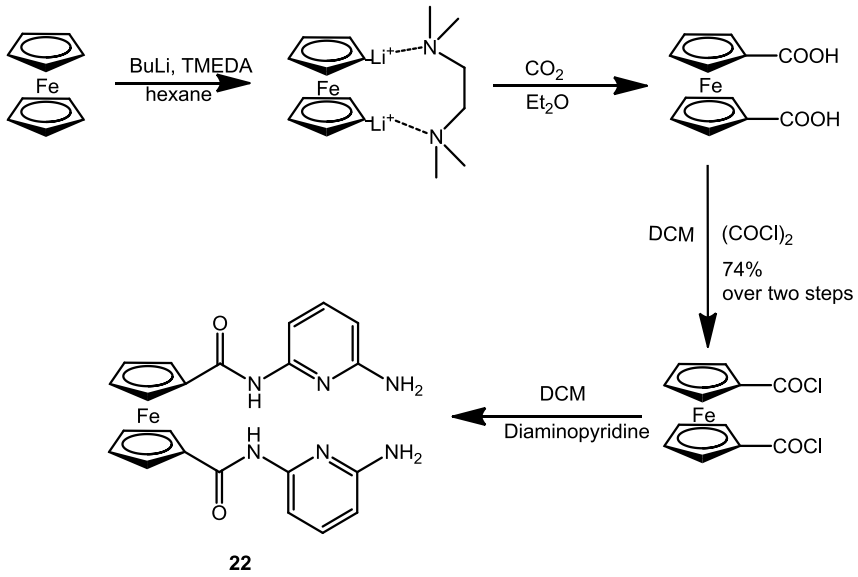

22

Scheme 2. Reaction scheme for **22**.

The chiral moiety was installed into the macrocyle through the use of **(*R*)-23**. This was obtained from (*R*)-Binol, which was treated with a base (potassium carbonate) and reacted with either bromoethylethanoate or bromoethylbutanoate in order to obtain macrocycles of different sizes. The resulting diesters were then saponified with NaOH, yielding chiral dicarboxylic acids which could be readily converted in the corresponding diacyl acid. This compound is rather air sensitive so it was prepared just before the cyclisation reaction.[8]

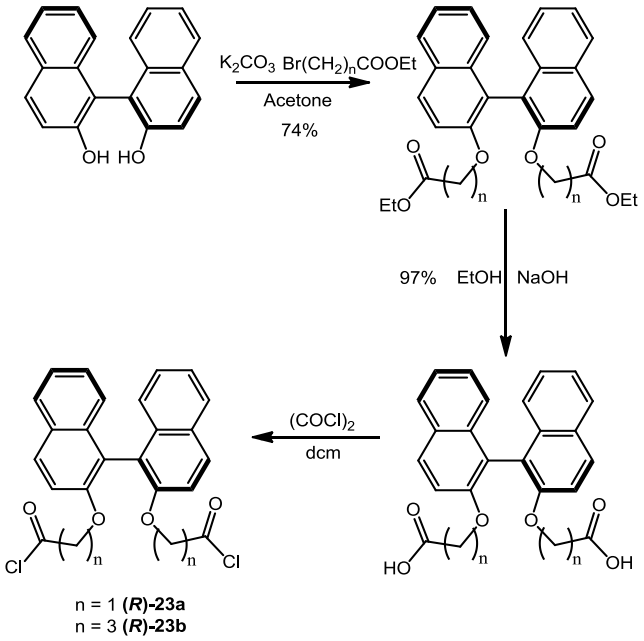

Scheme 3. Reaction scheme to obtain **(*R*)-23**

Obtaining the *n* = 2 macrocycle using this approach from bromoethylpropionate was impossible; under basic conditions, this compound undergoes β-elimination instead of the desired nucleophilic substitution (Scheme 4).

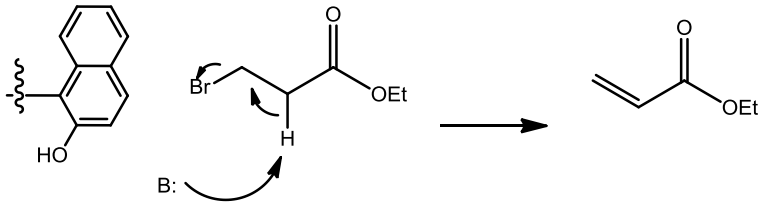

Scheme 4. β-elimination**.**

3.4 NMR studies

The presence of exchangeable protons is a good way to follow the formation of H-bonding host-guest systems. Upon the formation of the complex, the chemical shifts of the protons involved in the binding change with the addition of different aliquots of guest. From the magnitude of the shift and the molar equivalents of guest added, an evaluation of the

binding constant of the host guest system is also possible using software such as Wineqnmr®.[18]

3.4.1 Macrocycle (*R*)-16a

The two amide protons of **(*R*)-16a** possess two distinguishable sharp singlets whose chemical shifts are not affected by concentration; presumably the cavity protects them from the solvent and also prevents intermolecular interactions that broaden the signals and affect the chemical shifts. Moreover, using different NMR techniques (HSQC and HMBC) it was possible to assign the two peaks to the two different amide protons.[‡] The amide proton on the ferrocene side (Red arrow Figure 8) resonates more downfield than the one on the Binol side (Blue arrow Figure 8).

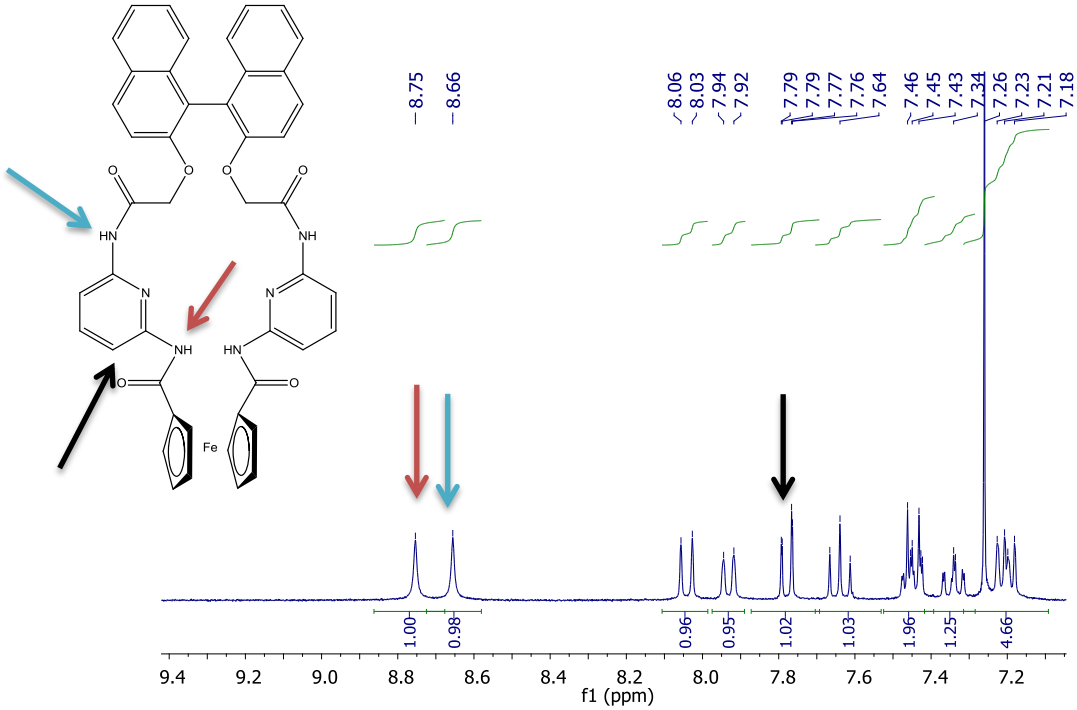

Figure 8 ^{1}H-NMR ($CDCl_3$ 500 MHz)of **(*R*)-16a** amides and aromatic protons. Red arrow amide on the ferrocene side; blue arrow amide on the Binol side.

[‡] NMR characterisation carried out by Dr. Neil Spencer

The assignment of these two signals is important for determining the orientation of binding. Upon titrating **(*R*)-16a** with cyclic ureas **17** and **18**, the signals for the proton closer to the ferrocene undergoes a downfield shift (Figures 9 and 11), this effect demonstrates the H-bonding nature of the *host-guest* interaction. Interestingly, the other amide proton did not change upon the addition of guest (Figure 10 and 12).

A downfield shift is also displayed by the ortho pyridine proton on the ferrocene side (black arrows, Figures 9 and 11) which is consistent with complexation. However, in the case of the guest protons, it could also be explained by intermolecular interactions between guest molecules. A proposed model of the interaction is shown in Figure 13.

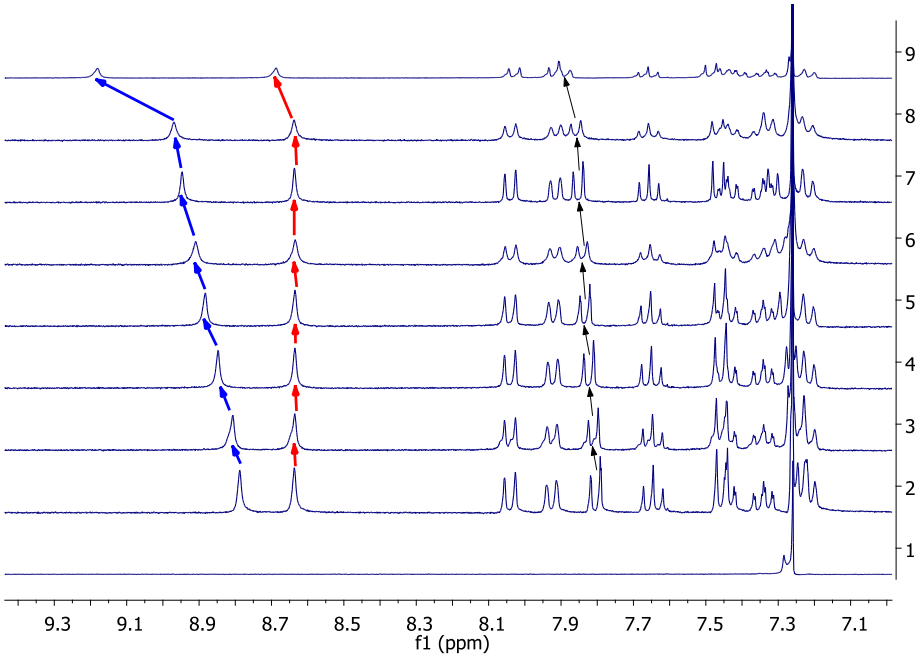

Figure 9: ^{1}H-NMR (300 MHz, $CDCl_3$) amide protons of **(*R*)-16a** + ethyleneurea, **17**. Ethylene urea spectrum 1; free **(*R*)-16a** spectrum 2; **(*R*)-16a** + 0.35 molecular equivalent of **17** spectrum 3; ; **(*R*)-16a** + 1.1 molecular equivalent of **17** spectrum 4; ; **(*R*)-16a** + 1.8 molecular equivalent of **17** spectrum 5; ; **(*R*)-16a** + 2.7 molecular equivalent of **17** spectrum 6; ; **(*R*)-16a** + 3.6 molecular equivalent of **17** spectrum 7; **(*R*)-16a** + 4.5 molecular equivalent of **17** spectrum 8; **(*R*)-16a** + 20 molecular equivalent of **17** spectrum 9.

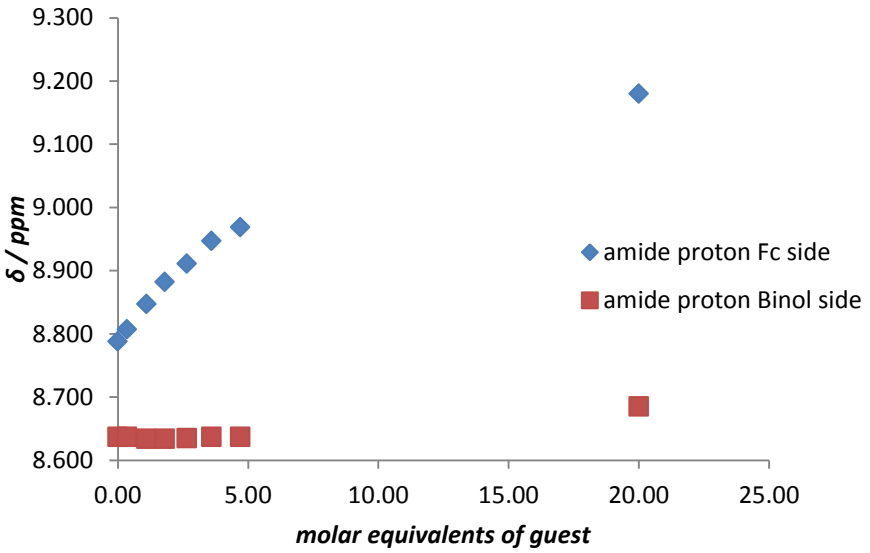

Figure 10 Chemical shift of the amide protons of **(*R*)-16a** upon the addition of **17.**

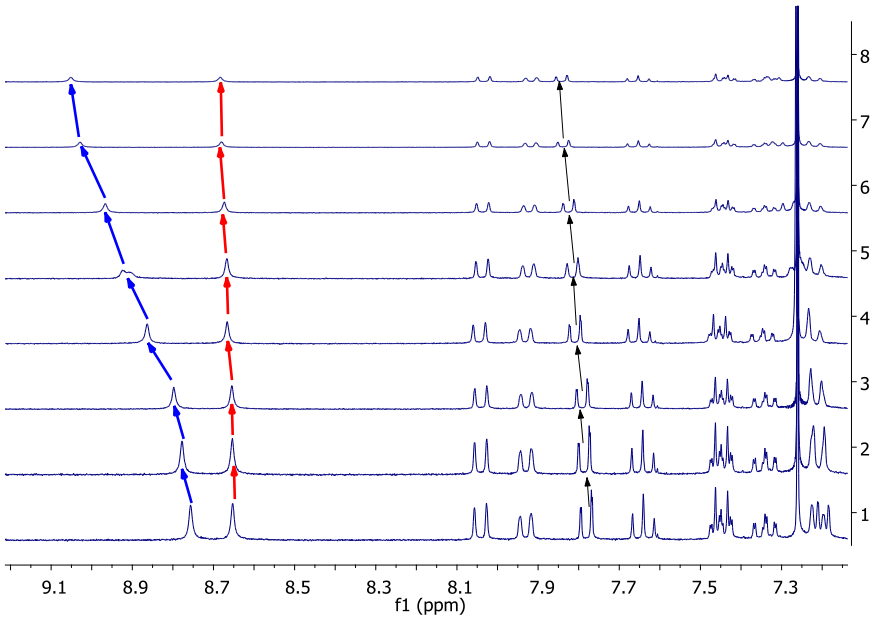

Figure 11: : ^{1}H-NMR (300 MHz, $CDCl_3$) amide protons of **(*R*)-16a** + 2,2'-ethyl propyleneurea, **18**. free **(*R*)-16a** spectrum 1; **(*R*)-16a** + 0.6 molecular equivalent of **18** spectrum 2; ; **(*R*)-16a** + 1.1 molecular equivalent of **18** spectrum 3; ; **(*R*)-16a** + 2.6 molecular equivalent of **18** spectrum 4; **(*R*)-16a** + 4.5 molecular equivalent of **18** spectrum 5; **(*R*)-16a** + 10.5 molecular equivalent of **18** spectrum 6; **(*R*)-16a** + 18 molecular equivalent of **18** spectrum 7; **(*R*)-16a** + 22.2 molecular equivalent of **18** spectrum 8.

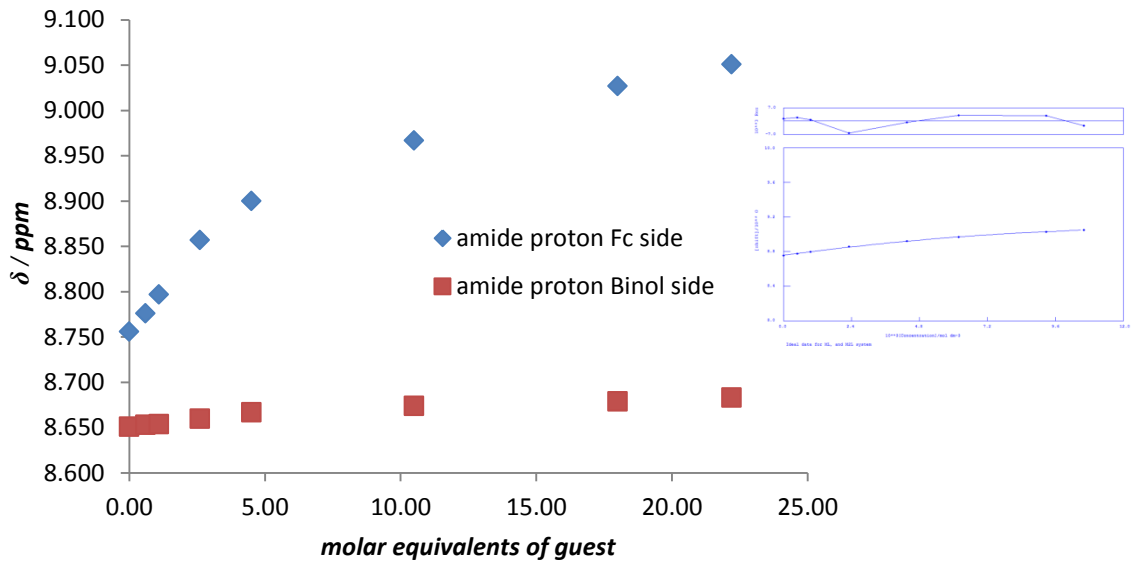

Figure 12 Chemical shift of the amide protons of **(*R*)-16a** upon the addition of **18.**

From the titration with **18** the determination of the binding constant ($CDCl_3$, 298 K) was carried out using Wineqnmr software:

K_1=245 M^{-1} ± 51

The fact that only one amide proton signal moves indicates that the cyclic ureas prefer to bind as H-bonding acceptors to the amides closest to the ferrocene unit. On the other hand, looking at the chemical shift of the pyridine moiety on the host and of the exchangeable protons on the guests it is possible to speculate whether the host acts also as a H-bonding acceptor on the pyridine nitrogen. Upon the addition of different aliquots of ethyleneurea the urea protons signal shifts downfield, as shown in Figure 14 and even more clearly in Figure 15.

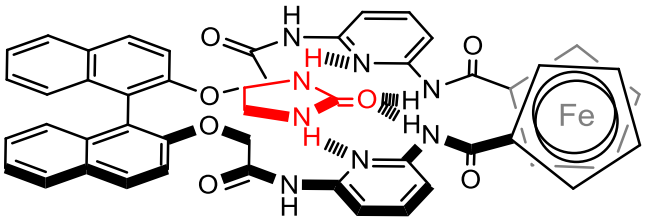

Figure 13. Proposed model of interaction between **(*R*)-16a** and **17**

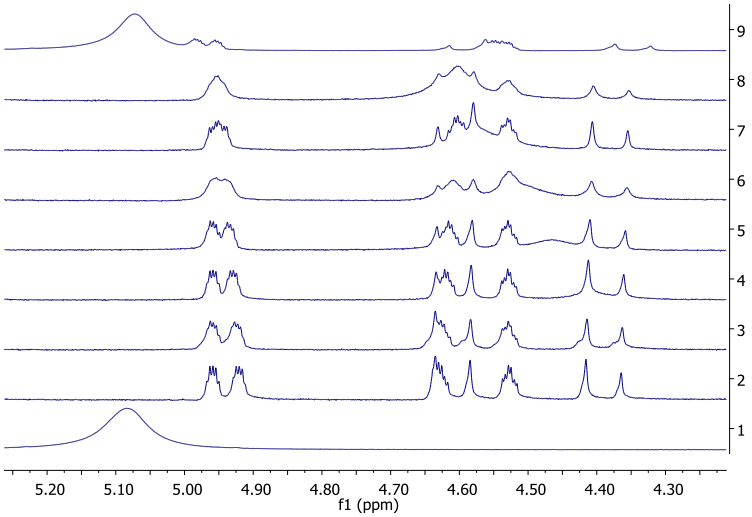

Figure 14 ^{1}H-NMR (300 MHz, $CDCl_3$) urea protons; **(*R*)-16a** + ethyleneurea, **17**. Ethylene urea spectrum 1; free **(*R*)-16a** spectrum 2; **(*R*)-16a** + 0.35 molecular equivalent of **17** spectrum 3; ; **(*R*)-16a** + 1.1 molecular equivalent of **17** spectrum 4; ; **(*R*)-16a** + 1.8 molecular equivalent of **17** spectrum 5; ; **(*R*)-16a** + 2.7 molecular equivalent of **17** spectrum 6; ; **(*R*)-16a** + 3.6 molecular equivalent of **17** spectrum 7; **(*R*)-16a** + 4.5 molecular equivalent of **17** spectrum 8; **(*R*)-16a** + 20 molecular equivalent of **17** spectrum 9.

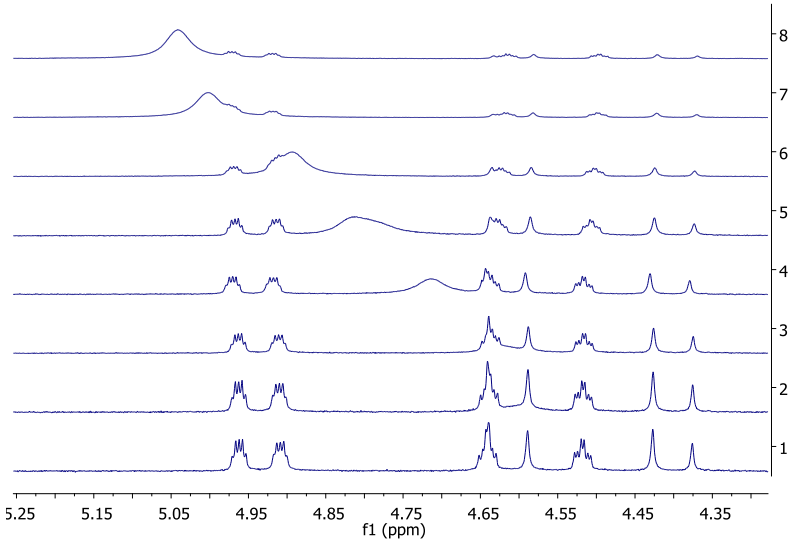

Figure 15::^{1}H-NMR (300 MHz, $CDCl_3$) amide protons of **(*R*)-16a** + 2,2' ethyl propyleneurea, **18**. free **(*R*)-16a** spectrum 1; **(*R*)-16a** + 0.6 molecular equivalent of **18** spectrum 2; ; **(*R*)-16a** + 1.1 molecular equivalent of **18** spectrum 3; ; **(*R*)-16a** + 2.6 molecular equivalent of **18** spectrum 4; **(*R*)-16a** + 4.5 molecular equivalent of **18** spectrum 5; **(*R*)-16a** + 10.5 molecular equivalent of **18** spectrum 6; **(*R*)-16a** + 18 molecular equivalent of **18** spectrum 7; **(*R*)-16a** + 22.2 molecular equivalent of **18** spectrum 8.

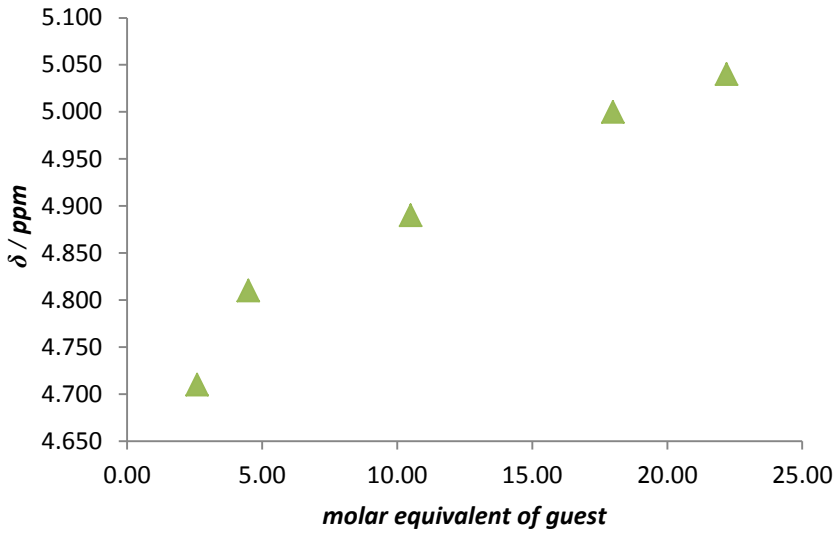

Figure 16 Chemical shift of the urea protons of **18** *vs.* the molar equivalents of guest added.

Bulky guests **19** and **(*R*)-20** do not give any evidence of hydrogen bonding. Upon addition of up to 15 molar equivalents the chemical shift of the two protons did not change (Figures 17 and 18). In the case of barbital the peak did not shift even upon the addition of a large excess of guest. No change is observed also in the spectra of the guests.

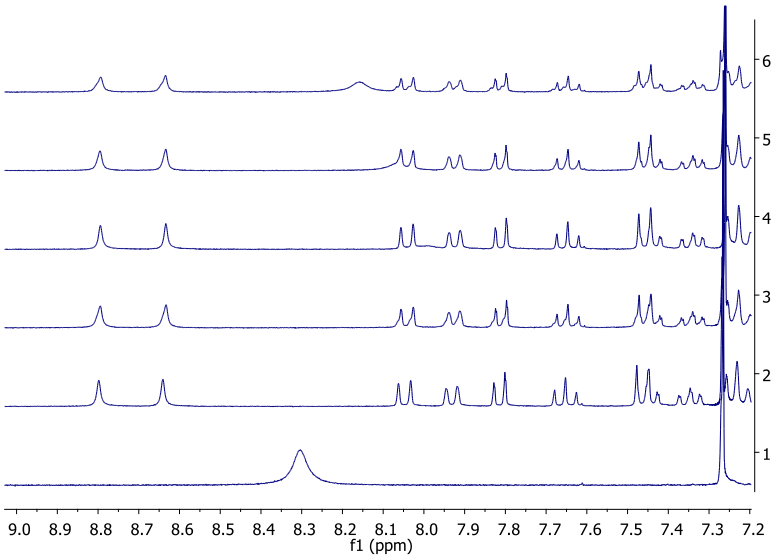

Figure 17 : ^{1}H-NMR (300 MHz, $CDCl_3$) amide protons of **(*R*)-16a** + barbital, **19** spectrum 1; free **(*R*)-16a** spectrum 2; ; **(*R*)-16a** + 0.1 molecular equivalent of **19** spectrum 3; ; **(*R*)-16a** + 0.5 molecular equivalent of **19** spectrum 4; **(*R*)-16a** + 1 molecular equivalent of **19** spectrum 5; **(*R*)-16a** + 2 molecular equivalent of **19** spectrum 6.

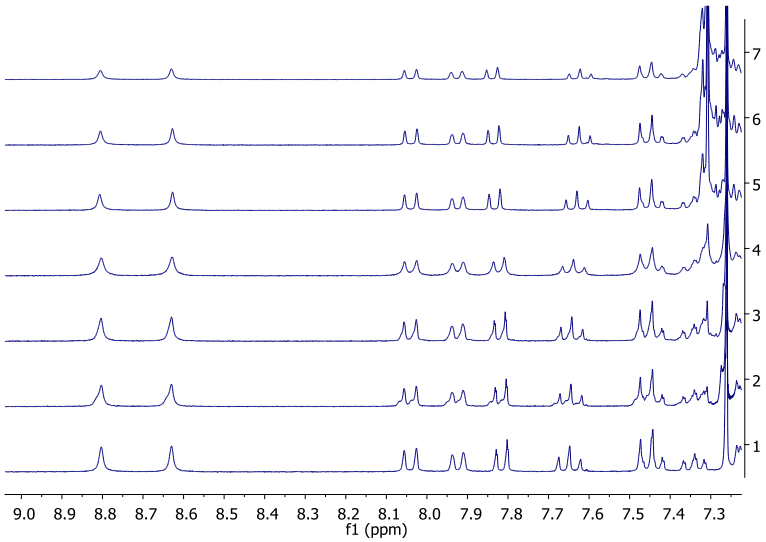

Figure 18: : ^{1}H-NMR (300 MHz, $CDCl_3$) amide protons of **(*R*)-16a** + (*R*)-2-Phenyl-butyrric acid, **20**, free **(*R*)-16a** spectrum 1; **(*R*)-16a** + 0.5 molecular equivalent of **20** spectrum 2; **(*R*)-16a** + 1 molecular equivalent of **20** spectrum 4; **(*R*)-16a** + 2 molecular equivalent of **20** spectrum 5; **(*R*)-16a** + 7 molecular equivalent of **20** spectrum 5; **(*R*)-16a** + 12 molecular equivalent of **20** spectrum 6; **(*R*)-16a** + 15 molecular equivalent of **20** spectrum 7.

3.4.2 Macrocycle (*R*)-16b

(*R*)-16b possesses a larger cavity which allows the amide protons to be more accessible by molecules of solvent, leading to the signals of the amide protons being broader than the corresponding signals in **(*R*)-16a** (Figure 19).

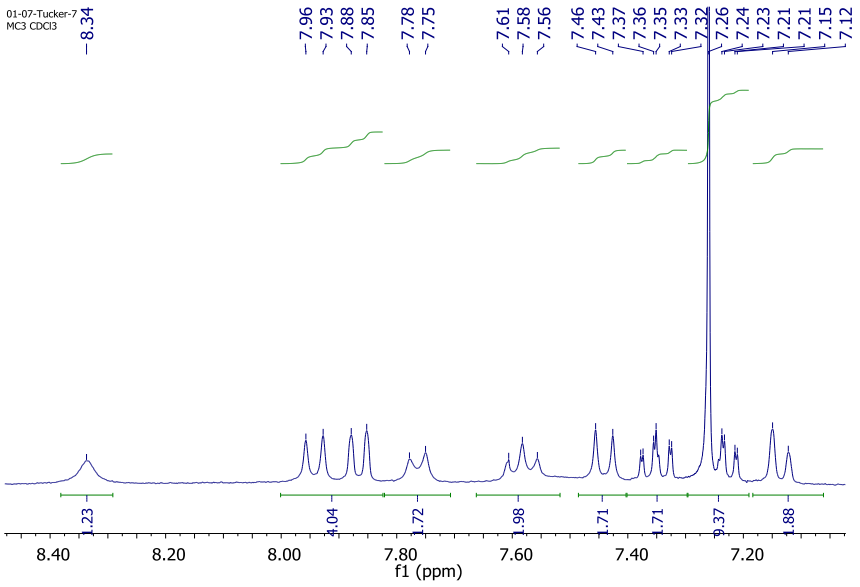

Figure 19 ^{1}H-NMR of **(*R*)-16b** (300 MHz, $CDCl_3$) aromatic region.

Nevertheless, interactions between **(*R*)-16b** and the two enantiomers of the chiral guest 2-Phenyl-butanoic acid, **20** could be qualitatively assessed by following the signal of the exchangeable amide protons (Figures 20 and 21).

The upfield shift experienced by the signal for one of the amides undergoes (red arrows Figures 20 and 21) seems to contradict an interaction based on H-bond donation from the host to the guest. However, the second amide proton, which in the spectrum of the free host is not recognisable, shows a downfield shift (blue arrows, Figures 20 and 21). Even though the changes in the spectra are rather subtle, the shift is demonstrated by the disappearance of an aromatic signal due to the overlapping with the broad amide signal. The evident upfield shift, (max $\Delta\delta \approx 0.2$ ppm) of the other amide proton could, therefore, be explained by a shielding effect by the phenyl ring on the guest. During these experiments the guests were dissolved in a stock solution of the host, in order to avoid shifts of the amide proton signals due to the concentration. The magnitude of the shift is comparable for the same concentration of each enantiomer added, demonstrating that the interaction is not enantioselective.

A preliminary NMR assessment of the interaction between the macrocycle **(*R*)-16b** and ethylene urea, **17**, displayed a rather small downfield shift ($\Delta\delta \approx 0.19$ ppm) of the amide proton upon the addition of 11 equivalents of **17** (from a stock solution of the host). The spectra are shown in the appendixes (Figure 46 in the Appendix). However, the signal for the other amide proton signal is not identifiable in the spectrum and therefore it is not clear if it would undergoes a larger downfield shift upon the addition of guest.

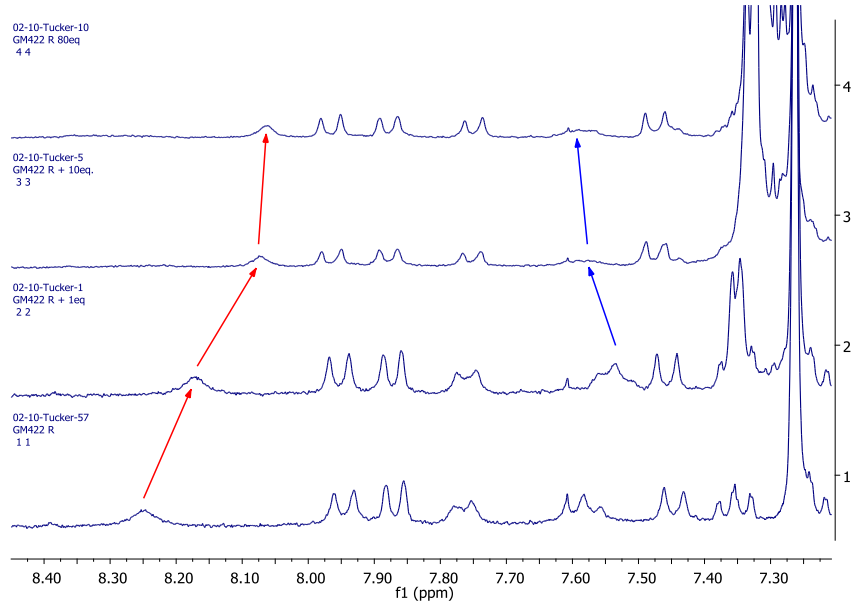

Figure 20 ^{1}H-NMR (300 MHz, $CDCl_3$) amide protons of **(*R*)-16b**+ (*R*)-2-Phenyl-butyrric acid, **(*R*)-20**, free **(*R*)-16b** spectrum 1; **(*R*)-16b** + 1 molecular equivalent of **(*R*)-20** spectrum 2; **(*R*)-16b**+ 10 molecular equivalent of **(*R*)-20** spectrum 3; **(*R*)-16b** + 50 molecular equivalent of **(*R*)-20** spectrum 4.

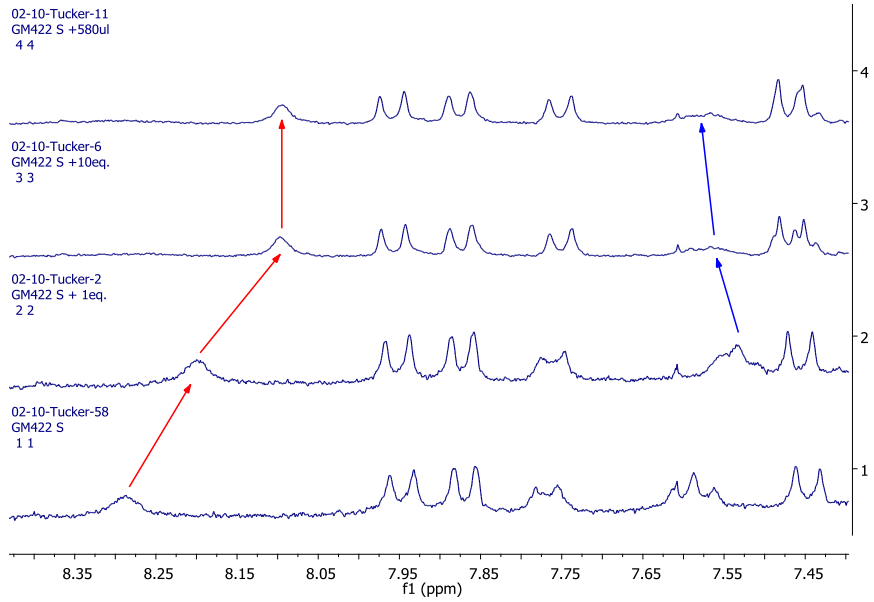

Figure 21 ^{1}H-NMR (300 MHz, $CDCl_3$) amide protons of **(*R*)-16b** + (*S*)-2-Phenyl-butyrric acid **(*S*)-20**, free **(*R*)-16b** spectrum 1; **(*R*)-16b** + 1 molecular equivalent of **(*S*)-20**spectrum 2; **(*R*)-16b** + 10 molecular equivalent of **(*S*)-20**spectrum 3; **(*R*)-16b** + 50 molecular equivalent of **(*S*)-20**spectrum 4.

3.5 Electrochemistry

Both the hosts showed a rather high potential (>900 mV *vs.* decamethylferrocene) due to the presence of two electron-withdrawing groups on the ferrocene. For this reason ferrocene was used as the internal reference allowing smaller potential windows for the analysis. The potentials of the two hosts *vs.* Fc and dmfc are shown in Table 1.

Table 1 Electrode potential of the two macrocycles *vs.* ferrocene (Fc) and decamethylferrocene (dmfc) in 0.1 M TBA·PF_6 in dcm determined by SWV (± 2mV). [a] determined by CV (±5 mV).

	Fc	**dmfc**
(*R*)-16a	453	1000[a]
(*R*)-16b	430	972

3.5.1 Macrocycle (*R*)-16a

Cyclic voltammetry of **(*R*)-16a** displayed electrochemical reversibility in dichloromethane with anodic peak current proportional to the square root of the scan rate. In addition to this, the anodic and cathodic peak currents were approximately the same magnitude (i_{pc}/i_{pa} *ca*. 1.08).

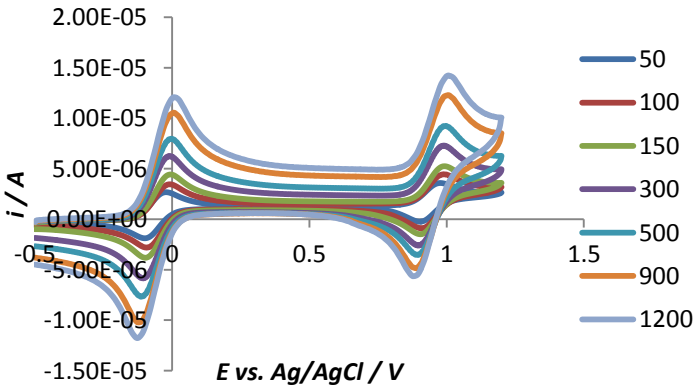

Figure 22 Cyclic voltammograms of **(*R*)-16a** in 0.1 M TBA·PF_6 in dcm, dmfc internal reference at different scanrates as indicated in the legend.

Addition of aliquots of ethylene urea, **17**, caused a negative shift in the electrode potential. The direction of the shift is in agreement with the formation of the host-guest system based on H-bonds.[11] As already demonstrated by the NMR studies, the host acts as an H-bond donor through the amide proton on the ferrocene side. For this reason the interaction with the guest causes the electron cloud to increase around the ferrocene unit. This results in a lower potential being needed to oxidise the redox unit compared to the free host. However, the shift obtained is rather small, upon the addition of more than 40 molar equivalents of ethylene urea, **17**, the potential decreased by ca. 20 mV (Figure 23).

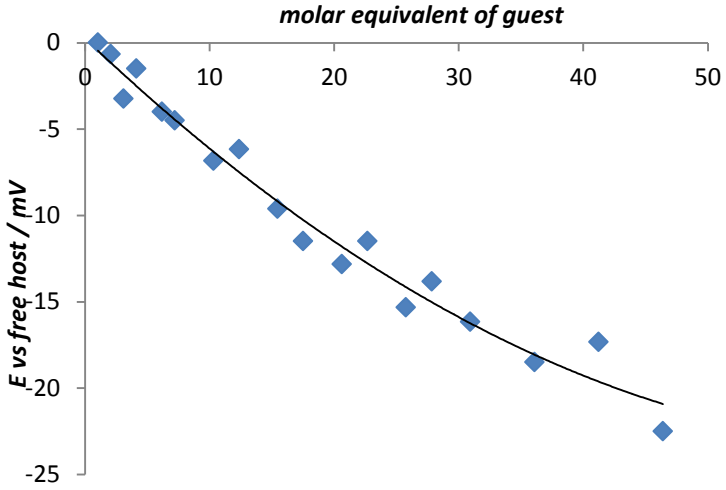

Figure 23 Electrode potential of **(*R*)-16a** *vs.* molar equivalents of ethyleneurea, **17**, added. Determined by CV in a 0.1 M dcm solution of TBA·PF_6 and dmfc as internal reference.

Considering the NMR titration of **(*R*)-16a** with (*R*)-phenylbutirric acid, **(*R*)-20** which did not show any change in the spectrum of the hosts, it is not surprising that a square wave voltammetric titration of this host with both the enantiomers of phenylbutirric acid did not show any shift in potential (Figure 24), proving the cavity was small to interact with this bulky guest.

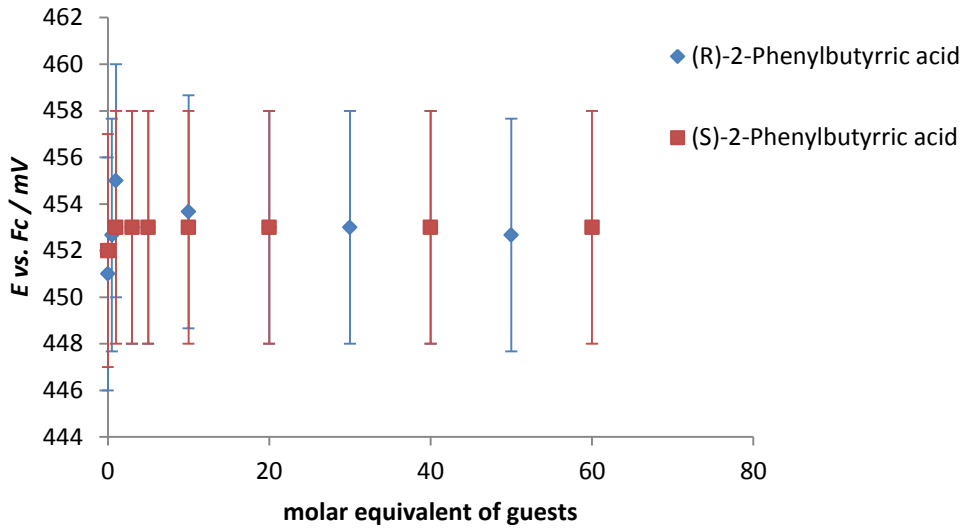

Figure 24 Electrode potential of **(*R*)-16a** upon the addition of the two enantiomers of 2-Phenylbutyrric acid, **(*R*)-20** and **(*S*)-20**.

3.5.2 Macrocycle (*R*)-16b

Cyclic and square wave voltammetric studies in dichloromethane showed (Figure 25) that **(*R*)-16b** also displayed electrochemical reversibility, with the peak current proportional to the square root of the scan rate.

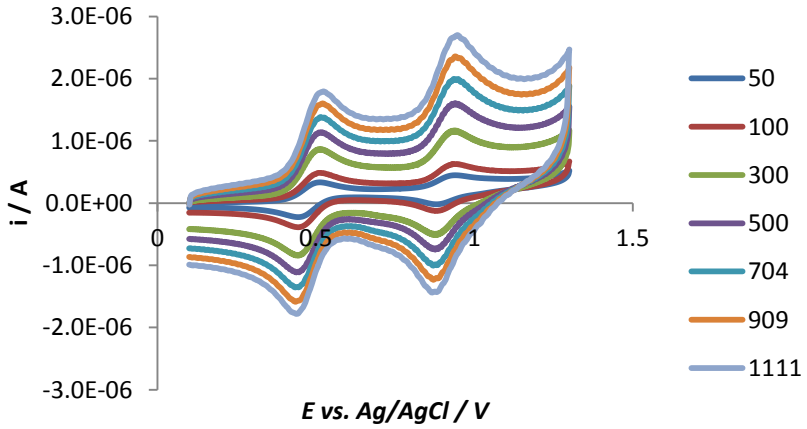

Figure 25 Cyclic voltammograms of **(*R*)-16b** in 0.1 M TBA·PF_6 in dcm, dmfc internal reference at different scanrates as indicated in the legend.

On the addition of ethylenurea, **17**, an unexpected *two-wave* behaviour was observed, with a new wave growing at higher potentials with respect to the free host (Figure 26). The positive shift is not in agreement with an H-bonding interaction on the ferrocene side; such an interaction, as shown previously, is associated with a negative shift in the potential. A positive shift may mean that the host binds the guest on the Binol side donating H-bonds, and at the same time acting as an H-bond acceptor to the pyridine nitrogens. The latter interaction is then reflected by the potential of the ferrocene unit. Upon the addition of 20 molar equivalents of **17** the system becomes more irreversible (**Figure 26**).

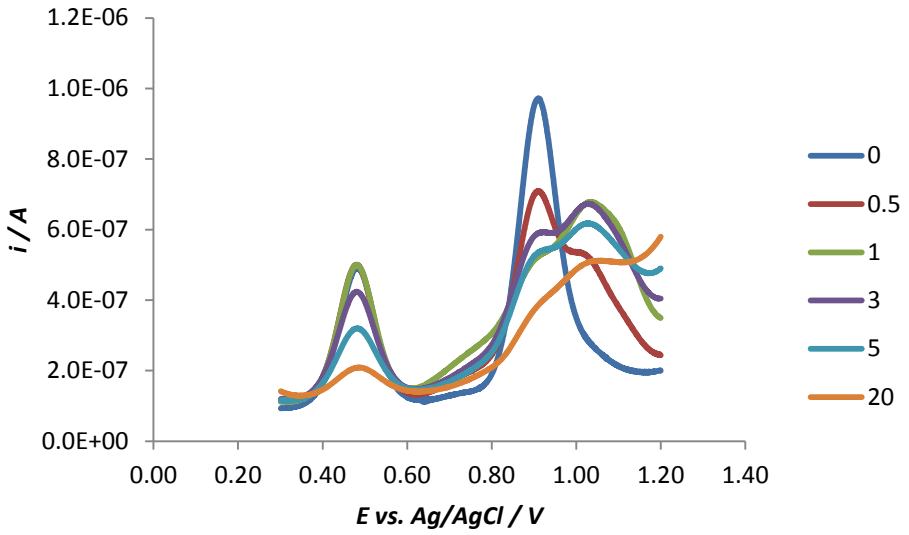

Figure 26 Square wave voltammetric titration of **(*R*)-16b** with ethylene urea, **17**. In 0.1 M TBA·PF_6 in dcm and ferrocene as internal reference.

Studies on the enantioselectivity of **(*R*)-16b** have been carried out using phenyl butyrric acid, **20** as a guest. As already shown via NMR, **(*R*)-16b** displays a moderate interaction with **20**. This interaction is confirmed by square wave voltammetry, with the redox unit undergoing a positive shift upon the addition of aliquots of the two enantiomers of the guest. However, the shift is small with a max shift of ca. 10 mV and, as shown in Figure 27, the binding was not enantioselective.

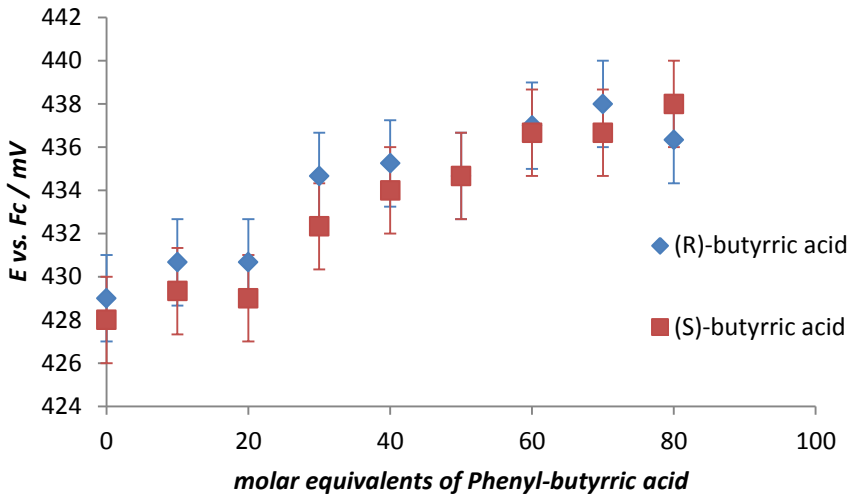

Figure 27 Electrode potential of **(*R*)-16b** upon the addition of **(*R*)-20** and **(*S*)-20**, determined via SWV (±2 mV).

As in the case of **17** a positive shift of the potential can be explained by an interaction between the acidic proton of the carboxylic group of the guest and the pyridine nitrogen of the host, while the carbonyl group might interact with the amide proton on the side of the Binol unit of **(*R*)-16b**.

The interaction of **(*R*)-16b** with another chiral guest, mandelic acid, **21** was also assessed with square wave voltammetry. As for the other guests studied with **(*R*)-16b**, the addition of each enantiomer of mandelic acid, **21** caused a positive shift in the electrode potential (Figures 28 and 29).

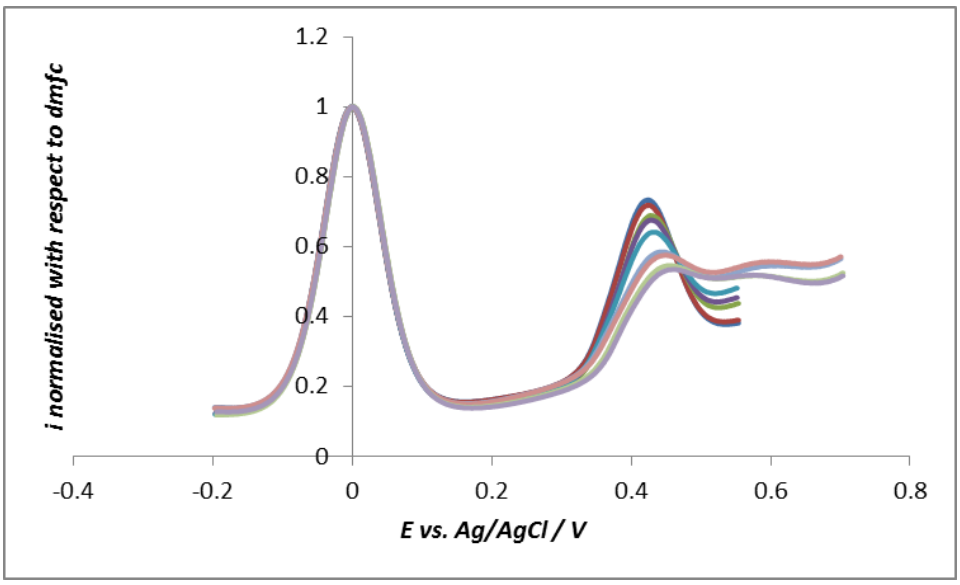

Figure 28. Square wave voltammetric titration of **(*R*)-16b** with ethylene urea, **(*R*)-21**. In 0.1 M TBA·PF_6 in dcm and ferrocene as internal reference.

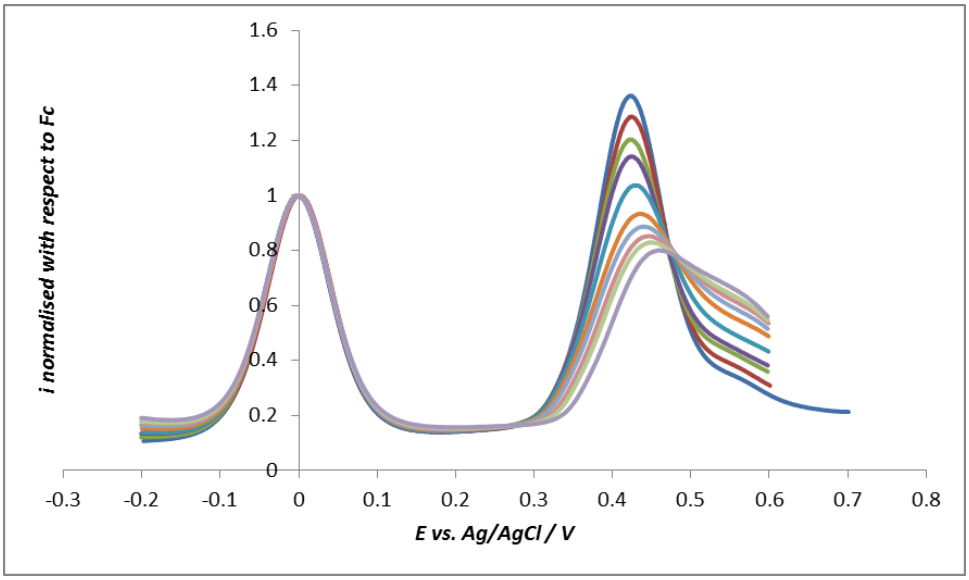

Figure 29. Square wave voltammetric titration of **(*R*)-16b** with ethylene urea, **(*S*)-21**. In 0.1 M TBA·PF_6 in dcm and ferrocene as internal reference.

Both the enantiomers of **21** caused a positive shift in the potential. Furthermore, the magnitude of the shift is slightly different and allows each enantiomer to be distinguished, although the effect is minimal (Figure 30).

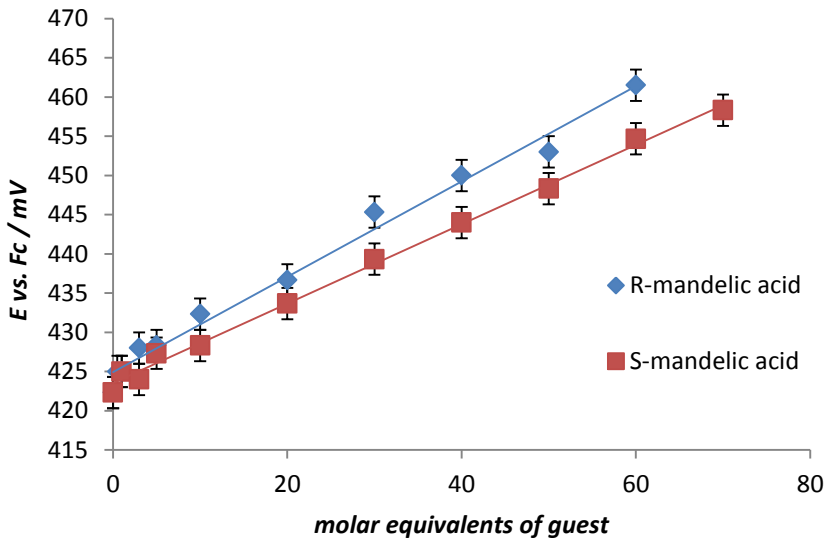

Figure 30 Electrode potential of **(*R*)-16b** upon the addition of different molar equivalents of mandelic acid, **21**. Determined by SWV (±2 mV) in a 0.1 M dcm solution of TBA·PF_6 and ferrocene as internal reference.

3.6 Interaction with other solvents: dmso and acetonitrile

During binding studies it is desirable to avoid solvents that may compete with the analyte in binding the host. Competitive solvents generally reduce the binding constant of the host-guest interaction. In some cases however, very strong interactions between host and guest do not allow the constant to be determined in non-competitive solvents.[19]

Dimethyl sulphoxide is a very good solvent for a vast variety of both hydrophobic and hydrophilic compounds. This is due to the fact that although it is an aprotic solvent, the S-O bond is greately polarised. When **(*R*)-16a** was dissolved in dmso the solution turned black within minutes. This appeared to be just a solvatochromic effect. As shown in Figure 31 the amide and aromatic proton signals of **(*R*)-16b** shifted upon the addition of dmso and no degradation was noted.

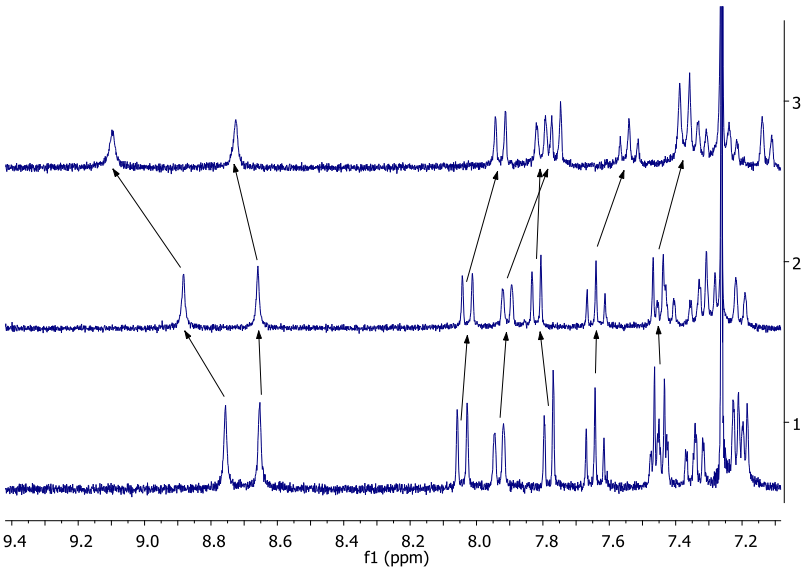

Figure 31 ^{1}H-NMR (300 MHz, $CDCl_3$) of **(*R*)-16a** upon the addition of different aliquots of dmso. Detail of the amide protons and aromatic region.

Another widely used solvent is acetonitrile, which is also an aprotic solvent with a greatly polarised bond, which allows it to be used to dissolve a vast range of analytes.

During the preliminary studies on **(*R*)-16b**, given the poor solubility of some guests in dcm, acetonitrile was used to dissolve either guests or hosts. However, when the macrocycle was dissolved in this solvent, it partially precipitated giving a red powder. Moreover, when dissolved in acetonitrile **(*R*)-16b** does not show electrochemical reversibility, as shown in Figure 32.

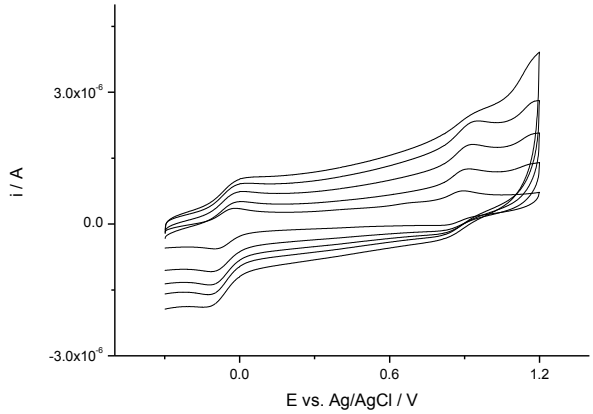

Figure 32 cyclic voltammetry of **(*R*)-16b** in a 0.1 M TBA·PF_6 solution in acetonitrile, dmfc used as internal reference.

3.7 Conclusions

The synthesis of two ferrocene-containing chiral macrocycles was accomplished. The binding site resembles the Hamilton receptors and for this reason barbiturate analytes could in principle be bound by up to 6 H-bonds. The host possess 4 protons that can be donated while it can accept two H-bonds via the lone pair on each pyridine moiety.

^{1}H-NMR studies on **(*R*)-16a** show that the two amide protons possess sharp peaks whose chemical shift does not change with the concentration. However, upon the addition of cyclic ureas their chemical shifts move downfield. It was also proved that the proton that shifts the most is the one on the ferrocene side demonstrating a preferential direction of the binding of **17** and **18**.

Bulkier guests **19** and **20** did not cause any shift of the amide proton, indicating that **(*R*)-16a** does not interact with them.

Electrochemical studies of the binding of ethylene urea, **17**, with **(*R*)-16a** showed that there is a small negative shift in the ferrocene unit potential (-20 mV) upon the addition of

up to 45 molar equivalents of guest which is the effect of the H-bond host-guest interaction. However, this shift is smaller than previously reported results.[11] Voltammograms of the titration of both the enantiomers of **20** with **(*R*)-16a** did not show any appreciable shift in the potential, confirming the absence of interaction with these guests.

(*R*)-16b has a larger cavity and for this reason the two amide protons possess broad signals the chemical shift of which is concentration dependant, and often overlap. However, upon the addition of either enantiomer of the chiral guest 2-phenylbutanoic acid one of the signals of the amide shows an unexpected upfield shift which is probably caused by a shielding effect of the phenyl ring on the guest. A subtle downfield shift of the other amide proton is also observed. In any case the effect is smaller than for **(*R*)-16a.**

Electrochemical studies show that the potential of the host shifts positively when titrated with (*R*) and (*S*)-2-phenylbutyrric acid, **20**. The direction of the shift might depend on how the guest binds to the host. As demonstrated with **(*R*)-16a**, if the guest is bound via the amide protons on the ferrocene side the potential shifts negatively upon the increase of the electronic cloud around the ferrocene unit. On the other hand the positive shift observed with this host can be explained by the guest binding the amide on the Binol side with a simultaneous H-bond donated to one pyridine unit. This would withdraw electrons from the redox unit causing a positive shift. The shift for the two enantiomers is of the same magnitude (+10 mV) and no enantioselectivity was therefore observed.

(*R*) and (*S*)-mandelic acid, **21**, also caused a positive shift in the potential. In this case the magnitude of the shifts for the two enantiomers is different, allowing chiral recognition. However, an additional wave at higher potentials is observed upon the addition of the guest.

The electrochemical titration of **(*R*)-16b** with ethylenurea, **17**, showed two-wave behaviour with a progressive loss of the reversibility upon the addition of the guest.

(*R*)-16a showed a solvatochromic effect when dissolved in dmso; on the other hand, **(*R*)-16b** was not stable when dissolved in acetonitrile.

To conclude the two macrocycles do not show an increase in selectivity compared to similar systems. This is probably due to the particular shape of the binding site, and consequently selectivity and chiral recognition could be higher with other guests, for example, chiral cyclic ethylene ureas.

3.8 References

(1) Gibson, S. E.; Lecci, C. *Angew. Chem., Int. Ed.* **2006**, *45*, 1364.
(2) Ogata, E.; Rasmusse.H *Biochemistry* **1966**, *5*, 57.
(3) Harold, F. M.; Baarda, J. R. *J. Bacteriol.* **1967**, *94*, 53.
(4) Roy, K.; Wang, C.; Smith, M. D.; Dewal, M. B.; Wibowo, A. C.; Brown, J. C.; Ma, S. G.; Shimizu, L. S. *Chem. Commun.* **2011**, *47*, 277.
(5) (a) Pedersen, C. J. *J. Am. Chem. Soc.* **1967**, *89*, 7017(b) Lehn, J. M.; Sauvage, J. P. *J. Am. Chem. Soc.* **1975**, *97*, 6700(c) Simmons, H. E.; Park, C. H. *J. Am. Chem. Soc.* **1968**, *90*, 2428(d) Park, C. H.; Simmons, H. E. *J. Am. Chem. Soc.* **1968**, *90*, 2431(e) Park, C. H.; Simmons, H. E. *J. Am. Chem. Soc.* **1968**, *90*, 2429(f) Graf, E.; Lehn, J. M. *J. Am. Chem. Soc.* **1976**, *98*, 6403(g) DeSantis, G.; Fabbrizzi, L.; Perotti, A.; Sardone, N.; Taglietti, A. *Inorg. Chem.* **1997**, *36*, 1998.
(6) (a) Kyba, E. P.; Siegel, M. G.; Sousa, L. R.; Sogah, G. D.; Cram, D. J. *J. Am. Chem. Soc.* **1973**, *95*, 2691(b) Kyba, E. B.; Koga, J.; Sousa, L. R.; Siegel, M. G.; Cram, D. J. *J. Am. Chem. Soc.* **1973**, *95*, 2692.
(7) Chang, S. K.; Hamilton, A. D. *J. Am. Chem. Soc.* **1988**, *110*, 1318.
(8) Ema, T.; Tanida, D.; Sakai, T. *Org. Lett.* **2006**, *8*, 3773.
(9) Ema, T.; Tanida, D.; Sakai, T. *J. Am. Chem. Soc.* **2007**, *129*, 10591.
(10) Carr, J. D.; Goles, S. J.; Hursthouse, M. B.; Light, M. E.; Tucker, J. H. R.; Westwood, J. *Angew. Chem., Int. Ed.* **2000**, *39*, 3296.
(11) Westwood, J.; Coles, S. J.; Collinson, S. R.; Gasser, G.; Green, S. J.; Hursthouse, M. B.; Light, M. E.; Tucker, J. H. R. *Organometallics* **2004**, *23*, 946.
(12) Saji, T.; Kinoshita, I. *J. Chem. Soc., Chem. Commun.* **1986**, 716.
(13) Medina, J. C.; Goodnow, T. T.; Rojas, M. T.; Atwood, J. L.; Lynn, B. C.; Kaifer, A. E.; Gokel, G. W. *J. Am. Chem. Soc.* **1992**, *114*, 10583.
(14) Oton, F.; Tarraga, A.; Espinosa, A.; Velasco, M. D.; Molina, P. *Dalton Trans.* **2006**, 3685.
(15) Arion, V. B.; Kravtsov, V. C.; Gradinaru, J. I.; Simonov, Y. A.; Gerbeleu, N. V.; Lipkowski, J.; Wignacourt, J. P.; Vezin, H.; Mentre, O. *Inorg. Chim. Acta* **2002**, *328*, 123.
(16) Ercolani, G.; Mandolini, L.; Mencarelli, P. *J. Chem. Soc., Perkin Trans. 2* **1990**, 747.
(17) Beer, P. D.; Graydon, A. R.; Johnson, A. O. M.; Smith, D. K. *Inorg. Chem.* **1997**, *36*, 2112.
(18) Hynes, M. J. *J. Chem. Soc., Dalton Trans.* **1993**, 311.
(19) Benesi, H. A.; Hildebrand, J. H. *J. Am. Chem. Soc.* **1949**, *71*, 2703.

4. Ferrocene receptors on gold surfaces

4.1 Self-Assembled Monolayers on Au surfaces

Self-assembling systems are constituted by molecular building blocks that spontaneously and reversibly form ordered hierarchical structures by means of non-covalent interactions.[1]

Over the past few decades, an increasing interest in monolayers formed by organic molecules has been demonstrated by the scientific community, in order to functionalise surfaces for very different purposes, e.g., sensing.[2] The first examples of studies on SAMs formed by disulphides adsorbed onto a gold surface date back to 1983.[3] However, studies on adsorbed inert and electro-active species, not necessarily organic, date back earlier.[4] Sulphur possesses a high affinity for gold, the enthalpy of the interaction is estimated to be 40-45 kcal mol^{-1}.[5] Therefore alkyl thiols and disulphides spontaneously adsorb onto gold surfaces, which results in their alkyl chains sticking out into solution.[6]

The formation of ordered SAMs not only depends on the affinity of the anchoring group for the surface, but also on Van der Waals interactions between molecular building blocks that form the monolayer. For this reason, in order to have well packed SAMs of aliphatic thiols, the alkyl chain should be of a suitable length.[5b] Monolayers of short ω-alkylthiols can be obtained with longer soaking times. However, this approach can lead to the formation of multilayers.[7] An important role in the packing of the monolayer is played by interactions between particular groups on the monolayer. For example when groups that can form H-bonds are present in the organic scaffold, the interactions between the building blocks might be expected to increase (Figure 1).[8]

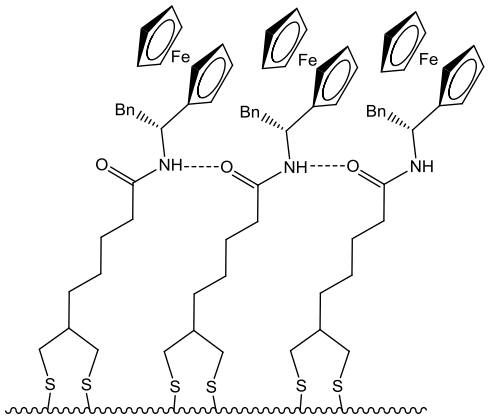

Figure 1: SAM formed by **sym** onto a gold surface

4.2 Electrochemical behaviour of diffusionless redox-active units

Electrochemically active groups attached to a surface work under diffusionless conditions, and for this reason they display different cyclic voltammograms to the free species in solution. The peak potential can be described using eq. (***4.1***)

$$E_p = E° - \frac{RT}{nF} \ln\left(\frac{b_O \Gamma_O}{b_R \Gamma_R}\right) \qquad (\textbf{\textit{4.1}})$$

Here E_p is the peak potential, $E°$ the standard potential of the species in solution and b_O, b_R, Γ_O and Γ_R are the adsorption coefficients and the surface coverages for the oxidised (*O)* and the reduced (*R)* form respectively. From this formula it is evident that if the species does not desorb during the redox process (i.e. $b_O = b_R$ and $\Gamma_O = \Gamma_R$) then the peak potential will correspond to the potential of the species in solution, this with the assumption that b_O and b_R do not vary with the scanning potential (Figure 2).[9]

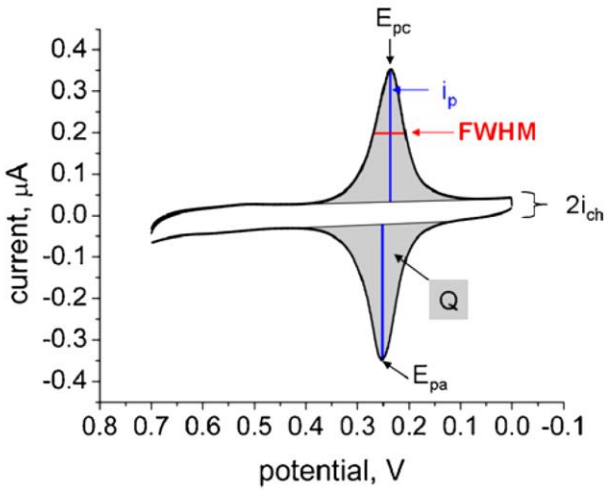

Figure 2. Schematic representation of a cyclic voltammogram of speciaes under diffusionless conditions.

As the scan-rate increases, however, a separation of the anodic and cathodic peaks is observed due to the non-rigidity of the linkage unit which allows a certain mobility of the redox unit. From this separation it is possible to determine the rate constant for electron transfer k_{ET}.[10]

$$k_{ET} = \frac{\alpha n F v_c}{RT} = (1-\alpha)\frac{\alpha n F v_a}{RT} \qquad (\textbf{4.2})$$

Here α is the transfer coefficient, and ideally is = 0.5. This parameter gives an indication on how symmetrical the electron transfer process is. *n, F, R* and *T* have their usual meanings while v_a and v_c are the scan-rate if we consider the anodic and cathodic peaks respectively.

At low scan-rates the anodic and the cathodic peaks of strongly adsorbed species fall at the same potential since they are not conditioned by mass transport and diffusion in solution. The shape and the potential of the peaks depends on the packing of the molecule on the surface. In some cases a spacer is added to the solution in order to separate the electro-active units; this leads to different patterns for the arrangement of the molecules on the surface that may affect the potential.[11]

In addition to the shape of the voltammograms, further evidence for the formation of a monolayer of electrochemically reversible redox-active units is the peak current being proportional to the scan-rate, according to equation (***4.3***).[12]

$$i_p = \frac{n^2F^2}{4RT}\nu A\Gamma \qquad (4.3)$$

Here i_p is the peak current in Amperes, ν the scan-rate in V/s and A the geometrical area of the electrode in cm^2.

This differs from the behaviour of systems in solution where, as already described in previous chapters, the peak current is proportional to the square root of the scan-rate.

Moreover, the presence of a monolayer (either electro-active or electro-inert) affects the electrochemical behaviour of other species in solution. The experiments described in this chapter were carried out in dcm in the presence of decamethylferrocene as internal reference. The monolayer on the electrode causes the separation between anodic and cathodic peaks (ΔE_p) of the diffusing species to increase to more than 59 mV, which is the expected value for ideal reversible systems under diffusion control. Assuming a one-electrode process and using equation (***4.4***), it is possible to evaluate the surface coverage from the quantity of charge exchanged during the oxidative process that is proportional to the area underneath the anodic peak.

$$\Gamma = \frac{Q}{nFA} \qquad (4.4)$$

Here Γ is the surface coverage, Q the quantity of charge exchanged during the redox process (in Coulombs) n the number of electron involved and A the geometrical surface area of the electrode (cm^2).

Theoretical coverage has previously been estimated for closely packed monolayers of ferrocene, approximating the bulky ferrocene units to spheres of 3.3 Å radius, and the value found of 4.5×10^{-10} mol / cm^2 was taken as maximum coverage possible for a monolayer.[13] Higher coverage values can be explained by the formation of multilayers.

Positive and negative interactions between the molecular units forming the monolayer change the shape of the peaks. In general, in the presence of positive interactions, i.e. when building blocks attract each other (e.g. H-bonds, Figure 1), the peaks appear narrower and sharper than the peak in the ideal case. By contrast, in the presence of negative interactions, i.e. repulsive, the peaks will be broader and flatter than the ideal case.[11] An estimation of these interactions and of the shape of the peaks can be done considering the full width of the half maximum high (*FWHM)* of the peak, according to eq. (***4.5***) which gives the value of the ideal case.

$$FWHM = 3.53\frac{RT}{nF} = \frac{90.6}{n} \qquad (\textbf{\textit{4.5}})$$

4.3 Ferrocene SAMs

Self-assembled monolayers of ω-alkyl thiols equipped with a reporting group bound to the α position have been widely described in the literature.[14] In particular gold electrodes have been functionalised with ferrocene-containing thiols[15] and disulphides[16] in order to exploit redox-processes in determination electron transfer kinetics as a means characterising the surface. There are now a number of examples of ferrocene based SAMs used for sensing applications.[16] In electrochemical sensing, in some cases (when double armed ferrocene thiols were examined Figure 3) an amplification of the sensing ability was found compared to the same species in solution due to the formation of a pseudo-macrocyclic species.[2b] An

earlier example of a receptor for catechol and indole, adsorbed on a gold electrode was also reported.[17]

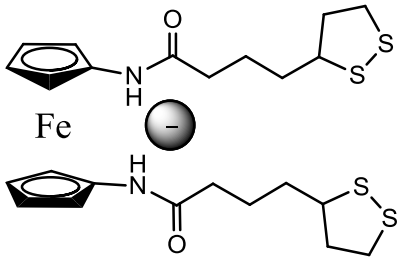

Figure 3: (*rac*)-lipoic acid used as tether unit in anion sensors self-assembled onto a gold surface

Usually functionalization occurs by soaking the electrode in a solution of the ferrocene thiol. Despite the fact that electrode functionalization is widely reported, the is no common consensus on the soaking time, which ranges from minutes[18] to several hours.[19] Moreover, the surface coverage is also affected by the roughness of the surface and also by the solvent in which the compound is dissolved.[12] Furthermore, in SAMs formed by ferrocene alkyl thiols with chains of different length, the redox unit can change its position upon the oxidation process.[20]

4.4 Lipoic acid as anchor group for SAMs on gold and synthesis of isolipoic acid

The naturally occurring *R* isomer of lipoic acid is a cofactor for many enzymes in which its disulphide is reduced to a dithiol.[21] Lipoic acid is commercially available as a racemic mixture and it has proven to be a better anchoring group for the immobilisation of organic molecules onto gold surfaces compared to analogous thiols due to the presence of two sulphides.[22] However, with the growing demand of chiral functionalised SAMs[23] a control over the absolute configuration of the thiol is strongly desirable. So far in cases where the stereochemistry plays a fundamental role, alkyl thiols have been used instead of lipoic acid.

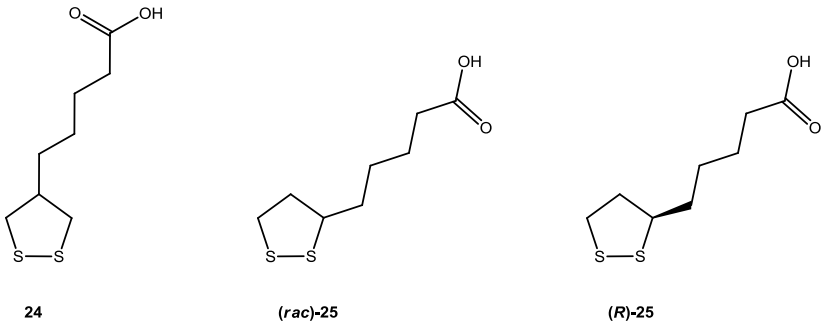

24 (*rac*)-25 (*R*)-25

Figure 4: isolipoic acid, (*rac*)-lipoic acid and (*R*)-lipoic acid

4.5 Aim of the studies and SAMs preparation

Isolipoic acid is an achiral version of the lipoic acid and, until recently, it had only been reported once as a tether unit[24] probably due to the rather laborious procedure to prepare it.[25] For this reason it was decided to undertake a relatively easier multistep preparation of this compound. The improved synthetic pathway implemented in Moody's group in Nottingham involved a nucleophilic substitution between diethyl malonate and 6-bromo-1-hexane, the malonate obtained was reduced to the diol. The diol was then converted into the mesilate, this step is the only one that involves chromatographic purification, all the other products can be obtained pure by distillation. The olefin was then oxidised with oxone and osmium tetroxide. The disulphide is then obtained by treatment of the carboxylic acid obtained with sulphur and sodium sulphite hydrate. The full pathway is shown in Scheme 1**.**

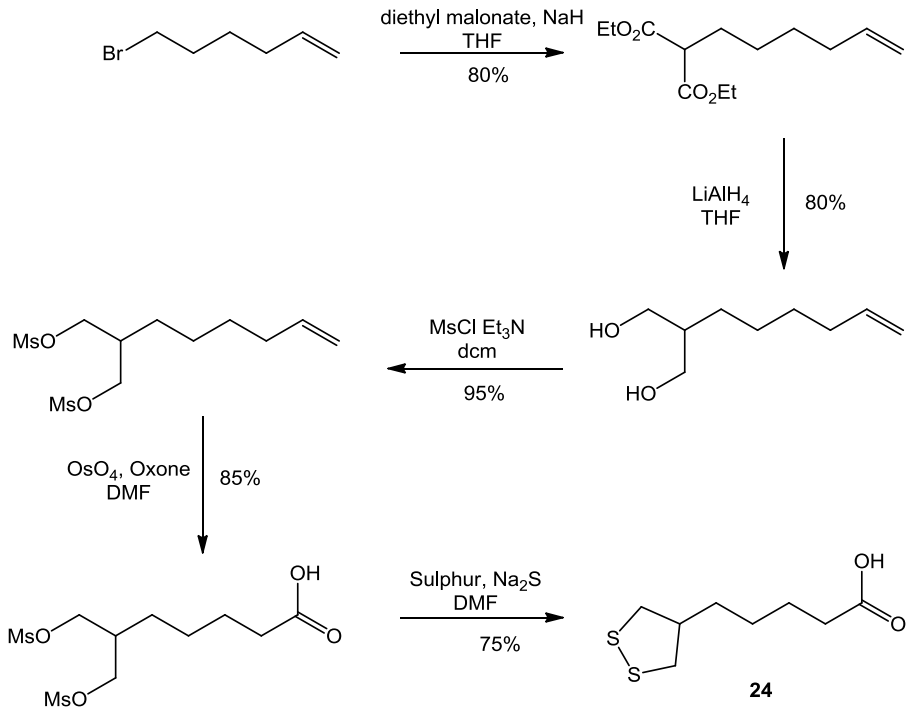

Scheme 1. Synthetic pathway to obtain isolipoic acid

Different chiral ferrocene lipoil amides **26, (*rac*)-27** and **(*R*)-27** have been prepared by Kevin Joly in Prof. Moody's group from isolipoic acid **24**, (*rac*)-lipoic acid, **(*rac*)-25**, and (*R*)-lipoic acid, **(*R*)-25**, using an amide coupling reaction with the chiral amine **(*R*)-1a**[26] (Scheme 3, Chapter 2).

In this chapter the recently reported results[27] on the electrochemical assessment of the self-assembled monolayers (SAMs) formed by **26, (*rac*)-27** and **(*R*)-27** onto monocrystalline gold surfaces are described in order to determine whether **26** can form SAMs in a similar fashion to analogous compounds **(*rac*)-27** and **(*R*)-27**. Preliminary ellipsometry results for determining the thickness of the monolayer are also discussed in this chapter. In order to estimate the maximum coverage of the surface obtained with the monolayers formed by the different compounds under study, no diluent (i.e. non-electroactive lipoic acid) was added to the solutions.

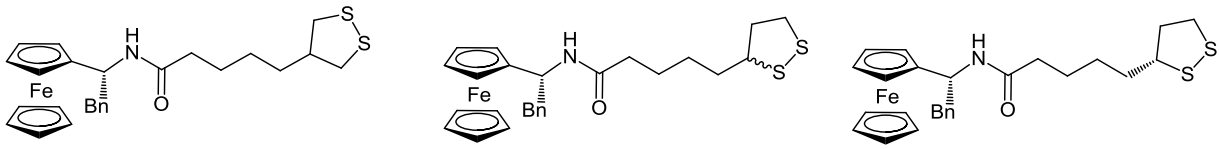

26 **(*rac*)-27** **(*R*)-27**

Figure 5. 26, **(*rac*)-27** and **(*R*)-27** amide obtained from amide coupling of **(*R*)-1a** with **24**, **(*rac*)-25** and **(*R*)-25**

SAMs of these compounds were prepared by soaking a gold electrode in dcm solutions of **26, (*rac*)-27** and **(*R*)-27** (ca. 1.5 mM). The electrode was previously mechanically polished on alumina slurry and then cleaned electrochemically in a solution of 1 M of sulphuric acid by cycling the potential several times.

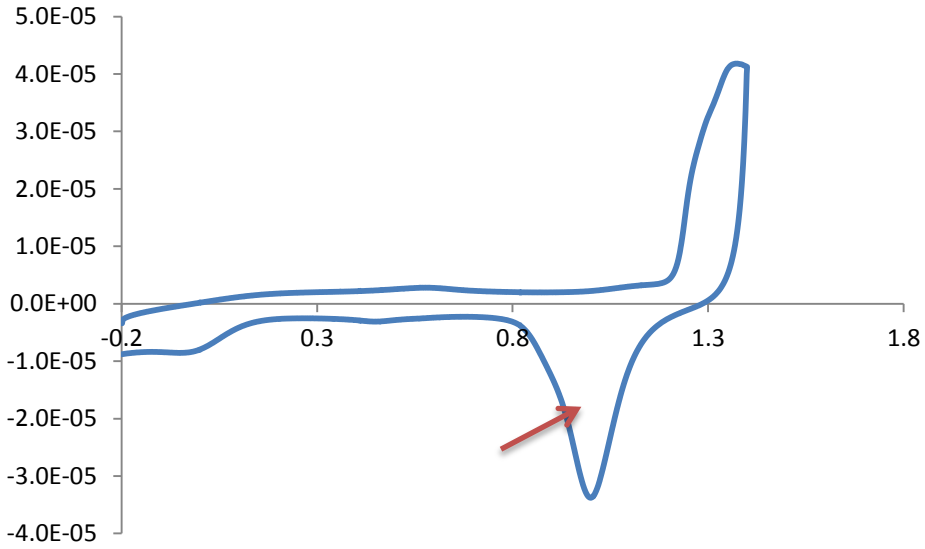

Figure 6. Cyclic voltammogram of the bare electrode in $H_2SO_{4\,(aq)}$ 0.1 M. From the area of the Au_2O_3 reductive desorbtion cathodic peak the roughness of the electrode surface can be evaluated. Red arrow indicates the reduction process of the gold oxide monolayer.

In this chapter we will refer to the geometrical area of the electrodes, however the roughness of the surface determines the formation and the packing of the monolayers. The real extension of the surface (and therefore its roughness) can be evaluated using different techniques, but most of these are *ex situ* (e.g. X-ray diffraction, microscopy).[28] In this case we preferred an *in situ* evaluation of the roughness of the surface directly from the pre-

treatment of the electrodes by determination of the Au_2O_3 monolayer formed during the oxidation process in an aqueous solution of sulphuric acid 0.1 M (Figure 6).[29] It was estimated that to reduce this thin oxide monolayer required a total quantity of current of 482 μC cm^{-2}.[30] Therfore form this value and considering the charge actually used during the cathodic process (red arrow, Figure 6) it is possible to determine the real area of the surface. The ratio between the real area and the geometrical area is the roughness coefficient. For the electrodes used it was evaluated to be ca. 2.

4.6 Cyclic voltammetry in dichloromethane

The polycrystalline gold electrodes were functionalised by soaking them in dichloromethane solutions (*ca.* 1.5 mM) of **26, (*rac*)-27** and **(*R*)-27**, in the dark at room temperature. Different soaking times were tried from a few minutes to several hours. They were then rinsed with dcm, dried and used in the electrochemical cell as working electrodes.

The results shown below in Table 1 refer to monolayers formed by soaking the electrode several hours (7-24h) in order to obtain an estimation of the maximum coverage of the surface. The three compounds studies showed comparable surface coverage calculated from eq. (***4.4***).

Table 1. [a] electrode potential of the species calculated from the CV in dcm vs. dmfc; [b] difference between anodic and cathodic peak; [c] ratio between anodic and cathodic peak currents; [d] surface coverage calculated from the area underneath the anodic wave.

	E°' / mV[a]	ΔE_p / mV[b]	i_{pa} / i_{pc}[c]	Γ / *mol* cm^{-2} [d]
26	579	45	0.95	3.0-4.4 × 10^{-10}
(*rac*)-27	532	38	1.01	3.0-4.3 × 10^{-10}
(*R*)-27	532	34	1.00	2.3-4.0 × 10^{-10}

In dichloromethane the voltammograms of the redox-active SAMs reflect the diffusionless condition of the redox units. The anodic and cathodic peaks occur at similar potentials (Table 1) and they are less than the peak separation expected for reversible species in solution. Besides, the formation of electrochemically reversible SAMs is proven by the linear dependence of the peak current with the potential scan-rate (Figure 7, Figure 8 and Figure 9) as determined from eq. (***4.3***).

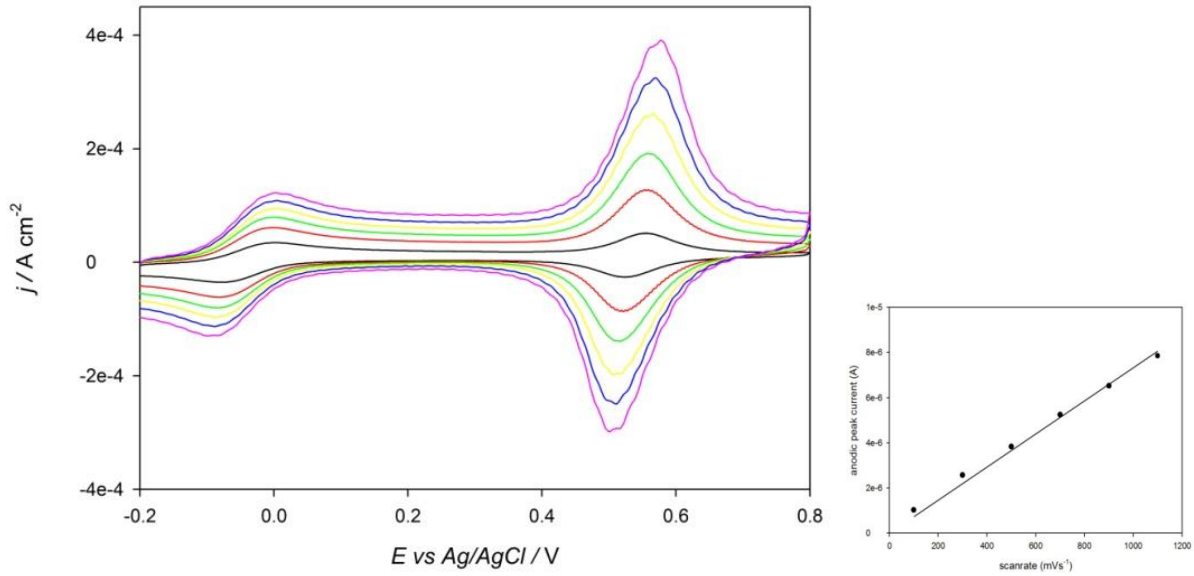

Figure 7. a) Cyclic voltammogram of a SAM of **26** on the gold working electrode in dcm (TBA·PF_6 0.1 M) *vs.* Ag/AgCl reference electrode and Pt wire as counter electrode. **b)** Potential scan-rate vs. peak current dependence.

Further evidence that the compounds give reversible electrochemistry is that the ratios between the anodic and the cathodic peaks are ca. 1 for all of the compounds studied. (Table 1).

From the peak separation it is also possible to determine the rate constant for electron transfer using Laviron's method as used by Schiffrin,[10-11,31] obtaining 45±2 s^{-1}, 44±6 s^{-1} and 39±1 s^{-1} respectively for **26, (*rac*)-27** and **(*R*)-27**. However, these values should only be used

for a comparison, since the peak separation is relatively small and the rate constant is more precise when large (ΔE > 200 mV, i.e. slower ET).[10] Moreover, the experiments were carried out without applying any ohmic drop correction. The IR-drop (ohmic drop) is a drop in the potential due to the current passing through a resistance. In these experiments the dcm electrolyte solutions act as resistance for the current passing through them. The effect of the potentials drop on a reversible species strongly adsorbed onto a surface is to shift the anodic peak to more positive potential and the cathodic peak to more negative potentials, these shifts increase with the scan-rate, giving similar voltammograms to those of quasi-reversible species. It has been demonstrated[32] that the errors made by calculating the rate constant from linear potential sweep voltammetric techniques, like cyclic voltammetry, are comparable to the effect of the ohmic drop.

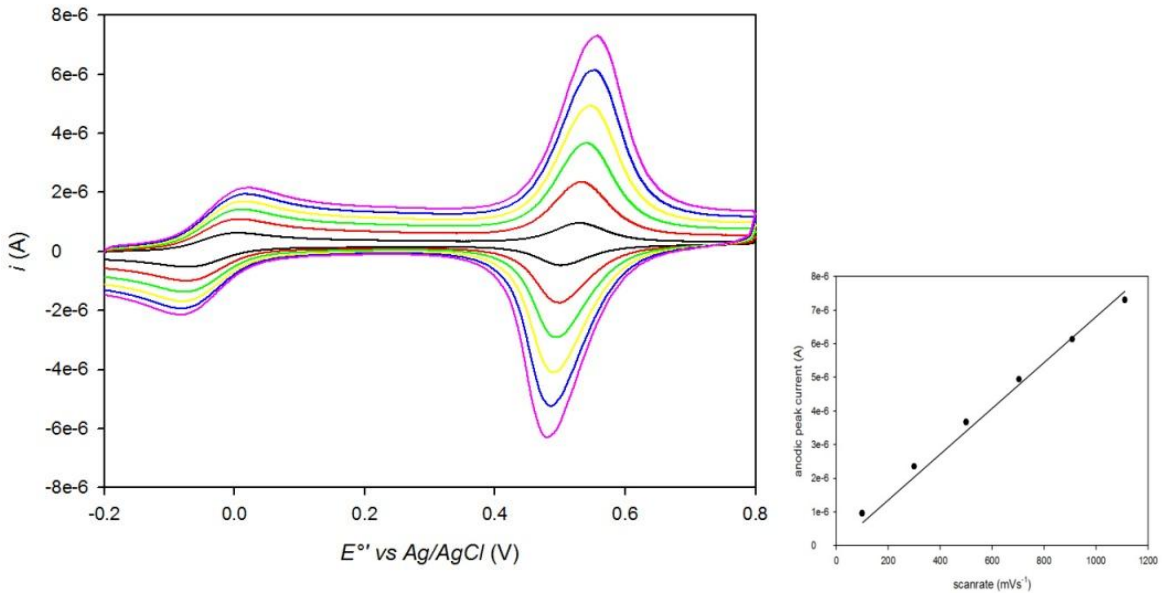

Figure 8. a) Cyclic voltammogram of a SAM of **(*rac*)-27** on the gold working electrode in dcm (TBA·PF_6 0.1 M) *vs*. Ag/AgCl reference electrode and Pt wire as counter electrode. **b)** Potential scan-rate vs. peak current dependence.

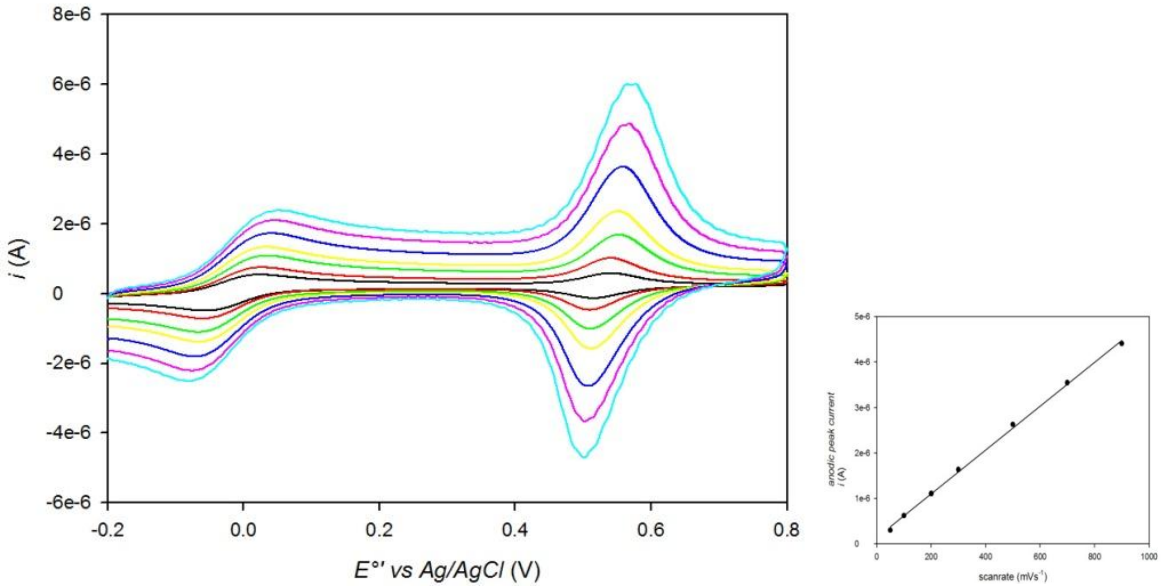

Figure 9. a) Cyclic voltammogram of a SAM of **(*R*)-27** on the gold working electrode in dcm (TBA·PF_6 0.1 M) *vs*. Ag/AgCl reference electrode and Pt wire as counter electrode. **b)** Potential scan-rate vs. peak current dependence

Regarding the shape of the peaks, as described in Section **4.2**, positive interactions are linked to narrower peaks, whereas negative interactions lead to broader peaks. From a closer analysis of the full-width-half-maxima (FWHM) of the cathodic peaks of **26, (*rac*)-27** and **(*R*)-27**, the interactions upon the oxidation process appear to be positive. On the other hand, looking at the FWHMs of the anodic peaks, they show a balance for **(*rac*)-27** and **(*R*)-27** and a small repulsive interaction for **26.** This can be explained by a reduced extent of the hydrogen bonding between the molecules. H-bonding might, in fact, contrast any repulsive interaction due to the charge of the oxidised species, ferrocenium.

At high scan-rates, the profile of the voltammograms appear distorted, whilst low conductivity of the solution (i.e. low concentration of electrolyte) can cause noise on the cyclic voltammograms. Since the electrolyte used in these experiments is the same as that used in other studies on SAMs containing ferrocene,[33] it is more likely that the noise is caused by electrical interference from the mains.

4.7 Cyclic voltammetry in water

In water the cyclic voltammograms of all the species display a rather different shape compared to experiments carried out in dcm, which show a certain asymmetry. The anodic peaks of **26, (*rac*)-27** and **(*R*)-27** appear broader and on the other hand, the cathodic peaks appear sharper (Figures 10, 11 and 12). As described in Section **4.2** this is due to repulsive interactions during the oxidation process and attractive interactions upon the reduction. This can be explained by the solvent interacting with the hydrophobic heads by interfering with the hydrogen bonds between the amides. On the other hand, water molecules can interact with the ferrocenium species, stabilising the otherwise repulsive interactions between adjacent molecules.

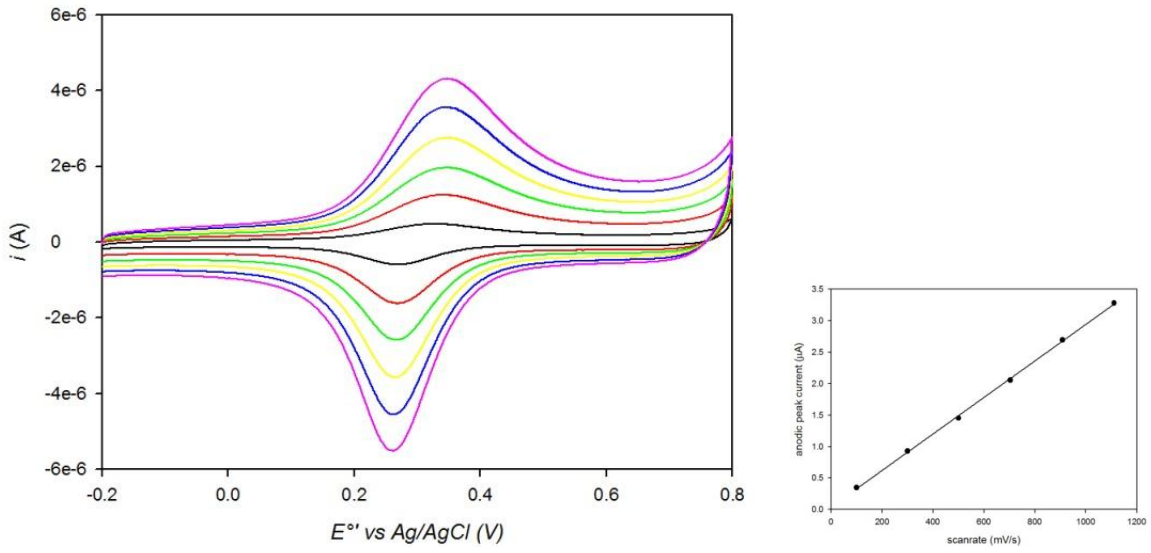

Figure 10. a) Cyclic voltammogram of a SAM of **26** on the gold working electrode in $NaPF_{6\,(aq)}$ 0.1 M *vs*. Ag/AgCl reference electrode and Pt wire as counter electrode. **b)** Potential scan-rate vs. peak current dependence

In spite of the high asymmetry of the voltammograms, all the species display electrochemical reversibility. The peak currents, in fact, are proportional to the scan-rate, as

required for electroactive species on surfaces, and also the ratio between the anodic and the cathodic currents is ca. 1, as shown in Table 2.

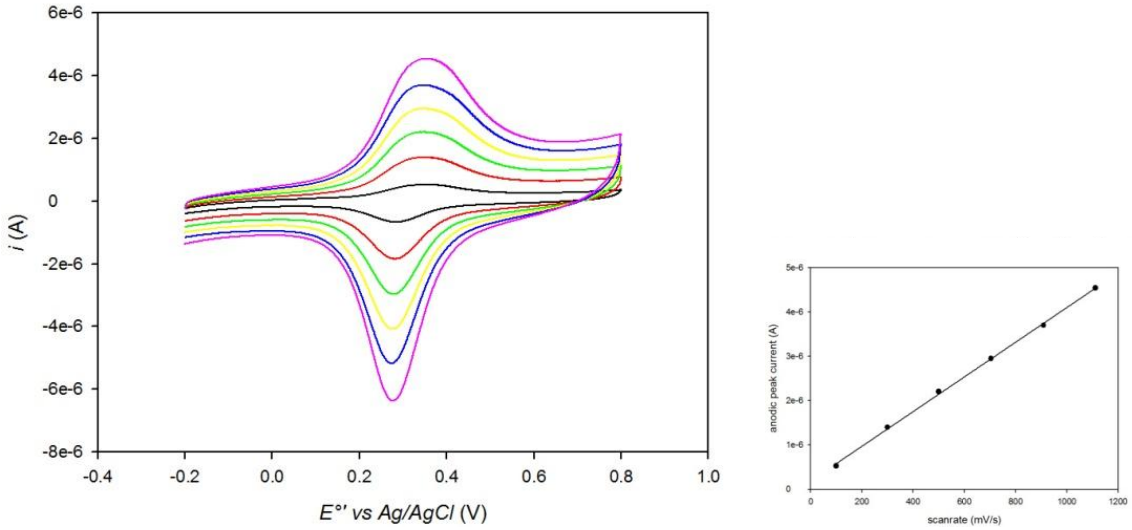

Figure 11. a) Cyclic voltammogram of a SAM of **(*rac*)-27** on the gold working electrode in $NaPF_{6\,(aq)}$ 0.1 M *vs*. Ag/AgCl reference electrode and Pt wire as counter electrode. **b)** Potential scan-rate vs. peak current dependence

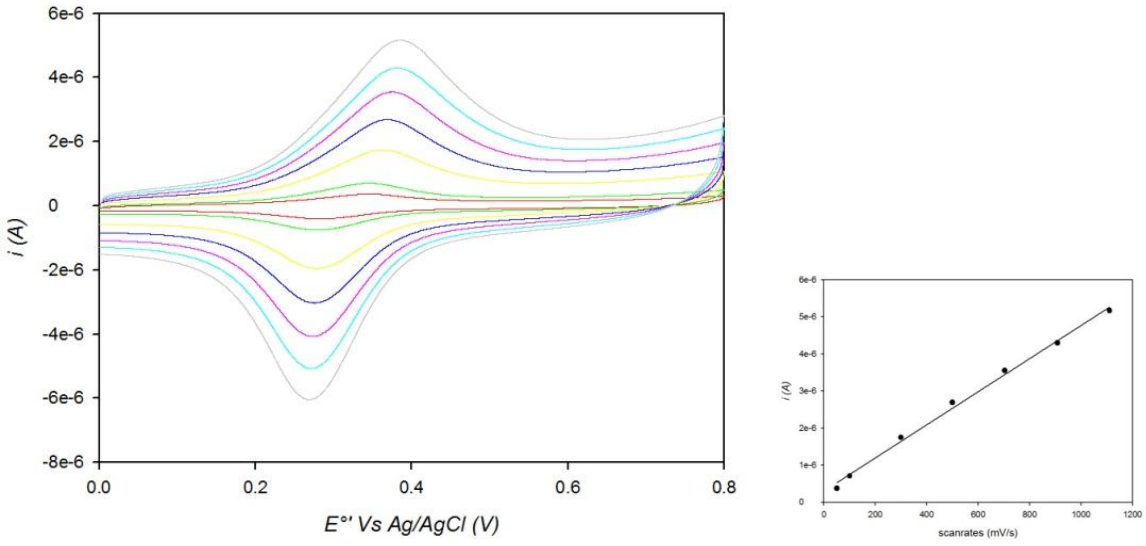

Figure 12. a) Cyclic voltammogram of a SAM of **(*R*)-27** on the gold working electrode in $NaPF_{6\,(aq)}$ 0.1 M *vs*. Ag/AgCl reference electrode and Pt wire as counter electrode. **b)** Potential scan-rate vs. peak current dependence

Table 2. [a] Electrode potential of the species calculated from the CV $NaPF_6$ (aq) vs. Ag/AgCl; [b] difference between anodic and cathodic peak; [c] ratio between anodic and cathodic peak currents.

	$E°'_{(aq)}$ / mV [a]	ΔE_p / mV [b]	i_{pa} / i_{pc} [c]
26	307	73	0.99
(*rac*)-27	313	61	1.03
(*R*)-27	321	67	1.00

From the differences in the peak potentials (ΔE_p) the electron transfer rate constant was evaluated for **26** in a similar way to that described for studies in dcm. The value obtained (180 s^{-1}) is comparable to previously reported results[15] and is corroborated by recent studies on similar compounds in aqueous electrolytes.[16]

It is worth noting that the three compounds under study possess different potentials in water (Table 2). In this case **26** shows the smaller potential of the series, an opposite result compared to similar experiments in dcm. Moreover, for **(*rac*)-27** and **(*R*)-27**, where in dcm they possess identical potential in water they display a difference. These results can be explained by the different packing that the species experience in the different solvents. Tighter packing causes the formal potential to increase.[34]

4.8 Ellipsometric assessment of the layer thickness

4.8.1 Introduction to the technique[35]

Ellipsometry is an optical and non destructive technique which uses elliptic polarised light to determine the refractive index of a thin layer on a reflecting surface. Elliptic polarised light

(Figure 13) can be divided into two directions of polarisation: *s* perpendicular to the plane of incidence; *p* parallel to the incidence plane. With an ellipsometer it is possible to estimate the *complex reflectance ratio*, ρ. This value corresponds to the ratio of the *s* and *p* components after being reflected by the surface and having travelled across the thin layer under study, r_s and r_p.

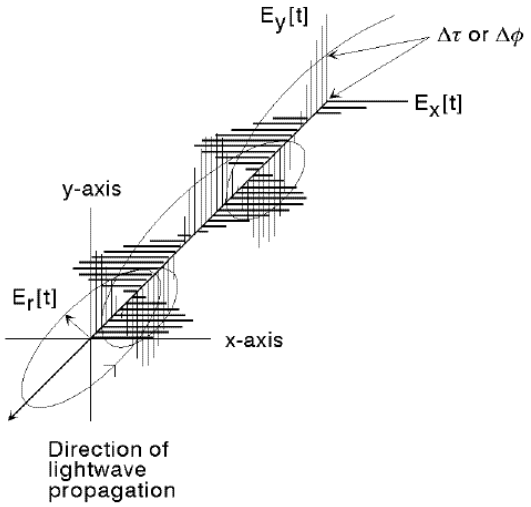

Figure 13. Elliptic polarised light. http://www.photonics.byu.edu/polarization.phtml

The ratio ρ can be parametrised, accordingly to eq. (***4.6***), in Ψ and Δ. However, the actual value of these two parameters can be obtained only by fitting the results with a layer model.

$$\rho = \frac{r_p}{r_s} = \tan(\Psi)e^{i\Delta} \qquad (\textbf{\textit{4.6}})$$

In Figure 14 a schematic representation of an ellipsometer is shown. It comprises a light source, a rotating polariser, a fixed analyser and a detector connected to a PC.

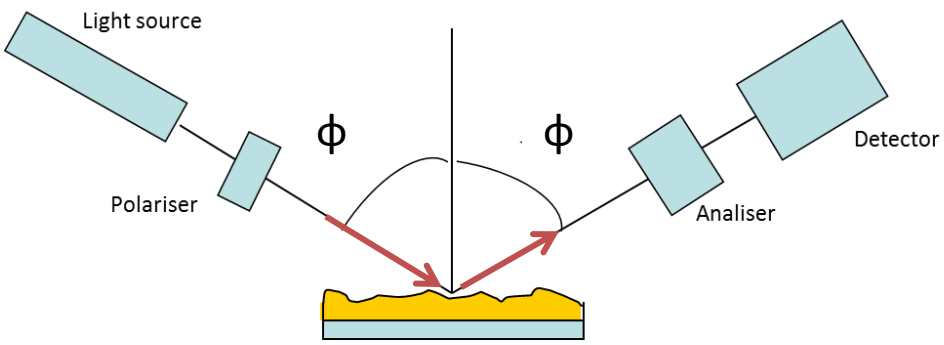

Figure 14. Schematic representation of an ellipsometer.

When the light hits the thin layer part of it is reflected without a change in the polarisation. However, part of it goes through it, refracted by the nature of the layer, according to Snell's law. This light, which can be further refracted if a multilayer is studied, is then reflected by the gold surface back into the monolayer and then into the first medium (usually air). The passages through the surface do not change the angles of reflection, but these cause a change in the polarisation parameters and this is what ellipsometry measures (Figure 15).

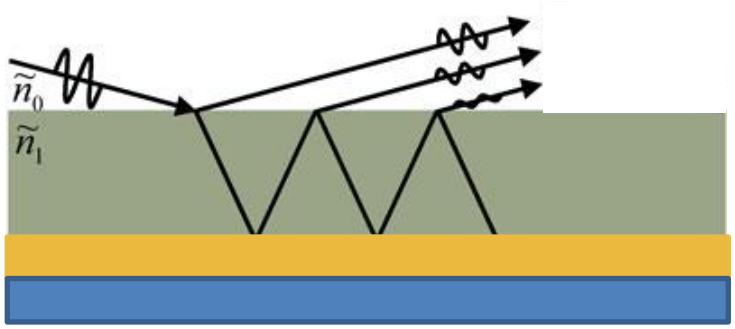

Figure 16. Schematic representation of light through a thin monolayer (gray) adsorbed on a gold surface (gold) attached to a glass surface (blue)

With this technique not only can the thickness of the thin layer be determined but also the nature of the monolayer can be assessed. For these reasons ellipsometry is a powerful analytical technique for materials applications, in particular for surface coating.[36] Moreover ellipsometry can be used to assess electroactive monolayers formed on gold.[37]

4.8.2 Results and discussion

The monolayers formed by **26, (*rac*)-27** and **(*R*)-27** were assessed by ellipsometry. In this case a gold coated glass surface was used to form the monolayer by immersing it in a dcm solution of the three compounds. The gold surface was previously cleaned by immersion in a piranha solution (H_2SO_4 : H_2O_2 = 1 : 1) for few minutes.

Before each experiment, the thickness of the bare gold was measured. It is possible that in spite of the careful cleaning of the surface, some impurities may be present. The software used takes into account the measurement of the blank (gold arrow Figure 17) and subtracts it from the thickness obtained (black arrow Figure 17), giving a value (red arrow Figure 17) which it is not correct. For this reason the thickness of the initial impurities (grey arrow Figure 17) should be added back to the value found in order to obtain the real thickness of the SAM under study (green arrow Figure 17). The thickness of the impurity monolayer was found using a model present in the software as a blank (**(a)** Figure 17).

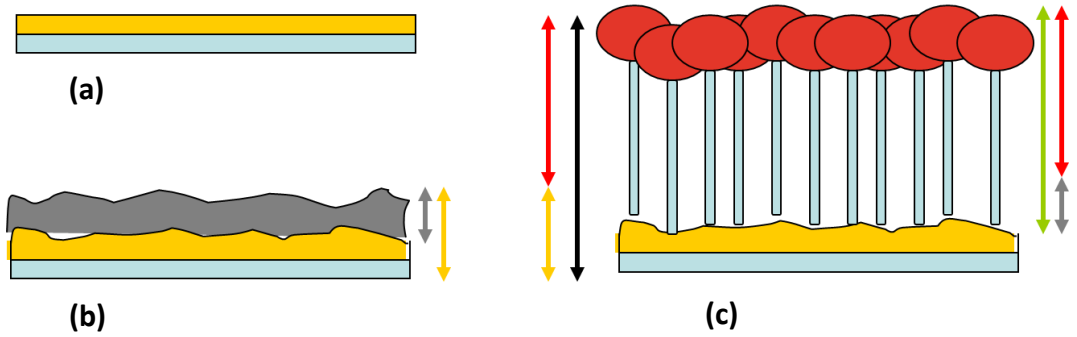

Figure 17. (a) schematic representation of a model of gold surface **(b)** schematic representation of the surface with impurities (**gold** arrow total length, **gray** arrow thickness of the impurities layer); **(c)** schematic representation of the SAM formation, assuming an higher affinity of the molecules forming the SAM for gold than the impurities present (**black** arrow total thickness, **red** arrow measured thickness using gold + impurities as a blank, **green** arrow thickness of the monolayer formed)

For these experiments only one piece of gold was available. The blank was calculated at the beginning of each experiment, then the gold layer was immersed in the solution for a certain amount of time, removed and rinsed with dry dcm, dried under a nitrogen flow and

then observed by ellipsometry and then washed again, dried and immersed back into the solution. This procedure is not ideal to determine how the layer grows as a function of soaking time; in fact during each rinsing and drying process some molecules can be displaced, and moreover the gold surface is more exposed to air and environmental impurities. For these reasons the following results should be regarded as an indication of the packing but not as a direct measure of the rate of monolayer growth.

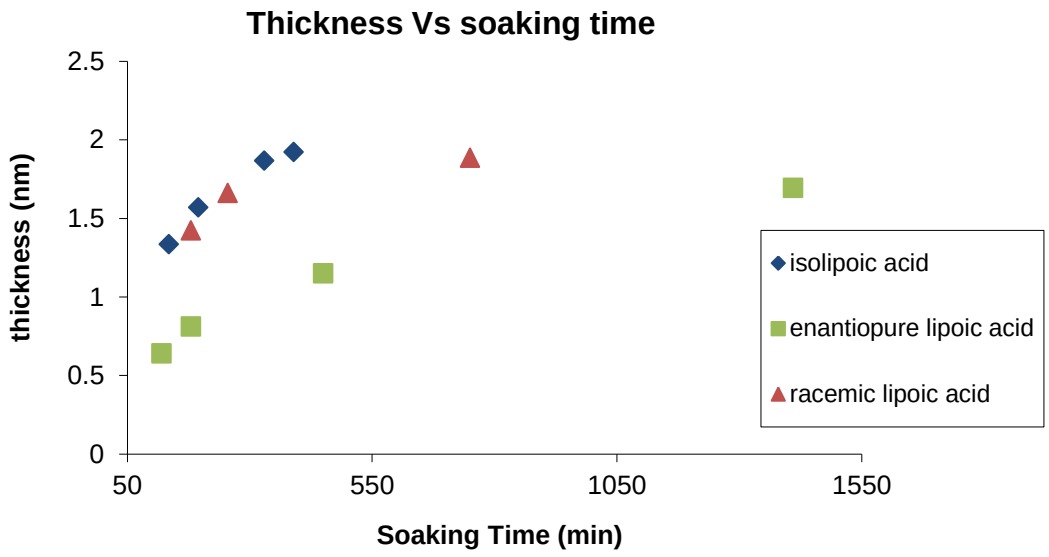

Figure 18. Thickness found with via ellipsometry *vs.* time the gold bid was soaked in the solution **26** blue diamonds, **(*rac*)-27** red triangles and **(*R*)-27** green squares

Table 3. [a] Maximum thickenss obtained with ellipsometry in nm, [b] calculated dimensions of each molecule using an *ab initio* molecular modelling

	Max thickness / nm [a]	Calculated thickness / nm [b]
26	1.91	1.63
(*rac*)-27	1.92	1.62
(*R*)-27	1.63	1.62

From Figure 18 it can be noted that all the compounds reach a maximum of thickness of less than 2 nm (exact values are shown in Table 3). The values obtained are larger than those calculated by an *ab initio* molecular modelling for the corresponding molecule.[‡] However, the molecular modelling calculates the distances between the nuclei, whereas the ellipsometry, being an optical technique, is affected by the interaction of the light with the electronic cloud of the molecules. This might justify the higher values obtained for some of the molecules under study with respect to the calculated length.

4.9 Conclusions

In conclusion in this chapter it has been shown that isolipoic acid, obtained through an improved synthetic pathway, can be used as a tether unit in molecules that can self-assemble onto surfaces. This unit, which does not bear any chiral centre, might find applications in the formation of SAMs where a strong control on the stereochemical configuration is required.

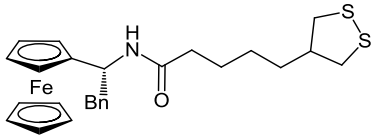

26

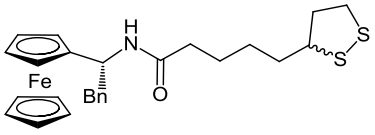

(*rac*)-27

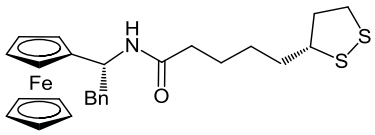

(*R*)-27

In particular, SAMs formed by **26, (*rac*)-27** and **(*R*)-27**,amides of isolipoic acid, (*rac*)-lipoic acid and (*R*)-lipoic acid with a chiral ferrocenyl amine, were assessed using electrochemical techniques both in organic and aqueous solvents. Moreover, preliminary optical studies were performed using ellipsometry.

[‡] Modelling carried out by Dr. John Wilkie

In organic solvents the three compounds under study show the characteristic cyclic voltammograms of electro-active species adsorbed onto the electrode: i.e. $\Delta E_p < 59$ mV and proportionality between the peak current and the scan-rate.

Moreover, positive interactions between adjacent redox units upon the oxidation have been determined; these can be explained by hydrogen-bonding between the amides. During the reduction event, a balance in the interaction has been determined for **(*rac*)-27** and **(*R*)-27** whereas a mild negative interaction was found for **26,** probably due to the repulsion between the ferrocinium ions.

Voltammograms of **26, (*rac*)-27** and **(*R*)-27** in water appear dramatically different from those showed in organic solvents. In fact, the high symmetry of the anodic and cathodic peak appear disrupted, with a broader anodic peaks and sharper, narrower cathodic peaks.

This behaviour is consistent with repulsive interactions during the oxidation process, which is probably due to solvent interfering with the hydrogen-bonds, and positive interactions in the reduction process which can be explained by the solvent stabilising the ferrocenium ions formed.

The kinetics of the electron transfer process was also investigated from the ΔE_p values. However, in dcm the results are affected by large errors since no correction for the ohmic drop was carried out. In water a slow electron transfer process was found.

Preliminary ellipsometry experiments on the monolayers have also been carried out, giving a maximum coverage that is in agreement with molecular modelling carried out on these compounds. These studies however must be regarded only as a comparison between the complexes and not as the real value, firstly because the thickness calculated for very thin

monolayers is affected by a large error and secondly because the model used for the fitting should be improved.

Future work will involve the study of SAMs of electrochemical chiral sensors for anions tethered to the surface by **24** and of comparison of these compounds with similar compounds tethered with acids **(*rac*)-25** and **(*R*)-25**. This will build on previous work in the Tucker group which has demonstrated that chiral ferrocenyl ureas, in solution[26] and adsorbed onto a gold surface,[38] can moderately sense different enantiomers of chiral carboxylates using electrochemical techniques.

4.10 References

(1) Lehn, J. M. *Angew. Chem., Int. Ed. Engl.* **1988**, *27*, 89.

(2) (a) Bayly, S. R.; Gray, T. M.; Chmielewski, M. J.; Davis, J. J.; Beer, P. D. *Chem. Commun.* **2007**, 2234(b) Beer, P. D.; Davis, J. J.; Drillsma-Milgrom, D. A.; Szemes, F. *Chem. Commun.* **2002**, 1716.

(3) Nuzzo, R. G.; Allara, D. L. *J. Am. Chem. Soc.* **1983**, *105*, 4481.

(4) Laviron, E. *J. Electroanal. Chem.* **1974**, *52*, 395.

(5) (a) Garg, N.; Lee, T. R. *Langmuir* **1998**, *14*, 3815(b) Dubois, L. H.; Nuzzo, R. G. *Annu. Rev. Phys. Chem.* **1992**, *43*, 437.

(6) Bain, C. D.; Whitesides, G. M. *Science* **1988**, *240*, 62.

(7) (a) Rincon, A. M.; Prados, P.; de Mendoza, J. *J. Am. Chem. Soc.* **2001**, *123*, 3493(b) Chun, K. M.; Kim, T. H.; Lee, O. S.; Hirose, K.; Chung, T. D.; Chung, D. S.; Kim, H. *Anal. Chem.* **2006**, *78*, 7597.

(8) Sek, S.; Misicka, A.; Bilewicz, R. *J. Phys. Chem. B* **2000**, *104*, 5399.

(9) (a) Laviron, E. *J. Electroanal. Chem.* **1974**, *52*, 355(b) Laviron, E. *J. Electroanal. Chem.* **1975**, *63*, 245.

(10) Laviron, E. *J. Electroanal. Chem.* **1979**, *101*, 19.

(11) Laviron, E. *J. Electroanal. Chem.* **1979**, *100*, 263.

(12) Bard, A. J.; Faulkner, L. R. *Electrochemical Methods, Fundamentals and Applications*; Wiley, 2001.

(13) Rowe, G. K.; Creager, S. E. *Langmuir* **1991**, *7*, 2307.

(14) Eckermann, A. L.; Feld, D. J.; Shaw, J. A.; Meade, T. J. *Coord. Chem. Rev.* **2010**, *254*, 1769.

(15) Frasconi, M.; D'Annibale, A.; Favero, G.; Mazzei, F.; Santucci, R.; Ferri, T. *Langmuir* **2009**, *25*, 12937.

(16) Cormode, D. P.; Evans, A. J.; Davis, J. J.; Beer, P. D. *Dalton Trans.* **2010**, *39*, 6532.

(17) Rojas, M. T.; Kaifer, A. E. *J. Am. Chem. Soc.* **1995**, *117*, 5883.

(18) Bandyopadhyay, K.; Patil, V.; Sastry, M.; Vijayamohanan, K. *Langmuir* **1998**, *14*, 3808.

(19) Chang, W. S.; Huh, K. S.; Cho, S. H.; Kim, J. G.; Whang, K. H., 2006.

(20) Viana, A. S.; Jones, A. H.; Abrantes, L. M.; Kalaji, M. *J. Electroanal. Chem.* **2001**, *500*, 290.

(21) Raddatz, G.; Bisswanger, H. *J. Mol. Model.* **1997**, *3*, 423.

(22) (a) Sharma, J.; Chhabra, R.; Andersen, C. S.; Gothelf, K. V.; Yan, H.; Liu, Y. *J. Am. Chem. Soc.* **2008**, *130*, 7820(b) Zhang, S.; Cardona, C. M.; Echegoyen, L. *Chem. Commun.* **2006**, 4461.

(23) (a) Amabilino, D. B. *Chem. Soc. Rev.* **2009**, *38*, 669(b) Parschau, M.; Passerone, D.; Rieder, K. H.; Hug, H. J.; Ernst, K. H. *Angew. Chem., Int. Ed.* **2009**, *48*, 4065.

(24) Fabianowski, W.; Coyle, L. C.; Weber, B. A.; Granata, R. D.; Castner, D. G.; Sadownik, A.; Regen, S. L. *Langmuir* **1989**, *5*, 35.

(25) Bergson, G.; Frisell, C. *Acta Chem. Scand.* **1964**, *18*, 2000.

(26) Willener, Y.; Joly, K. A.; Moody, C. J.; Tucker, J. H. R. *J. Org. Chem.* **2008**, *73*, 1225.

(27) Joly, K. M.; Mirri, G.; Willener, Y.; Horswell, S. L.; Moody, C. J.; Tucker, J. H. R. *J. Org. Chem.* **2010**, *75*, 2395.

(28) Trasatti, S.; Petrii, O. A. *Pure Appl. Chem.* **1991**, *63*, 711.

(29) Hoogvliet, J. C.; Dijksma, M.; Kamp, B.; van Bennekom, W. P. *Anal. Chem.* **2000**, *72*, 2016.

(30) Oesch, U.; Janata, J. *Electrochim. Acta* **1983**, *28*, 1237.

(31) Repo, E.; Ahlberg, E.; Murtomaki, L.; Kontturi, K.; Schiffrin, D. J. *Electrochim. Acta* **2009**, *54*, 6584.

(32) Roullier, L.; Laviron, E. *J. Electroanal. Chem.* **1983**, *157*, 193.

(33) Kondo, T.; Okamura, M.; Uosaki, K. *J. Organomet. Chem.* **2001**, *637*, 841.
(34) Seo, K.; Jeon, I. C.; Yoo, D. J. *Langmuir* **2004**, *20*, 4147.
(35) Tompkins, H. G. *A User's Giude to Ellipsometry*; Academic Press Inc: London, 1993.
(36) Dardona, S.; Jaworowski, M. *Appl. Phys. Lett.* **2010**, *97*.
(37) (a) Ohtsuka, T.; Sato, Y.; Uosaki, K. *Langmuir* **1994**, *10*, 3658(b) Viana, A. S.; Abrantes, L. M.; Jin, G.; Floate, S.; Nichols, R. J.; Kalaji, M. *Phys. Chem. Chem. Phys.* **2001**, *3*, 3411.
(38) Willener, Y. PhD Thesis, University of Birmingham, 2008.

5. Conclusions

In this thesis new chiral electrochemical receptors were described. For all of them the reporting unit is a ferrocene which can easily be functionalised by means of organic reactions. The differences between the receptors mainly concerned the binding site and the chiral feature.

Receptors equipped with a boronic acid binding site and central chiral moiety, have been proven to be able to discriminate between enantiomers of chiral diols, i.e. the potential of the adducts formed with either enantiomers were different from each other and from the potential of the free host, with a maximum difference of 51 mV found with the adducts formed with the two enantiomers of Binol and the chiral host with a benzyl side chain. The ratio between the thermodynamic constants of the equilibria of formation of the diasteromeric guests was assessed by NMR. The same host-guest system which showed the greatest difference in the potential possessed also the largest K_R/K_S ratio (≈19). The greater stabilisation of the adduct formed with *R*-Binol is to be assigned to a π-π interaction between host and guest, that, for geometrical reasons, is absent when the other enantiomer is bound. The large difference in the potential and in the thermodynamics for the two diasteromeric complexes allowed also the correlation between the potential of the host and the enantiomeric composition of a mixture of guest being linear in the region 100%-60% *ee* of (*S*)-Binol with the possibility of discrimination between 98% and 90% at a concentration of guest ten times lower than that used in similar NMR experiments. This is, to the best of our knowledge, the first electrochemical determination of a mixture of enantiomers. Similar host systems showed a good discrimination and also a discrete difference in the thermodynamics of of the formation of the two diasteromeric complexes with a variety of guests.

The second kind of receptor studied are ferrocene-containing macrocycles, where the chiral feature is installed by means of a Binol unit and the binding site is a diamido pyridine which can interact as H-bonding donor and acceptor. These systems have shown a discrete affinity for achiral cyclic ureas. However, small or no enantioselectivity with chiral guests was found. This is probably due to the geometry of the cavity which increases the selectivity. Future work may involve the binding of chiral cyclic ureas, i.e. naturally occurring biotin in addition to finding new guests which can be bound more selectively.

The formation of self assemblied monolayer formed with ferrocene amides of naturally occurring lipoic acid (in its (*R*) and racemic configuration) and the synthetic achiral isolipoic acid were assessed by electrochemical and optical techniques. The three compounds formed the monolayer in a similar way, proving that isolipoic acid is a tether group which can be substituted for the widely used lipoic acid when a strong control on the chiral configuration is required.

To conclude we demonstrated that chiral sensing can be performed with electrochemical techniques in a comparable way to other more widely described techniques, i.e. photoactive receptors and NMR.

General

All the products were used as received from Sigma-Aldrich, TCI, Fisher Scientific. All the solvents were used as received from Fischer and Sigma-Aldrich. Dry solvents were obtained using lab procedures or Solvent Purification System. Routine ^{1}H-NMR were recorded at 300 MHz on a Bruker AC 300 and AC III 300 ^{13}C-NMR were recorded at 75 MHz on a Bruker AC300 or at 100 MHz on a Bruker AC III 400, 2D NMR (COSY, HSQC, HMBC) recorder on a Bruker AC III 400. All the spectra were recorded at 298 K. NMR characterisation was performed with a Bruker drx500 at 300 K. NMR binding studies were performed with a Bruker AC 300 and AC III 300 at 298 K. Electrochemical studies were performed on a BAS 100W electrochemical analyser, with BAS 100W software for cyclic voltammetry and square wave voltammetry. A three electrode cell was used. The working electrode was a platinum (gold for SAMs experiments) disc electrode from Bioanalitical Systems. Inc. ($\phi = 1.6$ mm). Ag/AgCl was used as reference electrode. The auxiliary electrode was a Pt wire. Tetrabutyl ammonium hexafluorophosphate (TBA·PF_6) (0.1 M in dichloromethane) was used as supporting electrolyte. Either decamethyl ferrocene or ferrocene (in a concentration comparable to the concentration of the analyte) were used as internal reference for experiments in dichloromethane depending on the potential of the analyte.

Cells and glassware care

The cell and all the glassware used during the experiments were cleaned using one of the following methods:

- Ammonia : Hydrogen peroxide 1:1 (3/6 h)
- Piranha solution (sulfuric acid : H_2O_2 3:1) (1 h)
- Nitric acid : sulfuric acid 1:1 at 200 ˚C (1 h)

After any of the above methods the glassware should be rinsed several times (*ca.* 10) with MilliQ® water and dried in an oven overnight.

Working Electrodes pre-treatment

Pt and Au electrodes were mechanically polished before any experiment using an alumina water slurry on a microcloth pad, performing a figure of eight pattern for not less than 5 mins. Every 2-3 months of usage (or in case major scratches are present) each electrode

was polished with a diamond powder solution 3 µm (on a nylon pad). Gold electrodes used for SAMs formation and analysis were also electrochemically polished, running different scans (*ca.* 20) in a 0.1 M sulfuric acid solution. The scans should be carried out until the voltammogram is reproducible. In all cases the electrode was rinsed with MilliQ water and dried under a nitrogen flow.

(*R*)-*N*-(1-Phenylbutoxy)-phthalimide[1]

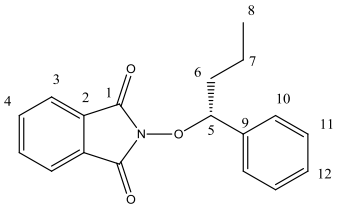

N-hydroxyphthalimide (2.18 g, 1.34 × 10^{-2} mol), (*S*)-1-phenylbutanol (1.0 g 6.7 × 10^{-3} mol) and PPh_3 (3.57 g, 1.3 × 10^{-3} mol) were placed in a 250 mL schlenk tube with 60 mL of dry THF. The mixture was cooled down at 0°C and DIAD (3 mL, 1.3 × 10^{-3} mol) added drop-wise over 10 min at the same temperature. The mixture was stirred at 0°C for 30 min and then allowed to warm up to r.t. (the mixture became cloudy with an orange suspension) and then it was stirred at 50°C for 4 days (mixture yellowish and clear). The solvent was evaporated obtaining a yellow oil. Pentane : diethyl eter 5:2 was added and the oil triturated with a glass rod to form a fluffy white solid that was filtered off and rinsed with Pentane : diethyl ether 1:1. The solution was evaporated to obtain a yellow oil that was dissolved in diethyl ether (30 mL) and washed with $NaHCO_{3\ (sat)}$ (15 mL ×2). The aqueous layers were combined together and extracted with diethyl ether (3 × 30 mL). The combined organic phases were dried over $MgSO_4$ and evaporated obtaining a yellow oil.

Purification chromatographic column: silica (light pet.et. : diethyl ether = 4 : 1 R_f target product = 0.38). 1.28 g of a white solid obtained (64%). The NMR data matched that give in the literature. ^{1}H NMR (300 MHz, $CDCl_3$) δ 7.78 – 7.60 (m, 4H, $H_{4,3}$), 7.51 – 7.27 (m, 5H, $H_{9\text{-}12}$), 5.33 (t, *J* = 7.1 Hz, 3H, H_5), 2.28 – 2.08 (dddd, *J* = 13.6, 9.9, 6.8, 5.7 Hz, 1H, H_{6a}), 1.99 – 1.80 (dddd, *J* = 13.5, 9.8, 7.3, 5.9 Hz, 1H, H_{6b}), 1.56 – 1.31 (m, 2H, H_7), 0.97 (t, *J* = 7.4 Hz, 3H, H_8) ^{13}C NMR (100 MHz, $CDCl_3$) δ 163.70 (C_1), 138.25 (C_2), 134.17 (C_{Ar}), 128.89 (C_{Ar}), 128.22 (C_{Ar}), 128.07 (C_{Ar}), 123.25 (C_{Ar}), 89.06 (C_5), 36.84 (C_6), 18.96 (C_7), 13.86 (C_8).

(*S*)-N-(1-Phenylbutoxy)-phthalimide[1]

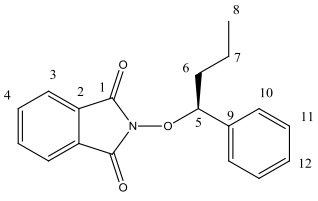

Same procedure used for (*R*)-N-(1-phenylbutoxy)-phthalimide was followed with the only change in the configuration of the starting alcohol. (*R*)-1-Phenylbutanol (1.0 g 6.7 × 10^{-3} mol), 2.18 g (1.3 × 10^{-}

^{2} mol) of N-hydroxyphthalimide; 3 mL of DIAD (1.5×10^{-2} mol); 4.10 g (1.56×10^{-2} mol) of PhP_3 in 60 mL of THF. After purification 1.5 g of a white solid obtained (76%). The NMR data matched that given in the literature ^{1}H NMR (300 MHz, $CDCl_3$) δ 7.83 – 7.59 (m, 4H, $H_{4,3}$), 7.51 – 7.27 (m, 5H, $H_{9\text{-}12}$), 5.35 (t, J = 7.1 Hz, 1H, H_5), 2.28 – 2.11 (m, 1H, H_{6a}), 1.99 – 1.80 (m, 1H, H_{6b}), 1.58 – 1.30 (m, 2H, H_7), 0.99 (t, J = 7.4 Hz, 3H, H_8). ^{13}C NMR (100 MHz, $CDCl_3$) δ 163.70 (C_1), 138.25 (C_2), 134.17 (C_{Ar}), 128.89 (C_{Ar}), 128.84 (C_9), 128.22 (C_{Ar}), 128.06 (C_{Ar}), 123.25 (C_{Ar}), 89.05 (C_5), 36.84 (C_6), 18.96 (C_7), 13.86 (C_8). ES+ *m/z*: 318.1 $[M+Na]^+$ 100%; 319.1 10%; HRMS: Calc. *m/z* 318.1106, found *m/z* 318.1111 $C_{18}\,H_{17}\,N\,O_3\,Na$

(*E*)-(*R*)-(*+*)-*O*-(1-Phenylbutyl)ferrocene-1-carboxaldoximine[2]

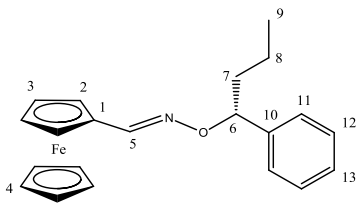

(*R*)-N-(1-Phenylbutoxy)-phthalimide (0.483 g, 1.64 x 10^{-3} mol) was dissolved in EtOH (15 ml) at 40°C. Hydrazine monohydrate (0.095 ml, 1.96 x 10^{-3} mol) was added dropwise under Ar. The mixture was refluxed for 1h. Ferrocene carboxyaldehyde (0.700 g 3.27 x 10^{-3} mol) was added at r.t. and the mixture was stirred overnight at r.t.. the crude was purified by chromatographic column (silica gel: light petroleum ether : diethyl ether 20:1) giving 0.490 g of a red oil which solidify upon standing under N_2 (83%). The NMR data matched that given in the literature ^{1}H NMR (300 MHz, $CDCl_3$) δ 7.97 (s, 1H, H_5), 7.45 – 7.21 (m, 5H, $H_{10\text{-}13}$), 5.12 (t, J = 6.9 Hz, 1H, H_6), 4.53 – 4.48 (m, 1H, H_{2a}), 4.48 – 4.42 (m, 1H, H_{2b}), 4.33 – 4.26 (m, 2H, H_3), 4.08 (s, 5H, H_4), 2.08 – 1.89 (m, 1H, H_{7a}), 1.86 – 1.68 (m, 1H, H_{7b}), 1.55 – 1.30 (m, 2H, H_8), 0.97 (t, J = 7.4 Hz, 3H, H_9). ES+ *m/z:* 361.2 $[M]^+$ 100%; 362.2 70%; 384.2 $[M+Na]^+$ 60%; HRMS: calc. *m/z:* 384.1027 found *m/z:* 384.1039 $C_{21}\,H_{23}\,N\,O\,Na$.

(*E*)-(*S*)-(-)-*O*-(1-Phenylbutyl)ferrocene-1-carboxaldoximine[2]

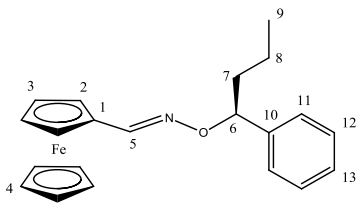

Same procedure as for (*E*)-(*R*)-(*+*)-*O*-(1-Phenylbutyl)ferrocene-1-carboxaldoximine but using (*R*)-N-(1-Phenylbutoxy)-phthalimide (0.511 g, 1.7×10^{-3} mol); 0.760 g (3.55×10^{-3} mol) of ferrocene carboxyaldehyde and 0.1 mL of hydrazine monohydrate (2.1×10^{-3} mol) in 15 mL of ethanol. Purification: chromatographic column (Silica gel, hexane : diethyl ether = 20 : 1) 0.385 g of a red solid obtained (63%). The NMR data matched that given in the literature ^{1}H NMR (300 MHz, $CDCl_3$) δ 7.98 (s, 1H, H_5), 7.42 – 7.19 (m, 5H, $H_{10\text{-}13}$), 5.13 (t, J = 6.9 Hz, 1H, H_6), 4.54 – 4.48 (m, 1H, H_{2a}), 4.48 – 4.43 (m, 1H, H_{2b}), 4.34 – 4.27 (m,

2H, H_3), 4.09 (s, 5H, H_4), 2.07 – 1.92 (m, 1H, H_{7a}), 1.85 – 1.71 (m, 1H, H_{7b}), 1.53 – 1.30 (m, 2H, H_8), 0.98 (t, J = 7.4 Hz, 3H, H_9). ^{13}C NMR (100 MHz, $CDCl_3$) δ 148.79 (C_5), 142.89 (C_{10}), 128.11 (C_{11}), 127.21 (C_{13}), 126.82 (C_{12}), 84.71 (C_6), 69.84 (C_{3a}), 69.65 (C_{3b}), 69.13 (C_4), 67.97 (C_{2a}), 67.16 (C_{2b}), 38.24 (C_7), 18.89 (C_8), 14.04 (C_9). ES+ *m/z:* 384.1 $[M+Na]^+$ 100%, 361.1 $[M]^+$ 10 %, 229.0 $[M\text{-}PhC_4H_8]^+$ 10% HRMS: calc. *m/z:* 384.1027 found *m/z:* 384.1025 $C_{21}H_{23}NONa$.

General procedure for the addition of the Grignard to (*E*)-(*R*)-(*+*)-*O*-(1-Phenylbutyl)ferrocene-1-carboxaldoximine[2]

Ferrocene oxime ether (1 eq) was dissolved in dry toluene. $BF_3{\cdot}OEt_2$ (3.5 eq) was added at -78°C, the mixture was stirred for 30' at the same temperature. The Grignard (3.5 eq) (BnMgCl and ^{i}PrMgCl commercially available as solutions in diethylether) was added with a syringe pump over 40' at -78°C. The mixture was stirred for 1h30' at the same temperature, and then quenched by adding 6 ml of a saturated solution of ammonium chloride to the mixture at -78°C. The mixture was warmed up to r.t. and washed with water (20 ml) and ethyl acetate (20 ml). The aqueous layer was extracted twice and the combined organic layers were washed with brine (35 ml), dried over $MgSO_4$ and evaporated.

(*1R,1'R*)-(*+*)-1-Ferrocenyl-2-phenyl-N-(1-phenylbutoxy)-1-ethylamine[2]

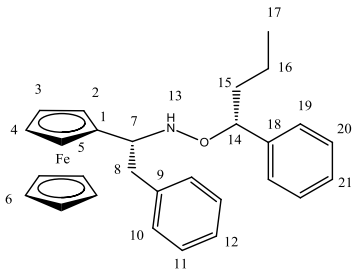

Ferrocene oxime ether 0.678g (1.88×10^{-4} mol) in 20 mL of dry toluene. Purification: chromatographic column (Silica gel, light pet.et./diethyl ether/triethylamine 95/5/0.5) gave 0.563 g (66%) of and orange solid. The NMR data matched that given in the literature ^{1}H NMR (300 MHz, $CDCl_3$) δ 7.43 – 7.06 (m, 10H, $H_{9\text{-}12,18\text{-}21}$), 5.75 (s, 1H, H_{13}), 4.56 (dd, J = 7.8, 5.8 Hz, 1H, H_{14}), 4.07 – 3.99 (m, 3H, $H_{2/5,7}$), 3.95 (s, 5H, H_6), 3.88 – 3.79 (m, 2H, $H_{3/4}$), 3.28 (dd, J = 13.1, 6.0 Hz, 1H, H_{8a}), 2.84 (dd, J = 13.1, 7.3 Hz, 1H, H_{8b}), 1.99 – 1.71 (m, 1H, H_{15a}), 1.66 – 1.23 (m, 3H, $H_{15b,16}$), 0.94 (t, J = 7.2 Hz, 3H, H_{17}), ^{13}C NMR (100 MHz, $CDCl_3$) δ 143.31 (C_{18}), 139.25 (C_9), 129.72 (C_{Ar}), 128.39 (C_{Ar}), 127.98 (C_{Ar}), 127.43 (C_{Ar}), 126.63 (C_{Ar}), 125.92 (C_{Ar}), 85.13 (C_{14}), 68.26 (C_6), 67.50 (C_{Fc}), 66.84 (C_{Fc}), 66.34 (C_{Fc}), 61.56 (C_7), 40.81 (C_8), 38.65 (C_{15}), 19.27 (C_{16}), 14.12 (C_{17}). ES+ *m/z:* 453.3 $[M]^+$ 100%, 476.2 $[M+Na]^+$ 70%, 289.1 50%, 492.2 $[M+K]^+$ 20%. HRMS calc. *m/z:* 476.1653 found *m/z:* 476.1649 $C_{28}H_{31}NONa^{56}Fe$.

(*1S,1'S*)-(-)-1-Ferrocenyl-2-phenyl-N-(1-phenylbutoxy)-1-ethylamine[2]

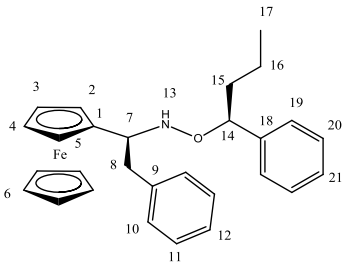

Ferrocene oxime ether 0.154g (4.26×10^{-4} mol) in 10 mL of dry toluene: Purification: chromatographic column (Silica gel, Light petroleum ether : diethyl ether = 20 : 1) 200 mg of a red solid obtained (quantitative yield). The NMR data matched that given in the literature ^{1}H NMR (300 MHz, $CDCl_3$) δ 7.50 – 7.00 (m, 10H, $H_{9\text{-}12,18\text{-}21}$), 5.76 (s, 1H, H_{13}), 4.58 (dd, *J* = 7.7, 5.9 Hz, 1H, H_{14}), 4.15 – 3.76 (m, 11H, $H_{Fc,7}$), 3.29 (dd, *J* = 13.1, 6.0 Hz, 1H, H_{8a}), 2.86 (dd, *J* = 13.1, 7.3 Hz, 1H, H_{8b}), 1.94 – 1.71 (m, 1H, H_{15a}), 1.69 – 1.17 (m, 3H, $H_{15b,16}$), 0.95 (t, *J* = 7.2 Hz, 3H, H_{17}). ^{13}C NMR (100 MHz, $CDCl_3$) δ 143.32 (C_{18}), 139.25 (C_9), 129.70 (C_{Ar}), 128.37 (C_{Ar}), 127.96 (C_{Ar}), 127.40 (C_{Ar}), 126.63 (C_{Ar}), 125.90 (C_{Ar}), 88.68 (C_1), 85.12 (C_{14}), 68.25 (C_6), 67.48 (C_{Fc}), 66.83 (C_{Fc}), 66.35 (C_{Fc}), 61.55 (C_7), 40.81 (C_8), 38.64 (C_{15}), 19.25 (C_{16}), 14.10 (C_{17}).ES+ *m/z:* 476.1 $[M+Na]^+$ 100% 289 10%. HRMS calc. *m/z:* 476.1653 found *m/z:* 476.1640 $C_{28}H_{31}NO\ Na^{56}Fe$.

(*1R,1'R*)-(*+*)-1-Ferrocenyl-2_methyl-N-(1-phenylbutoxy)-1-propylamine[2]

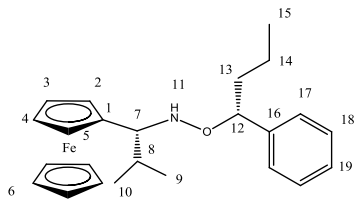

Ferrocene oxime ether 0.341g (9.4×10^{-4} mol) in 15 mL of dry Toluene. Purification of the crude by chromatographic column (silica gel, light pet.et. / diethyl ether 35 / 1) 0.300g of an orange solid obtained (79%). The NMR data matched that given in the literature ^{1}H NMR (300 MHz, $CDCl_3$) δ 7.47 – 7.27 (m, 5H, $H_{17\text{-}19}$), 5.93 (s, 1H, H_{11}), 4.66 (dd, *J* = 8.2, 5.5 Hz, 1H, H_{12}), 4.11 – 4.01 (m, 1H, H_{12}), 3.99 – 3.94 (m, 1H), 3.89 (s, 5H), 2.16 (dtd, *J* = 13.8, 6.9, 4.0 Hz, 1H), 1.98 – 1.74 (m, 1H), 1.72 – 1.32 (m, 1H), 0.94 (t, *J* = 7.2 Hz, 3H), 0.80 (d, *J* = 7.0 Hz, 3H), 0.72 (d, *J* = 6.8 Hz, 3H) ^{13}C NMR (100 MHz, $CDCl_3$) δ 143.59 (C_{16}), 128.49 (C_{Ar}), 127.49 (C_{Ar}), 126.62 (C_{Ar}), 84.96 (C_{12}), 69.30 ($C_{2/3}$), 68.20 (C_6), 67.16 ($C_{2/3}$), 66.54 ($C_{3/4}$), 66.46 ($C_{4/3}$), 64.39 (C_7), 38.80 (C_{13}), 29.85 (C_8), 19.74 (C_{15}), 19.38 (C_{14}), 16.64 ($C_{10/9}$), 14.06 ($C_{10/9}$).

(*1R,1'R*)-1-Ferrocenyl-2-(1-naphthyl)-N-(1-phenylbutoxy)-1-ethylamine

The Grignard was prepared *in situ* adding dropwise 1-(chloromethyl)-naphthalene (2.34 g, 1.32 x 10^{-2} mol) dissolved in dry diethyl ether (5 mL) to a two necked round bottom flask containing Mg (0.500 g) in 17 mL of diethyl ether. The mixture was then refluxed for 3h. The solution was then used as described in procedure for condition of the addition of the Grignard by assuming a concentration of 0.6 M.

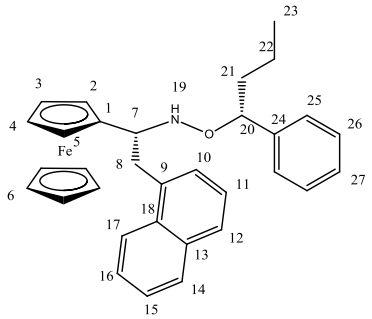

Purification chromatographic column (silica gel, light petroleum ether: Et_2O : Et_3N = 95 : 5 :0.5 R_f = 0.23) a red oil obtained. (yield 78 %). NMR shows the presence of 1-formyl naphthalene (same R_f of the target), product used in the next step without further purification. ^{1}H NMR (300 MHz, $CDCl_3$) δ 8.23 (d, *J* = 8.1 Hz, 1H, H_{17}), 7.85 (dd, *J* = 7.5, 1.9 Hz, 1H, H_{14}), 7.70 (d, *J* = 8.3 Hz, 1H, H_{12}), 7.59 – 7.16 (m, 8H, H_{Ar}), 7.03 (d, *J* = 6.1 Hz, 1H, H_{10}), 5.90 (s, 1H, H_{19}), 4.65 (dd, *J* = 7.7, 5.9 Hz, 1H, H_{20}), 4.07(dd, *J* = 2.4, 1.2 Hz, 1H, H_{8a}) 4.04 – 3.90 (m, 4H, $H_{2\text{-}5}$), 3.87 (s, 5H, H_6), 3.56 – 3.52 (dd, *J* = 2.5, 1.2 Hz, 1H, H_{8b}), 3.01 (dd, *J* = 14.9, 10.2 Hz, 1H, H_7), 1.96 – 1.81 (m, 1H, H_{21a}), 1.72 – 1.46 (m, 1H, H_{21b}), 1.47 – 1.06 (m, 2H, H_{22}), 0.95 (t, *J* = 7.3 Hz, 3H, H_{23}), ^{13}C NMR (100 MHz, $CDCl_3$) δ 143.21 (C_9), 135.32 ($C_{18/13/24}$), 133,78 ($C_{18/13/24}$), 132.26 ($C_{18/13/24}$), 129.08 (C_{Ar}), 128.59 (C_{Ar}), 128.46 (C_{Ar}), 128.17 (C_{Ar}), 127.51 (C_{Ar}), 126.75 (C_{Ar}), 126.67 (C_{Ar}), 125.60 (C_{Ar}), 125.29 (C_{Ar}), 125.21 (C_{Ar}), 124.41 (C_{Ar}), 85.19 (C_{20}), 68.67 (C_{Fc}), 68.27 (C_{Fc}), 68.18 (C_{Fc}), 67.51 (C_{Fc}), 66.71 (C_{Fc}), 65.51 (C_{Fc}), 60.61 (C_{Fc}), 38.77 ($C_{8/21}$), 38.71 ($C_{8/21}$), 19.31 (C_{22}), 14.16 (C_{23}). ES+ 526.3 $[M+Na]^+$ 100%, 542.3 $[M+K]^+$ 20%,

General Procedure for the cleavage of the chiral auxiliary[2]

The corresponding alkoxy amine was dissolved in acetic acid (5-10 ml) and THF (0.5-1 ml). Water (6-12 ml) was added and the mixture gets milky white-orange. Zn dust (>40 eq) was added and the mixture was sonicated at 40°C for 3-6h (the reaction was consider finished when all the suspension dissolves in the aqueous solvent). The Zn dust was filtered off on celite and profusely washed with water and diethyl ether. The aqueous layer was extracted and washed with diethyl ether, then basified with NaOH 4M till pH 9. Ammonium chloride was added to remove the emulsion and then extracted with ethyl acetate. The combined

organic layers were washed with brine, dried over $MgSO_4$ which was filtered off and the solvent was then removed under vacuum.

(*R*)-1-ferrocenyl-2-phenyl-ethylamine[2]

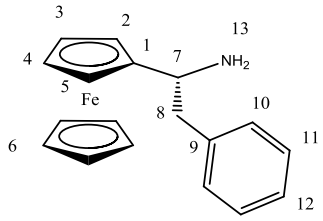

Purification Chromatographic column (Silica gel DCM - DCM:MeOH 10%) a yellow solid obtained (88%). The NMR data matched that given in the literature ^{1}H NMR (300 MHz, $CDCl_3$) δ 7.42 – 7.04 (m, 5 H, $H_{10\text{-}12}$), 4.34 – 4.02 (m, 9 H, $H_{1\text{-}6}$), 3.93 (dd, *J* = 8.9, 4.6 Hz, 1 H, H_7), 3.01 (dd, *J* = 13.2, 4.5 Hz, 1 H, H_{8a}), 2.73 (dd, *J* = 13.2, 9.0 Hz,1 H, H_{8b}), 1.80 (bs, 2 H, H_{13}). ^{13}C NMR (100 MHz, $CDCl_3$) δ 138.75 (C_9), 129.41 (C_{10}), 128.39 (C_{11}), 126.41 (C_{12}), 68.36 (C_6), 67.57 ($C_{3/4}$), 67.49 ($C_{3/4}$), 66.95 ($C_{2/5}$), 65.41 ($C_{2/5}$), 52.24 (C_7), 45.51 (C_8). TOF ES^+ *m/z:* 328.1 $[M+Na]^+$ and 289 $[M\text{-}NH_2]^+$

(*S*)-1-ferrocenyl-2-phenyl-ethylamine[2]

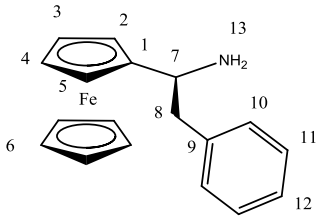

Purification: chromatographic column (silica gel DCM - DCM : MeOH 10%). A yellow solid obtained (20%). The NMR data matched that given in the literature ^{1}H NMR (300 MHz, $CDCl_3$) δ 7.48 – 7.03 (m, 5H, $H_{9\text{-}12}$), 4.33 – 4.06 (m, 2H, $H_{2\text{-}6}$), 4.05 – 3.90 (m, 1H, H_7), 3.12 (s, 2H, H_{13}), 3.04 (dd, *J* = 13.3, 4.2 Hz, 1H, H_{8a}), 2.79 (dd, *J* = 13.2, 8.6 Hz, 1H, H_{8b}). ^{13}C NMR (101 MHz, $CDCl_3$) δ 138.75 (C_9), 129.41 (C_{10}), 128.39 (C_{11}), 126.41 (C_{12}), 68.36 (C_6), 67.57 ($C_{3/4}$), 67.49 ($C_{3/4}$), 66.95 ($C_{2/5}$), 65.41 (C_7), 52.24 (C_7), 45.51 (C_8). ES^+ *m/z:* 289.1 $[M\text{-}NH_2]^+$

(R)-1-ferrocenyl-2-methyl-propylamine[2]

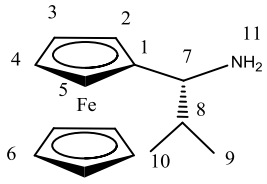

Purification: chromatographic column (Silica gel DCM -→ DCM:MeOH 10%) a yellow solid obtained (22%). The NMR data matched that given in the literature ^{1}H NMR (300 MHz, $CDCl_3$) δ 4.36 – 4.02 (m, 7 H, $H_{2,5,6}$), 3.86 (s, 2 H, $H_{3,4}$), 3.53 (d, *J* = 5.4, 1 H, H_7), 1.70 (dd, *J* = 12.7, 6.5 Hz, 1 H, $H_{9/10}$), 0.85 (dd, *J* = 24.8, 6.7 Hz, 1 H, $H_{9/10}$). ^{13}C NMR (75 MHz, $CDCl_3$) δ 94.53 – 91.27, 68.35, 67.32, 67.22, 65.09, 56.51, 34.85, 18.84. ES+ *m/z*: 241.1 $[M\text{-}NH_2]$ 100% 242.1 10%

(*R*)-1-ferrocenyl-2-naphthyl-ethylamine

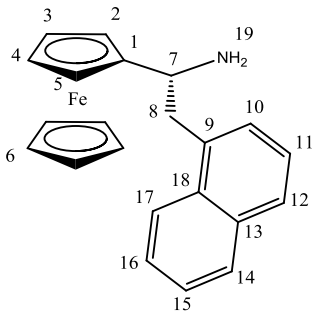

Purification: chromatographic column (Silica gel DCM -→ DCM:MeOH 10%) a yellow solid obtained (20%). ^{1}H NMR (300 MHz, $CDCl_3$) δ 8.06 (d, *J* = 7.8 Hz, 1H, H_{17}), 7.87 (dd, *J* = 7.3, 2.2 Hz, 1H, H_{14}), 7.75 (d, *J* = 8.2 Hz, 1H, H_{12}), 7.61 – 7.26 (m, 4H, $H_{10,11,15,16}$), 4.44 – 4.31 (m, 1H, H_7), 4.22 – 4.02 (m, 8H, $H_{2\text{-}6}$), 3.46 (dd, *J* = 13.5, 4.4 Hz, 1H, H_{8a}), 3.10 (dd, *J* = 13.6, 9.1 Hz, 1H, H_{8b}), 1.56 (bs, 2H, H_{19}), ^{13}C NMR (100 MHz, $CDCl_3$) δ 135.41, 133.99, 132.11, 128.84, 127.67, 127.17, 125.85, 125.53, 125.41, 123.87, 94.83, 77.04, 68.31, 67.46, 66.95, 65.12, 51.38, 43.53.ES+ *m/z:* 378.0 [M+Na] 100%; 339.0 [M-NH_2]60 %; 379 20%; 340 10%; HRMS Calc. 378.0921 found 378.0917 $C_{22}H_{21}N$ Na ^{56}Fe.

Ferrocenyl methyl amine[3]

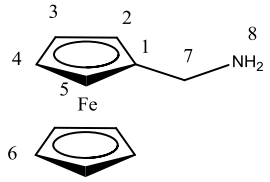

0.494 g (2.3 × 10^{-3} mol) of ferrocenecarboxyaldehyde 2.13 g (2.8 × 10^{-2} mol) of ammonium acetate were added dissolved in 30 mL of methanol at 0°C. The mixture was stirred at this temperature for 30 min. Sodium cyano borohydride (0.121 g, 2 × 10^{-3} M) was added portionwise at 0°C and the mixture stirred at r.t. overnight. The solvent was evaporated and the product purified via a chromatographic column (Silica gel, DCM -> DCM 10% MeOH -> DCM 10% MeOH 1% Et_3N). a yellow solid obtained (0.160 g, 33%). The NMR data matched that given in the literature ^{1}H NMR (300 MHz, $CDCl_3$) δ 4.22 (s, 2H), 4.21 – 4.05 (m, 7H), 3.56 (s, 2H).ES+ 199.31 [M-NH_2].

General procedure for NMR experiments

1 mL $CDCl_3$ solutions of the amines (conc. range 2 - 4.5 × 10^{-2} M) were prepared. Phenyl formyl boronic acid was weighed out in a vial and equimolar quantity of the amines was added from the solution prepared. The solution was then diluted up to 10 mL obtaining solution of a mM concentration. (conc. range 2 – 4.5 × 10^{-3} M). $CDCl_3$ solutions of the guest were also prepared (conc. range 1.1 – 4.4 × 10^{-2} M).

200 µL of the imine hosts **2a-d** (ca. 8 × 10^{-7} mol) were placed in a vial. Experiments involved the study of the formation of the adduct with either guest (1:1 host : guest) for

characterisation and the preparation of 1:1:1, 1:1:2 and 1:2:1 (host: *R*-guest : *S*-guest)* for the determination of K_R/K_S.† Aliquots of guest were then added accordingly.

Electrochemical titrations

Aliquots (*ca*. 200 µL, range 1 – 8 × 10^{-7} mol) of **2a-c** solutions prepared as described above, were diluted up to 10 mL with the electrolyte solution (TBA·PF_6 0.1 M in dichloromethane, decamethyl ferrocene used as internal reference). The mixture was stirred and purged with Ar for 5 min. Guests solution were prepared in the same electrolyte solution without the internal reference.

Electrochemical determination of *ee*

Solutions of different enantiomeric composition of Binol, **3**, or hydrobenzoin, **4** were prepared in 10 mL volumetric flasks in a way to obtain a total quantity of guest of ca. 4 × 10^{-6} mol. Aliquots of **2a-c** (*ca.* 4 × 10^{-7} mol) were added to the flasks then diluted to 10 mL with electrolyte solution. This resulted in solution of the host and a 10-fold excess molar quantity of the enantiomeric mixture of guest. **(*R*)-3 : (*S*)-3** mixtures prepared: 0.1 : 9.9 (98% ee); 0.3 : 9.7 (94% ee); 0.5 : 9.5 (90% ee); 0.7 : 9.3 (86% ee); 1 : 9.0 (80% ee); 1.3 / 8.7 (74% ee); 1.5 : 8.5 (70% ee); 1.7 : 8.3 (66% ee); 2.5 : 7.5 (50% ee); 5 : 5 (0% ee); 7 : 3 (-40% ee). **(*S,S*)-4 : (*R,R*)-4** mixtures prepared: 0.1 : 9.9 (98% ee); 0.2 : 9.8 (96% ee); 0.3 : 9.7 (94% ee); 0.5 : 9.5 (90% ee); 1 : 9 (80% ee); 3 : 7 (40% ee); 5 : 5 (0% ee); 7 : 3 (-40% ee). All the solution were prepared in the presence of molecular sieve 3 Å and left standing for 4 h.

(*S*)-1,2,4-butanetriol

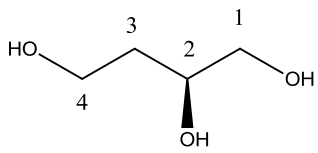

To a stirring solution of BH_3 SMe_2 (30 mL of a 2 M solution in THF 0.06 mol 3.75 eq) and $B(OMe)_3$ (6 mL, 0.0538 mol, 3.32 eq) (*S*)-malic acid (2.18 g, 0.0162 mol, 1 eq) dissolved in 10 mL of THF was added dropwise at 0°C. The mixture was stirred for further 5 min at the same temperature and then overnight at r.t.. 15mL of methanol were added over 1 h (hydrogen evolution). The solvent was then evaporated and methanol (50 mL) added and evaporated three times obtaining a colourless oil. Purification: chromatographic column: silica (dcm : MeOH 9 : 1)

* For adduct **(*R,R*) and (*R,S*)-8b** formed by ^{i}Pr host **(R)-2b** and Binol **3** the ratio was 1:2:2; 1:2:4 and 1:4:2.
† K_{RR}/K_{SS} when hydrobenzoin, **4**, is the guest.

the product was not UV active for this reason permanganate dip was used to develop TLCs. A colourless oil was obtained (1.48 g, 86%). ^{1}H NMR (300 MHz, MeOD) δ 3.83 – 3.60 (m, 3H, $H_{1,2}$), 3.53 – 3.38 (m, 2H, H_4), 1.82 – 1.47 (m, 2H, H_3). ^{13}C NMR (75 MHz, MeOD) δ 69.31 (C_2), 66.08 (C_1), 58.54 (C_4), 35.69 (C_3). EIMS showed an isotopic pattern identical to the one present in SigmaAldich database for the commercial product.

(2S,4S)-4-(Hydroxymethyl)-2-ferrocenyl-1,3-dioxane[4]

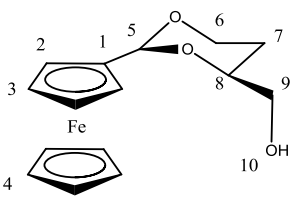

Ferrocene carboxyaldehyde (1.032 g 4.8 x 10^{-3} M) was placed in a 25 mL flask and trimethyl orthoformiate (6 mL) was added along with a catalytic quantity of PTSA (44 mg). The mixture was stirred at 80°C overnight. Potassium carbonate (5 g) was then added and the mixture cooled down to r.t.. Potassium carbonate was filtered off on celite and washed with diethyl ether. The solvent was evaporated yielding a dark red oil that was dried under vacuum for one day before being used in the next step without further purification. The oil obtained previously was dissolved in 5 mL of chloroform and (*S*)-(-)-1,2,4-butanetriol (0.498 g, 4.7 × 10^{-3} M) dissolved in 10 mL of chloroform was then added with PTSA (44 mg). The mixture was then stirred overnight at r.t. in the presence of molecular sieves 3Å. Potassium carbonate was then added, the reaction was stirred for 10 min and then the potassium carbonate was filtered on celite. The solvent was evaporated obtaining a red oil. The product was recrystallized by redissolving it in boiling toluene and allowing it to stand at -20°C for 5 days. (0.850 g 59%). The NMR data matched that given in the literature. ^{1}H NMR (300 MHz, $CDCl_3$) δ 5.41 (s, 1H, H_5), 4.37 – 4.30 (m, 2H, $H_{6,Fc}$), 4.30 – 4.11 (m, 9H, $H_{Fc,8}$), 4.02 – 3.83 (m, 2H, H_6), 3.74 – 3.55 (m, 2H, H_9), 2.03 (dd, J = 7.8, 5.3 Hz, 1H), 1.95 – 1.76 (m, 1H, H_{7a}), 1.47 – 1.35 (m, 1H, H_{7b}). ^{13}C NMR (75 MHz, $CDCl_3$) δ 100.18 (C_5), 77.17 (C_1), 68.87 (C_4), 68.03 (C_3), 66.62($C_{2/8}$), 66.49 (C_6), 66.43($C_{2/8}$), 65.77 (C_9), 26.84 (C_7).

(2S,4S)-4-(Methoxymethyl)-2-ferrocenyl-1,3-dioxane[4]

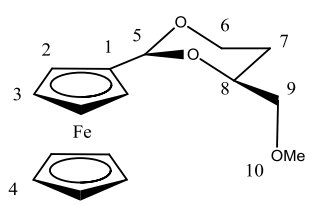

0.290 g of NaH (60% w:w, 7.25 × 10^{-3} mol) were washed with hexane and placed in a 100 mL flask with 15 mL of THF. 0.850 g of (2*S*,4*S*)-4-(hydroxymethyl)-2-ferrocenyl-1,3-dioxane (2.8 × 10^{-3} mol 1eq.) dissolved in 20 mL of THF were added over 1.5 h at 0°C. 0.200 mL of methyl iodide (3.21 × 10^{-3} mol) were added at the same temperature. The

mixture was stirred overnight at r.t.. Purification: chromatographic column (silica gel, hexane : diethyl ether = 4 : 1). 0.855 g of a red oil obtained (96%). The NMR data matched that given in the literature ^{1}H NMR (300 MHz, $CDCl_3$) δ 5.38 (s, 1H, H_5), 4.40 – 4.29 (m, 2H, H_6), 4.29 – 4.19 (m, 2H, H_2), 4.17 (s, J = 4.5 Hz, 5H), 4.11 (t, J = 1.9 Hz, 2H), 4.06 – 3.95 (m, 1H), 3.90 (ddd, J = 12.2, 11.6, 2.6 Hz, 1H), 3.54 (dd, J = 10.3, 6.1 Hz, 1H), 3.47 – 3.38 (m, 4H, H_{10}), 1.78 (ddd, J = 23.9, 12.0, 5.1 Hz, 1H,), 1.49 (dtd, J = 13.2, 2.6, 1.4 Hz, 1H).

(*S*)-α-Boronoferrocenecarboxyaldehyde[4]

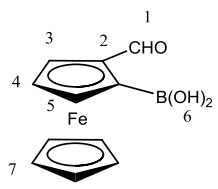

(2S,4S)-4-(Methoxymethyl)-2-ferrocenyl-1,3-dioxane (0.790 g, 2.5×10^{-3} mol) was dissolved in 10 mL of dry diethyl ether. The mixture was cooled at -78°C and ^{t}BuLi (1.7 mL of a 1.7 M pentane solution, 2.8×10^{-3} mol), the mixture was then stirred at the same temperature for 10 min and then for 1h20' at r.t. $B(O^{i}Pr)_3$ (0.9 mL, 3.75×10^{-3} mol) was added to the mixture at -78°C and THF (10 mL) was added right after. The mixture was stirred for further 2h. Reaction quenched with water end extracted with diethyl ether (×3). The organic phases joined together were dried over $MgSO_4$ and evaporated.

Purification: chromatographic column (silica gel, diethyl ether) 0.140 g obtained (16%) the product undergoes acetal hydrolysis onto the column yielding (*S*)-α-Bromoferrocenecarboxyaldehyde (0.150 g). The NMR data matched that given in the literature ES+ *m/z*: 383.1 $[M+Na]^+$ 100% HRMS *m/z:* calc. 383.0729; *m/z:* found 383.0726 for $C_{16}H_{21}{}^{11}BO_5Na^{56}Fe$

0.130 g (3.61×10^{-4} mol) of (2*S*, 4*S*, S_{Fc})-4-(Methoxymethyl)-2-[α-formylferrocenyl)-1,3-dioxane were dissolved in 4 mL of dichloromethane and 3 mL of water were then added. *p*-toluen sulfonic acid (0.02 g, 1.05×10^{-4} mol) the biphasic mixture was then stirred overnight at r.t.. The organic phase was separated and the aqueous layer extracted with dcm (10 mL ×2). The organic phases joined togheter were then dried over Magnesium sulphate and evaporated. 0.09 g of a dark red solid obtained (97%). The NMR data matched that given in the literature ^{1}H NMR (400 MHz, $CDCl_3$) δ 9.88 (s, 1H, H_1), 7.01 (s, 2H, H_6), 5.25 – 5.05 (m, 1H, H_3), 4.97 – 4.78 (m, 2H, $H_{4,5}$), 4.30 (s, 5H, $H_{,}$ H_7) ^{13}C NMR (100 MHz, $CDCl_3$) δ 197.43 (C_1), 82.32 (C_3), 78.73 ($C_{4/5}$), 77.08 ($C_{4/5}$), 70.73 (C_7).

(*S*)-α-(pinacolboronate)-ferrocenecarboxyaldehyde

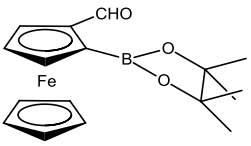

0.150 g (5.8×10^{-4} mol) of (*S*)-α-Boronoferrocenecarboxyaldehyde were dissolved in 5 mL of dichloromethane. 0.213 g(1.8×10^{-3} mol) of pinacol were added and the mixture was stirred overnight at r.t..

Purification: chromatographic column (Silica gel, AcOEt : hexane 3.5 : 10 - AcOEt). 0.100 g obtained (51 %) of a red solid obtained. ^{1}H NMR (400 MHz, $CDCl_3$) δ 10.39 (s, 1H), 5.14 (dd, *J* = 2.3, 1.4 Hz, 1H), 4.82 (dt, *J* = 8.2, 2.3 Hz, 2H), 4.27 (s, *J* = 46.7 Hz, 5H), 1.39 (d, *J* = 1.6 Hz, 12H). ES+ *m/z:* 363.2 $[M+Na]^+$ HRMS calc. *m/z:* 363.0831 found *m/z:* 363.0824 $C_{17}H_{21}{}^{11}BO_3Na^{56}Fe$.

1,1 bis(chlorocarbonyl)ferrocene[5]

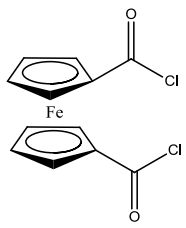

Ferrocene (5.423 g 0.0292 mol) was dissolved in 240 ml of hexane and added dropwise to a stirring solution of *n*-BuLi (1.6M in hexane) (0.072 mol) and TMEDA (10 ml 0.0667 mol) in 10 ml of hexane. The mixture was stirred overnight. An orange solid was obtained, the product was used in the next step without purification.

In a 1 L beacker was placed an excess of dry ice and 1 L of diethyl ether. The mixture obtained previously was poured in the beaker and stirred until all the dry ice has sublimed. A yellow solid suddenly formed; which was filtered off and washed with Et_2O. This was then dissolved in a NaOH 0.1 M (40 ml) solution and washed with DCM (2 x 40 ml). The aqueous layer is acidified with HCl conc. The solid formed was filtered off and washed with toluene and dried under vacuum. 5.033 g (63%)

1,1 ferrocene dicarboxylic acid (5.033 g, 0.0184 mol) was placed in a 250 ml 3 necked round bottomed flask with 15 ml of dry DCM. Oxalyl chloride (9.6 ml, 0.11 mol) in 35 ml of dry DCM was added dropwise at 0°C. The mixture was warmed up to r.t. and stirred overnight. The solvent was evaporated and the dark red solid obtained was purified using a Soxhlet extractor with pentane to give 4.023 g of a red solid (70 %). The NMR data matched that given in the literature ^{1}H-NMR (300 MHz, $CDCl_3$) δ: 5.05 (t, *J* = 1.8 Hz, 4H) 4.76 (t, *J* = 1.8, 4H) also ferrocene mono acid chloride present in a ratio bis : mono = 2 : 1

1,1' bis[((6-amidopyridyl)amino)carbonyl]ferrocene[5]

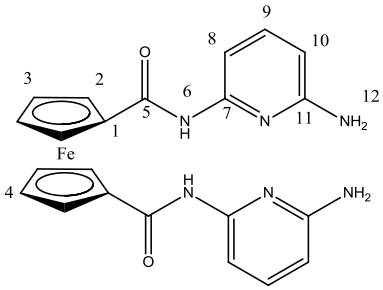

1,1' bis(chlorocarbonyl)ferrocene (0.534 g; 1.71 x 10^{-3} mol) was dissolved in 40 ml of dry THF and added dropwise to a mixture of 2,6 diaminopyridine (0.404 g; 3.70 x 10^{-3} mol) and triethylamine (0.05 ml; 3.59 x 10^{-4} mol) in 10 ml of dry THF at 0°C over a period of 30'. The mixture was allowed to warm up to r.t. and stirred for 48h. The solid present was filtered off and the solvent evaporated. A dark red solid was obtained. The crude was purified by chromatographic column (basic alumina, DCM-MeOH 5%) to give 0.116 g (16%).The NMR data matched that given in the literature ^{1}H-NMR (300 MHz, $CDCl_3$) δ: 8.03 (s, 2H, H_6); 7.60 (d, 2H, $H_{10/8}$); 7.45 (t, 2H, H_9); 6.26 (d, 2H, $H_{10/8}$); 4.83 (t, 4H, H_2); 4.50 (t, 4H, H_3); 4.34 (s, 4H, H_{12})

ES^+ found 457.2 $[M+H]^+$ and 479.4 $[M+Na]^+$

(*R*)-2,2 bis[(ethoxycarbonyl)methoxy]-1,1-binaphthol[6]

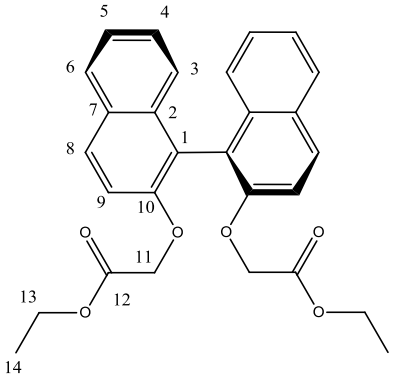

1,1-binaphthol (1 g; 3.49 x 10^{-3} mol) was refluxed with K_2CO_3 (1.72 g, 1.24 x 10^{-2} mol) and ethylbromoacetate (2 ml, 1.80 x 10^{-2} mol) in 20 ml of acetone for 24h. The white solid present was filtered off and the solvent was evaporated. Purification of the crude by chromatographic column (Basic alumina, n-hexane : ethyl acetate 5:1) gave 1.183 g (74%). The NMR data matched that given in the literature ^{1}H-NMR (300 MHz, $CDCl_3$) δ: 7.95 (d, J= 8.8 Hz, 2H, H_8); 7.86 (d, J= 8.1 Hz, 2H, H_6); 7.34 (d, J= 8.8 Hz; 4H, H_9); 7.21 (m, 4H, $H_{5,4}$); 4.54 (s, 4H, H_{11}); 4.11 (q, J = 7.2 Hz, 4H, H_{13}); 1.16 (t, J= 7.2, 6H, H_{14}); ^{13}C-NMR (300 MHz, $CDCl_3$) δ: 169.74 (C_{12}); 154.18 (C_{Ar}); 134.35 (C_{Ar}); 130.23 (C_{Ar}); 130.03 (C_{Ar}); 128.27 (C_{Ar}); 126.87 (C_{Ar}); 126.04 (C_{Ar}); 124.53 (C_{Ar}); 120.83 (C_{Ar}); 116.09 (C_{Ar}); 67.70 (C_{11}); 61.37 (C_{13}); 14.43 (C_{14}) ES^+ found 481.3 $[M+ Na]^+$

(*R*)-(2'-Carboxymethoxy-[1,1']binaphthalenyl-2-yloxy)-acetic acid[6]

(*R*)-2,2 bis[(ethoxycarbonyl)methoxy]-1,1-binaphthol (1.183 g, 2.58 x 10^{-3} mol) was refluxed with a NaOH 33% solution (6 ml) in 6 ml of ethanol for 30h. The solvent was evaporated and the solid obtained dissolved in water (20 ml). HCl conc. was added dropwise, a white solid

formed was extracted with DCM (2 x 25 ml), the organic layers united were washed with water (40 ml), dried over Na_2SO_4 and evaporated to give 1.005 g of a white solid (97%). The NMR data matched that given in the literature ^{1}H-NMR (300 MHz, $CDCl_3$) δ: 7.98 (d, *J*= 9.1 Hz, 2H, H_3); 7.89 (d, *J*= 8.1 Hz, 2H, H_2); 7.38 (t, *J*= 8.1, 2H, $H_{4/5}$); 7.32 (d, *J*= 8.1 Hz, 2H, H_6), 7.25 (ap.t. *J*= 8.1 Hz, 2H, $H_{4/5}$), 7.12 (d, *J*= 8.1 Hz, 2H, H_1); 4.60 (AB sys, *J*= 16.7 Hz, 4H, H_7); 3.64 (broad s, 2H, H_{13}). ^{13}C-NMR (75 MHz, $CDCl_3$) δ: 172.55 (C_{12}); 152.63 (C_{Ar}); 133.74 (C_{Ar}); 130.18 (C_{Ar}); 129.94 (C_{Ar}); 128.12 (C_{Ar}); 126.96 (C_{Ar}); 125.35 (C_{Ar}); 124.55 (C_{Ar}); 119.94 (C_{Ar}); 114.80 (C_{Ar}); 66.40 (C_{11}) ES$^+$ found 425.4 $[M+Na]^+$

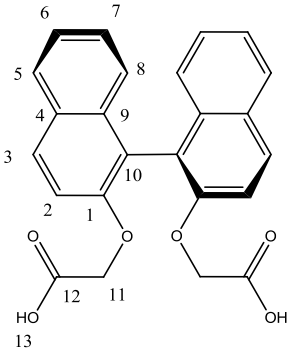

Macrocycle (*R*)-16a

Oxalyl chloride (0.165 ml, 1.92 x 10^{-3} mol) in 10 ml of dry DCM was added dropwise at 0°C to (2'-Carboxymethoxy-[1,1']binaphthalenyl-2-yloxy)-acetic acid (0.130 g, 3.23 x 10^{-3} mol) in 5 ml of dry DCM. One drop of DMF was added. The mixture was stirred at r.t. for 5h. the solvent was evaporated giving a brown oil (0.178 g) that was used in the next step without purification. ^{1}H-NMR (300 MHz, $CDCl_3$) δ: 8.00 (d, *J*= 9.19 Hz, 2H); 7.90 (d, *J* = 8.04, 2H); 7.28 (m, 8H); 4.84 (s, 4H). (R)-2,2-bis[(chlorocarbonyl)methoxy]-1,1-binaphthol (0.170 g 3.87 x 10^{-4} mol) dissolved in 35 ml of dry THF and 1,1' bis[((6-amidopyridyl)amino)carbonyl]ferrocene (0.150 g, 3.29 × 10^{-4} mol) and triethylamine (0.100 ml, 7.17 x 10^{-4} mol) dissolved in 35 ml of dry THF were simultaneously added dropwise to 40 ml of dry THF under vigorous stirring at r.t., over a period of 30'. The mixture was stirred overnight. The solvent was evaporated and the orange solid obtained dissolved in DCM and washed with a solution of $NaHCO_3$ (sat). The organic layer dried over $MgSO_4$ and evaporated. Purification: Chromatographic column: (silica gel, n-hexane : AcOEt 1:1). 0.04 g obtained (30%) of an orange solid. ^{1}H-NMR (500 MHz, $CDCl_3$, 300 K) δ: 8.75 (s, 2H, H_5); 8.62 (s, 2H, H_{11}); 8.04 (d, *J* = 8.7 Hz, 2H, H_{16}); 7.92 (d, *J* = 8.1 Hz, 2H, H_{23}); 7.80 (d, *J* = 7.8 Hz, 2H, H_{10}); 7.64 (t, *J* = 8.1 Hz, 2H, H_9); 7.45 (t, *J* = 9.2 Hz, 4H, $H_{15,22}$); 7.34 (m, 2H, H_{21}); 7.22 (t, *J* = 7.81 Hz, 4H, $H_{8,10}$); 4.96 (m, 2H H_{2a}); 4.92 (m, 2H, H_{2b}); 4.63 (m, 2H, H_{1a}); 4.52 (m, 2H, H_{1b}); 4.60-4.40 (dd, *J*= 15.45 Hz,

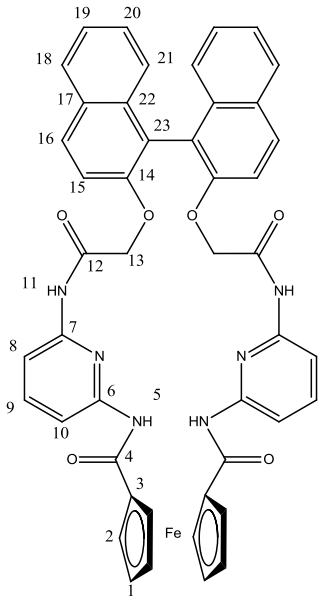

4H, H_{13}); ^{13}C-NMR (125 MHz, $CDCl_3$, 300 K) δ: 168.40 (C_4); 167.06 (C_{12}); 152.81 (C_{14}); 149.79 (C_6); 148.50 (C_7); 140.29 (C_9); 133.55 (C_{18}); 130.96 (C_{16}); 130.40 (C_{17}); 128.39 (C_{23}); 127.51 (C_{21}); 125.44 (C_{20}); 125.16 (C_{22}); 120.34 (C_{19}); 116.21 (C_{15}); 111.97 (C_{10}); 110.06 (C_8); 77.41 (C_3); 73.10 (C_{1a}); 72.59 (C_{1b}); 70.98 (C_{2a}); 70.22 (C_{2b}); 69.88 (C_{13}) ES+ found 845.1 $[M+Na]^+$ HRMS: found 845.1780 $[C_{46}H_{34}N_6O_6NaFe]$ Elem. Anal. calc. C 62.20, H 4.00, N 9.26 $C_{46}H_{34}N_6O_6Fe{\cdot}CH_2Cl_2$ found C 62.53, H 4.01, N 8.95.

(*R*)-2,2 bis[(ethoxycarbonyl)propoxy]-1,1-binaphthol[6]

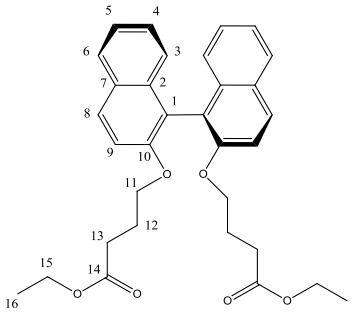

(*R*)-Binol (0.242 g, 8.45 × 10^{-4} mol) was dissolved in 10 ml of acetone. K_2CO_3 (0.498 g, 3.60 × 10^{-3} mol) and stirred for 10' at r.t. 4-bromoethylbutyrate (0.4 ml, 2.80 x 10^{-3} mol) was added and the mixture was refluxed for 72h. The white solid formed was filtered off and the solvent evaporated giving a pale yellow oil. This was dissolved in Dichloromethane (15 ml) and washed with water (2 x 20 ml). The organic layer was dried over $MgSO_4$ and evaporated. Purification of the crude by chromatographic column (basic alumina, n-hexane : AcOEt 5:1) gave 0.342 g of a pale yellow oil. The NMR data matched that given in the literature ^{1}H-NMR (300 MHz, $CDCl_3$) δ: 7.94 (d, 2H, H_3); 7.86 (d, 2H, H_6); 7.41 (d, 2H, H_8); 7.21 (m, 6H, $H_{4,5,9}$); 3.98 (m, 8H, $H_{13,15}$); 1.85 (m, 4H, H_{11}); 1.71 (m, 4H, H_{12}); 1.18 (t, 6H, H_{16}) ES+ found 537.1 $[M+Na]^+$

(2'-Carboxypropoxy-[1,1']binaphthalenyl-4-yloxy)-acetic acid[6]

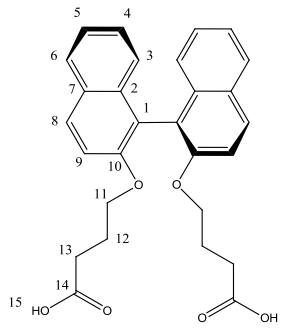

(R)-2,2 bis[(ethoxycarbonyl)propoxy]-1,1-binaphthol (0.342 g, 7.09 x 10^{-4} mol) was dissolved in ethanol (5 ml) and $NaOH_{(aq)}$ 2M (5 ml) was added. The mixture was refluxed overnight. The solvent was evaporated and the white solid obtained partitioned between DCM (25 ml) and HCl 1N (aq) (30 ml). The organic layer was washed with $NaHCO_3$ (sat) (15 ml), dried on $MgSO_4$ and evaporated giving 0.247 g of a white solid (77 %). The NMR data matched that given in the literature ^{1}H-NMR (300 MHz, $CDCl_3$) δ: 7.94 (d, 2H, H_3); 7.86 (d, 2H, H_6); 7.41 (d, 2H, H_8); 7.32 (t, 2H,); 7.21 (t, 2H); 7.16 (d, 2H); 4.04 (m, 2H); 3.92 (m, 2H); 2.09 (m, 2H); 1.61 (m, 2H) ^{13}C-NMR (75 MHz, $CDCl_3$) δ: 180.34 (C_{14}); 154.45 (C_{Ar}); 134.48 (C_{Ar}); 129.78 (C_{Ar}); 129.75 (C_{Ar}); 128.33 (C_{Ar}); 126.67 (C_{Ar});

125.75 (C_{Ar}); 124.03 (C_{Ar}); 120.88 (C_{Ar}); 116.02 (C_{Ar}); 68.59 (C_{13}); 30.11 (C_{11}); 24.67 (C_{12}). ES+ found 481.2 $[M+Na]^+$

Macrocycle (*R*)-16b

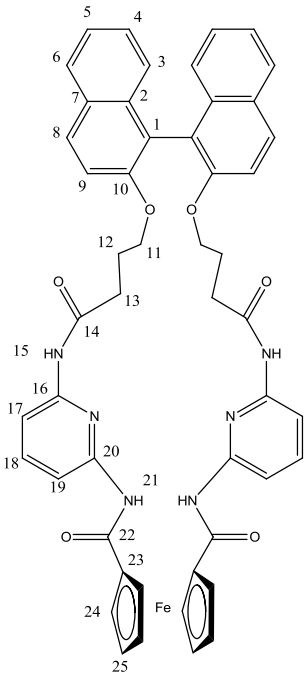

(2'-Carboxypropoxy-[1,1']binaphthalenyl-4-yloxy)-acetic acid (0.063 g 1.37 x 10^{-4} mol) was dissolved in 10 ml of dry DCM. Oxalyl chloride (0.100 ml, 1.15 x 10^{-3} mol) dissolved in 5 ml of DCM was added dropwise at 0°C. Few drops of DMF were added. The mixture was stirred at R.T. for 7h. The solvent was evaporated and a brown oil obtained 0.070 g. This compound is not isolated and it is used in the next stage without further purification. (R)-2,2-bis[(chlorocarbonyl)propoxy]-1,1-binaphthol (0.069 g 1.39 x 10^{-4} mol) dissolved in 20 ml of dry THF and bis[((6-amidopyridyl)amino)carbonyl]ferrocene (0.070 g 1.53 x 10^{-4} mol) with triethylamine (0.1 ml 7.17 x 10^{-4} mol) dissolved in 20 ml of dry THF were added simultaneously dropwise to 15 ml of dry THF vigorously stirred over a period of 1h. The mixture was stirred under N_2 overnight. The solvent was evaporated and the dark-red solid obtained dissolved in DCM (15 ml) and washed with $NaHCO_3$ (20 ml) and water (20 ml). the organic layer was dried on $MgSO_4$ and evaporated. Purification: Chromatographic column (silica gel, *n*-hexane : AcOEt 1:1) and a further chromatographic column (silica gel, DCM-MeOH 2%). 0.04 g (33%) of a red-orange solid obtained. ^{1}H-NMR (300 MHz, $CDCl_3$) δ: 8.33 (s, broad, $H_{21/15}$); 7.93 (d, J = 8.79 Hz , 2H, $H_{21/15}$); 7.86 (d, J= 8.09 Hz, 2H); 7.76 (m, 2H); 7.56 (m, 2H); 7.44 (d, J = 9.12 Hz, 2H); 7.34 (t, J = 6.96 Hz, 4H); 7.23 (t, J = 8.05 Hz, 2H); 7.13 (d, J = 8.41 Hz, 2H); 4.95 (s, 2H); 4.89 (s, 2H), 4.54 (s, 4H); 4.08 (m, 2H); 3.93 (m, 2H); 2.36 (m, 2H); 2.20 (m, 2H); 1.95 (m, 2H); 1.91 (m, 2H) ^{13}C-NMR (100 MHz, $CDCl_3$) δ: 167.55 ($C_{14/22}$); 167.53 ($C_{14/22}$); 154.30 (C_{Ar}); 149.64 (C_{Ar}); 149.37 (C_{Ar}); 140.65 (C_{Ar}); 134.13 (C_{Ar}); 129.62 (C_{Ar}); 129.55 (C_{Ar}); 127.94 (C_{Ar}); 126.48 (C_{Ar}); 125.41 (C_{Ar}); 124.00 (C_{Ar}); 121.18 (C_{Ar}); 116.81 (C_{Ar}); 109.78 (C_{Ar}); 109.75 (C_{Ar}); 77.55 (C_{23}); 72.96 (C_{24a}); 72.70 (C_{24b}); 70.43 (C_{25b}); 70.02 (C_{25b}); 69.28 (C_{13}); 65.83 (C_{11}); 45.86 (C_{12}); TOF ES$^+$ found 901.2 $[M+Na]^+$; HRMS calc. 901.2413 found 901.2420 $C_{50}H_{42}N_6O_6NaFe$, Elem. Anal. calc. C 68.34, H 4.82, N 9.56 for $C_{50}H_{42}N_6O_6Fe$, found C 68.35, H 4.88, N 9.58.

Crystal Structure of (*R,R*)-8a

$C_{45}H_{34}BFeNO_2.C_7H_8$ (crystals grown from toluene solution), M_r = 779.53, orange crystal, crystal dimensions: 0.16 x 0.08 x 0.03 mm, monoclinic, space group: *P*21, *a* = 11.7546(3), *b* = 8.5825(2), *c* = 19.6622(6) Å, β = 103.959(1)°, *V* = 1925.02(9) Å^3, *Z* = 2, ρ_{calcd} = 1.345 Mg/m$_3$, μ = 0.437 mm^{-1},$\lambda_{Mo\text{-}K\alpha}$ = 0.71073 Å, *T* = 120(2) K, $2\vartheta_{max}$ = 27.42°, 4685 reflections measured, 4235 observed reflections, R_1 = 0.0592 (observed reflections), *wR* = 0.1307 (all data), GOF = 1.164, largest diff. peak and hole: 0.451 and -0.535 e.Å^{-3}, Flack parameter = 0.08 (3).[7] The dataset was measured on a Bruker APEXII CCD diffractometer at the window of a Bruker FR591 rotating anode. The data collection was driven by COLLECT[8] and processed by DENZO[9] and EvalCCD.[10] An absorption correction was applied using TWINABS.[11] The structure was solved using ShelXS-97[12] and refined by a full-matrix leastsquares procedure on F_2 in ShelXL-97.[12] The crystal was a non-merohedral twin with the two domains related by -2.6° about the reciprocal axis (0 2 -5). The refined percentage ratio of the twin domains was 57:43. All non-hydrogen atoms were refined with anisotropic displacement parameters. All hydrogen atoms were added at calculated positions and refined by use of a riding model with isotropic displacement parameters based on the equivalent isotropic displacement parameter (U_{eq}) of the parent atom. Figures were produced using ORTEP3 for Windows.[13] The CIF for the crystal structure of **(*R,R*)-8a** has been deposited with the CCDC and has been given the deposition number 765703.

References

(1) Moody, C. J. *Chem. Commun.* **2004**, 1341.
(2) Willener, Y.; Joly, K. A.; Moody, C. J.; Tucker, J. H. R. *J. Org. Chem.* **2008**, *73*, 1225.
(3) Kraatz, H. B. *J. Organomet. Chem.* **1999**, *579*, 222.
(4) Riant, O.; Samuel, O.; Flessner, T.; Taudien, S.; Kagan, H. B. *J. Org. Chem.* **1997**, *62*, 6733.
(5) Beer, P. D.; Graydon, A. R.; Johnson, A. O. M.; Smith, D. K. *Inorg. Chem.* **1997**, *36*, 2112.
(6) Ema, T.; Tanida, D.; Sakai, T. *J. Am. Chem. Soc.* **2007**, *129*, 10591.
(7) Flack, H. D. *Acta Crystallographica Section A* **1983**, *39*, 876.
(8) Hooft, R. W. W. *COLLECT, Data software, Nonius B. V. (Delft)* **1998**.
(9) Otwinowski, Z.; Minor, W. In *Methods Enzymol.*; Carter, C. W., Sweet, R. M., Eds.; Academic Press: New York, 1997; Vol. 276.
(10) Duisenberg, A. J. M.; Kroon-Batenburg, L. M. J.; Schreurs, A. M. M. *J. Appl. Crystallogr.* **2003**, *36*, 220.
(11) Sheldrick, G. M. *TWINABS. Brucker AXS Inc. Madison, Wisconsin (USA)* **2007**.
(12) Sheldrick, G. M. *Acta Crystallographica Section A* **2008**, *64*, 112.
(13) Farrugia, L. J. *J. Appl. Crystallogr.* **1997**.

A.1 Appendix to Chapter 2

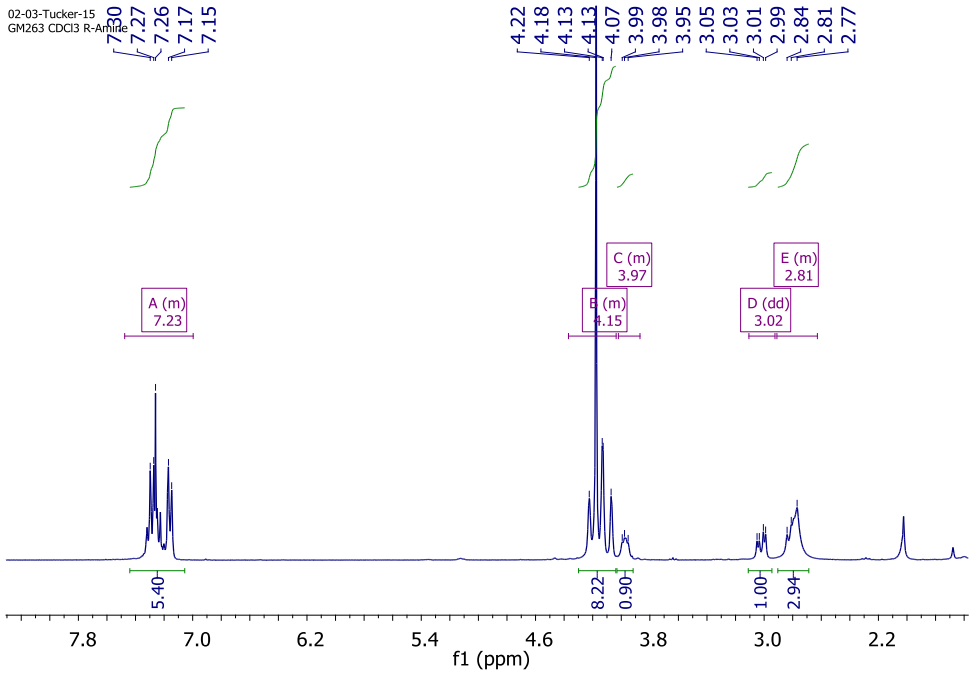

Figure 1. (*R*)-1a ^{1}H-NMR (300 MHz, $CDCl_3$)

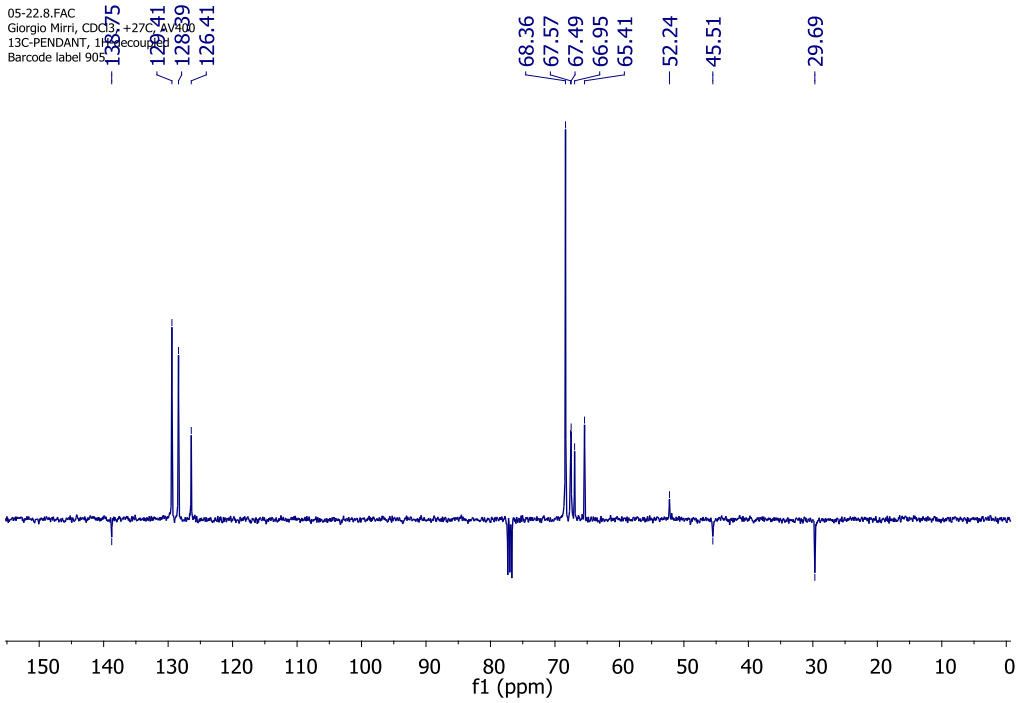

Figure 2. (*S*)-1a, ^{13}C-NMR (100 MHz, $CDCl_3$)

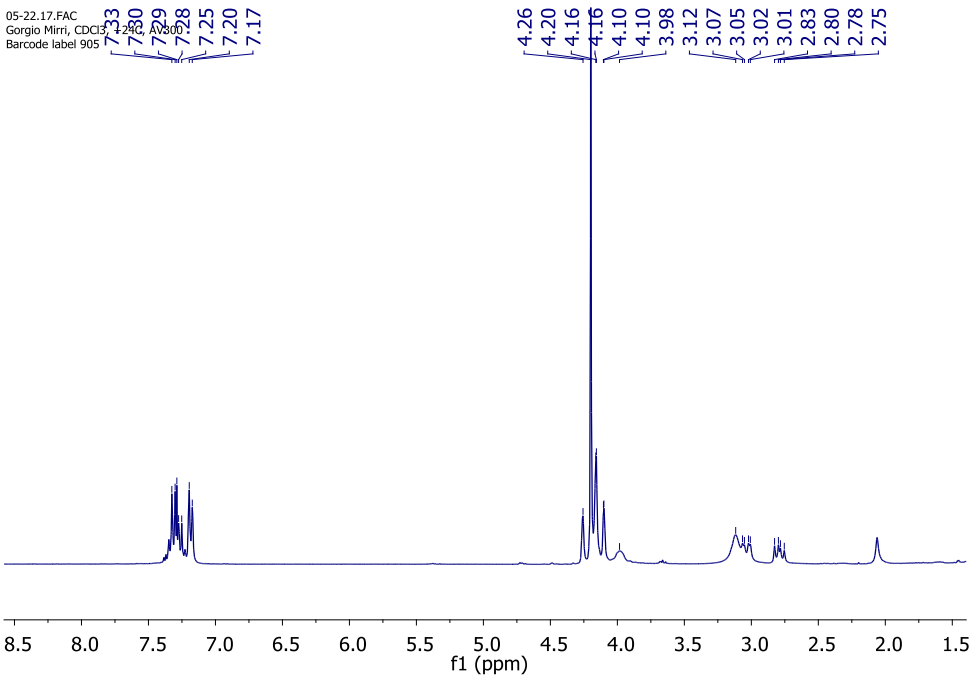

Figure 3. (*S*)-1a ^{1}H-NMR (300 MHz, $CDCl_3$)

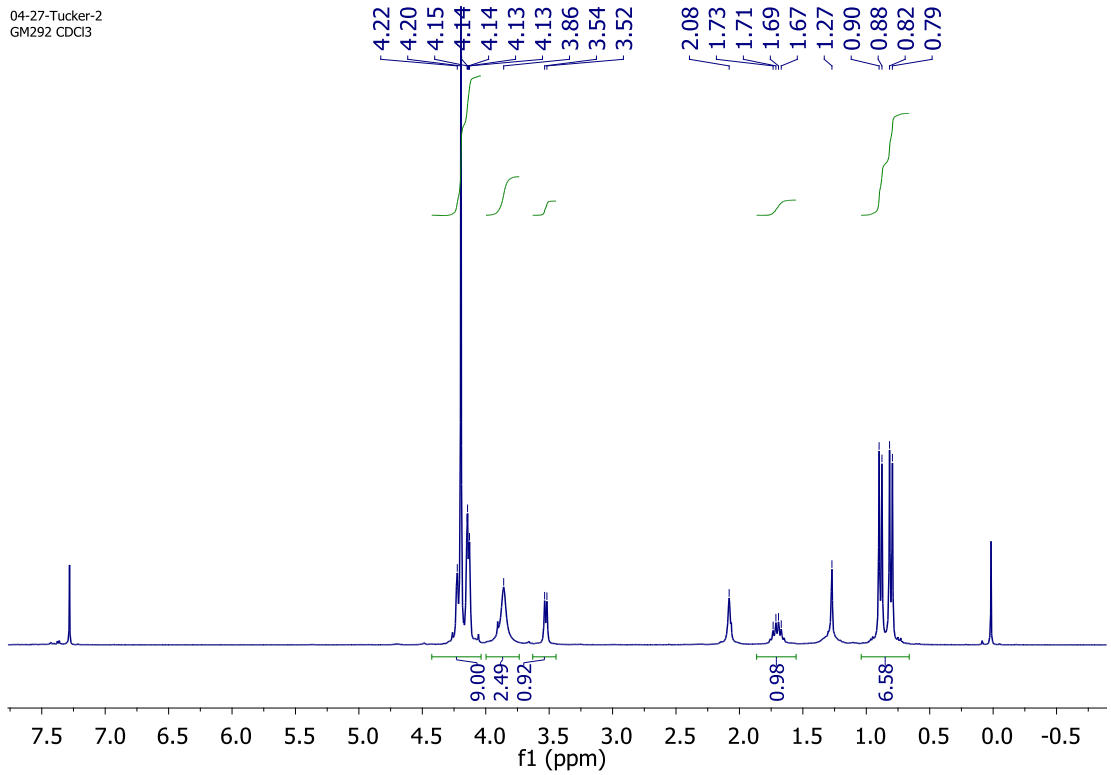

Figure 4. (*R*)-1b ^{1}H-NMR (300 MHz, $CDCl_3$)

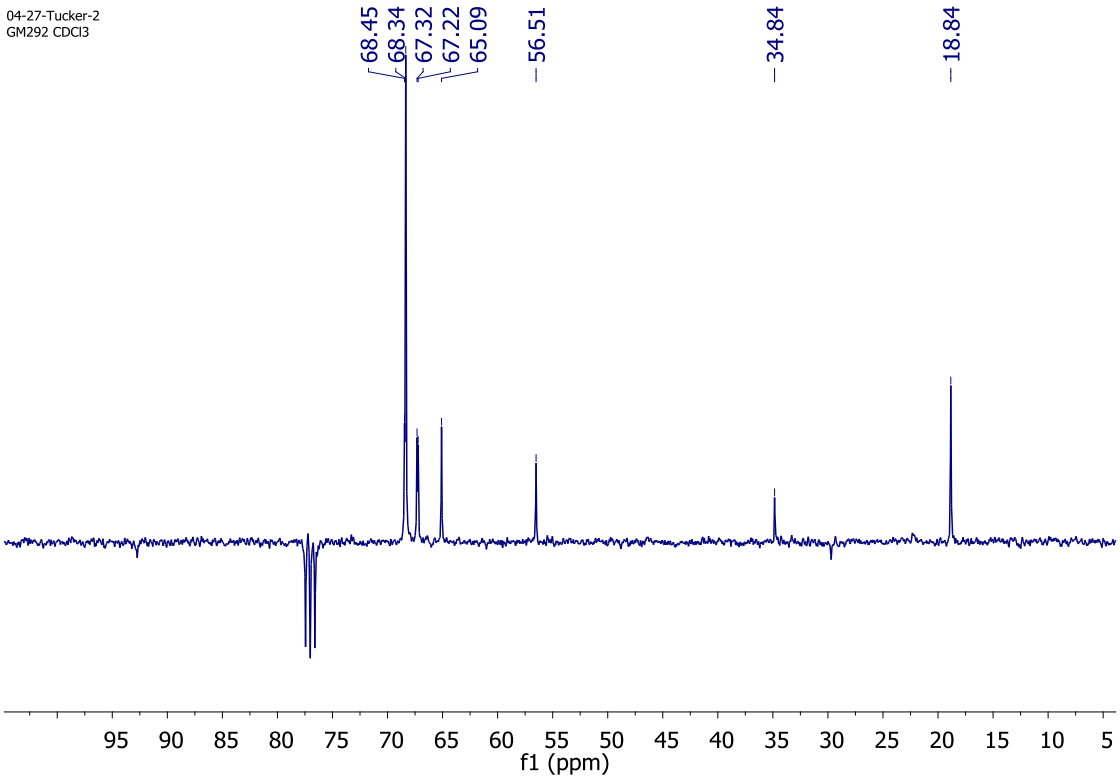

Figure 5. (*R*)-1b ^{13}C-NMR (100 MHz, $CDCl_3$)

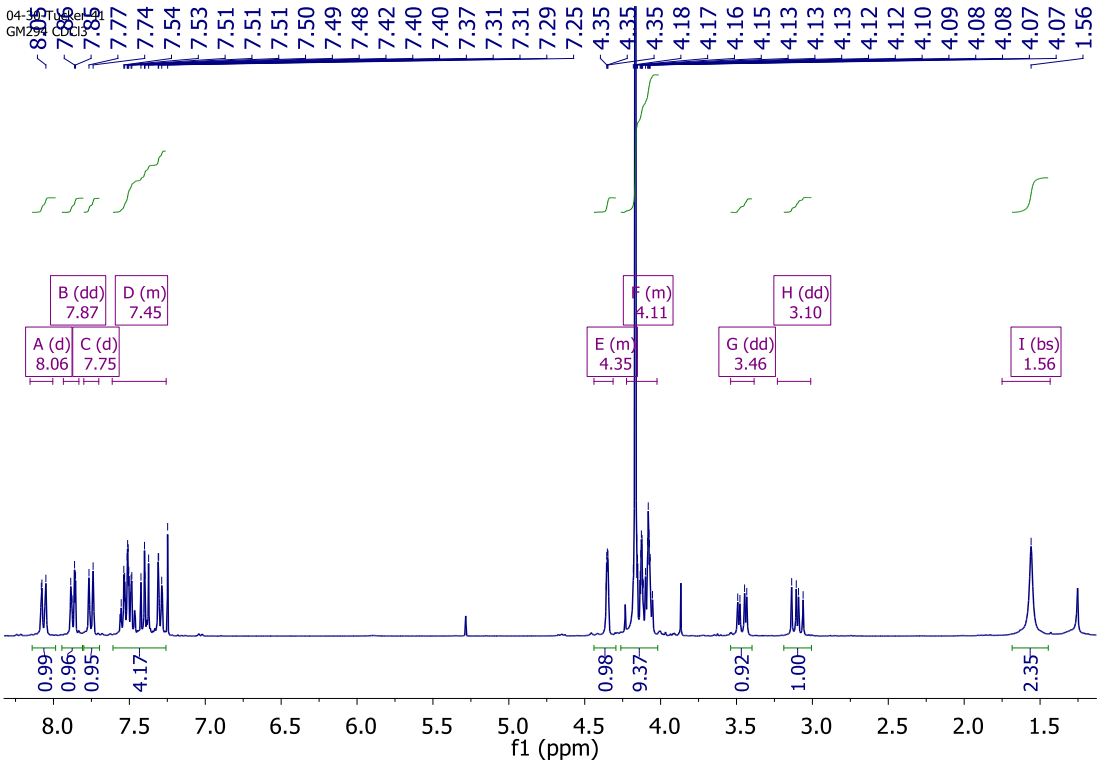

Figure 6. (*R*)-1c ^{1}H-NMR (300 MHz, $CDCl_3$)

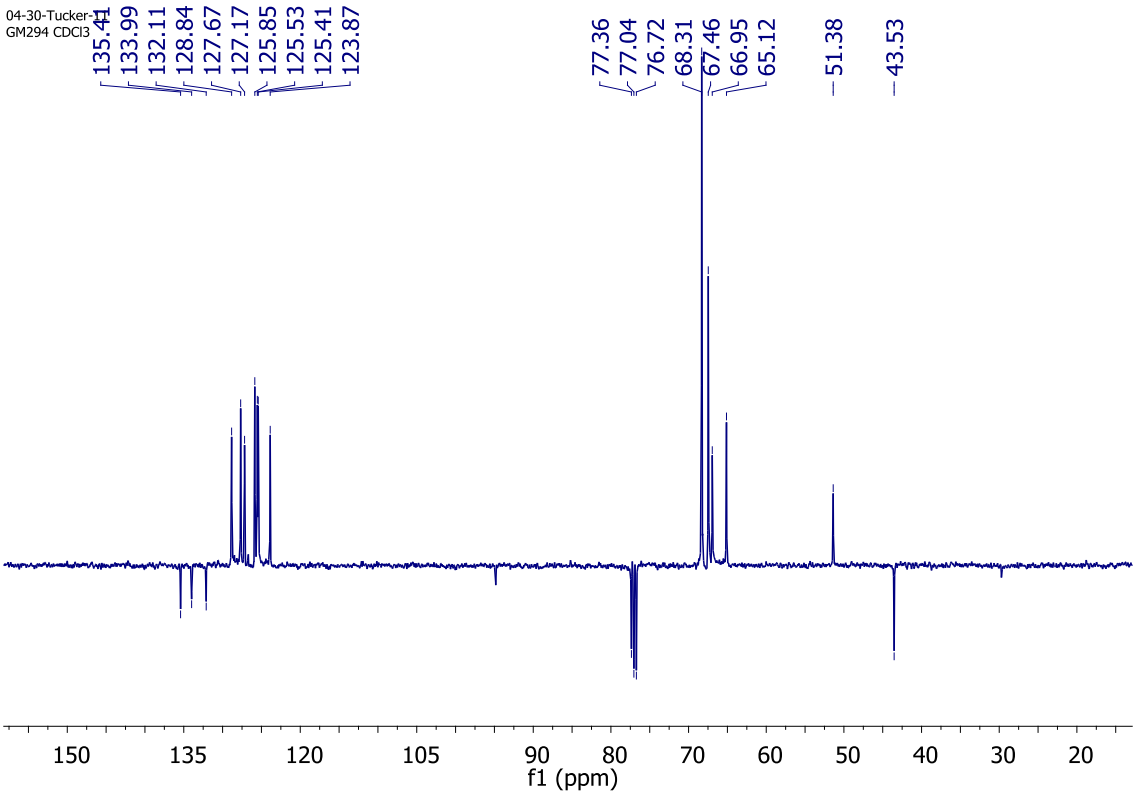

Figure 7. (*R*)-1c ^{13}C-NMR (100 MHz, $CDCl_3$)

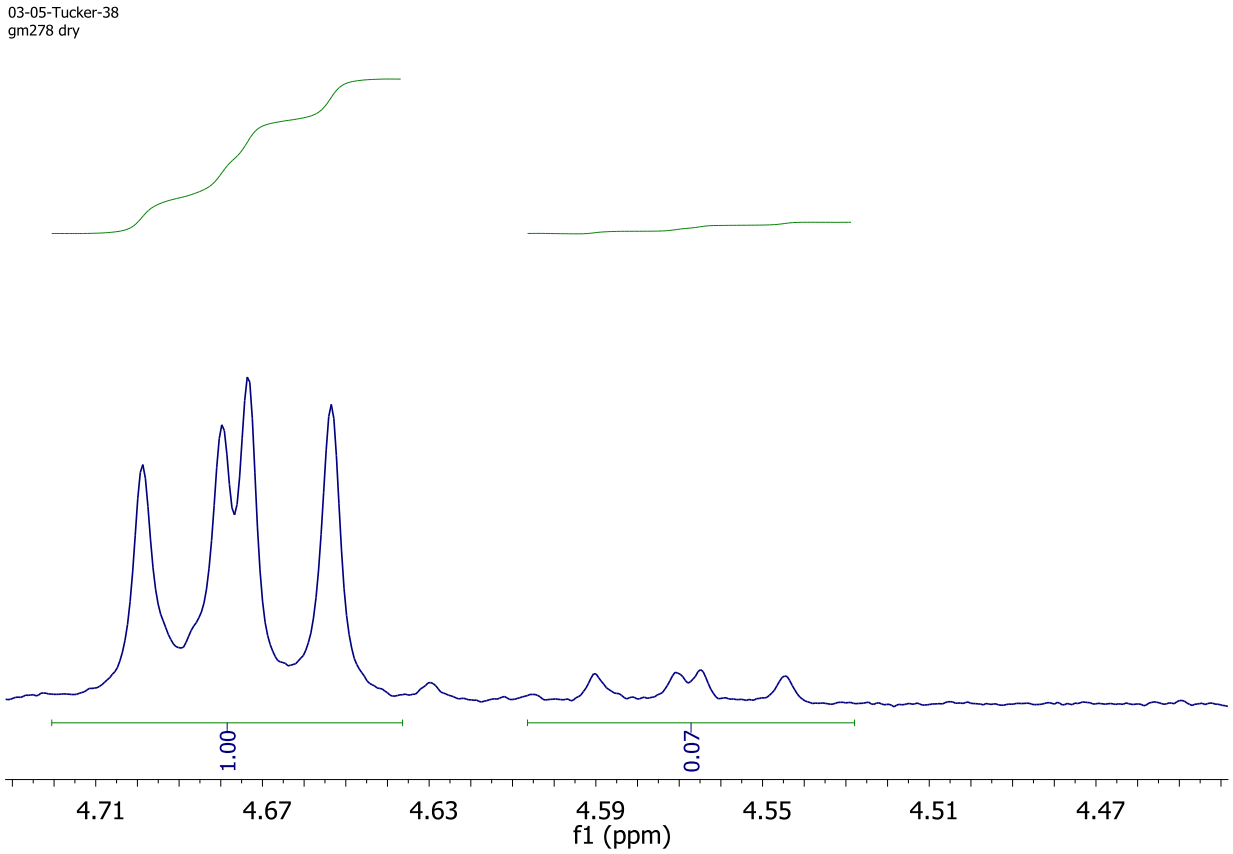

Figure 8 (*1R,1'R*)-1-Ferrocenyl-2-(1-naphthyl)-N-(1-phenylbutoxy)-1-ethylamine (precursor to **(*R*)-1c**). Determination of the diasteromeric excess (87% *de*)

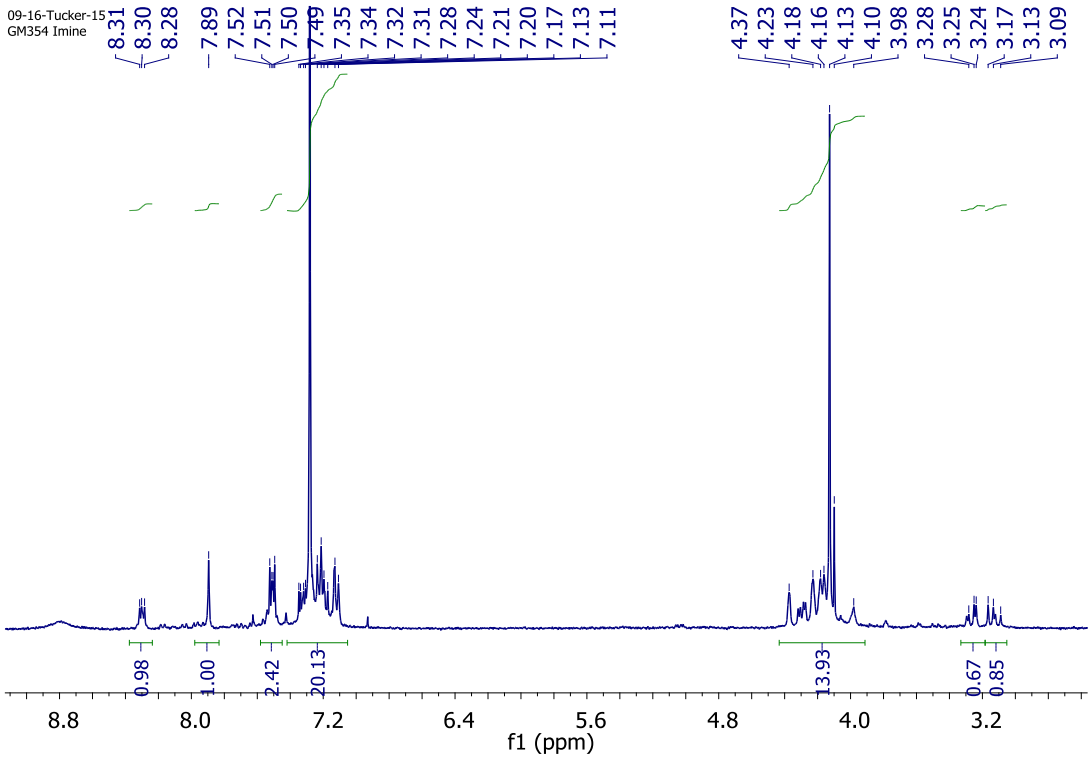

Figure 9. (*R*)-2a ^{1}H-NMR (300 MHz, $CDCl_3$)

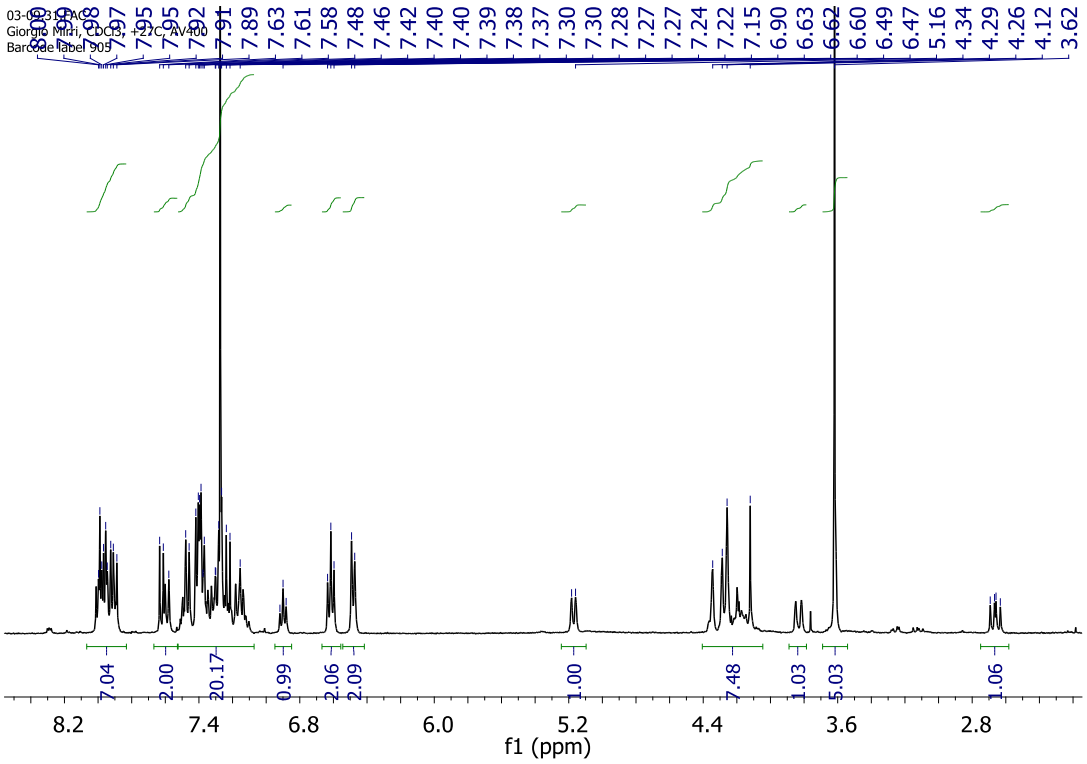

Figure 10. (*R,R*)-8a ^{1}H-NMR (300 MHz, $CDCl_3$)

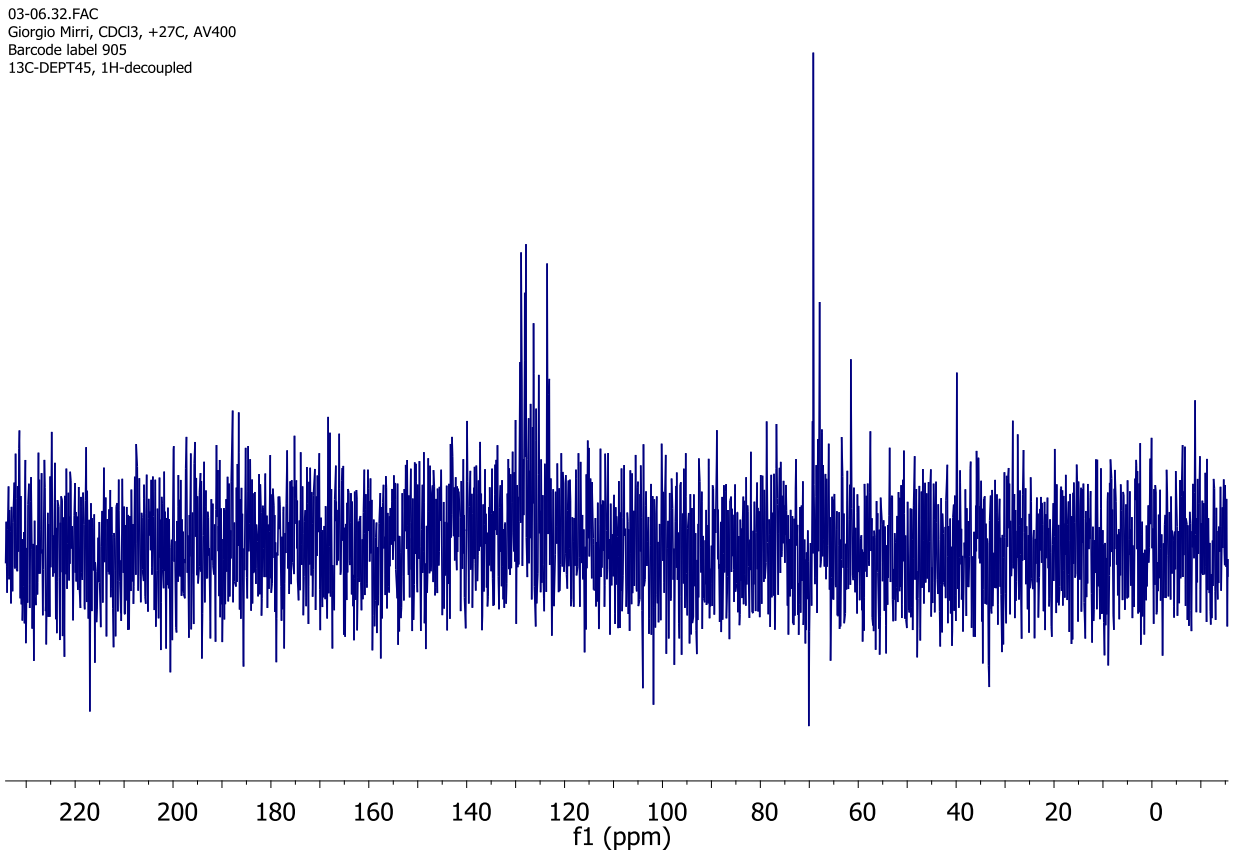

Figure 11 (*R,R*)-8a ^{13}C-NMR (100 MHz, $CDCl_3$)

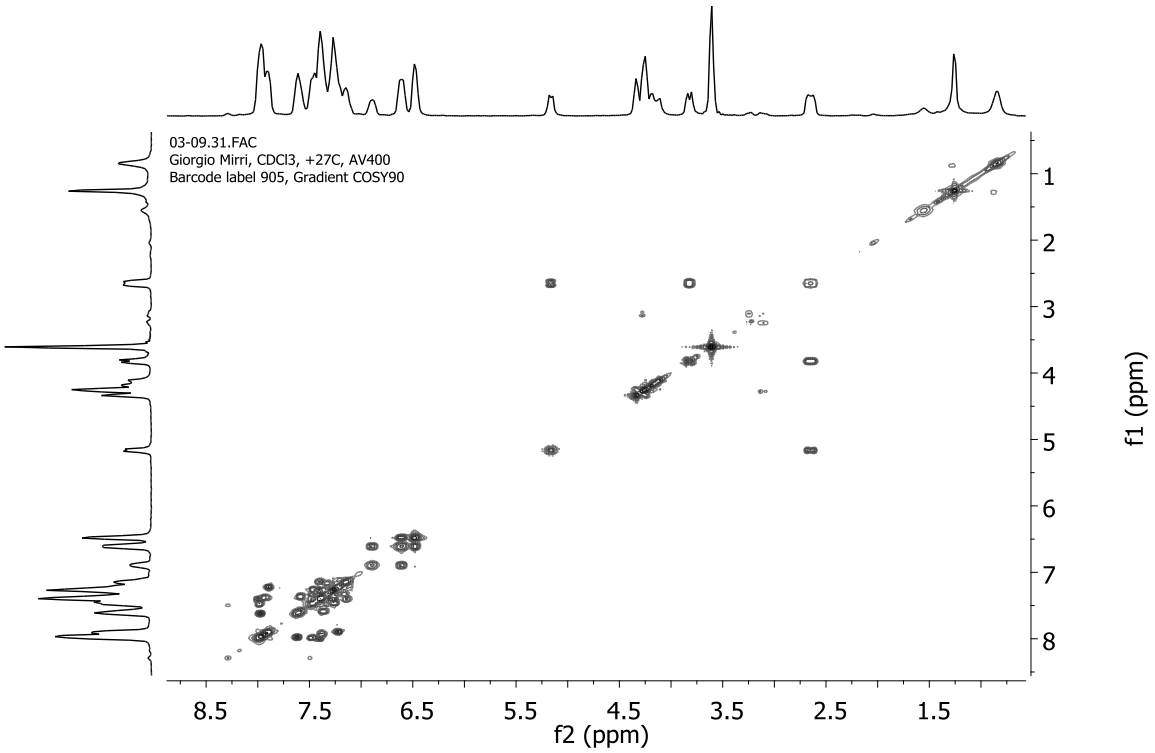

Figure 12 (*R,R*)-8a ^{1}H-^{1}H (COSY)-NMR (400 MHz, $CDCl_3$)

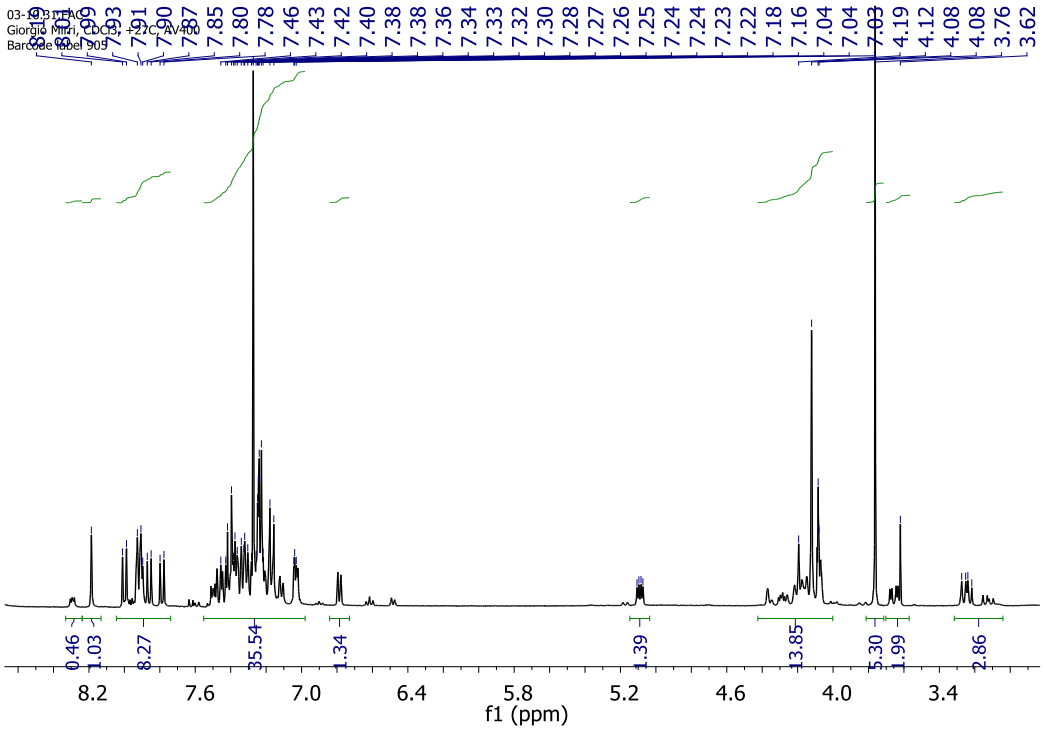

Figure 13. (*R,S*)-8a ^{1}H-NMR (300 MHz, $CDCl_3$)

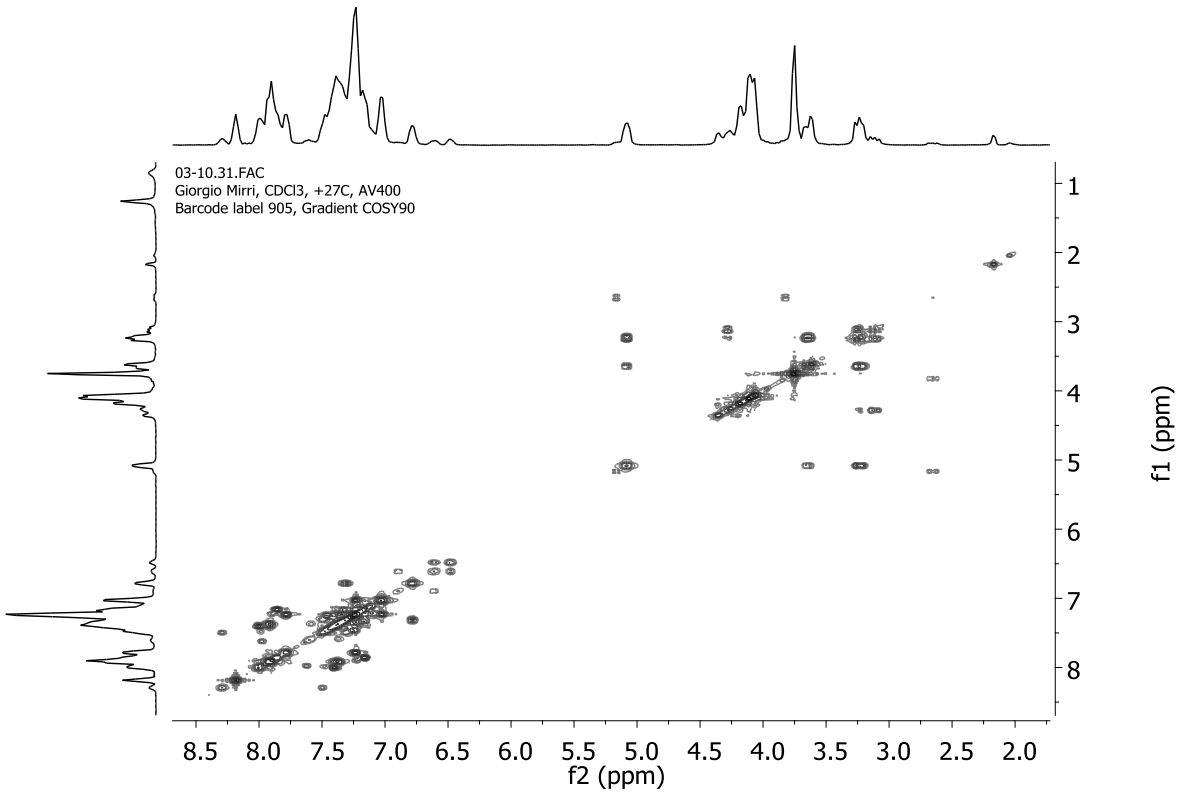

Figure 14. (*R,S*)-8a ^{1}H-^{1}H (COSY)-NMR (400 MHz, $CDCl_3$)

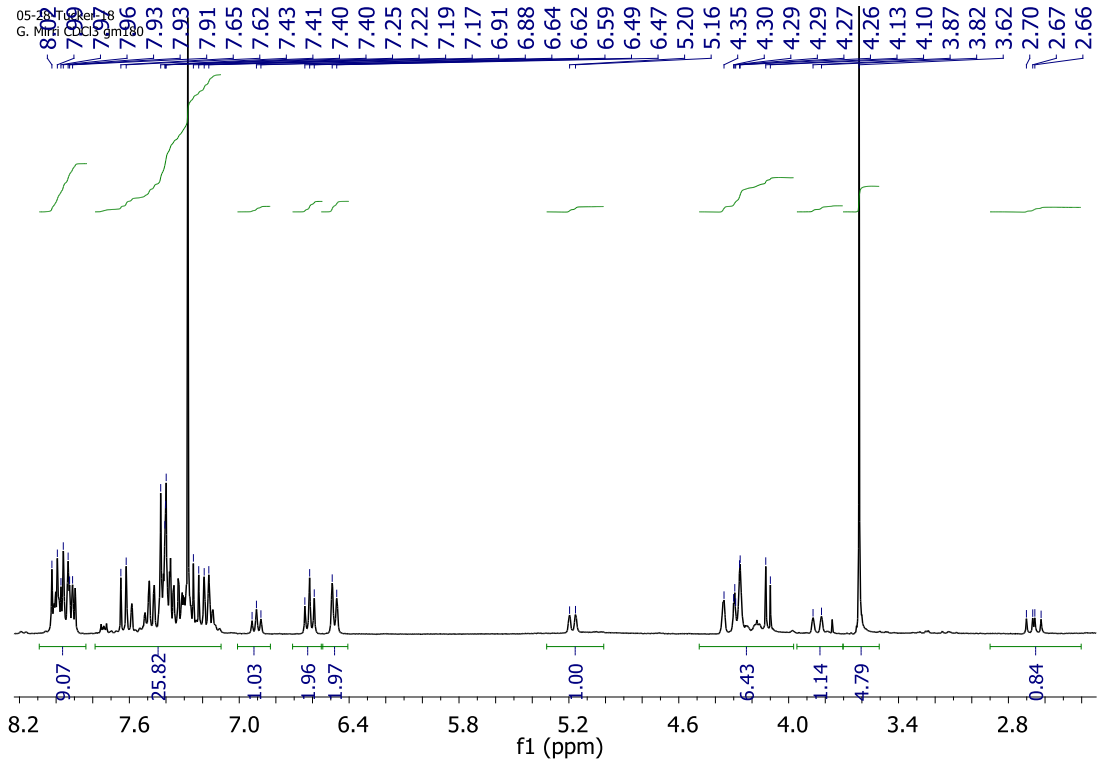

Figure 15. (*S,S*)-8a ^{1}H-NMR (300 MHz, $CDCl_3$)

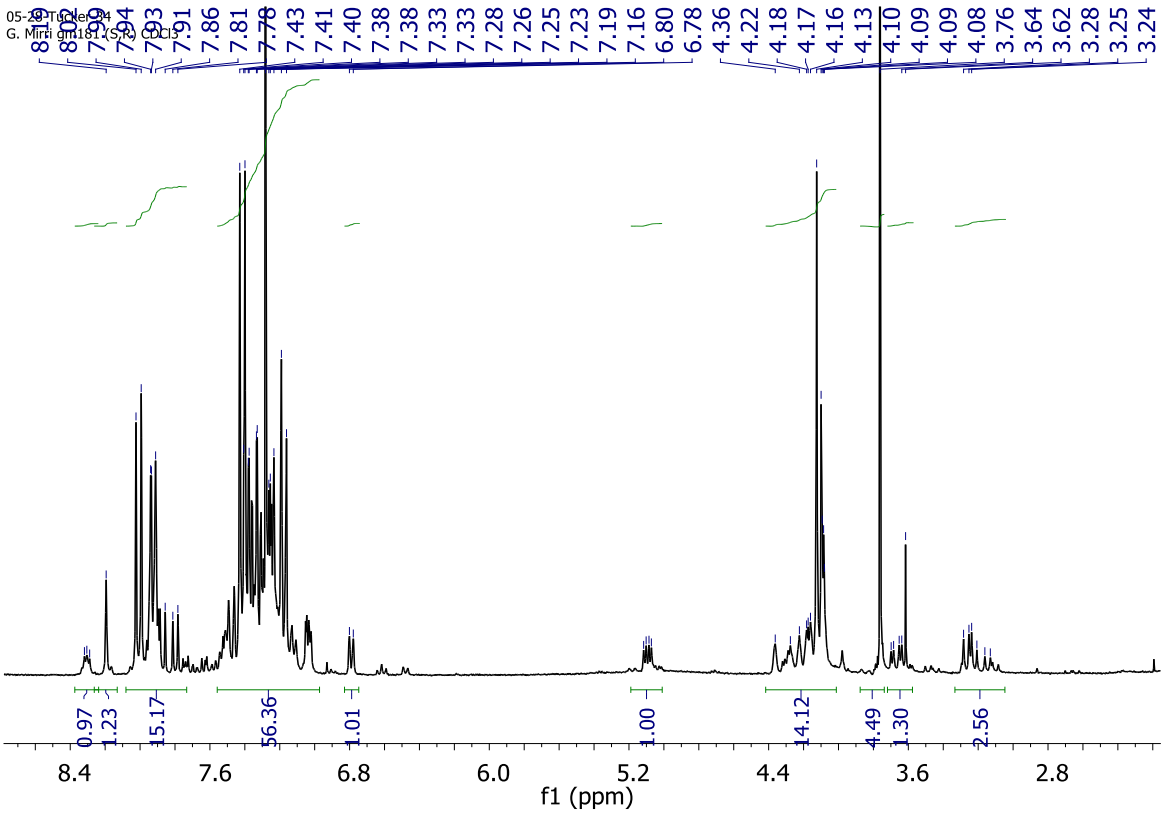

Figure 16. (*S,R*)-8a ^{1}H-NMR (300 MHz, $CDCl_3$)

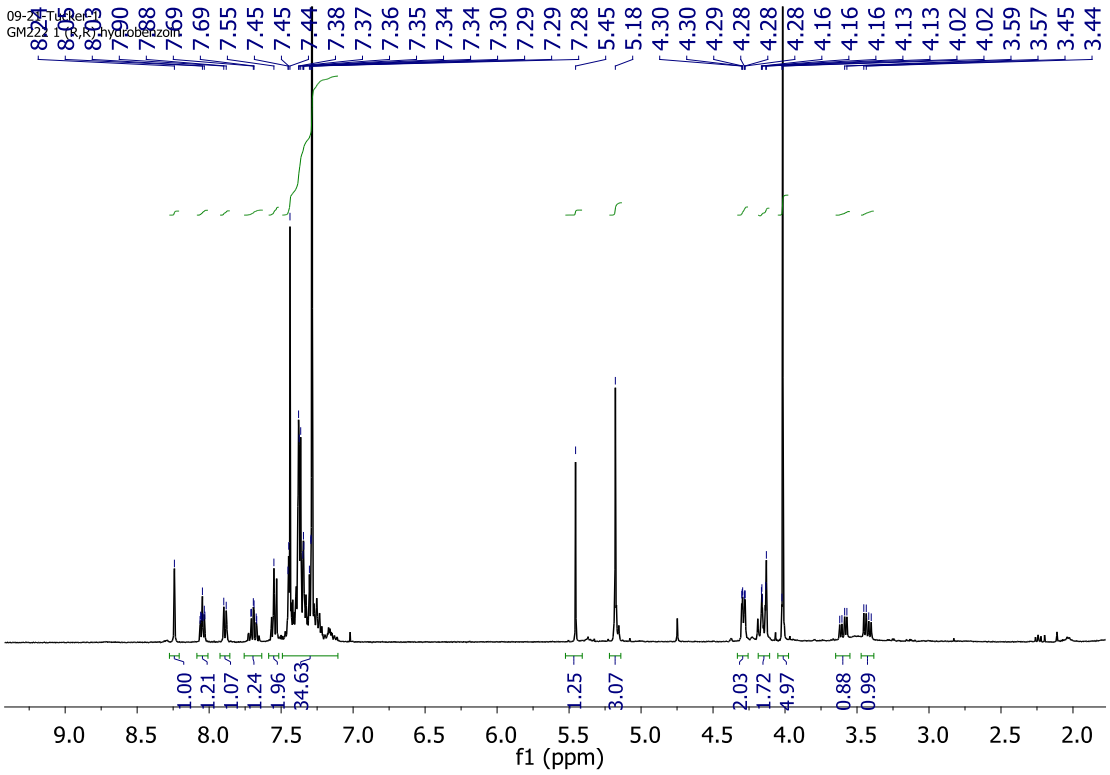

Figure 17. (*R,R,R*)-9a ^{1}H-NMR (400 MHz, $CDCl_3$)

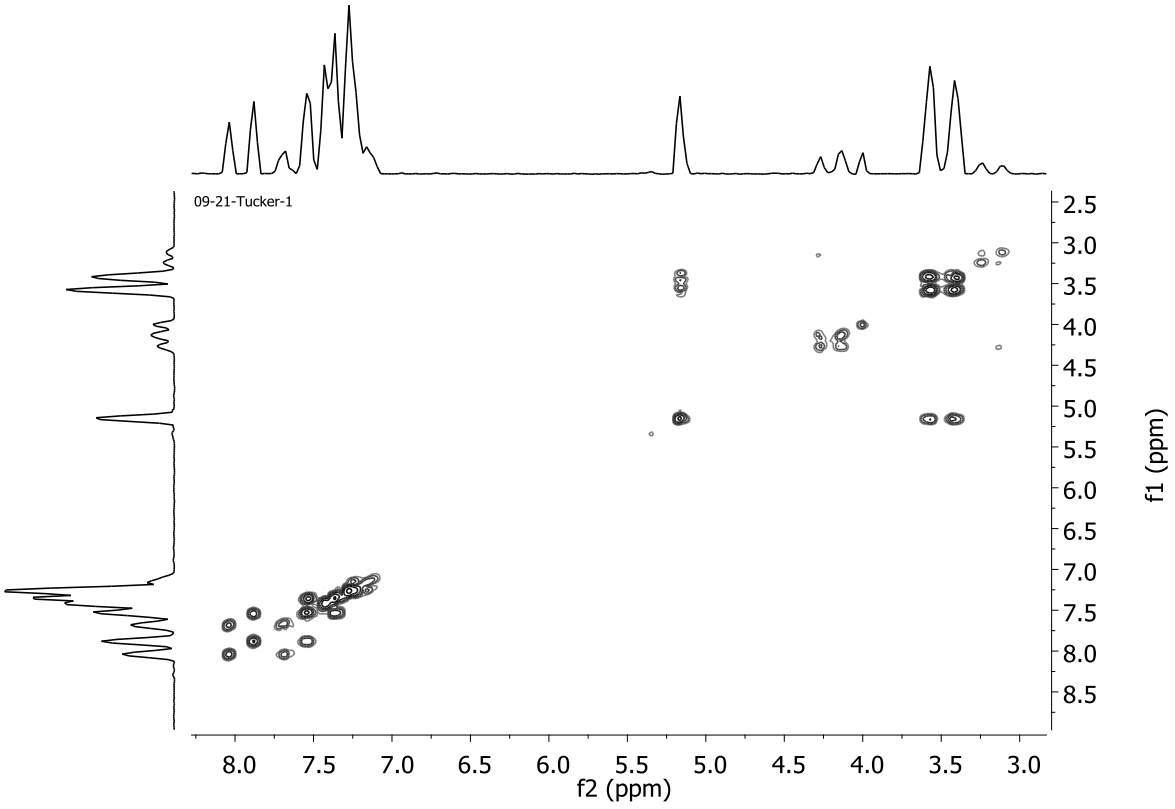

Figure 18. (*R,R,R*)-9a ^{1}H-^{1}H (COSY)-NMR (400 MHz, $CDCl_3$)

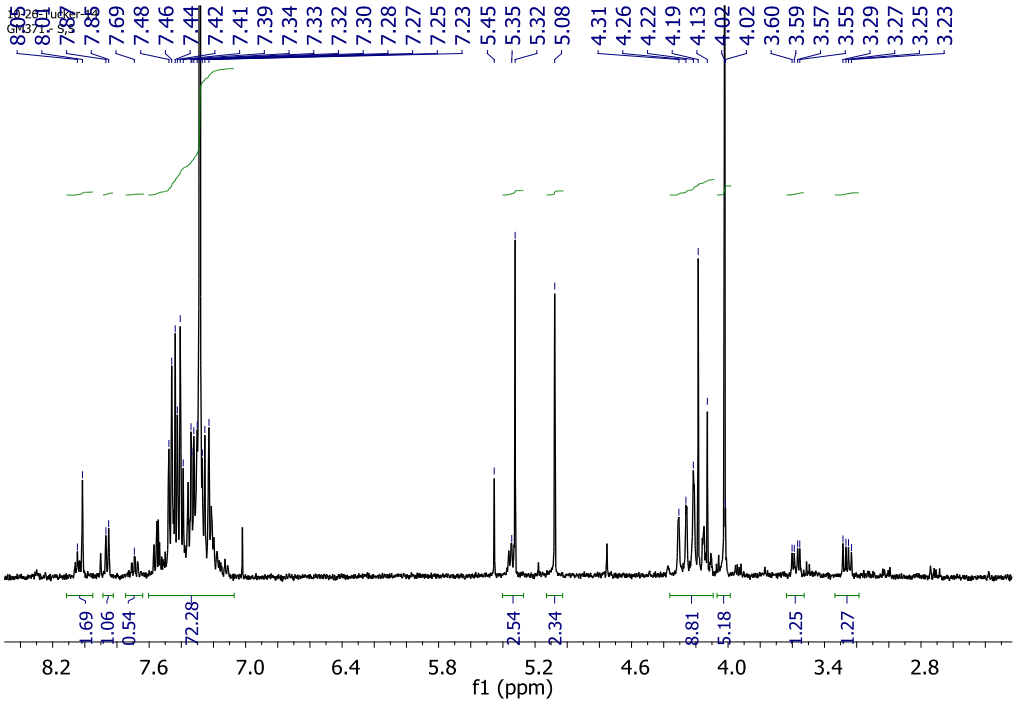

Figure 19. (*R,R,R*)-9a ^{1}H-NMR (400 MHz, $CDCl_3$)

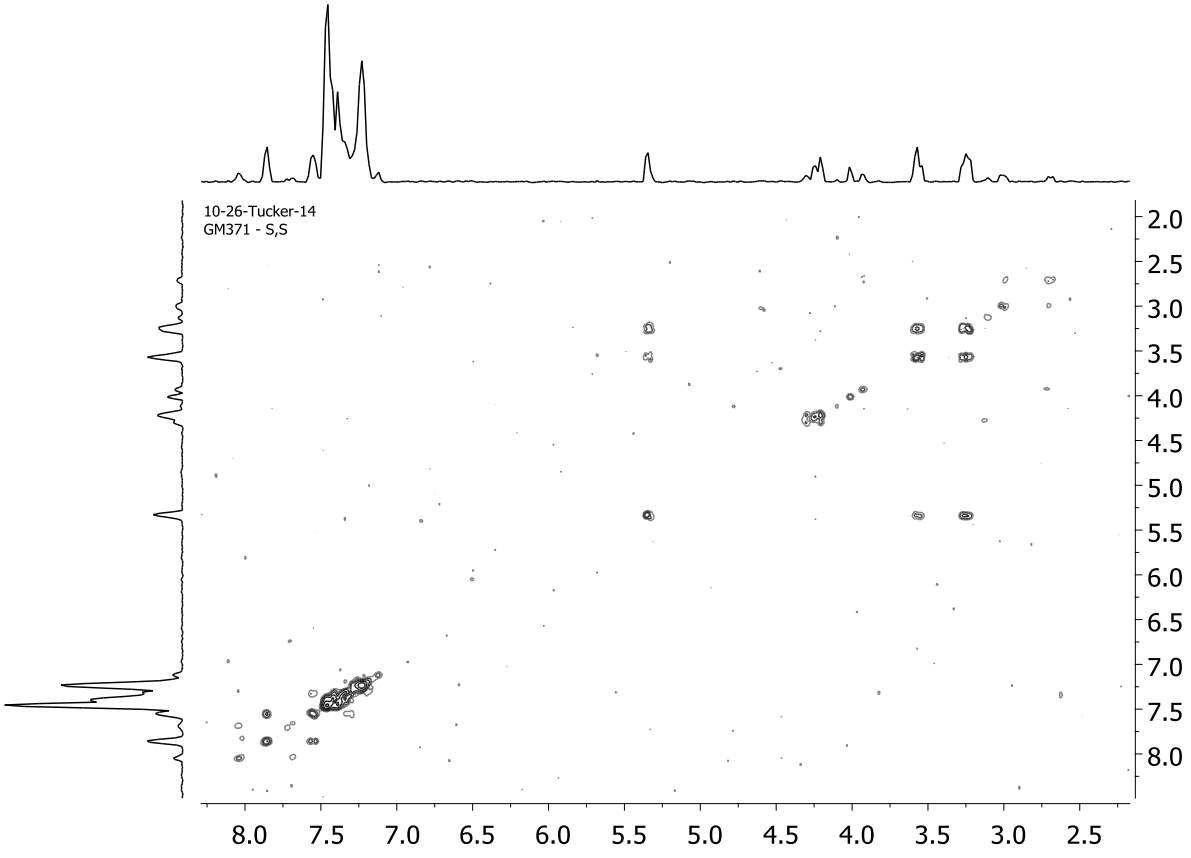

Figure 20. (*R,S,S*)-9a ^{1}H-^{1}H (COSY)-NMR (400 MHz, $CDCl_3$)

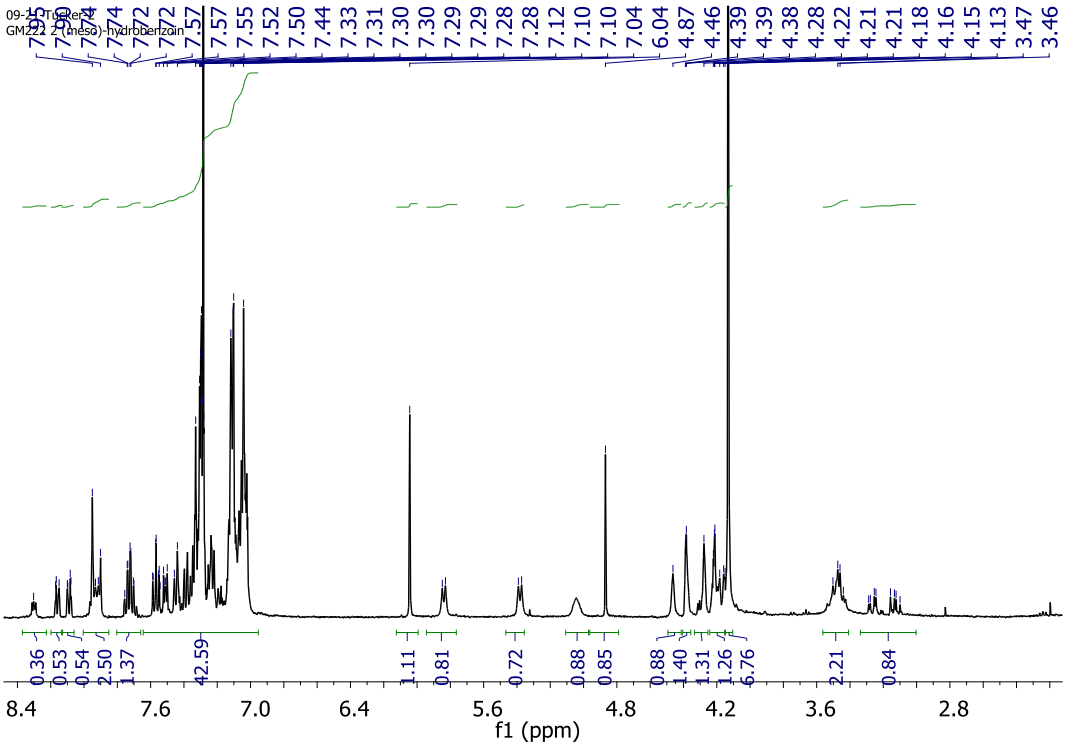

Figure 21. (*R,meso*)-9a ^{1}H-NMR (400 MHz, $CDCl_3$)

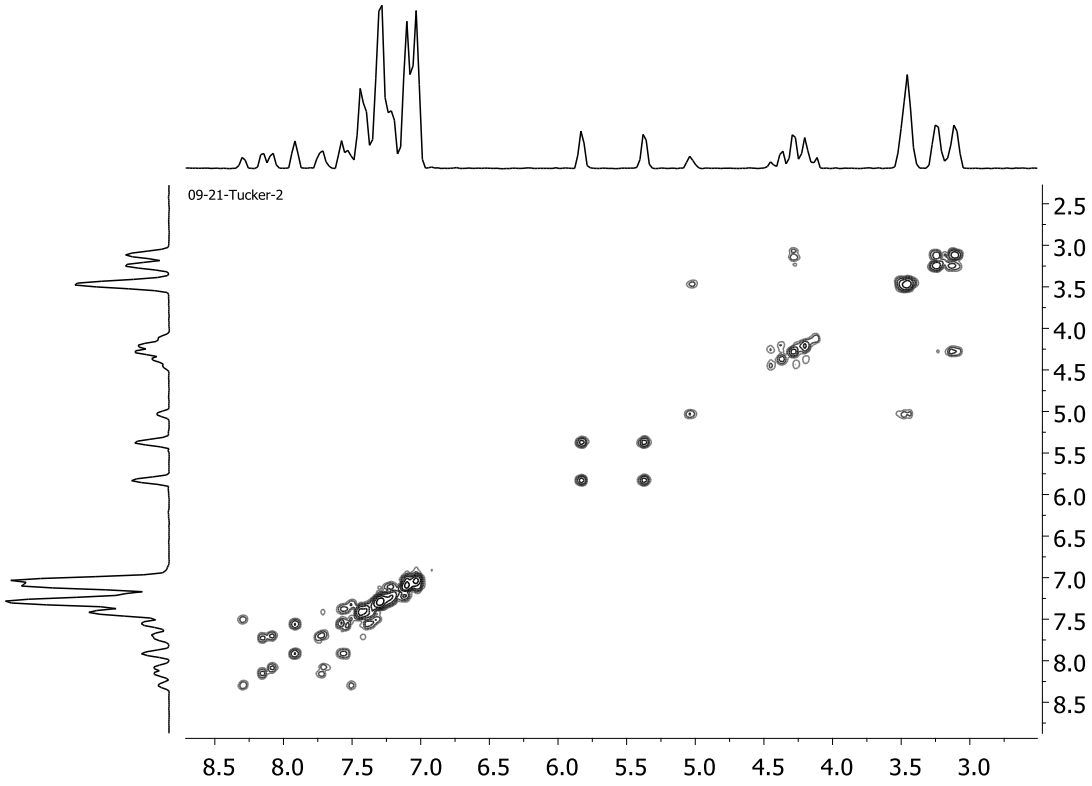

Figure 22. (*R,meso*)-9a ^{1}H-^{1}H (COSY)-NMR (400 MHz, $CDCl_3$)

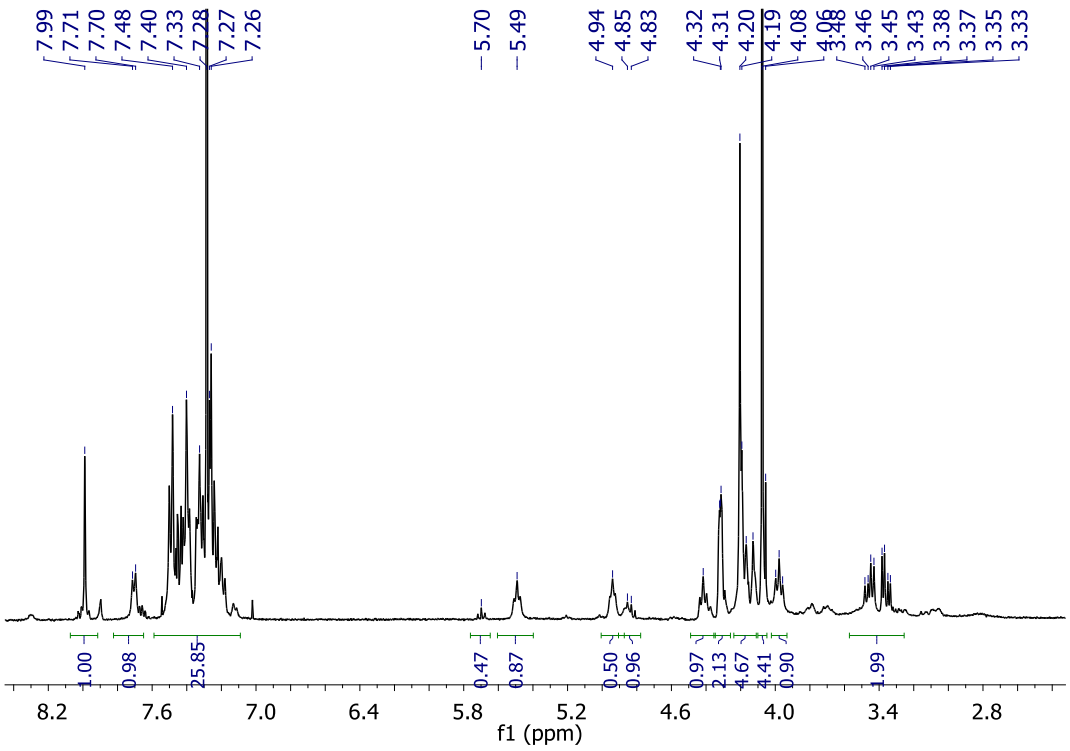

Figure 23. (*R,R*)-10a ^{1}H-NMR (300 MHz, $CDCl_3$)

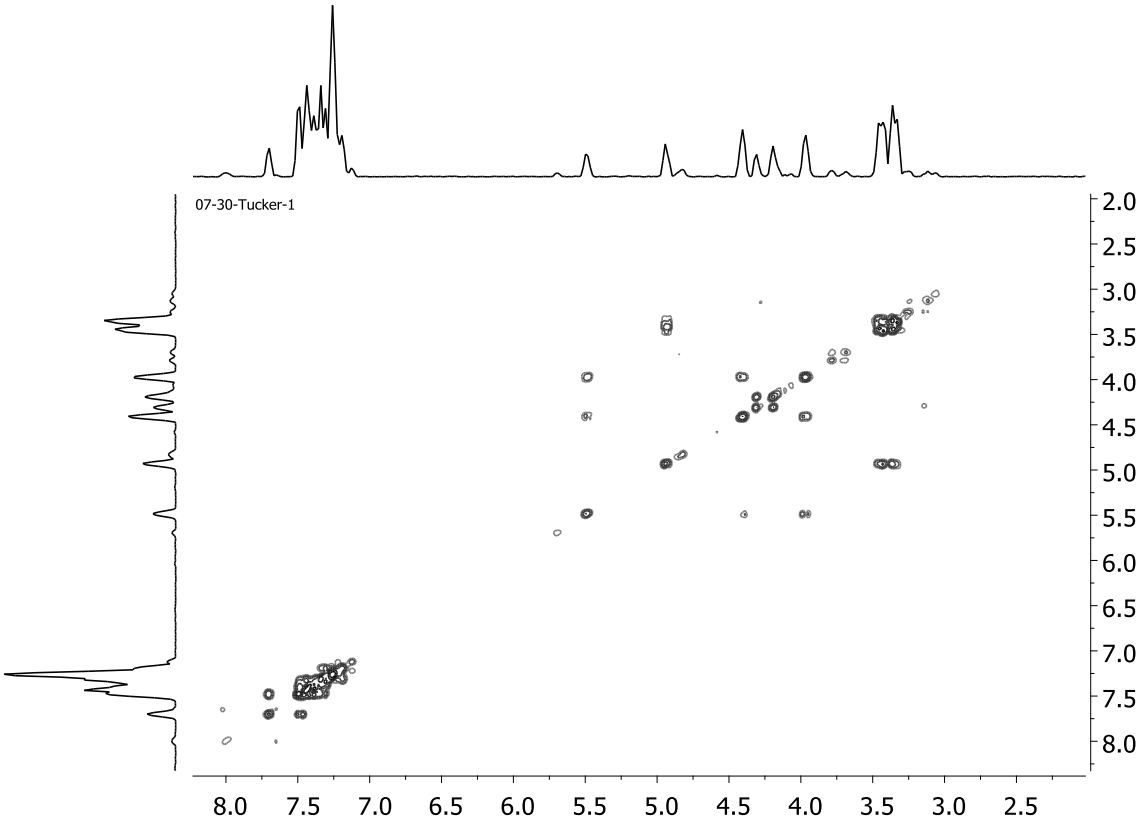

Figure 24. (*R,R*)-10a ^{1}H-^{1}H (COSY)-NMR (400 MHz, $CDCl_3$)

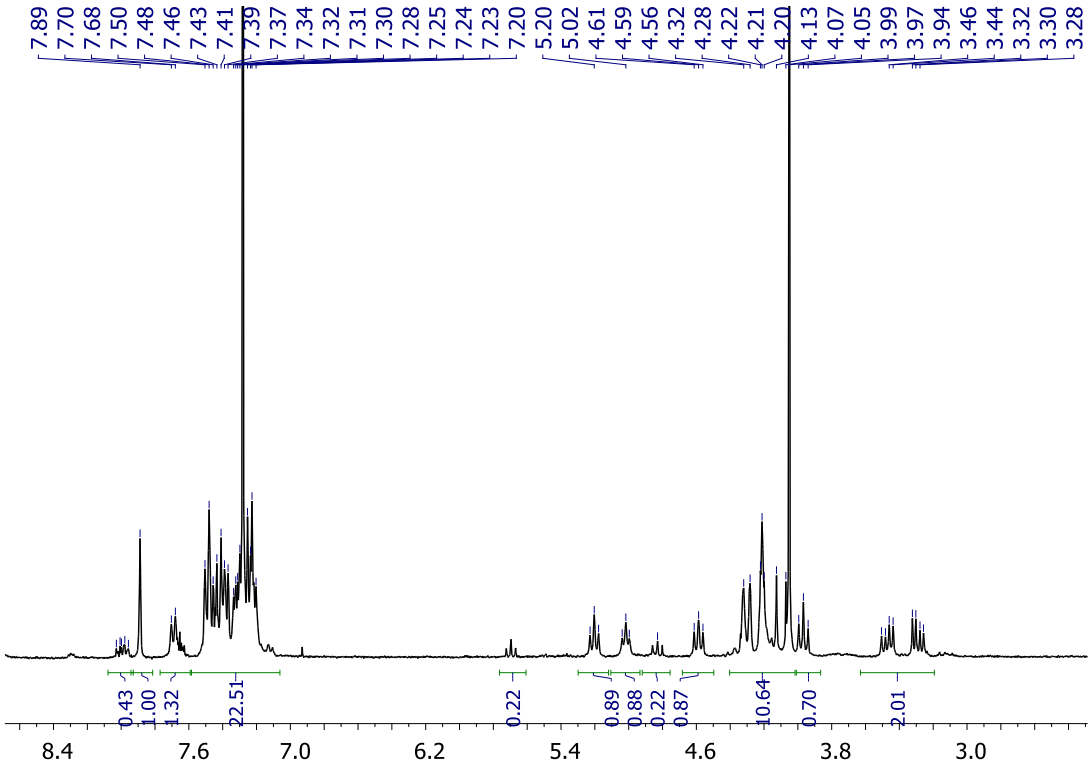

Figure 25. (*R,S*)-10a ^{1}H-NMR (300 MHz, $CDCl_3$)

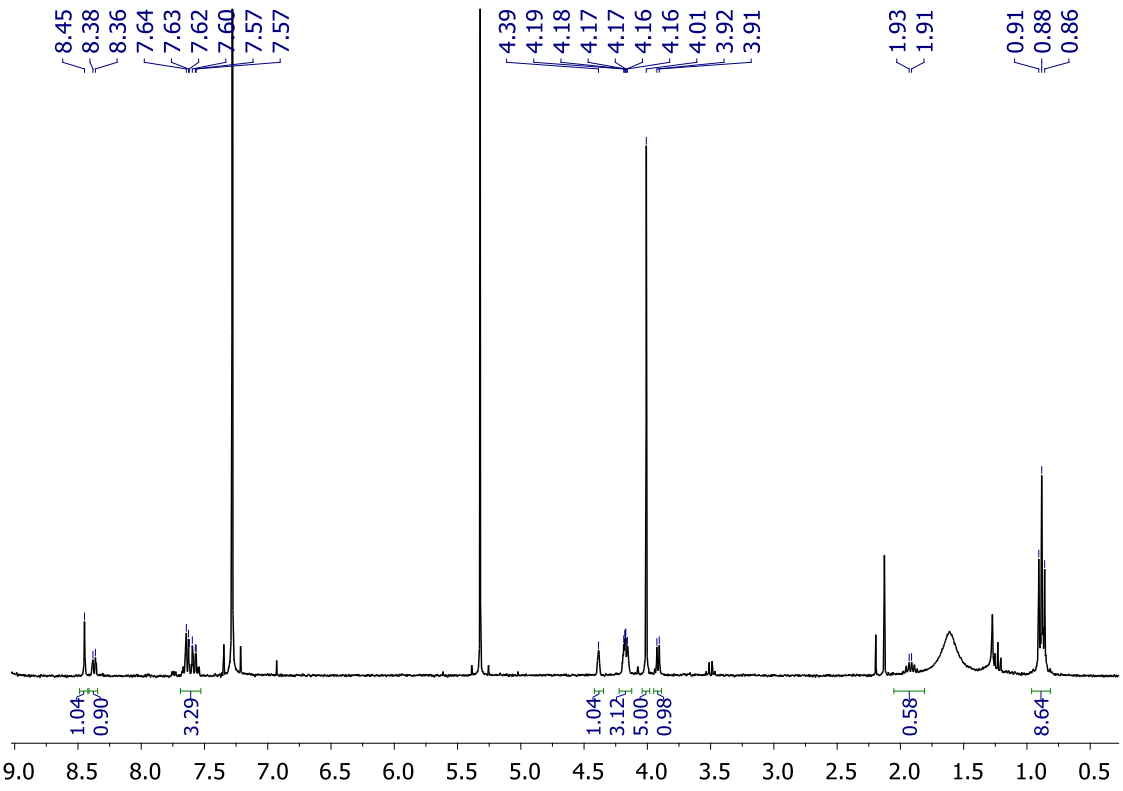

Figure 26. (*R*)-2b ^{1}H-NMR (300 MHz, $CDCl_3$)

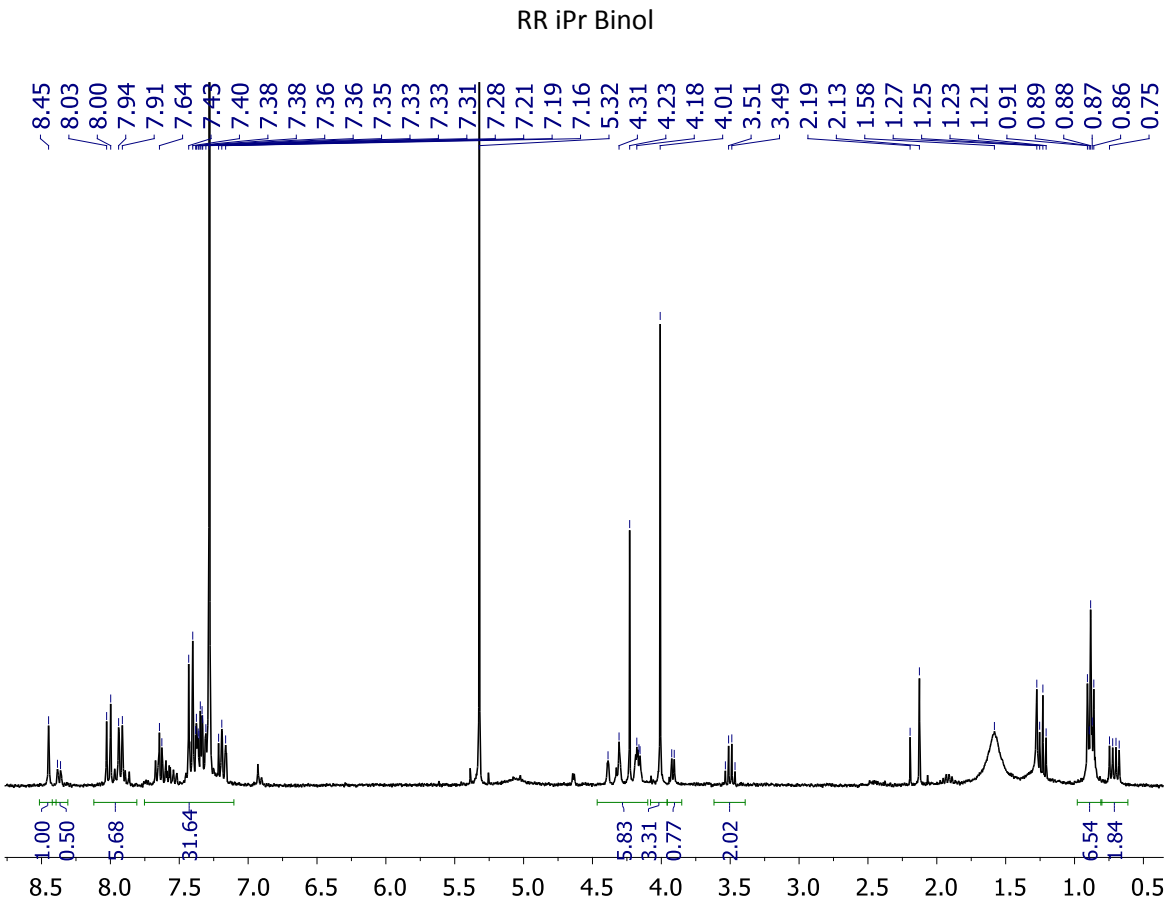

Figure 27. (*R,R*)-8b ^{1}H-NMR (300 MHz, $CDCl_3$)

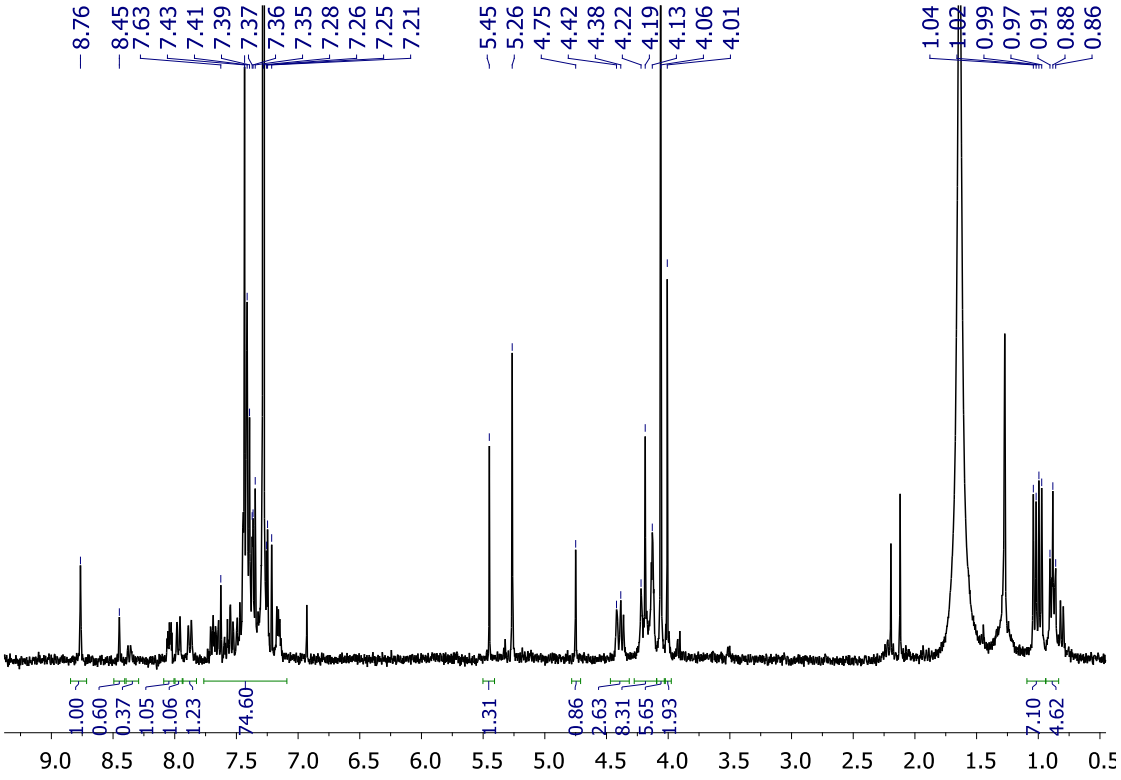

Figure 28. (*R,R,R*)-9b ^{1}H-NMR (300 MHz, $CDCl_3$)

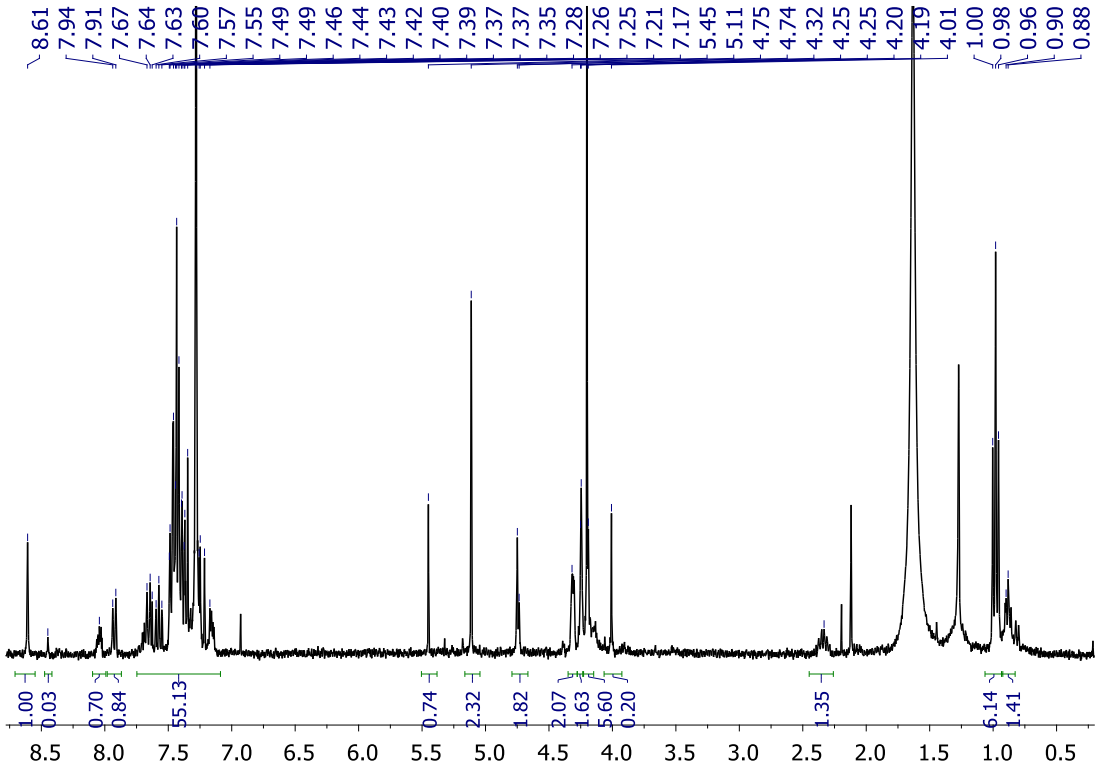

Figure 29. (*R,S,S*)-9b ^{1}H-NMR (300 MHz, $CDCl_3$)

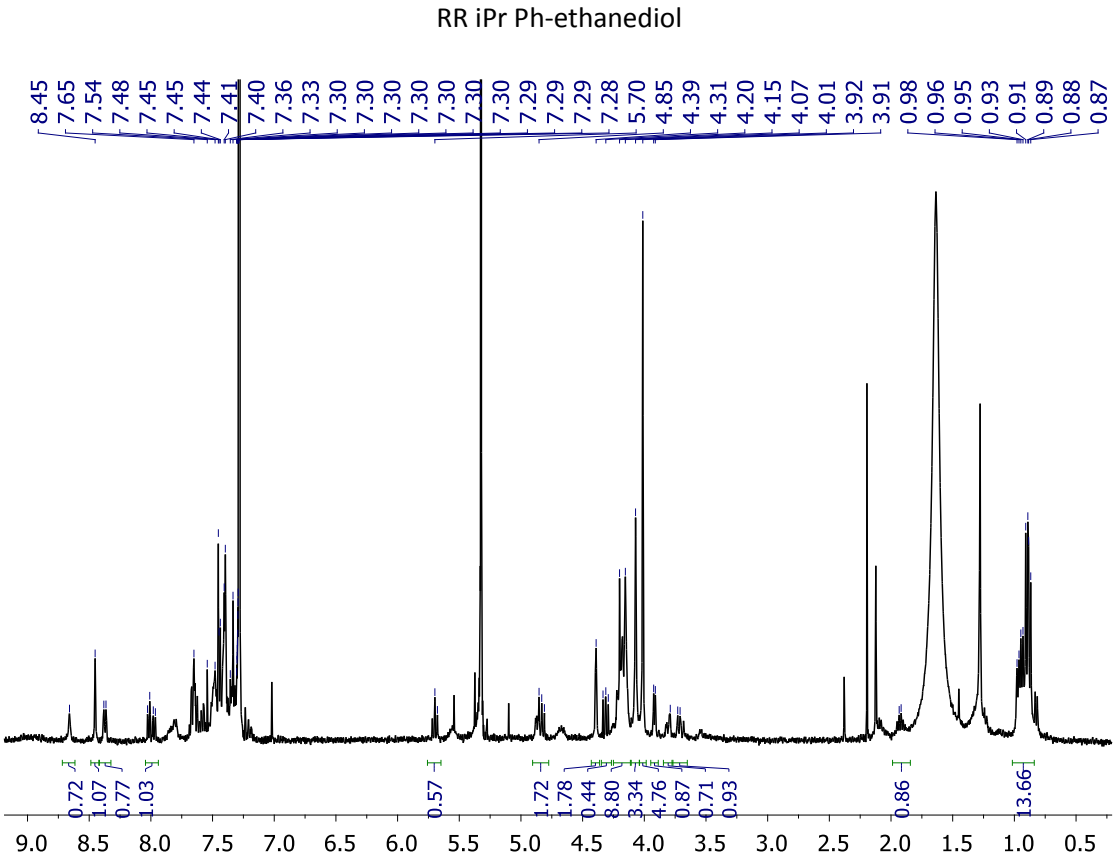

Figure 30. (*R,R*)-10b ^{1}H-NMR (300 MHz, $CDCl_3$)

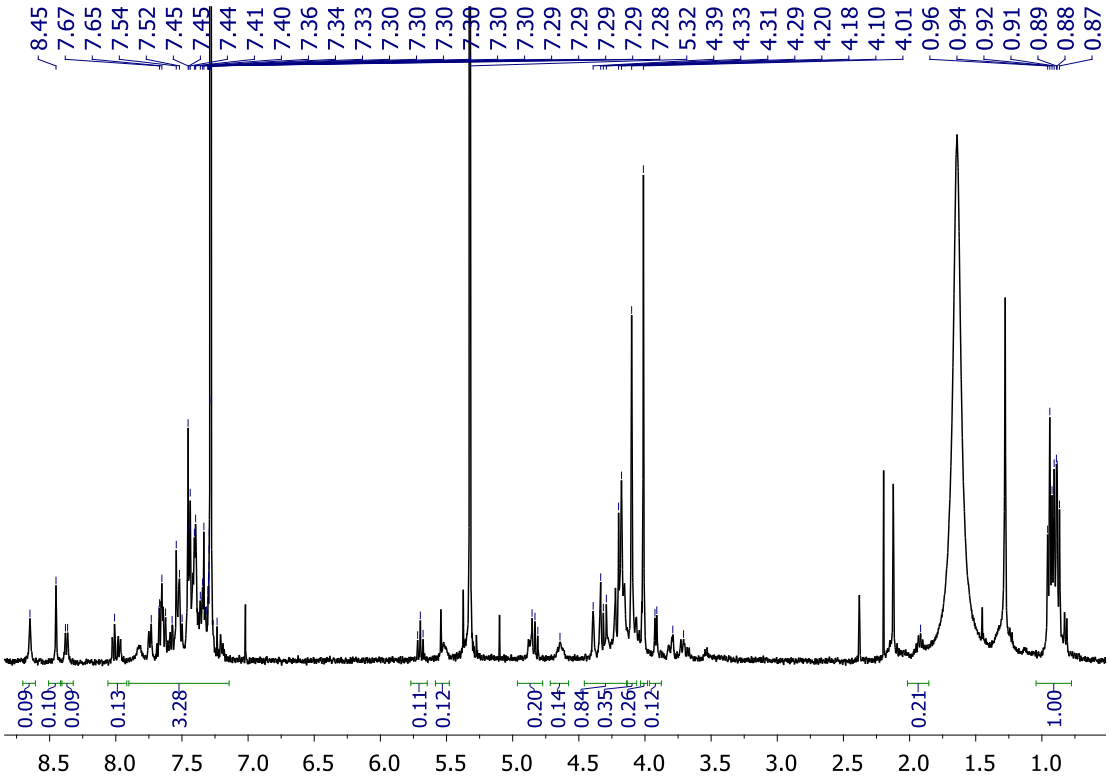

Figure 31. (*R,R*)-10b ^{1}H-NMR (300 MHz, $CDCl_3$)

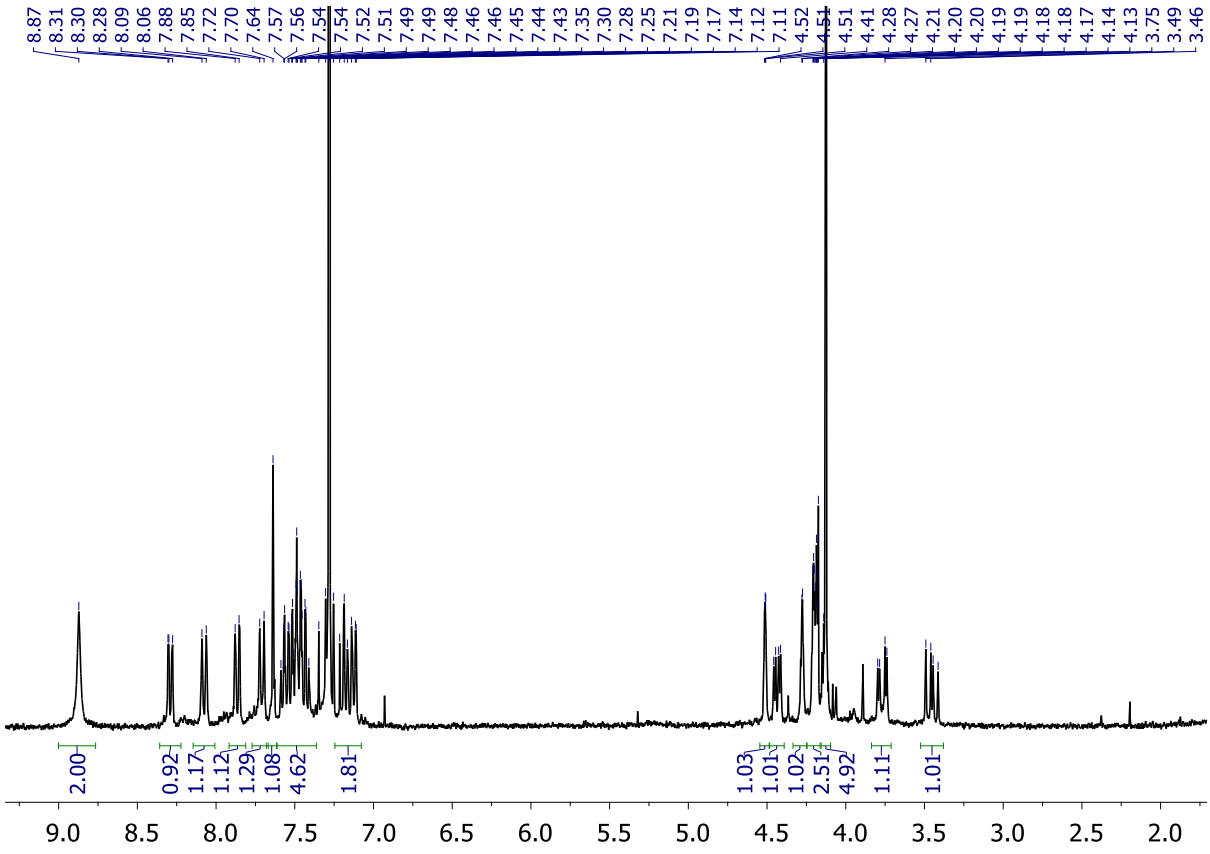

Figure 32. (*R*)-2c ^{1}H-NMR (300 MHz, $CDCl_3$)

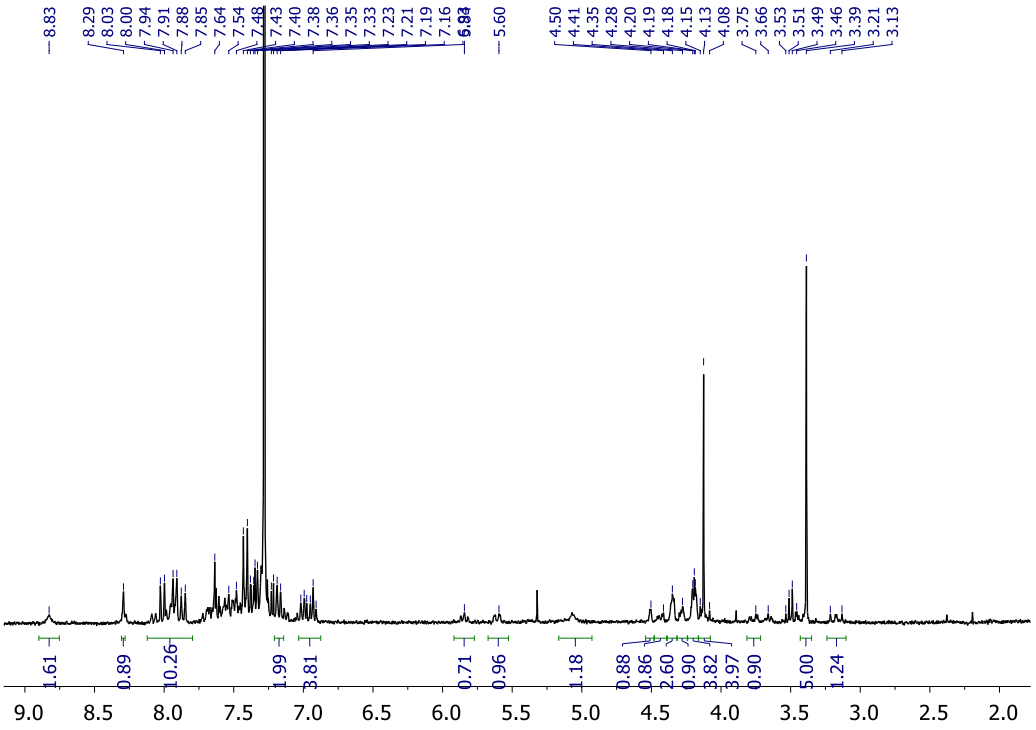

Figure 33. (*R,R*)-8c ^{1}H-NMR (300 MHz, $CDCl_3$)

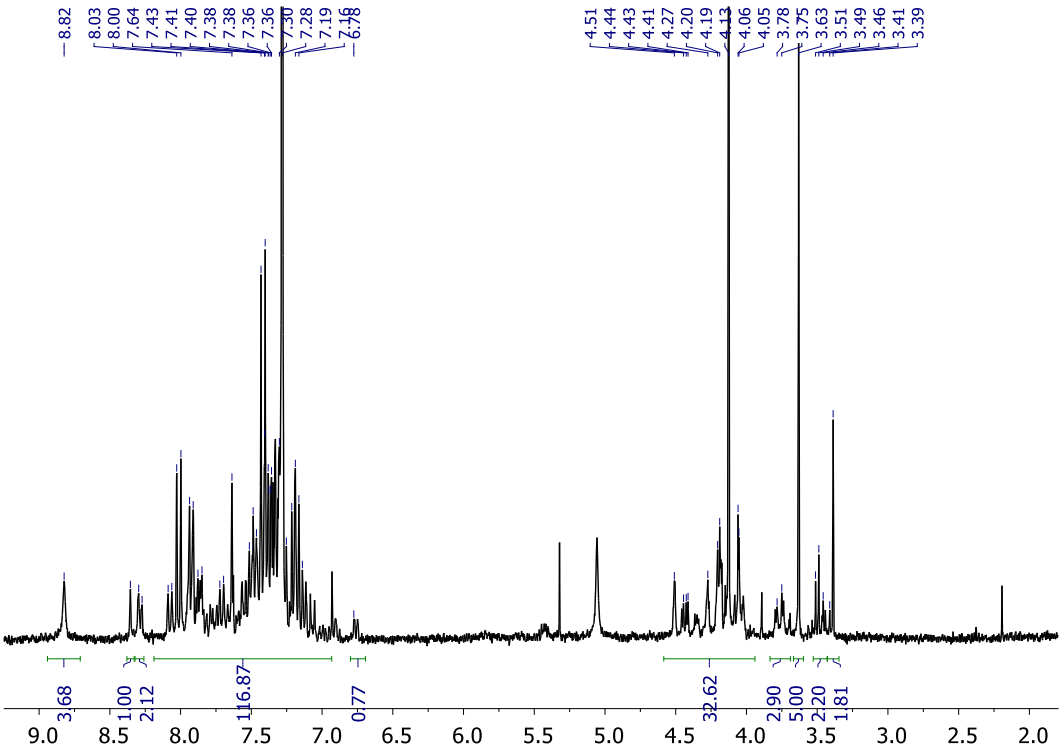

Figure 34. (*R,S*)-8c ^{1}H-NMR (300 MHz, $CDCl_3$)

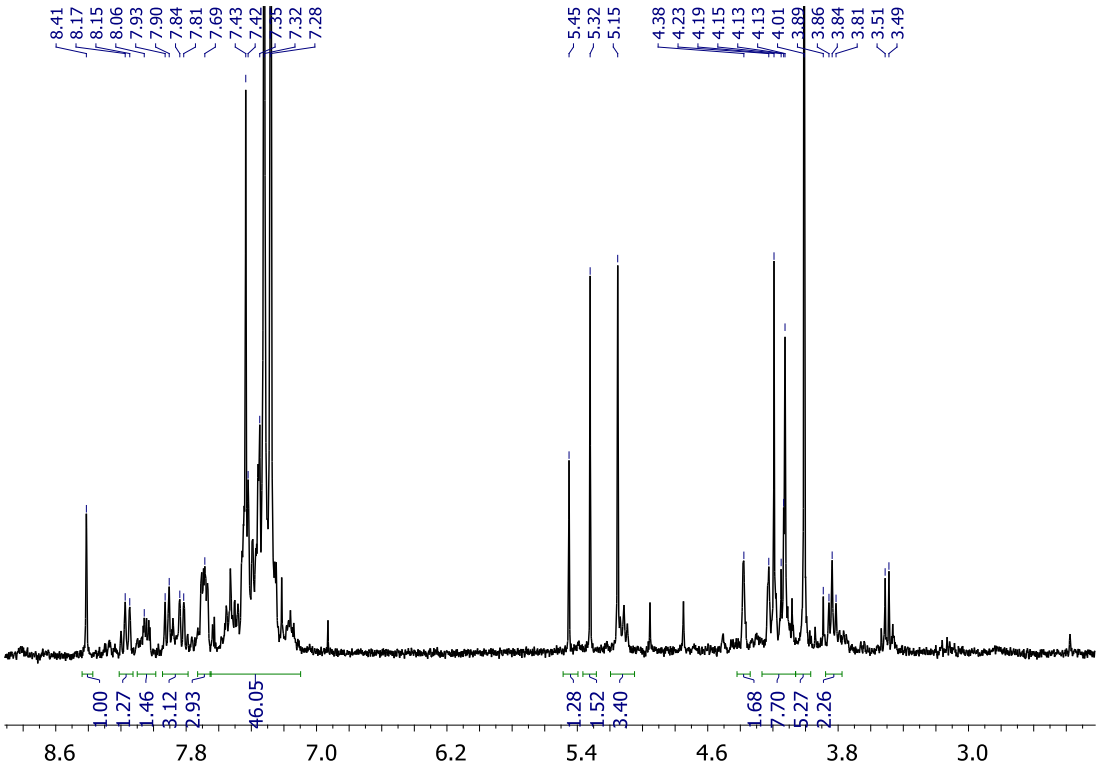

Figure 35. (*R,R,R*)-9c ^{1}H-NMR (300 MHz, $CDCl_3$)

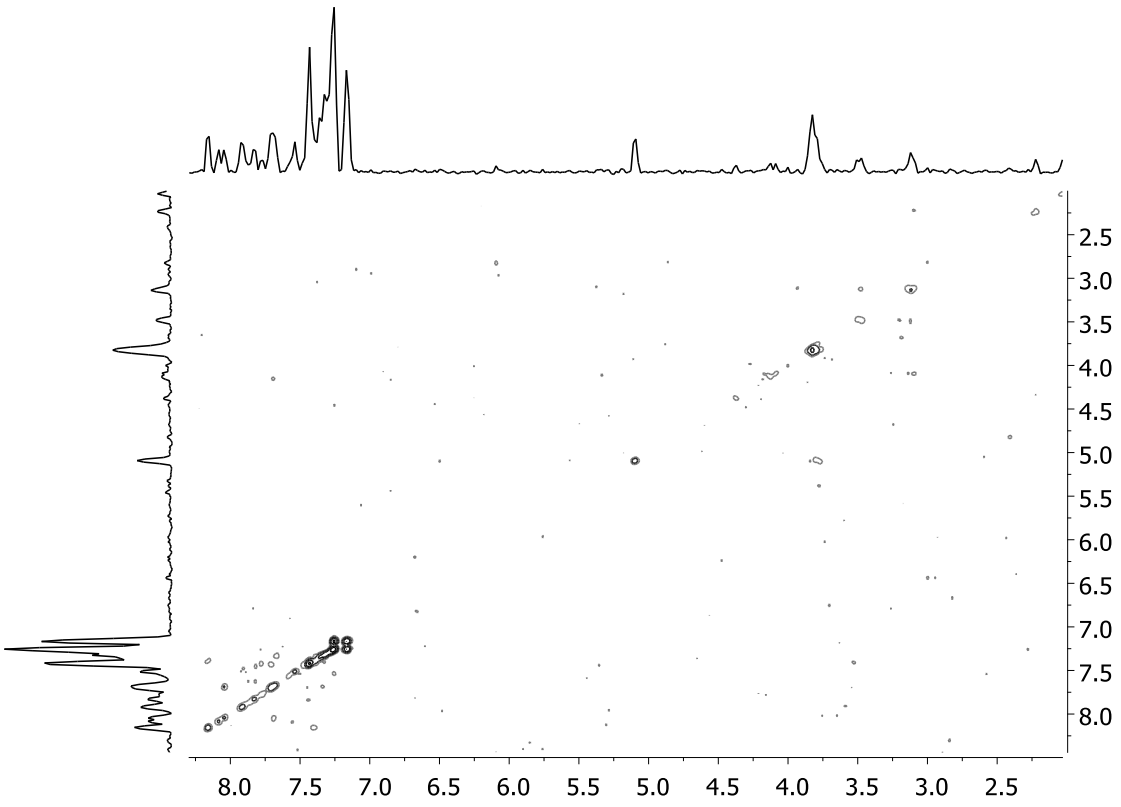

Figure 36. (*R,R,R*)-9c ^{1}H-^{1}H (COSY)-NMR (400 MHz, $CDCl_3$)

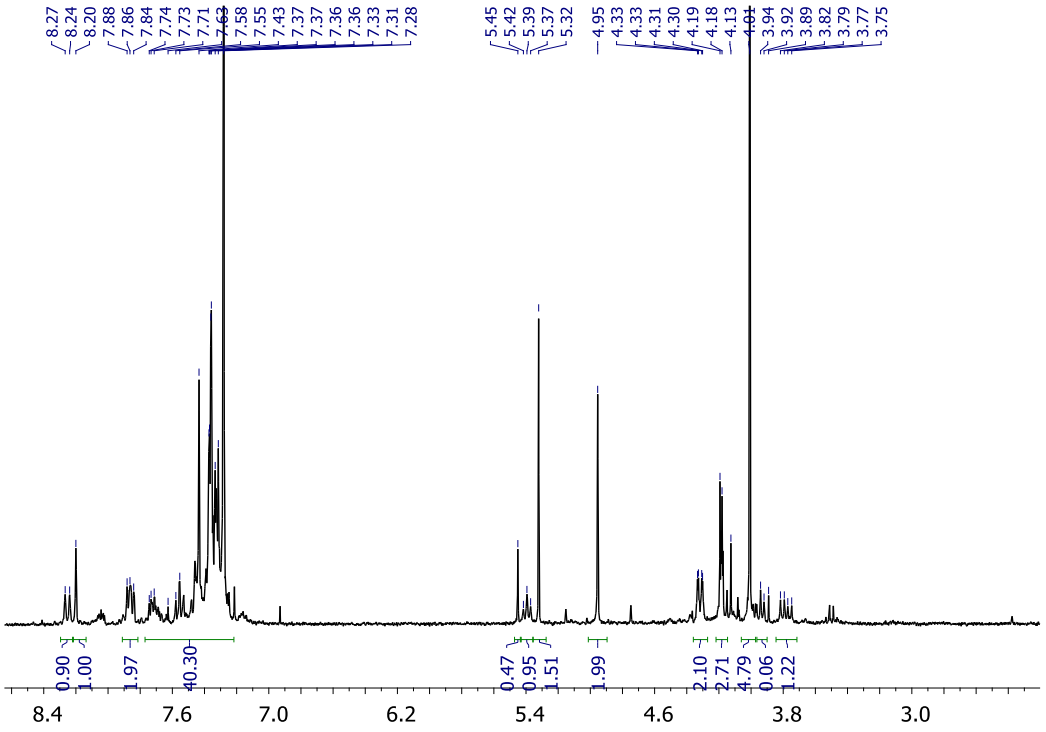

Figure 37. (*R,S,S*)-9c ^{1}H-NMR (300 MHz, $CDCl_3$)

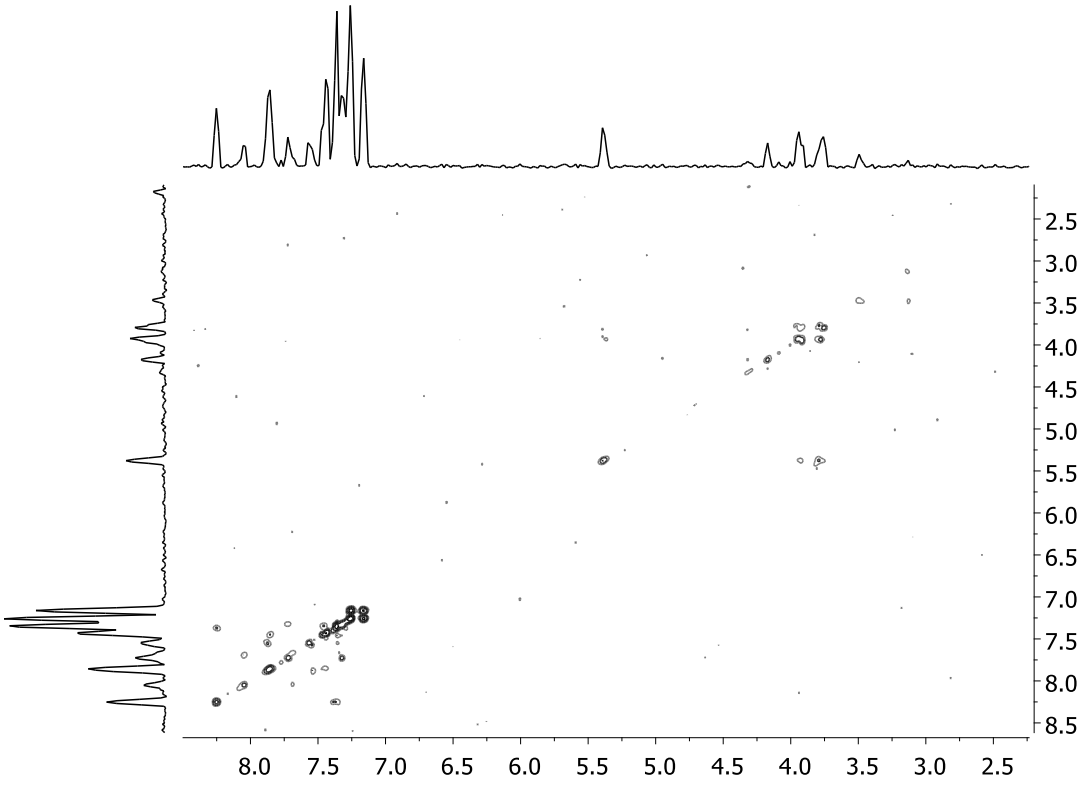

Figure 38. (*R,S,S*)-9c ^{1}H-^{1}H (COSY)-NMR (400 MHz, $CDCl_3$)

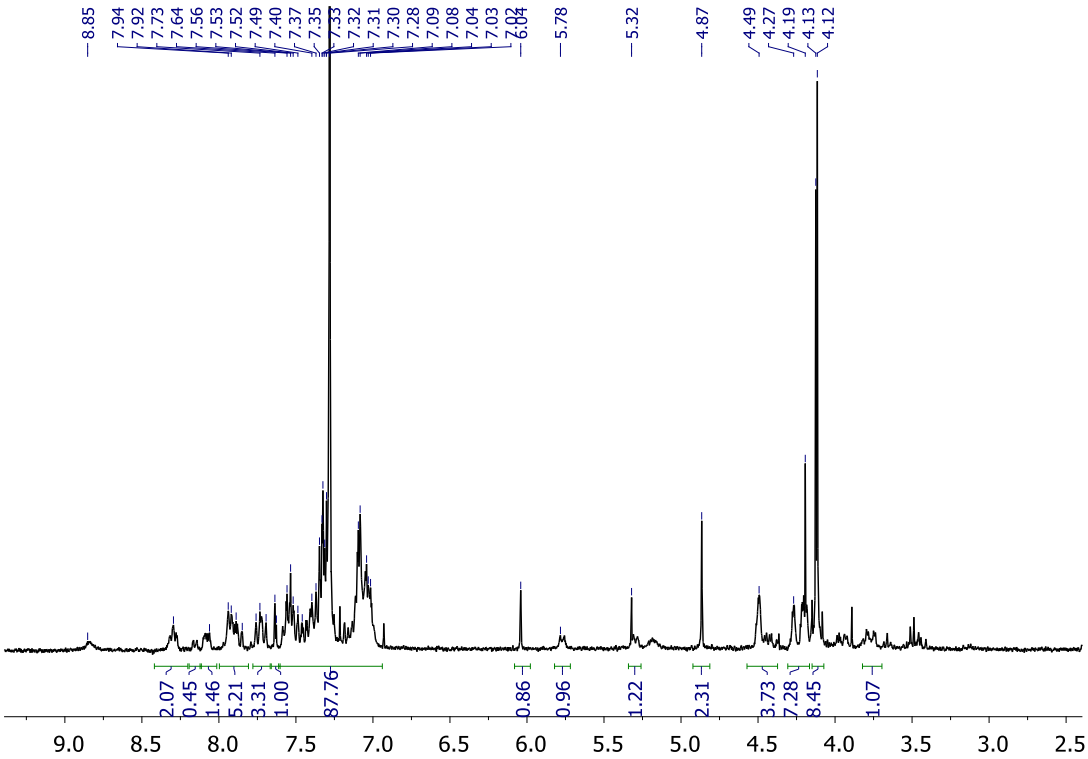

Figure 39. (*R,meso*)-9c ^{1}H-NMR (300 MHz, $CDCl_3$)

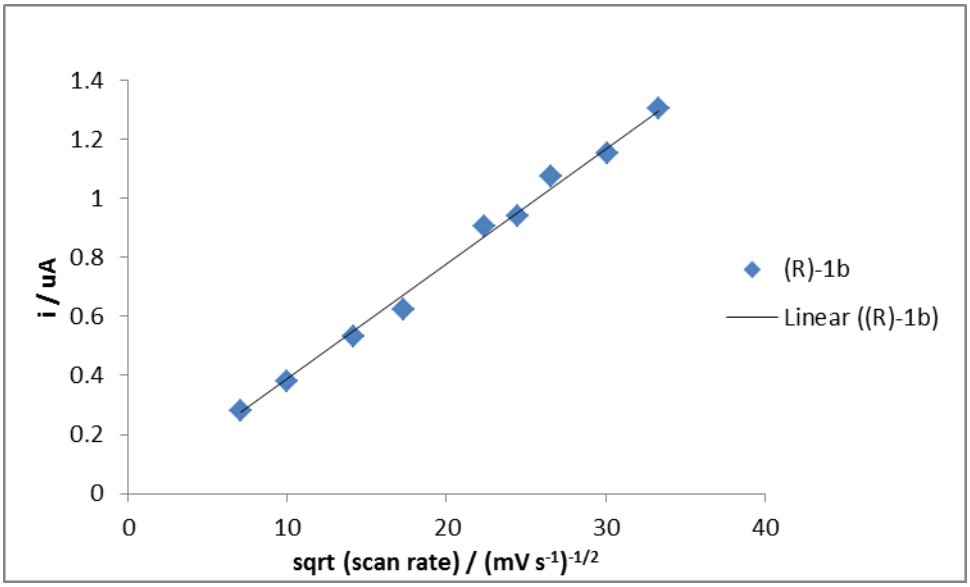

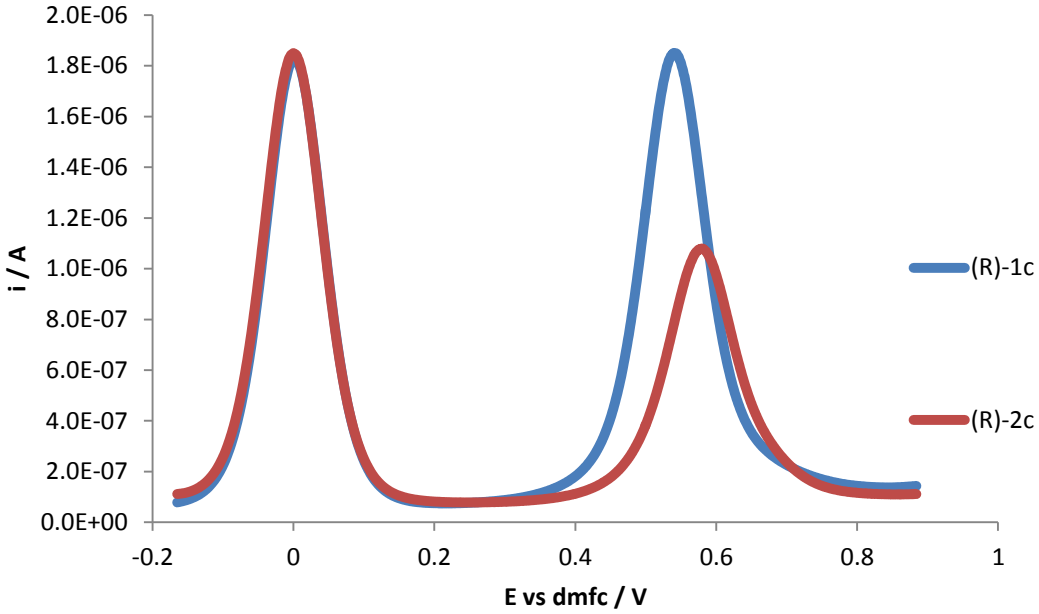

Figure 40. SWV of **(*R*)-1c** and **(*R*)-2c** in dcm *vs.* dmfc (TBA·PF_6 0.1 M)

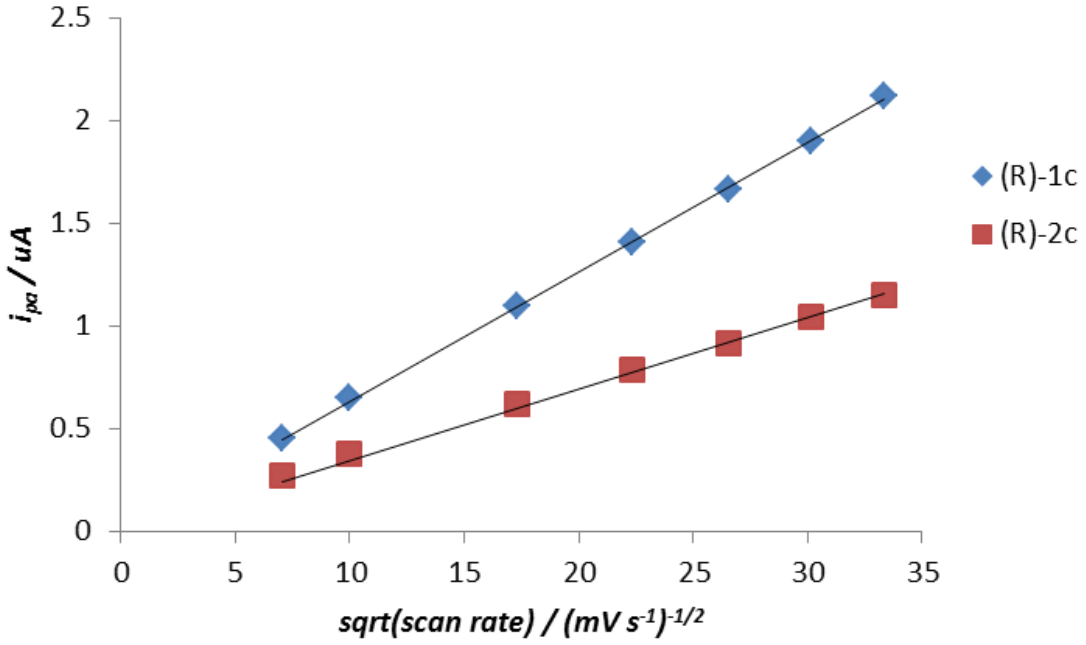

Figure 41. current *vs.* sqrt (scan rate) of **(*R*)-1c** and **(*R*)-2c** in dcm *vs.* dmfc (TBA·PF_6 0.1 M) from CV

Operator:Administrator Timebase:HPLC_7_1 Sequence:manual

Page 1-1
16/10/2009 10:58 AM

803 GM215 (3% IPA in Hexane)

Sample Name:	**GM215 (3% IPA in Hexane)**	*Injection Volume:*	**20.0**
Vial Number:	**1**	*Channel:*	**UV_VIS_1**
Sample Type:	**unknown**	*Wavelength:*	**210**
Control Program:		*Bandwidth:*	**n.a.**
Quantif. Method:	**default**	*Dilution Factor:*	**1.0000**
Recording Time:	**16/10/2009 10:23**	*Sample Weight:*	**1.0000**
Run Time (min):	**31.08**	*Sample Amount:*	**1.0000**

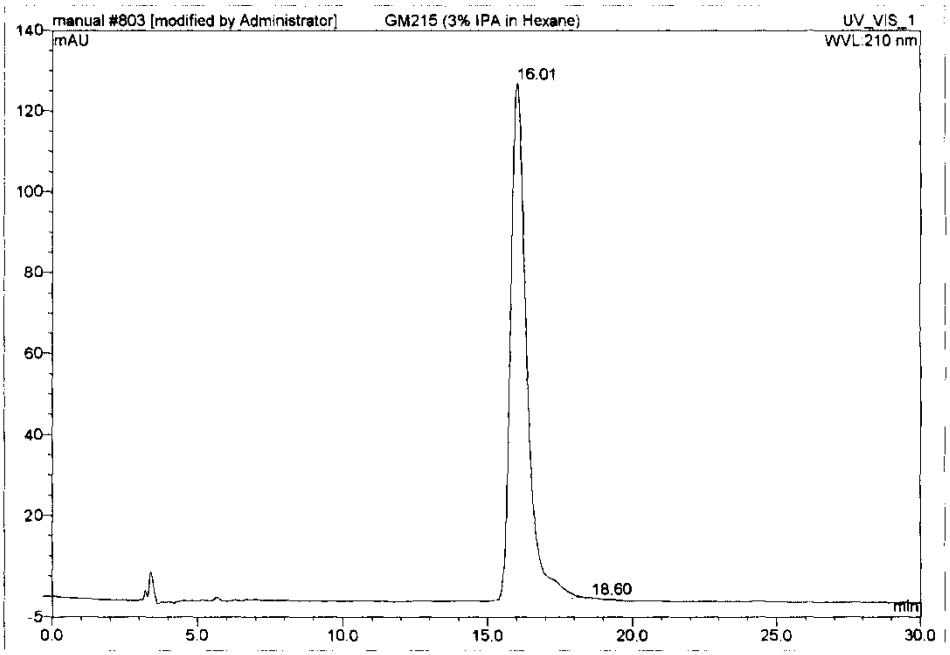

No.	Ret.Time min	Peak Name	Height mAU	Area mAU*min	Rel.Area %	Amount	Type
1	16.01	n.a.	127.796	79.599	95.87	n.a.	BM *
2	18.60	n.a.	0.001	3.433	4.13	n.a.	MB*
Total:			127.797	83.031	100.00	0.000	

DEFAULT/Integration

Chromeleon (c) Dionex 1996-2006
Version 6.80 SP1 Build 2238

Figure 42. Chiral HPLC (OD column) of **(*R*)-1a**

Operator:Administrator Timebase:HPLC_7_1 Sequence:manual

Page 1-1
16/10/2009 10:57 AM

802 GM197 (3% IPA in Hexane)

Sample Name:	**GM197 (3% IPA in Hexane)**	*Injection Volume:*	**2.0**
Vial Number:	**1**	*Channel:*	**UV_VIS_1**
Sample Type:	**unknown**	*Wavelength:*	**210**
Control Program:		*Bandwidth:*	**n.a.**
Quantif. Method:	**default**	*Dilution Factor:*	**1.0000**
Recording Time:	**16/10/2009 9:49**	*Sample Weight:*	**1.0000**
Run Time (min):	**30.73**	*Sample Amount:*	**1.0000**

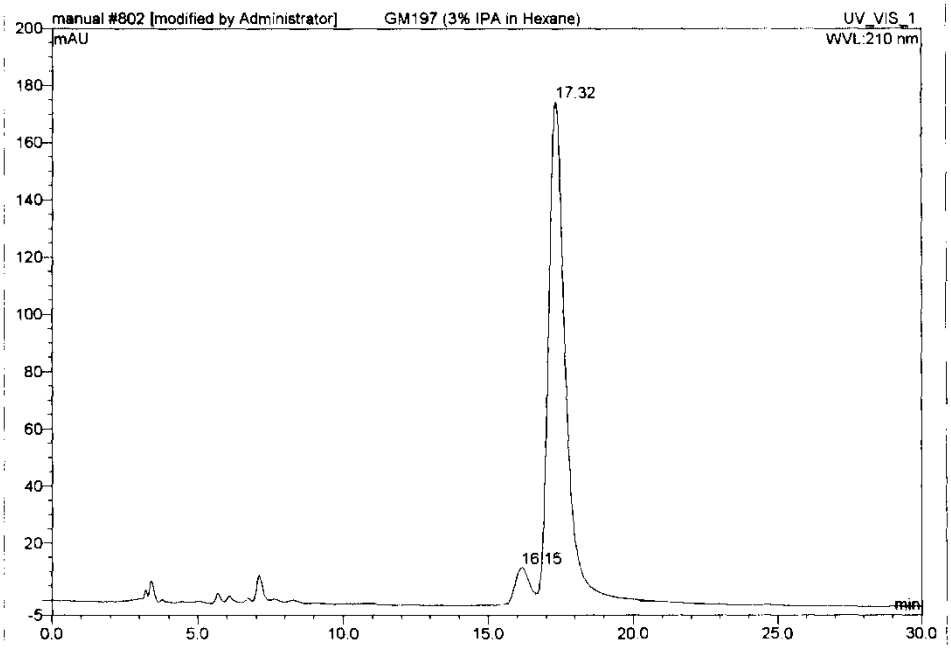

No.	Ret.Time min	Peak Name	Height mAU	Area mAU*min	Rel.Area %	Amount	Type
1	16.15	n.a.	13.078	7.551	5.83	n.a.	BM
2	17.32	n.a.	175.476	121.919	94.17	n.a.	MB
Total:			188.554	129.469	100.00	0.000	

DEFAULT/Integration

Chromeleon (c) Dionex 1996-2006
Version 6.80 SP1 Build 2238

Figure 43. Chiral HPLC (OD column) of **(*S*)-1a**

Appendix to Chapter 3

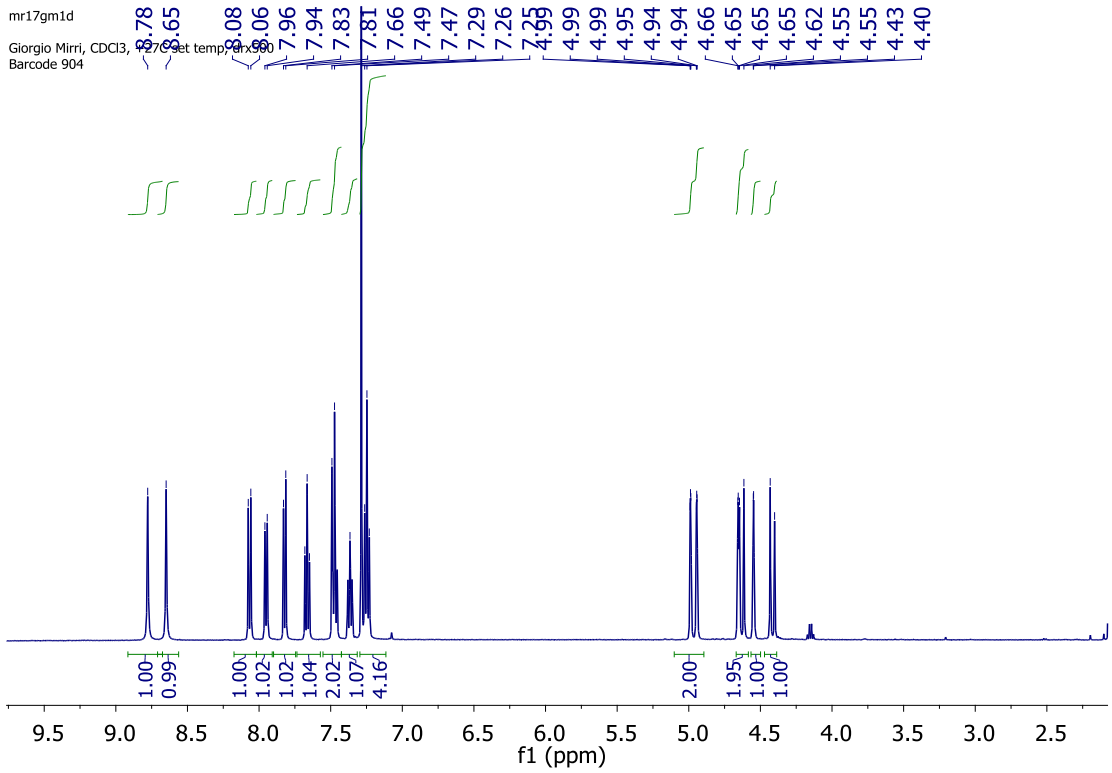

Figure 44 (*R*)-16a ^{1}H-NMR (500 MHz, $CDCl_3$)

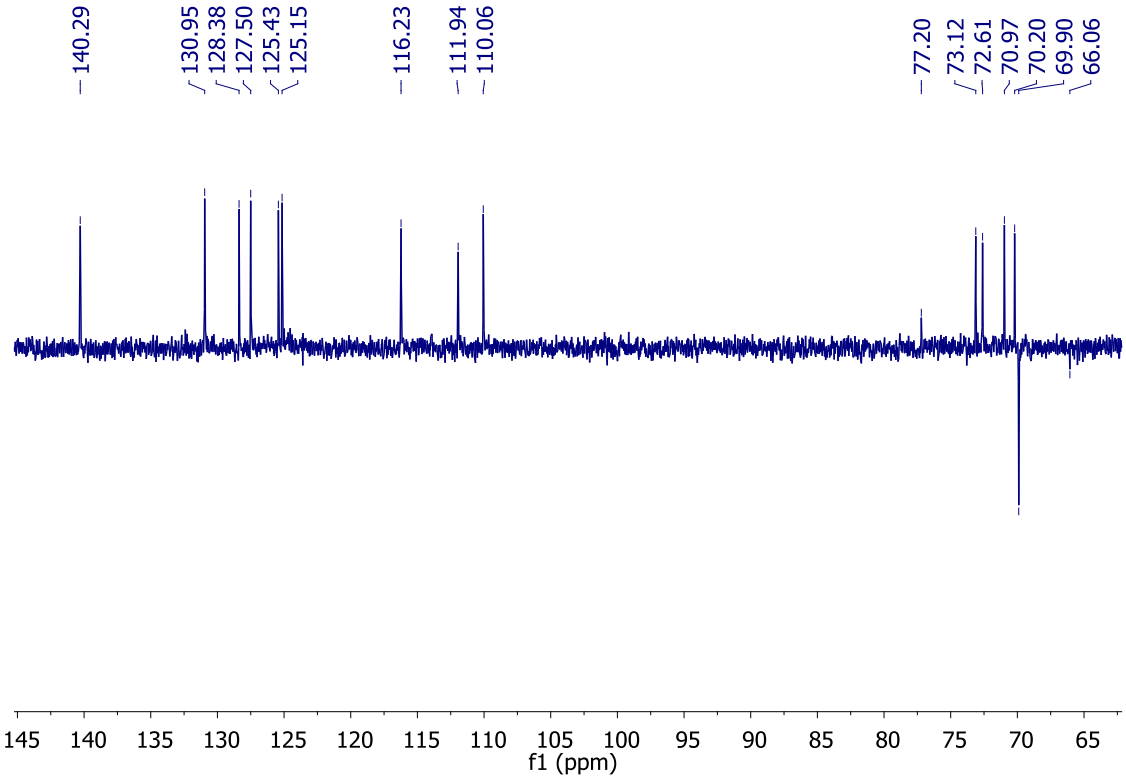

Figure 45. (*R*)-16a ^{1}H-NMR (125 MHz, $CDCl_3$)

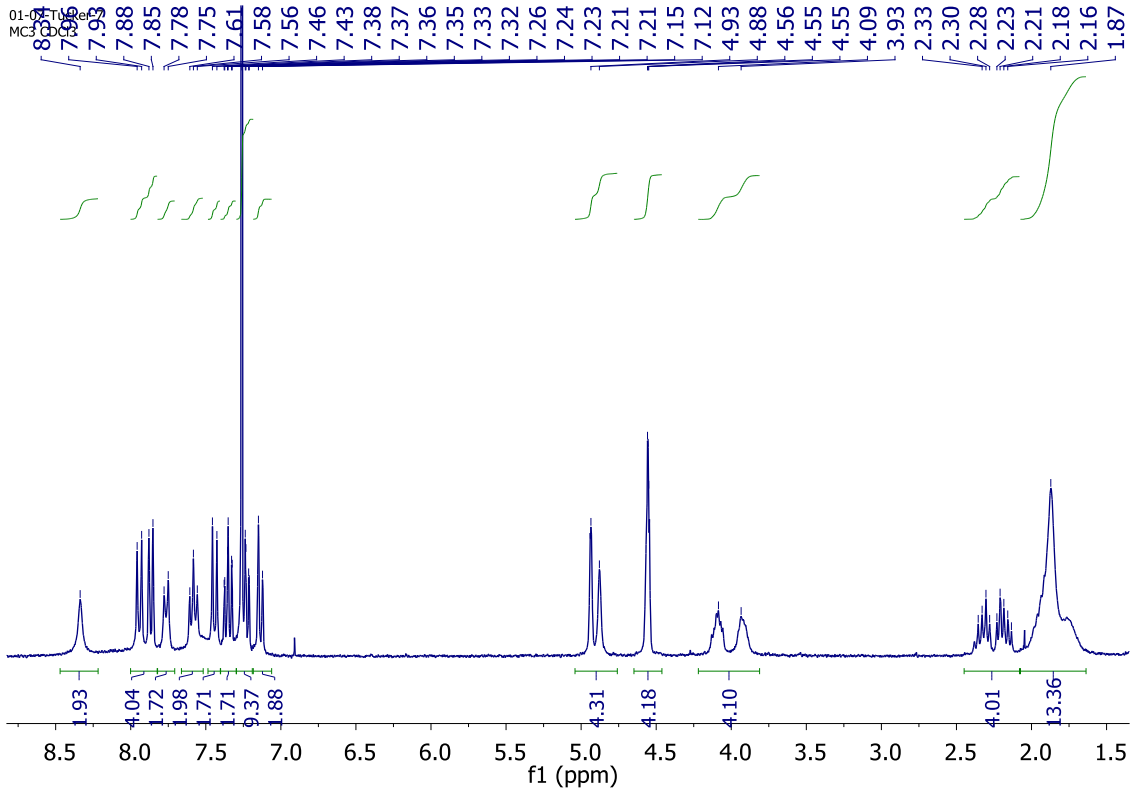

Figure 46. (*R*)-16b ^{1}H-NMR (400 MHz, $CDCl_3$)

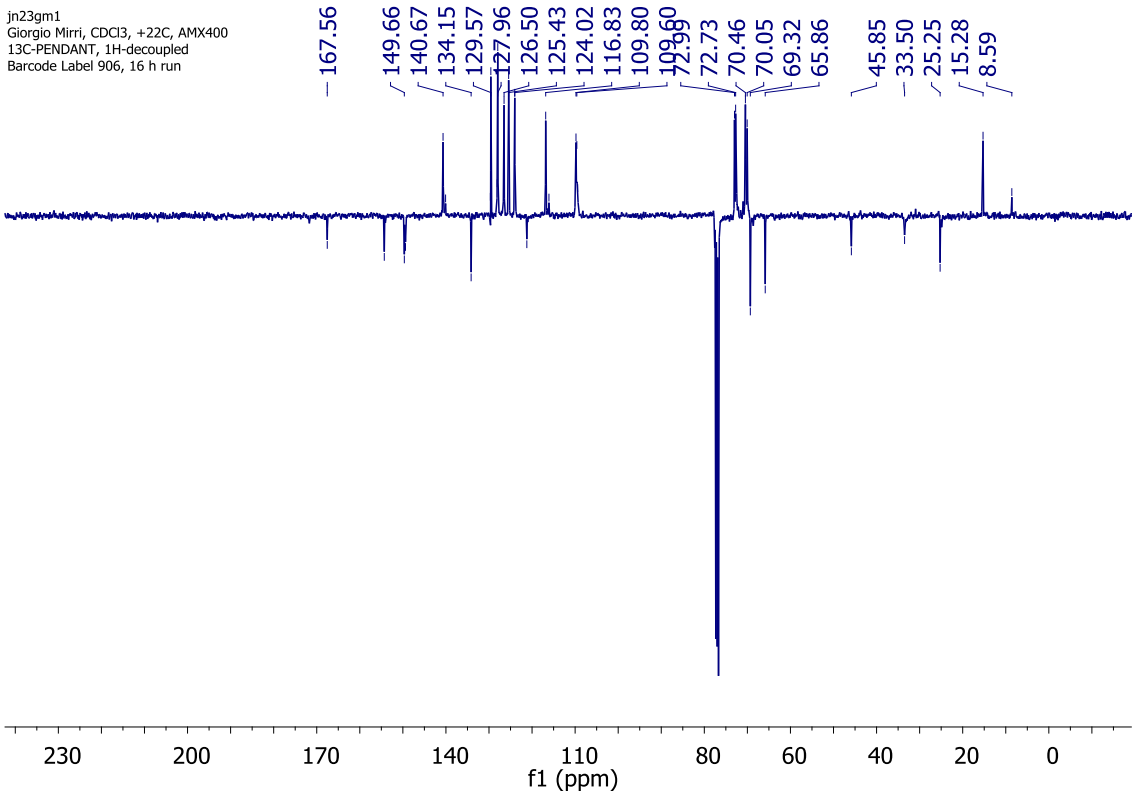

Figure 47. (*R*)-16b ^{13}C-NMR (100 MHz, $CDCl_3$)

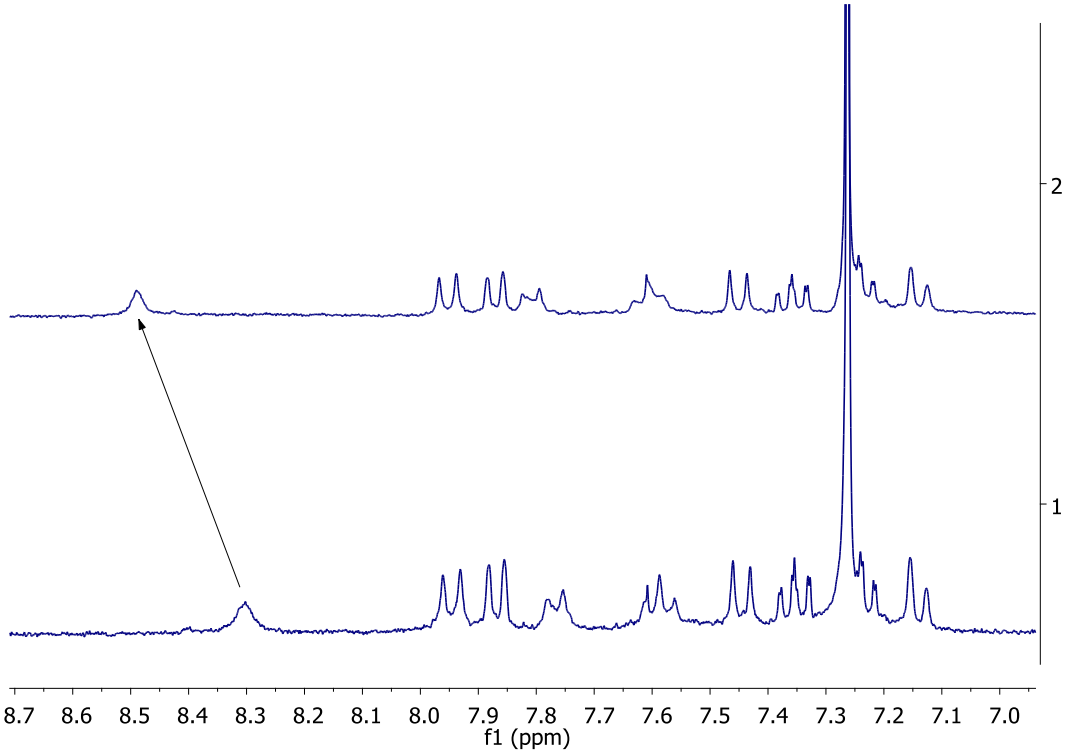

Figure 48. ^{1}H-NMR (300 MHz, $CDCl_3$) of **(*R*)-16b** (spectrum 1) and **(*R*)-16b** + excess of **17** (spectrum 2)

Appendix to Chapter 4

Calculations

All ab initio calculations in this work have been performed using the Gaussian03 (G03) software package[1], the Lanl2DZ basis set[2-5] and a combination of Barone's 1-parameter modified Perdew-Wang 91 exchange functional[6] and the Perdew-Wang 91 correlation functional (MPW1PW91)[7].

References

1. Gaussian 03, Rev. E.01. M. J. Frisch, G. W. Trucks, H. B. Schlegel, G. E. Scuseria, M. A. Robb, J. R. Cheeseman, J. A. Montgomery, J. T. Vreven, K. N. Kudin, J. C. Burant, J. M. Millam, S. S. Iyengar, J. Tomasi, B. M. V. Barone, M. Cossi, G. Scalmani, N. Rega,, H. N. G. A. Petersson, M. Hada, M. Ehara, K. Toyota,, J. H. R. Fukuda, M. Ishida, T. Nakajima, Y. Honda, O. Kitao,, M. K. H. Nakai, X. Li, J. E. Knox, H. P. Hratchian, J. B. Cross,, J. J. C. Adamo, R. Gomperts, R. E. Stratmann, O. Yazyev,, R. C. A. J. Austin, C. Pomelli, J. W. Ochterski, P. Y. Ayala,, G. A. V. K. Morokuma, P. Salvador, J. J. Dannenberg,, S. D. V. G. Zakrzewski, A. D. Daniels, M. C. Strain,, D. K. M. O. Farkas, A. D. Rabuck, K. Raghavachari,, J. V. O. J. B. Foresman, Q. Cui, A. G. Baboul, S. Clifford,, B. B. S. J. Cioslowski, G. Liu, A. Liashenko, P. Piskorz,, R. L. M. I. Komaromi, D. J. Fox, T. Keith, M. A. Al-Laham,, A. N. C. Y. Peng, M. Challacombe, P. M. W. Gill, and W. C. B. Johnson, M. W. Wong, C. Gonzalez, and J. A. Pople, *Gaussian, Inc., Wallingford CT*, 2004.
2. T. H. Dunning Jr. and P. J. Hay, in *Modern Theoretical Chemistry*, Ed. H. F. Schaefer III, Vol. 3 (Plenum, New York, 1976) 1-28
3. P. J. Hay and W. R. Wadt, *J. Chem. Phys.*, **82** (1985) 270-83.
4. W. R. Wadt and P. J. Hay, *J. Chem. Phys.*, **82** (1985) 284-98.
5. P. J. Hay and W. R. Wadt, *J. Chem. Phys.*, **82** (1985) 299-310.
6. C. Adamo and V. Barone, *J. Chem. Phys.*, 1998, **108**, 664-675.
7. J. Perdew, K. Burke and Y. Wang, *Phys. Rev. B.*, 1996, **54**, 16533-16539.